MECHANICAL ENGINEERING BULLETIN
Vol 12 1981

HC 421

mechanical engineering bulletin

VOL 12 • NO 1 • MARCH 1981

Editor

S. K. Ghosh

★

Editorial Board

D. Bhaduri

D. K. Shastri

S. Dasgupta

A. Das Sharma

P. K. Chowdhury

CONTENTS

		PAGE
1.	Optimization of hand hoist by analytic-structural modelling *by Jerzy Kowalski and Waclaw Szyc*	.. 3
2.	Calculation of the oil flow rate for proper operation of a scoop type fluid coupling *by Jhankar Basu*	.. 17
3.	Welding of copper without preheat - a study *by N.D. Das*	.. 20
4.	Erosion, corrosion and fouling of tubes in fluidized bed boilers *by Prabir Basu and M. Debnath*	.. 26
5.	State level R&D committee: inherent constraints defeat basic objectives	.. 32
6.	News and Views	.. 34

On front cover

Photograph of single spindle turret lathe developed by MERADO, Ludhiana. Details on page 34.

mechanical engineering bulletin

VOL 12 • NO 2 • JUNE 1981

Editor

S. K. Ghosh

★

Editorial Board

D. Bhaduri

D. K. Shastri

S. Dasgupta

A. Das Sharma

P. K. Chowdhury

CONTENTS

PAGE

1. Critical consideration on the limits of operation of fluid couplings
   by Jhankar Basu, G.S. Patki and S. Ramachandra .. 41

2. Open solar regeneration of lithium chloride brine
   by M. Prasad and P. Kumar .. 47

3. Free mass impact damper having larger clearances
   by S.V. Bhave and P.P. Chikate .. 53

4. Determination of the relative effect of the process variables on overcut in ECM
   by D.K. Pramanik .. 60

5. News and Views .. 63

On front cover

CMERI has recently completed investigations on castellated beams. Photograph shows such a beam under deflection and strain measuring test.

mechanical engineering bulletin

VOL 12 • NO 3 • SEPTEMBER 1981

Editor
S. K. Ghosh

★

Editorial Board
D. Bhaduri
D. K. Shastri
S. Dasgupta
A. Das Sharma
P. K. Chowdhury

CONTENTS

PAGE

1. Some effects of electrolyte flow mode on the anode shape in ECM
   by V.K. Jain and P.C. Pandey .. 69

2. Angular defocusing of paraboloidal reflectors with obtuse rim angle and truncated bottom
   by M. Prasad and S.K. Mazumdar .. 75

3. Fatigue in rolling contact - some salient features
   by C.S. Chandrasekharamurthy and A. Ramamohana Rao .. 82

4. Pedal pump for lift irrigation
   by G.K. Verma, R.K. Varma and K.N. Rao .. 87

5. News and Views .. 91

On front cover

Prototype of tractor-pulled combine harvester designed and developed by MERADO, Ludhiana. Details on page 93.

mechanical engineering bulletin

VOL 12 • NO 4 • DECEMBER 1981

Editor

S. K. Ghosh

★

Editorial Board

D. Bhaduri

D. K. Shastri

S. Dasgupta

A. Das Sharma

P. K. Chowdhury

CONTENTS

PAGE

1. Solar still regenerator for brine
   By M. Prasad, P. Kumar and B.C. Raychaudhuri .. 99

2. Energy losses in smooth pipe bends
   by Usha S. Powle .. 104

3. Metallurgical investigation into tube failures in power plants
   by A.B. Mondal, B.K. Ghosh, A. Basu and S. Jana .. 110

4. A review of surface roughness measurement technique
   by R.A. Agarwal, M.P. Kumaraswamy and S.K. Basu .. 116

5. News and Views .. 132

On front cover

Photo shows plasma cutting in operation. MERADO, Durgapur has developed the technique, and optimised parameters for cutting stainless steel.

OPTIMIZATION OF HAND HOIST BY ANALYTIC-STRUCTURAL MODELLING

JERZY KOWALSKI* AND WACLAW SZYC**

Abstract

The paper deals with mathematical models for optimisation of worm geared and planetary geared hoists. The models, presented here, show generalised and quantified optimisation models, taking into consideration the alternative designs, and provide information for final decision regarding materials to be used, to enable the designer to select the most effective alternative. For optimisation, the scale function, in regard to weight of the hoist, the length between the inner edges of the hook when pulled up and the efficiency have been assumed.

Introduction

The optimal design method for gearbox and transmission system was formulated[1-4] by using quantified models. V.V. Pavlov[5] formulated three tier system of mathematical modelling clearly demarkating between quantified, logical and structural models. For optimal design objective, the significance of the logic is compromised to rationalize the solution obtained from computerised model, with a view to selecting the optimal variant in design considering certain reproducible sets of variables and parameters.

*Research and Development Centre of Engineering Industry, Tekoma, Warsaw, Poland.

**Technical University of Poznan, Poland.

One of the present authors suggested[6] a two levelled partition of optimization models. The 'analytic-structural' model at the lower level of abstraction, contains the principles of quantified model with the rules and step sequence, necessary to create the same, while choosing between the alternative designs.

The designer has to formulate, in closed form, the objective function and the various constraints.

In analytic-structural model, one may find the following -

(i) The general form of the objective function (scaling function) with the decisive vectors formulating the alternate design and with the specification of the replaceable components and characteristics and repeatability of the decisive vector component in the multi-component objective function.

(ii) The constraint matrix consisting of parts independent of the particular solution of the design variant and the part appropriate to the particular variant and the specification and characteristics of the constraints in regard to replaceability and type, and the repeatability of the variables within the set of constraints.

(iii) Sets of non-material parameters

appearing in the constraints belonging to two distinct groups (as explained later in the text) and implication of other associated parameters with the parameters belonging to the first group.

(iv) The network diagram showing correlations of material parameters (occuring in the objective function) enabling us to decide about the proper material to be selected.

Thus, the analytic-structural model suggested here, provides greater opportunities to penetrate into the structure of the optimised object, than a Pavlov's model.

The present paper deals with the principles and procedures of formulating an analytic-structural model for design of hand hoists. Diagrams, showing the typical hoists, viz, the worm-geared hoist[7] and planetary geared hoist[8] are shown in Fig 1.

Analytic-structural model for optimization of worm geared hoist

Geometric models of hoist elements, are presented in Fig 2. s = 1,2,3,4 design pair variants, are assumed. Variant 1 : cast housing, and uniform hoisting chain wheel; Variant 2: cast housing, and sectional hoisting chain wheel; Variant 3 : composed housing, and uniform hoisting chain wheel; Variant 4 : composed housing, and sectional hoisting chain wheel.

The objective function takes the form

$$f(\vec{x}) = k_G \frac{G(\vec{x}_G)}{G_o} + k_l \frac{l(\vec{x}_l)}{l_o} +$$

$$k_\eta \frac{\eta_o}{\eta(\vec{x}_\eta)} = min \qquad .. (1)$$

where, $k_G + k_l + k_\eta = 1$

The decisive vector of hoist weight, should be expressed as follows

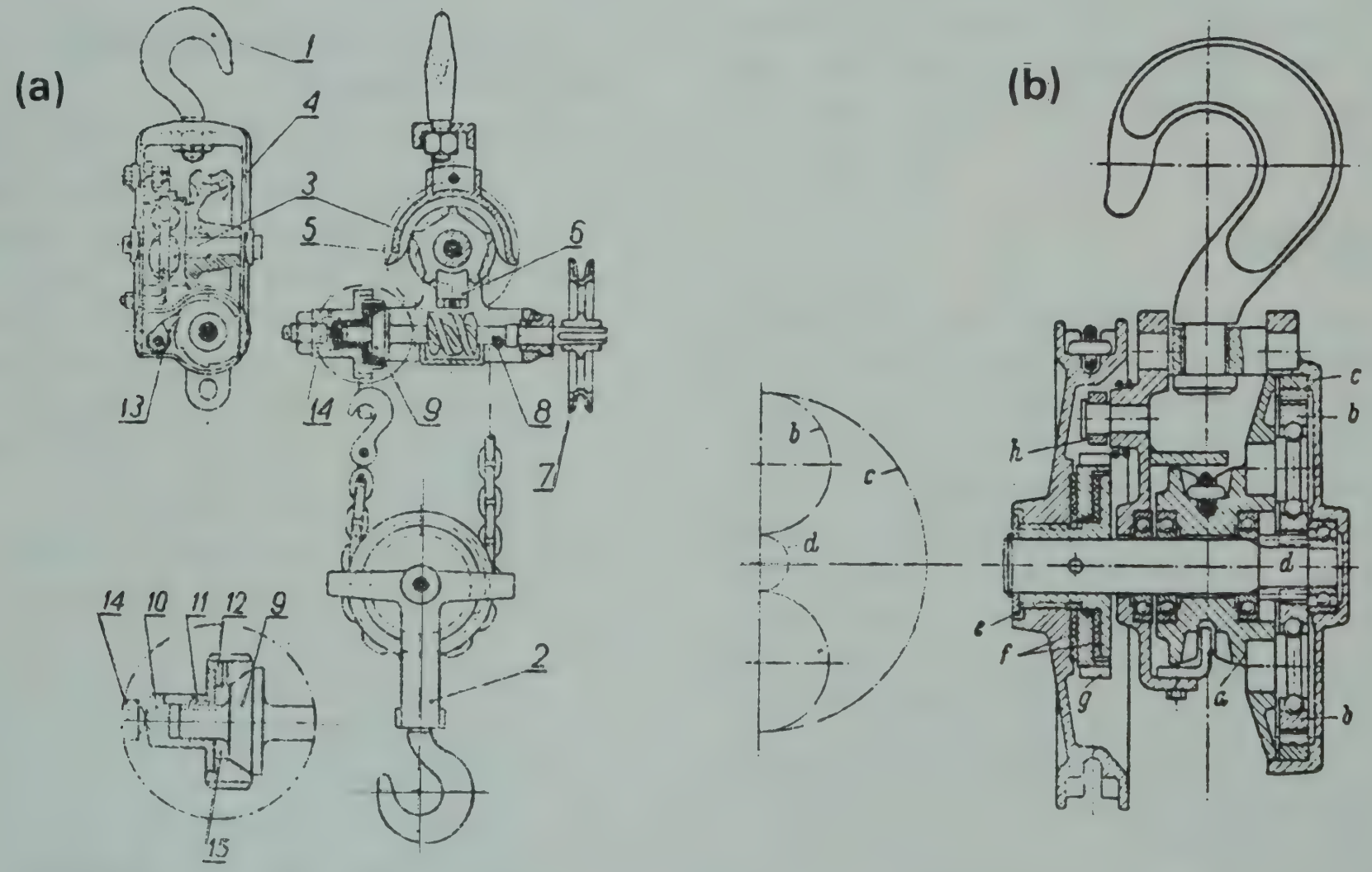
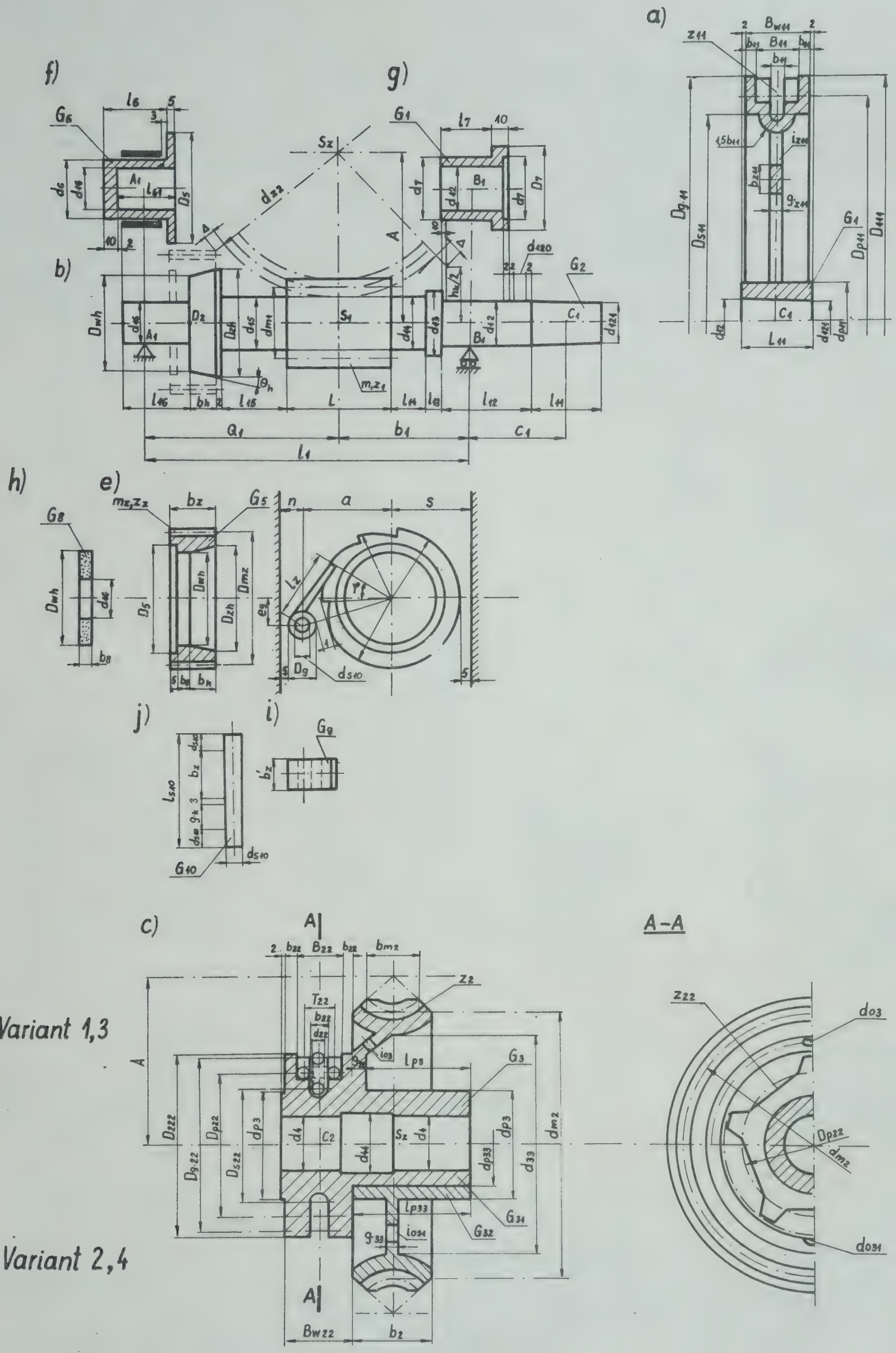
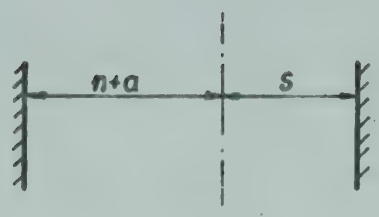


Fig 1
Design diagrams of the typical hoists. (a) worm geared hoist, (b) planetary geared hoist

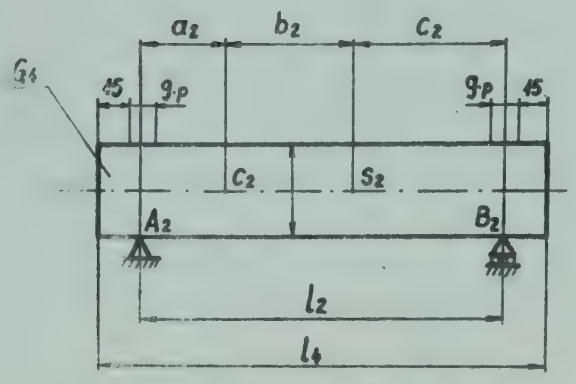


(Fig contd)

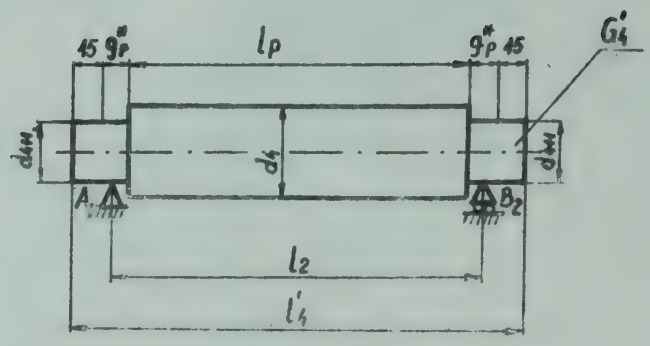
d)



Variant 1,2



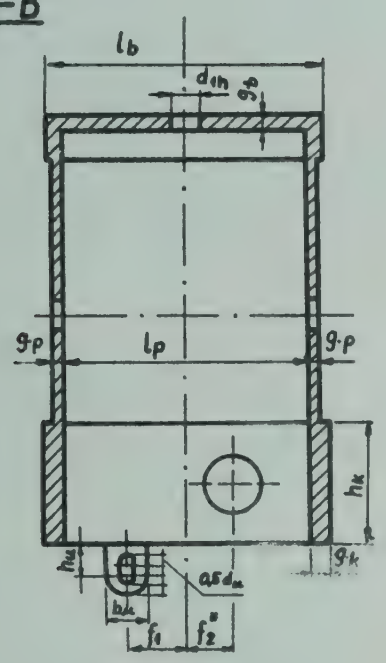
Variant 3,4



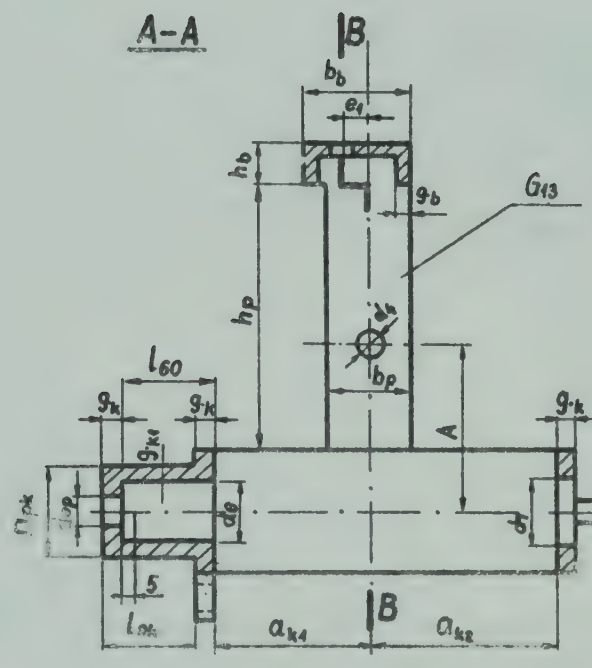
k)

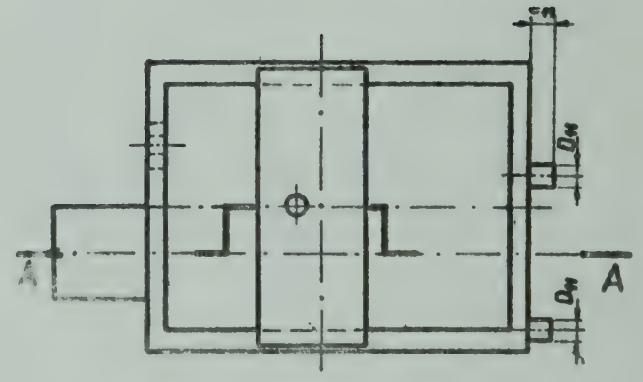
Variant 1,2

B-B



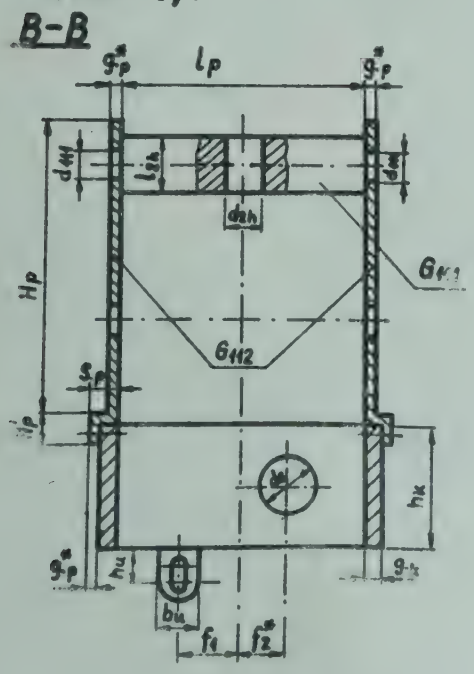
A-A

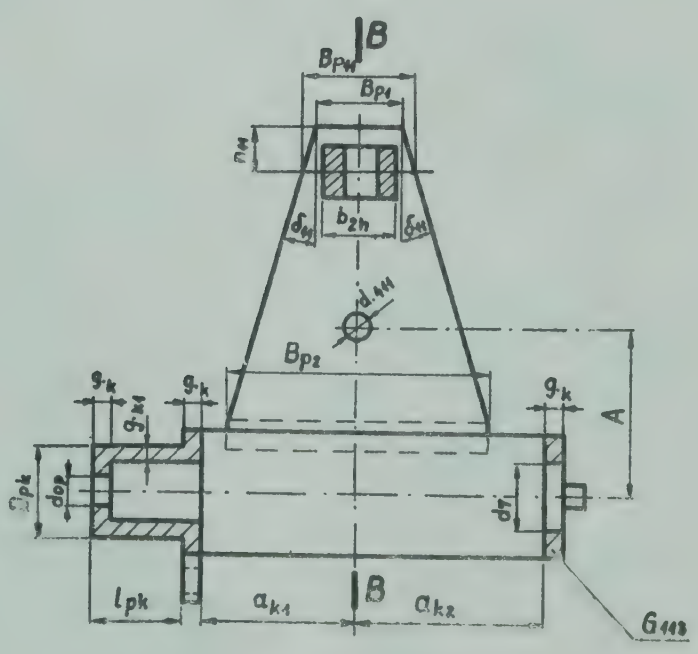


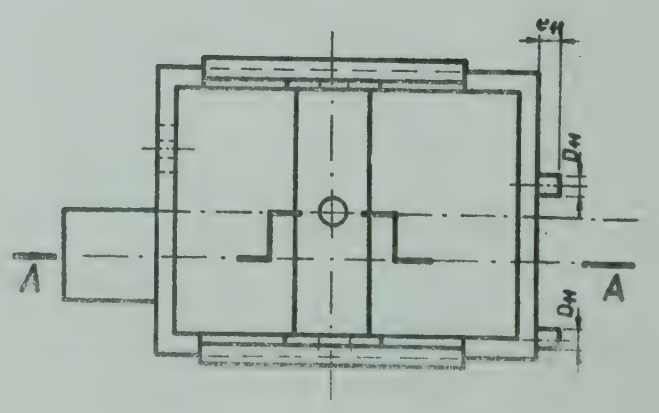


Variant 3,4

B-B







(Fig contd)

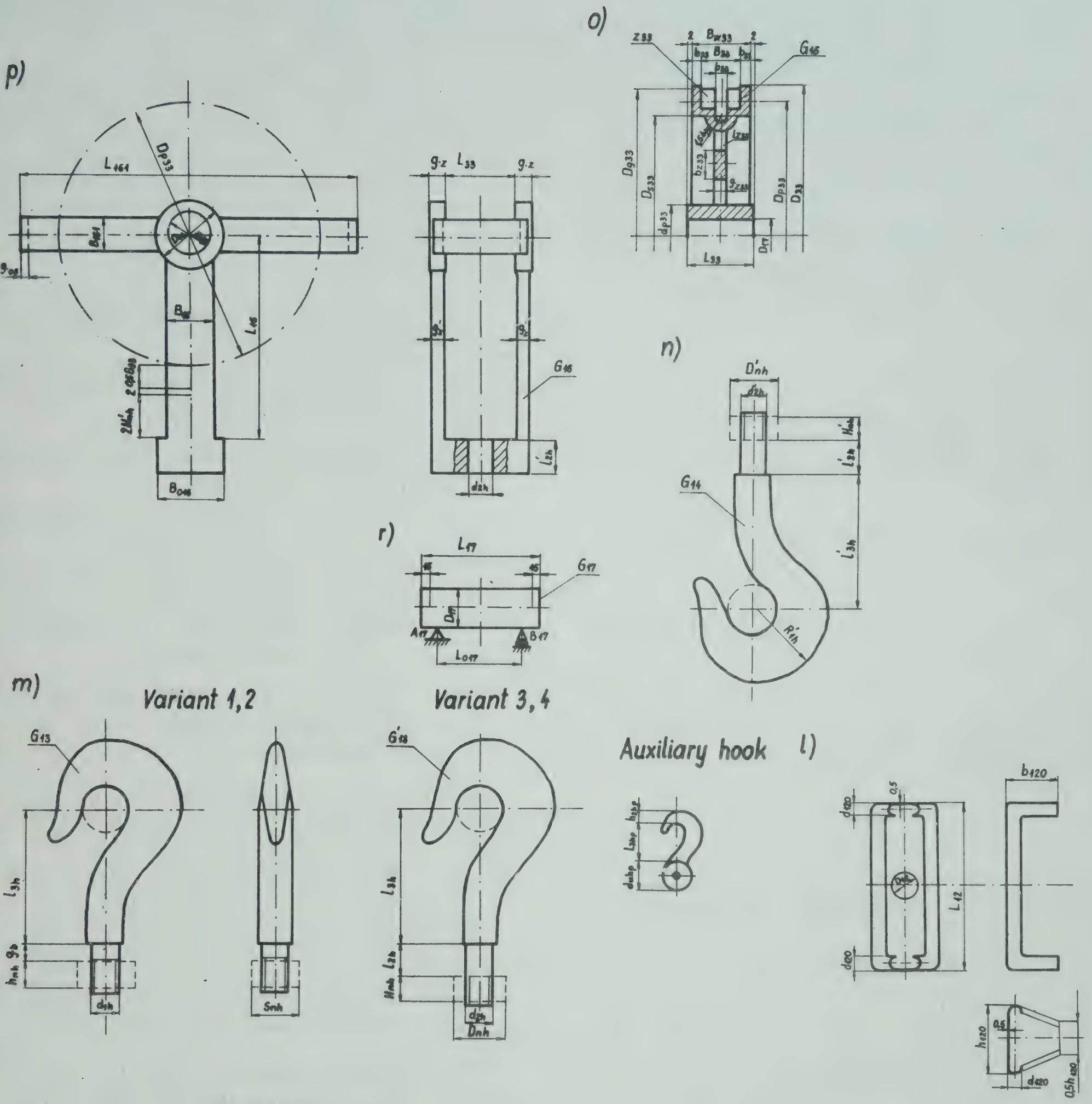


Fig 2

Geometric models of worm geared hoist. (a) drive chain wheel, (b) worm with brake outer plate, (c) hoisting chain wheel with worm-wheel, (d) axle of hoisting chain wheel, (e) ratchet-wheel creating the brake inner plate, (f) brake mounting, (g) worm sleeve, (h) felting ring, (i) ratchet, (j) ratchet pin, (k) housing, (l) chain guard, (m) upper hook, (n) lower hook, (o) chain wheel of lower hook, (p) lifting sling, and (r) lifting sling axle

$$\vec{x}_G = \vec{x} = [z_{11}, A, \vec{x}_{10}, l_{16}, d_{16}, d_{12}, D_{zh},$$
$$\theta_h, z_{22}, d_4, \vec{x}_{20}, b_z, l_z, d_{s10}, g_k, h_k,$$
$$z_{33}, g_z, g'_z, D_{17}, (g_b, h_b, b_b, b_p)_{1,2}$$
$$\nabla(g^*_p, n_{11}, B_{p1}, \delta_{11}, d_{111})_{3,4}] \quad .. (2)$$

$$(.....)_{s=1,2} \equiv (.....)_{1,2}$$

where decisive subvectors

$$\vec{x}_{10} = (m,\ i \wedge z_1)$$
$$\vec{x}_{20} = (m_z,\ z_z) \quad .. (3)$$

i being gear transmission ratio.

Decisive vector of length between the hook inner edges in the pull up state, takes the form

$$\vec{x}_1 = [A, \vec{x}_{10}, h_k, z_{33}, D_{17}, (h_b)_{1,2}$$
$$\nabla (g^*_p)_{3,4}] \quad .. (4)$$

Decisive vector for the efficiency

$$\vec{x}_\eta = (A,\ \vec{x}_{10}) \quad .. (5)$$

Designations of the decisive vector components are given in Fig 2. Hoist weight

$$G = \sum_{j=1}^{17} G_j \quad .. (6)$$

where the replaceable components are

$$(G_3)_{1,3} \nabla (G_{31},\ G_{32})_{2,4}$$
$$(G_{11})_{1,2} \nabla (G_{111},\ G_{112},\ G_{113})_{3,4}$$
$$(G_4)_{1,2} \nabla (G'_4)_{3,4} \quad .. (7)$$

In eqn (1) G_o, l_o, η_o are respectively : hoist weight, length between the hook inner edges in the pull up state, object efficiency for initial design, (ie, to be used for optimization), but k_G, k_l, k_η, are the scaling factors. Considering, that first two parts in the optimization criterion (eqn 1) are partially dependent, while the third part is independent, one may sugges the scaling factor ratio as 0.35:0.25:0. for this case.

The particular components of the sca ling function have the following character multinominal, linear, and rational. Th component repeatability for the decisiv vector is as follows: $\vec{x}_{20}$ (8 times), b_z (times) $d_{12}, D_{zh}, \theta_h, g_k$ (5 times), $A, \vec{x}_{10}, d_1$ (4 times).

The constraints imposed on the desig are as follows

W_1 : stress condition for worm gear tooth under unit pressure[9],

W_2 : stress condition for worm-wheel tooth in bending[9],

W_3 : condition determining braking torque

W_4 : stress condition for the unit pressure on the brake frictional surface

W_5 : stress condition for bending of ratchet-wheel tooth,

W_6 : stress condition for the unit pressure between ratchet tooth and ratchet-wheel tooth,

W_7 : stress condition for ratchet pin bending,

W_8 : stress condition for the unit pressure between ratchet and pin,

W_9 : condition limiting hoisting force,

W_{10} : stress condition for the axle of the hoisting chain wheel,

W_{11} : stress condition for the axle of the hoisting chain wheel at the worm-wheel,

W_{12} : stiffness condition for the axle of the hoisting chain wheel on the deflection at the worm-wheel,

W_{13} : stress condition for the unit pressure in A_2-bearing of the axle of hoisting chain wheel,

W_{14} : stress condition for the unit pressure in B_2-bearing of the axle of hoisting chain wheel,

W_{15} : stress condition of worm for the unit pressure in A_1-bearing,

W_{16} : stress condition in D_1-section of the bearing pin,

W_{17} : stress condition of worm for the unit pressure in B_1-bearing,

W_{18} : stress condition of worm in the section under B_1-bearing,

W_{19} : stress condition of worm for meshing plane (point S_1),

W_{20} : stiffness condition of worm for deflection of the point S_1,

W_{21} : stiffness condition of worm for angle of rotation of A_1-bearing,

W_{22} : stress condition for the unit pressure between key and hub of driving chain wheel,

W_{23} : design condition determining minimal length of brake cone,

W_{24} : design condition determining minimal thickness of felting ring,

W_{25} : design condition determining minimal width of felting ring,

W_{26} : condition enabling the assembly of ratchet-wheel and ratchet,

W_{27} : condition determining perfect mesh of the ratchet[7],

W_{28} : design condition determining worm diameter d_{12},

W_{29} : stress condition for housing cage,

W_{30} : stress condition for housing cage lug,

W_{31} : stress condition for bending of axle of lifting sling,

W_{32} : stress condition for the unit pressure between the lifting sling and its axle,

W_{33} : stress condition for the unit pressure between the lifting sling axle and chain wheel of lower hook,

W_{34} : design condition determining the width of lifting sling base,

W_{35} : design condition determining the maximal pitch diameter of chain wheel of lower hook,

W_{36} : design condition determining the maximal diameter of hub of the housing cage,

W_{37} : stress condition for tension of the lifting sling arms,

$(W_{38})_{1,2}$: stress condition for the housing beam (cast steel-by Huber-Mises-Hencky's hypotehsis; cast iron-by Mariotte-de St Venant-Poncelet's hypothesis),

$(W_{39})_{1,2}$: stress condition for the housing arms,

$(W_{40})_{1,2}$: condition enabling the upper hook assembly,

$(W_{41})_{2,4}$: stress condition for the unit pressure between key and worm-wheel hub,

$(W_{38})_{3,4}$: bending stress condition of the housing cross-bar,

$(W_{39})_{3,4}$: tensile stress condition of the housing carrying strips,

$(W_{42})_{3,4}$: stress condition for shearing of pin of the upper hook cross-bar,

$(W_{43})_{3,4}$: stress condition for the unit pressure between cross-bar pin and the carrying strip,

$(W_{44})_{3,4}$: stress condition for shearing of the carrying strips,

$(W_{45,46})_{3,4}$: design conditions determining the lengths of carrying strips.

The constraint matrix is given in Fig 3. One may separate in the matrix, the part

Variable / Constraint	z_{41}	A	$\bar{X}_{40}$	l_{46}	d_{46}	d_{42}	D_{zh}	θ_h	z_{22}	d_4	$\bar{X}_{20}$	b_z	l_z	d_{540}	g_k	h_k	z_{33}	g_z	g'_2	D_{47}	Variant 1,2 g_b	h_b	b_b	b_p	Variant 3,4 $g^x_{p_0}$	n_H	B_{p11}	δ_{11}	d_{444}
$W_{1,2}$		×	×						×																				
W_3		×	×				×	×	×		×																		
W_4		×	×				×		×		×																		
$W_{5,6}$			×				×	×	×		×	×																	
$W_{7,8}$			×				×	×	×		×	×		×															
W_9	×	×	×						×																				
$W_{10,11,12,13,14}$		×	×						×	×	×										×				×				
$W_{15,16}$	×	×	×	×	×		×	×	×		×	×			×	×													
$W_{17,18}$	×	×	×	×		×	×	×	×		×	×			×	×													
W_{19}	×	×	×	×			×	×	×		×	×			×	×													
$W_{20,21}$	×	×	×	×	×	×	×	×	×		×	×			×	×													
W_{22}		×	×			×			×																				
W_{23}							×	×			×																		
W_{24}					×						×																		
W_{25}							×	×			×	×																	
W_{26}		×	×								×			×															
W_{27}											×		×	×															
W_{28}		×	×			×																							
W_{29}	×	×	×								×	×			×	×													
W_{30}															×														
$W_{31,32}$																		×		×									
$W_{33,34}$																				×									
W_{35}																	×												
W_{36}					×										×	×													
W_{37}																			×	×									
$(W_{38})_{1,2}$		×	×						×		×	×			×	×					×	×	×						
$(W_{39})_{1,2}$		×	×						×	×	×	×				×					×			×					
$(W_{40})_{1,2}$		×	×						×		×	×			×	×	×				×		×	×					
$(W_{44})_{2,4}$		×	×						×	×	×																		
$(W_{38})_{3,4}$		×	×								×														×				
$(W_{39})_{3,4}$																									×	×	×	×	×
$(W_{42})_{3,4}$																													×
$(W_{43})_{3,4}$																									×				×
$(W_{44})_{3,4}$																									×	×			
$(W_{45})_{3,4}$		×	×													×										×	×	×	
$(W_{46})_{3,4}$		×	×													×										×	×	×	

Fig 3
Matrix of constraints for worm geared hoist

independent of the particular variants of design, and the proper parts for the particular variants. In the common part occur 37 constraints, but the constraints W_{38}, W_{39} are replaceable for variants (1,2) and variants (3,4).

Constraints $(W_{40})_{1,2}$ and $(W_{41})_{2,4}$ are proper for variants indicated, so are constraints $(W_{42}/W_{46})_{3,4}$. All constraints have inequal form, and are of various types: non-linear, non-rational, rational, linear. The variable repeatability in the constraint set, is as follows: $\vec{x}_{10}$ (32 times, $\vec{x}_{20}$ (30 times), A (27 times), z_{22} (26 times), b_z (17 times), D_{zh} (15 times), θ_h, h_k (14 times), g_k (12 times).

In the constraint matrix, do not occur too many numbers of couplings by particular variables, except constraints W_{15}/W_{21} and $(W_{38}/W_{40})_{1,2}$.

Non-material parameter vector of the first group, takes the form

$$\vec{p}_1 = (Q,\ P_{max},\ L_h) \qquad .. (8)$$

where, Q = hoisting capacity, 250 kp $\leqslant Q \leqslant$ 10000 kp[7], P_{max} = maximal hoisting force, L_h = total life of gear transmission.

Non-material parameter vector of the second group should be expressed as follows

$$\vec{p}_2 = [\alpha_o, n_2, f_w, x_h, \alpha_{11}, \theta_{A1a}, (d_{1h} \wedge h_{nh} \wedge s_{nh} \wedge l_{3h})_{1,2} \nabla (d_{2h} \wedge l_{2h} \wedge H_{nh} \wedge D_{nh} \wedge l_{3h})_{3,4}, h_{2hp} \wedge l_{3hp} \wedge d_{uhp}, d'_{2h} \wedge l'_{2h} \wedge H'_{nh} \wedge D'_{nh} \wedge l'_{3h} \wedge R'_{1h} \Delta, \eta_k, \eta_b] \quad .. (9)$$

where α_o = transverse pressure angle, n_2 = worm rotational speed, f_w = coefficient of load character for worm gear, x_h = factor of brake reliability, θ_{A1a} = A_1-bearing allowable angle of rotation, η_k = chain wheel efficiency, η_b = shaft bearing efficiency.

Parameters of the first kind Q and P_{max} implicate the values of certain other parameters associated with them, concerning dimensions of hooks and chains represented below

$$1.2Q \rightarrow (d_{1h}, h_{nh}, S_{nh}, l_{3h}, G_{13})_{1,2} \nabla (d_{2h}, l_{2h}, H_{nh}, D_{nh}, l_{3h}, G'_{13})_{3,4}$$

$$1.1Q \rightarrow (d'_{2h}, l'_{2h}, H'_{nh}, D'_{nh}, l'_{3h}, R'_{1h}, G_{14})$$

$$Q \rightarrow P_c \rightarrow (d_{22}, T_{22}, B_{22}, h_{2hp}, l_{3hp}, d_{uhp})$$

$$P_{max} \rightarrow (d_{11}, T_{11}, B_{11}) \quad .. (10)$$

where P_c = force acting on the hoisting chain wheel.

The network diagram showing correlations of material parameters is given in Fig 4. The material properties are systemized in several groups. The outer group encloses the material specific gravities, occuring only in the scaling function. Remaining, inner groups, viz, allowable unit pressures

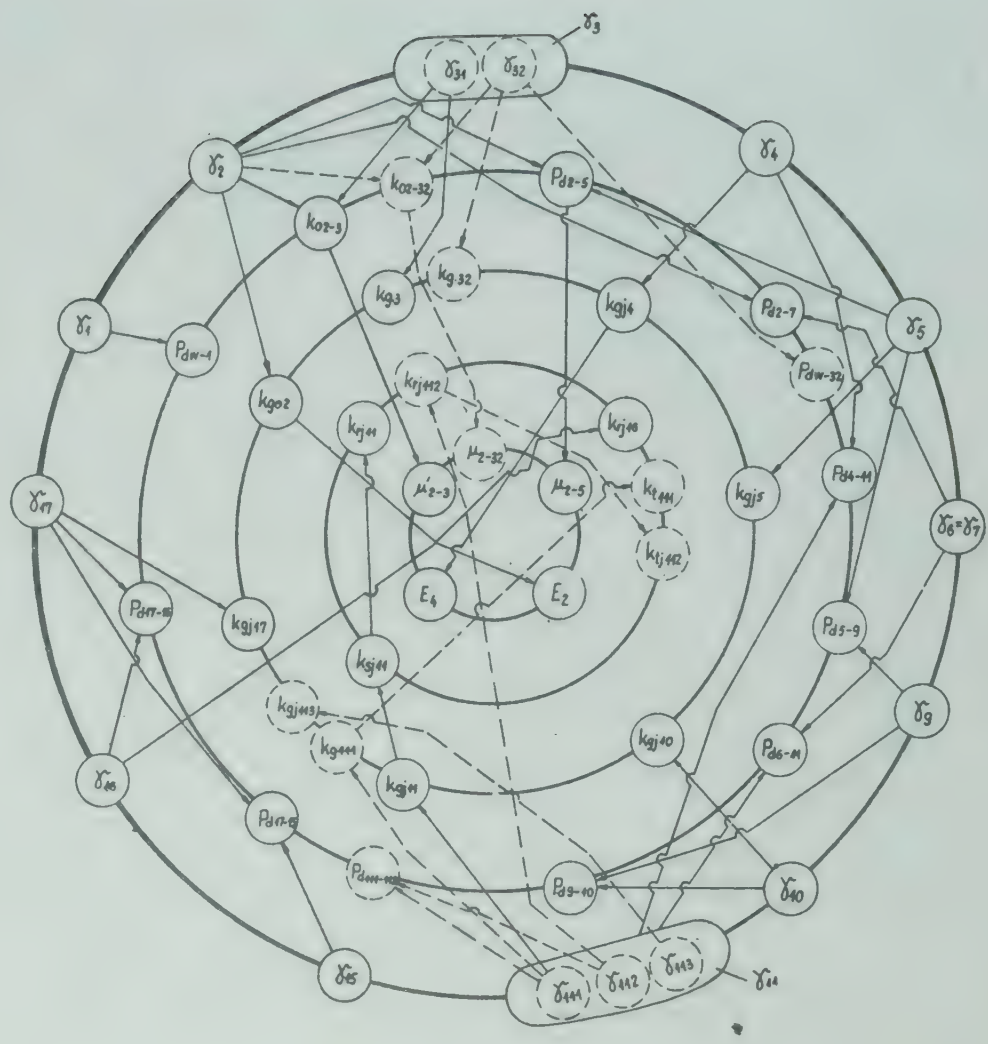


Fig 4

Network diagram of material parameter correlations for worm geared hoist

depending on the properties of mating elements p_{dk-l} (for teeth k_{o2-m}), allowable bending pulsatory stresses k_{gjn} and oscillatory stresses k_{gop} (for worm-wheel teeth k_{gm}), allowable pulsatory tensile, torsional and shearing stresses k_{rjq}, k_{sju}, k_{tjv}, moduli of elasticity E_w, coefficients of friction μ_{y-z} (for worm-wheel teeth, the apparent coefficient of friction in the mesh μ'_{2-m}), occur only in the constraints. In the outer envelope are located the parameters, whose values may be chosen according to the designer's requirement, and they automatically imply the variation of corresponding inner parameters.

The network diagram of material parameter correlations, illustrating the connection net, existing between particular material groups, should be supplied by the outer material parameter matrix, ie, the parameters occuring in the optimization criterion. It explains the way how material parameters occuring in the constraints have an effect on the scaling function (Fig 5).

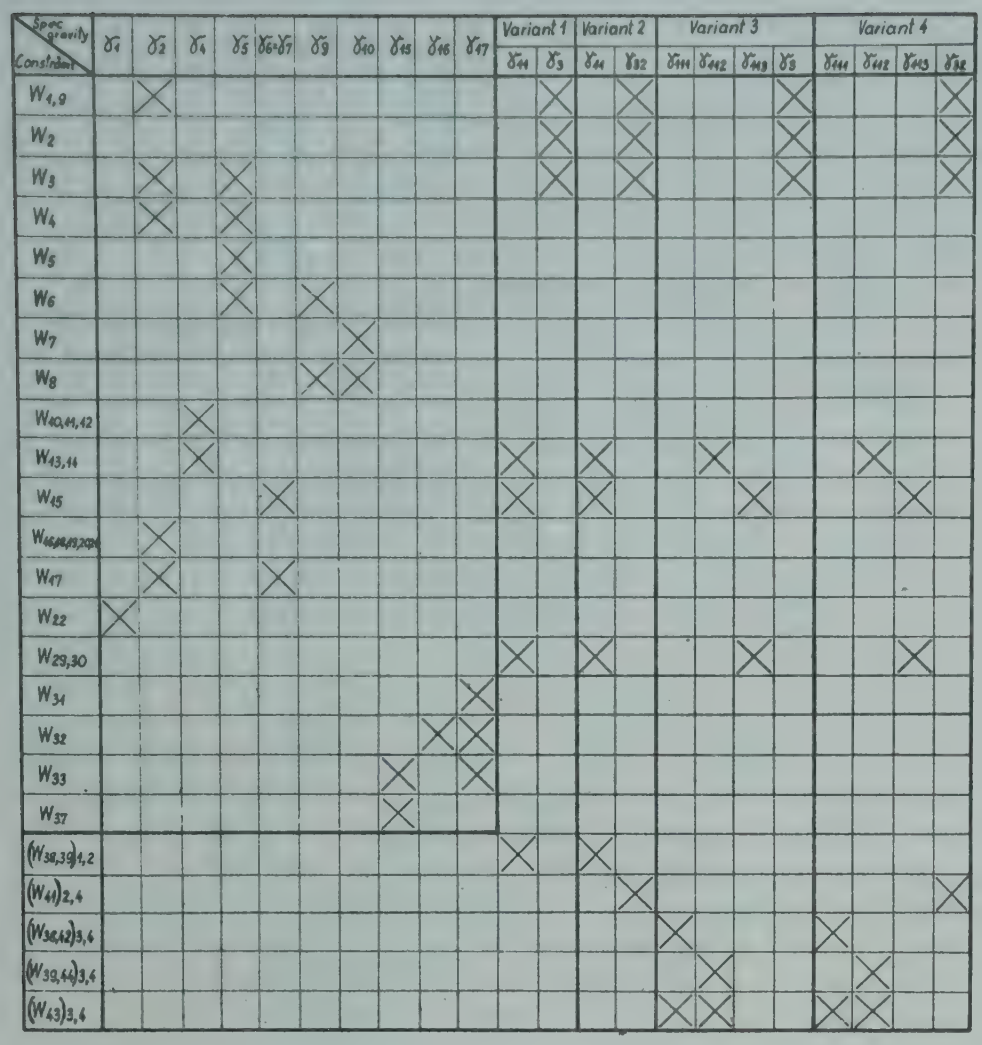


Fig 5

Matrix of outer material parameters for worm geared hoist

Analytic-structural optimizational model for planetary geared hoist

Geometric models of hoist elements are presented in Fig 6. Regarding the design compactness, the alternate design pair structure, was not considered.

The scaling function takes the form (eqn 1), moreover the decisive vector of hoist weight, should be expressed as follows:

$$\vec{x}_G = \vec{x} = [z_{11}, d_{m1}, l_1, m, z_1, i, b_2, d_{21} \wedge l_{211} \wedge D_{21} \wedge G_{143} \wedge l_{212} \wedge D_{212} \wedge G_{62}, l_2, d_{22} \wedge l_{22} \wedge D_{22} \wedge G_{144}, D_{p7} \wedge D_{k7} \wedge D_{z7} \wedge z_{k7}, d_5, l_5, z_{22}, d_8, d_{10}, m_z, z_z, b_z, l_z, d_{12}, a_{14}, g_{14}, g_{k14}, d_{14}, g_{t14}, z_{33}, g_z, g'_z, D_{20}] \quad .. (11)$$

Decisive vector of length between the hook inner edges in the pull up state, takes the form

$$\vec{x}_1 = (z_1, i, a_{14}, z_{33}, D_{20}) \quad .. (12)$$

but decisive vector of the object efficiency

$$\vec{x}_\eta = x_\eta = i \quad .. (13)$$

Hoist weight

$$G = \sum_{j=1}^{20} G_j \quad .. (14)$$

The component repeatability for the vector of hoist weight is as follows: b_2 (7 times), d_{21} (6 times), m, z_1, b_z (5 times).

The constraints imposed on the design are as follows :

W_1 : condition of adjacency for the planetary gear,

W_2 : stress condition for unit pressure on sun wheel tooth, (old formulae[10])

W_3 : stress condition for bending of sun wheel tooth (old formulae[11]),

W_4 : stress condition for unit pressure on planet wheel tooth,

W_5 : stress condition for bending of planet wheel tooth,

W_6 : stress condition for bending of planet wheel pin,

W_7 : stress condition for the unit pressure between pin and cage[9],

W_8 : condition determining braking torque,

W_9 : stress condition for press sleeve hub,

W_{10} : stress condition for the unit pressure in the screw joint of press sleeve of driving chain wheel,

W_{11} : stress condition for the unit pressure on the brake frictional surface,

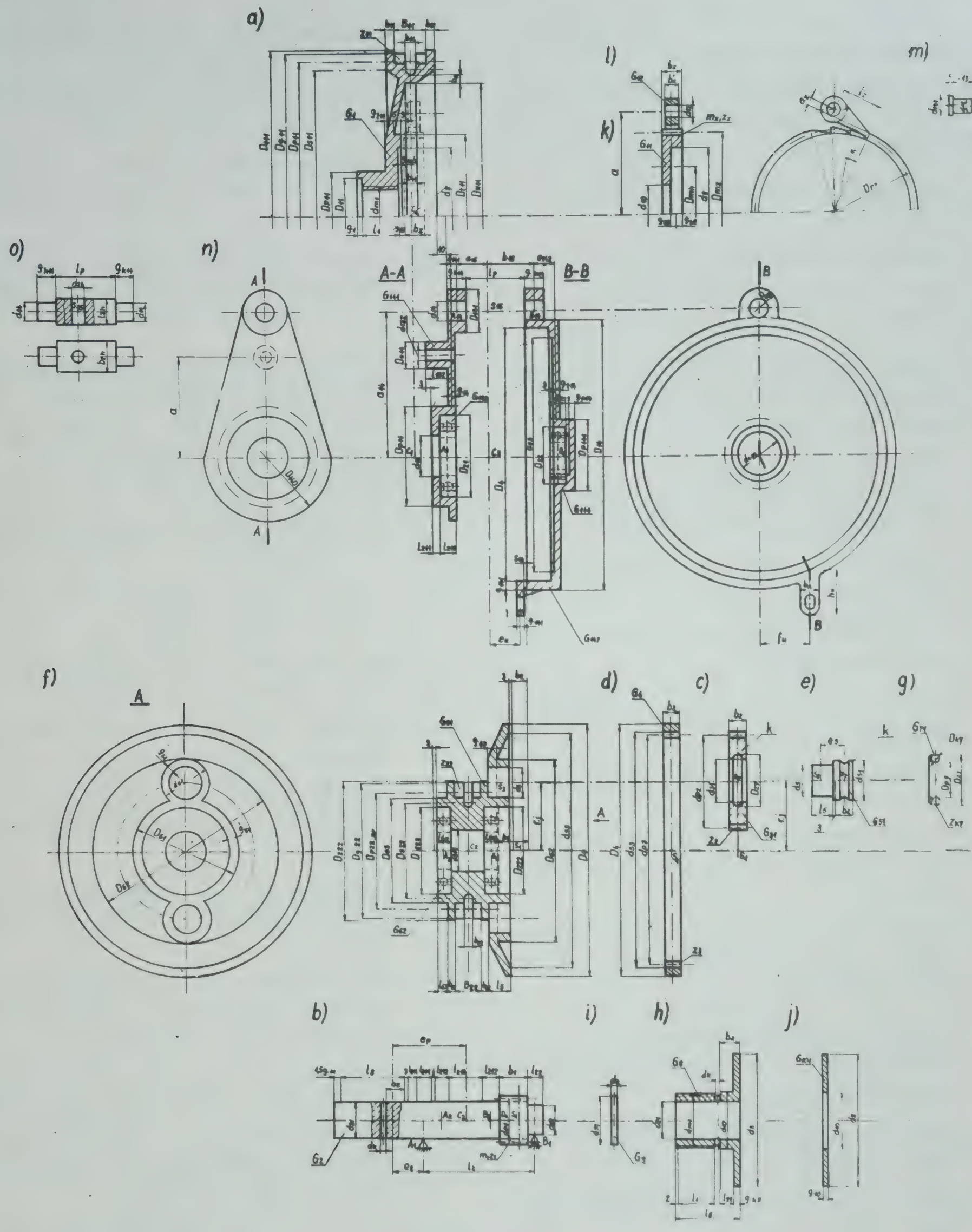


Fig 6

Geometric models of planetary geared hoist. (a) drive chain wheel, (b) drive shaft with sun wheel, (c) planet wheel, (d) internal fixed gear, (e) planet wheel pin, (f) hoisting chain wheel creating the planetary cage, (g) ringless bearing, (h) press sleeve with self-locking thread, (i) safetying pin, (j) ferrodic-disk, (k) ratchet-wheel, (l) ratchet, (m) ratchet pin, (n) housing with bearings, and (o) upper hook cross-bar

W_{12} : stress condition for the bending of ratchet-wheel tooth,

W_{13} : stress condition for the unit pressure between teeth of ratchet and ratchet wheel,

W_{14} : stress condition for bending of ratchet pin,

W_{15} : stress condition for the unit pressure between ratchet and pin,

W_{16} : condition limiting hoisting force,

W_{17} : stress condition for driving shaft at the place where the section changes, located by the sun wheel (point D_1),

W_{18} : stress condition for driving shaft at the bearing place (point B_2),

W_{19} : total-life condition of the driving shaft bearing A_1 12,

W_{20} : total-life condition of the driving shaft bearing B_1 12,

W_{21} : total-life condition of ringless bearing of planet wheel 12,

W_{22} : stress condition for shearing of driving shaft pin,

W_{23} : stress condition for the unit pressure between the pin and the press sleeve,

W_{24} : stiffness condition for the driving shaft due to the deflection of sun wheel (point S_1),

W_{25} : stress condition for the unit pressure between the upper hook cross-bar and housing,

W_{26} : stress condition for bending of the upper hook cross-bar,

W_{27} : stress condition for the upper hook lug,

W_{28} : stress condition for the right part of housing,

W_{29} : stress condition for the left part of housing,

W_{30} : stress condition for tension of th lower hook lug,

W_{31} : stress condition for bending of axle of the lifting sling,

W_{32} : stress condition for the unit pressure between lifting sling and its axle,

W_{33} : stress condition for the unit pressure between lifting sling axle and chain wheel of lower hook,

W_{34} : design condition determining the width of lifting sling base,

W_{35} : design condition determining the maximal pitch diameter of the chain wheel of lower hook,

W_{36} : condition determining proper mesh of the ratchet,

W_{37} : stress condition for tension of lifting sling arms,

W_{38} : design condition determining the root diameter of sun wheel,

W_{39} : design condition determining the diameter of the pin of planet wheel,

W_{40} : design condition determining the lug diameter of upper hook cross-bar,

W_{41} : design condition determining the pin diameter of upper hook cross-bar,

W_{42} : design condition determining the nominal diameter of self-locking thread of press sleeve,

W_{43} : condition eliminating the possibility of collision between upper hook nut and riser head with the hole for cross-bar pin, located in the left part of housing,

W_{44} : condition eliminating the possibility of collision between the chain and lower hook lug,

W_{45} : condition eliminating the possibility of collision between upper hook nut and chain.

The constraint matrix is given in Fig 7. ne variable repeatability in the cons-raint set, is as follows: i (21 times), $_{22}$ (20 times), b_2 (17 times), d_{21} (15 imes), z_1, l_2, g_{14} (11 times).

The constraint matrix does not show too any numbers of couplings by particular ariables, except constraints W_{17}, W_{24} and $_{25}, W_{27}, W_{28}$.

The non-material parameter vector of he first kind takes the form (eqn 8), but non-material parameter vector of the second kind, should be expressed as follows

$$\vec{p}_2 = [\alpha_o, n_2, x_h, g_{60}, d_{2h}\hat{}l_{2h}\hat{}H_{2h}\hat{}D_{nh} \hat{}l_{3h}, h_{2hp}\hat{}l_{3hp}\hat{}d_{uhp}, d'_{2h}\hat{}l'_{2h} \hat{}H'_{2h}\hat{}D'_{nh}\hat{}l'_{3h}\hat{}R'_{1h}, \eta_k, \eta_b] \quad .. (15)$$

The implications of associated parameters with the parameters of the first kind, are as follows:

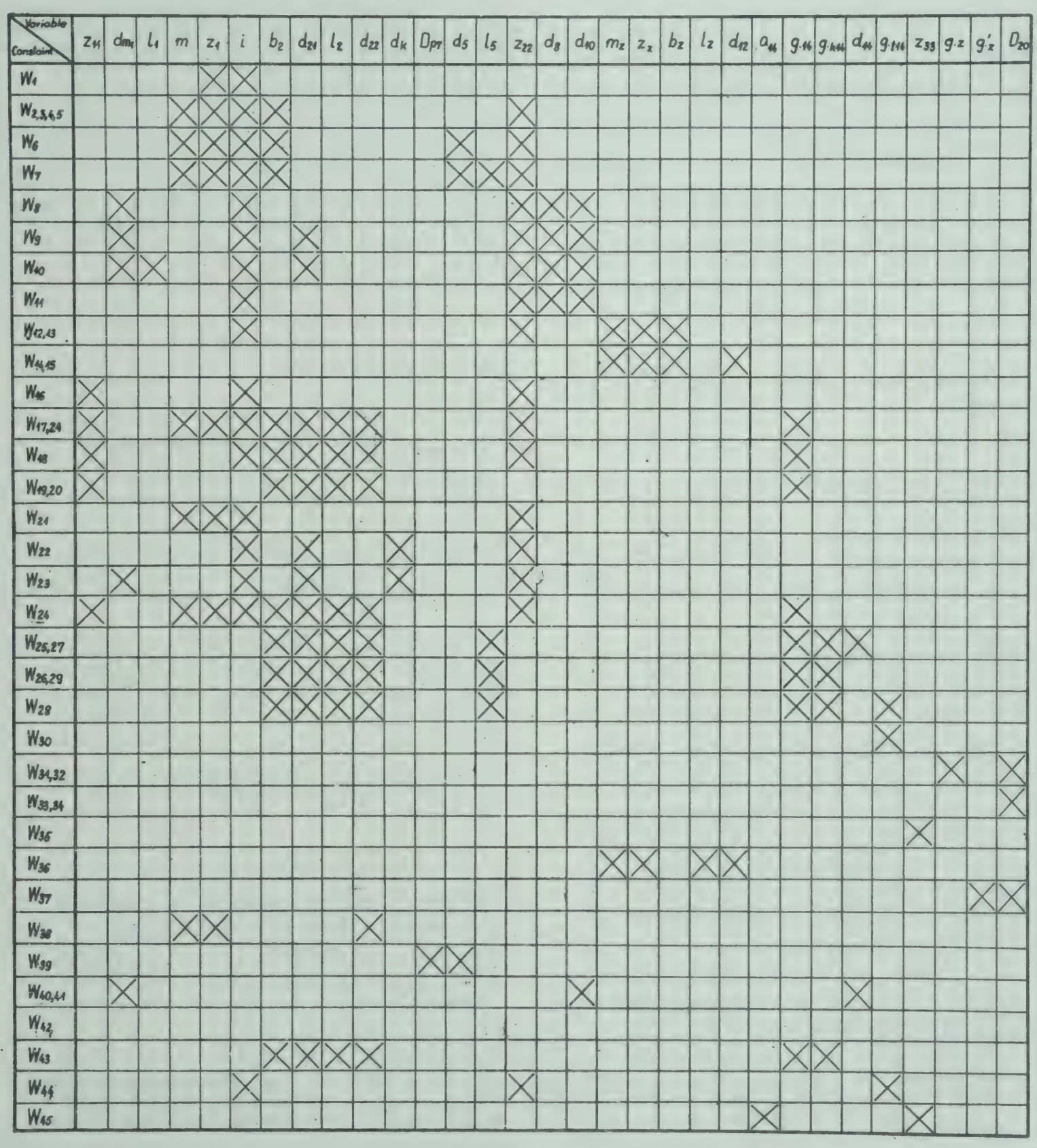


Fig 7
Matrix of constraints for planetary geared hoist

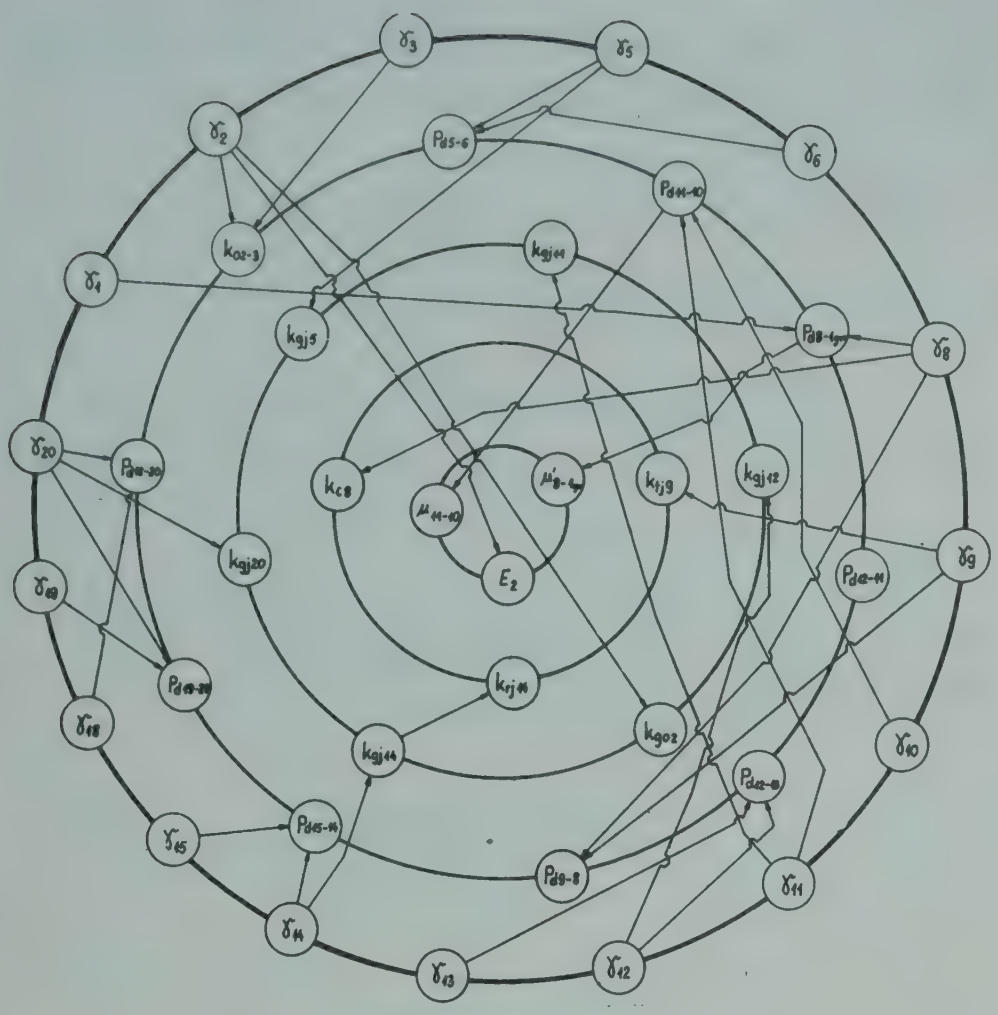


Fig 8
Network diagram of material parameter correlations for planetary geared hoist

Spec. gravity / Constraint	γ_1	γ_2	γ_3	γ_5	γ_6	γ_8	γ_9	γ_{10}	γ_{11}	γ_{12}	γ_{13}	γ_{14}	γ_{15}	γ_{18}	γ_{19}	γ_{20}
$W_{2,4}$		X	X													
$W_{3,17,18,24}$		X														
W_5			X													
W_6				X												
W_7				X	X											
$W_{8,9}$	X					X		X	X							
W_{10}								X	X							
W_{11}	X					X										
W_{12}									X							
W_{13}									X	X						
W_{14}										X						
W_{15}										X	X					
W_{22}							X									
W_{23}						X	X									
W_{25}												X	X			
$W_{26,17,28,33}$												X				
W_{34}																X
W_{32}															X	X
W_{33}														X		X
W_{37}															X	

Fig 9
Matrix of outer material parameters for planetary geared hoist

$$1.2Q \rightarrow (d_{2h}, l_{2h}, H_{nh}, D_{nh}, l_{3h}, G_{16}),$$

$$1.1Q \rightarrow (d'_{2h}, l'_{2h}, H'_{nh}, D'_{nh}, l'_{3h}, R'_{1h}, G_{17}),$$

$$Q \rightarrow P_c \rightarrow (d_{22}, T_{22}, B_{22}, h_{2hp}, l_{3hp}, d_{uhp}),$$

$$P_{max} \rightarrow (d_{11}, T_{11}, B_{11}) \qquad .. (16)$$

The network diagram showing correlations of material parameters is presented in Fig 8, but the matrix of outer material parameters is given in Fig 9. Network diagram and matrix construction are analogous to worm geared hoist.

Conclusions

With the 'analytic-structural' models, formulated in this paper, it was possible to optimise the various parameters of the hoist in a quantified manner, thus making them directly useful to designers. This optimal design method of hand hoists was offered for use by Research and Development Centre for cranes and transport systems of Bytom, Poland.

References

[1] J. Kowalski, 'Optimal synthesis of double reduction helical gear units by nonlinear programming', ASME publication, No 77-DET-171.

[2] J. Kowalski, 'Optimal synthesis of double reduction Bevel/helical gear units by nonlinear programming', ASME publication, No 77-DET-172.

[3] J. Kowalski, 'Optimal synthesis method of mechanical transmissions', Proceedings of the Fifth World Congress on Theory of Machines and Mechanisms (1979), published by ASME.

[4] J. Kowalski, 'Double reduction planetary gear unit - computer-aided design', *Strojarstvo* (in print).

[5] V.V. Pavlov, 'Matematitsheskiye modelyi protsessov mekhanosborky v avtomatizirovannykh sistemakh technologhytsheskovo proyektirovanyia', **Avtomatizatsyia technoghytsheskovo proyektirovanyia**, *Izd standartov*, Moscow (1977).

[6] J. Kowalski, 'Basis of machine construction optimal design. Part 1: Elements of creating theory of optimizational models', Seminary Materials for SEM-095/80. Universidade de São Paulo, Escola de Engenharia de São Carlos.

(Continued on page 19)

CALCULATION OF THE OIL FLOW RATE FOR PROPER OPERATION OF A SCOOP TYPE FLUID COUPLING

JHANKAR BASU*

Abstract

The rate of oil flow through a scoop type or variable speed fluid coupling is an important factor for proper operation of the coupling. An attempt has been made here to analyse the factors, viz, heat developed under high slip and oil stability in the torus. This analysis will also help for selection of the oil pump and heat exchanger for a scoop type fluid coupling.

Introduction

As a special version of constant filling fluid couplings, the scoop type fluid couplings have been developed. Fig 1 shows the general arrangements of a scoop type coupling. These couplings are favoured for achieving different output speeds of the drive. Here, a pump continuously delivers oil from the tank to the coupling, and at the same time, oil is continuously removed from the coupling through a scoop tube. Oil from the coupling is returned to the tank.

The end of the radially displaceable scoop tube decides the inside diameter of the oil levels in the torus. For different filling percentages, the capacity of the coupling varies. Fig 2 shows the curves for variation of torque against output speed for different filling percentages[1]. Depending upon the characteristic curve of the driven machine, the desired speed can be achieved by adjusting the oil filling.

For designing such a coupling, the oil flow rate is an important factor for selection of the oil pump and other allied equipment. But, no method has yet been developed for determining the required oil flow rate. An attempt has been made in this paper to analyse the factors, which affect the oil flow rate for proper operation of the couplings.

Calculation of oil flow rate

As shown in Fig 1, oil from the pump flows inside the torus and flows out through the scoop tube, fitted inside the casing. The flow of oil inside the torus and the casing can be considered to be forced vortex. For a steady condition, oil levels will maintain fixed positions. If r_1 and r_2 be the inside radii of the oil levels inside the torus and casing respectively, then pressures p_1, p_2 on both sides of the narrow passage between the torus and casing will be

$$p_1 = \frac{\omega^2 \rho}{g} (r_0^2 - r_1^2) \text{ and}$$

$$p_2 = \frac{\omega^2 \rho}{g} (r_0^2 - r_2^2)$$

where, ω = input angular speed of the coupling, r_0 = radius of angular passage, and ρ = density of oil.

*Central Mechanical Engineering Research Institute, Durgapur 9.

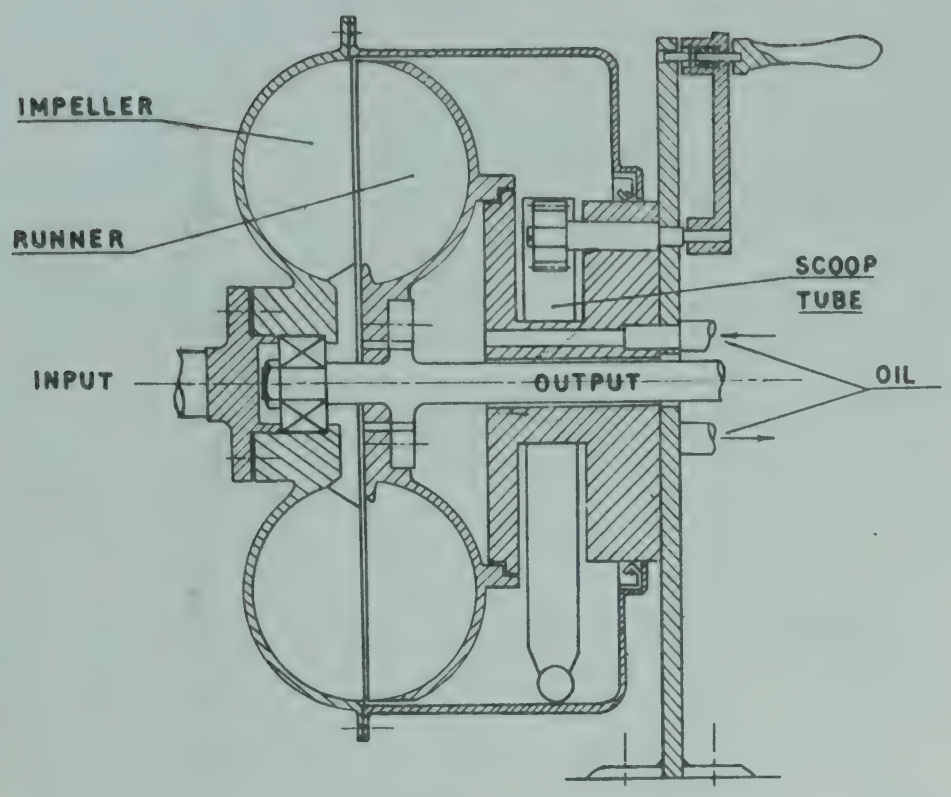


Fig 1
General arrangement of a scoop type fluid coupling

So, rate of oil flow through the narrow passage will be

$$q = \sqrt{\frac{2(p_1 - p_2)g}{\rho}} \times a$$

where a = area of the narrow passage.

Therefore,

$$q = a\sqrt{\omega^2(r_1^2 - r_2^2)}$$
$$= \omega a \sqrt{r_1^2 - r_2^2} \quad .. (1)$$

During steady operation:

inflowing oil = q = oil flow through narrow passage.

The radius r_2 is decided by the position of the scoop tube end. The capacity of the tube should be sufficient enough to allow inflowing oil to flow out.

The value of r_2 varies between the limiting positions of the scoop tube. r_1 is decided for the required range of the coupling. So, for a particular value of a, the value of q, ie, pump capacity, can be calculated. Moreover, it is seen that for particular values of r_1 and r_2, the value of q can be varied by varying the area of the narrow passage, ie, a. The value of a can be varied by providing one baffle between the torus and the casing. Holes are drilled along the outermost periphery of the baffle to achieve the required values of a. The pump capacity is thus reduced by reducing the area of the annular passage.

However, oil flow inside the coupling also helps to remove heat developed inside the coupling. From Fig 2, it is evident that slippage of coupling increases for reduction of output speed. Because of increased slippage, input power is lost and absorbed in the coupling. This increases the temperature of the coupling. To avoid excessive rise of temperature, the rate of oil flow through the coupling plays an important role. Hot oil carries the heat from the coupling to tank. The pump delivers oil to the coupling through a heat exchanger which cools down the oil.

The major part of the heat is carried away by the outflowing oil. A small part of heat is also convected to atmosphere. But, since it is very small it can be neglected.

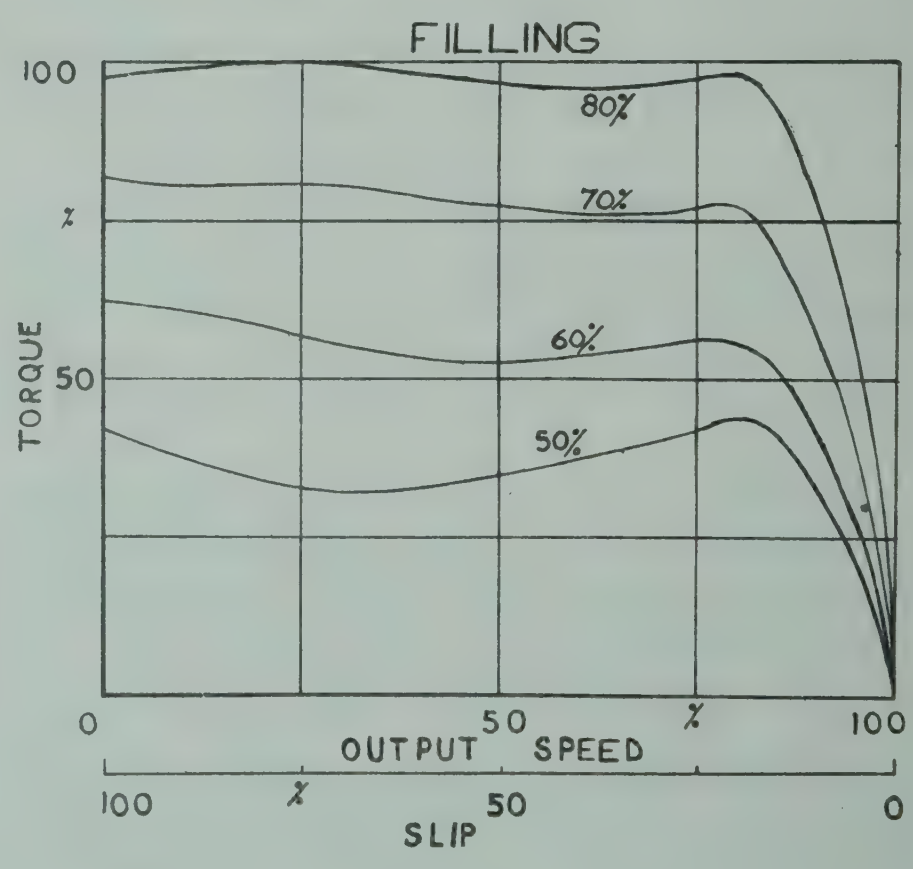


Fig 2
Influence of filling percentage on the torque slip characteristic

Heat generated in the coupling depends on the input power and slip of the coupling. Thus,

heat generated, H = loss of input power

$$= S \times K_Q n_1^3 D^5$$

where, n_1 = input speed, D = outside diameter, K_Q = a constant, depending upon coupling geometry, slip and percentage filling of oil, and S = slip.

This heat H will raise the temperature of the coupling material and enclosed oil. During steady state, the temperature of the coupling will not increase. The heat H will be carried away by the outflowing oil. If this steady temperature be T_{all} and temperature of inflowing oil be T_a, then we can write

$$H = Q \times \rho \times C \times (T_{all} - T_a)$$

where Q = rate of outflowing oil, and C = specific heat of oil.

So, we can write,

$$Q \times \rho \times C \times (T_{all} - T_a) = S \times K_Q n_1^3 D^5$$

$$\text{or } Q = \frac{S \times K_Q n_1^3 D^5}{\rho C (T_{all} - T_a)} \quad \ldots (2)$$

From the equation it is evident that for an allowable temperature T_{all} of oil, the value of Q will be maximum when slip is maximum and power input is maximum. The input power will be maximum when the coupling will run with full filling and at maximum input speed. The slip will be maximum for minimum output speed.

Thus, from eqn (2) the maximum value of Q for allowable temperature rise can be calculated for the desired output speed and maximum power capacity. For a coupling, fully filled with oil input power can be calculated from standard equations[2]. The corresponding value of area of the narrow passage a can be found out from eqn (1).

From the value of Q, the necessary pump and the cooler are selected.

Acknowledgement

The author wishes to thank the Director, CMERI, for his kind permission to publish this paper.

References

[1] R. Keller, 'The start up of hydrodynamic couplings', VDI Report No 73/1963, pp 33-41.

[2] G.S. Patki and B.S. Gill, 'The effect of number of blades on the performance of hydrodynamic couplings and dynamometers', *Mech Engg Bull*, 7(3) 80-88 (1976).

(Continued from page 16)

OPTIMIZATION OF HAND HOIST BY ANALYTIC-STRUCTURAL MODELLING

[7] A. Rachalski, 'Budowa dźwignic', **Mechanik Poradnik Techniczny**, *Warszawa: Państwowe Wydawnictwa Techniczne*, Tom IV, cz III (1957).

[8] A. Vierling, 'Hube-und Fördermittel', **Dubbels Taschenbuch für den Maschinenbau**, Springer-Verlag, Berlin/Göttingen/Heidelberg, (1963).

[9] G. Niemann, **Maschinenelemente**, Bd I u II, Springer-Verlag, Berlin/Göttingen/Heidelberg (1961).

[10] G. Niemann, H. Glaubitz, 'Zahnflankenfestigkeit geradverzahnter Stirnräder', *VDI-Zeitschrift*, Bd 93 (1951).

[11] G. Niemann, H. Glaubitz, 'Zahnfußfestigkeit geradverzahnter Stirnräder', *VDI-Zeitschrift*, Bd 92 (1950).

[12] SKF-Wälzlager in Kraftfahrzeugen, Schweinfurt (1966).

WELDING OF COPPER WITHOUT PREHEAT - A STUDY

N.D. DAS*

Abstract

The welding of copper is difficult due to its high thermal conductivity. A high heat input is therefore required to weld copper, making it necessary to preheat copper before welding. Generally copper is welded by gas welding and inert gas welding processes. But in both the processes, extensive preheating and interpass heating are necessary. An extensive investigation was carried out to weld copper by manual metal arc welding process without preheat. In this process, attempt was made to induce high arc voltage instead of high current, so that total heat input remains the same. The results of the investigation are reported in this paper.

Introduction

Copper is one of the purest metals produced commercially with purity exceeding 99.9 per cent. Copper and its alloys are widely used in different industrial applications Welding is one of the oldest fabrication techniques used to fabricate copper items.

The principal factors which influence the welding of copper are : (1) Melting point and thermal capacity, (2) Thermal conductivity, (3) Fluidity and freezing characteristics, (4) Gas porosity, (5) Reaction with oxygen, (6) Tendency to crack when hot, and (7) Metallurgical changes during welding. Among these factors, it is difficult to control factors (5) to (7).

Oxygen does not attack copper at ordinary temperature, but when heated in air to redness, copper becomes covered with a film of oxides. The red oxide (Cu_2O) predominates while the black oxide (CuO) is present as an outer layer. The oxides are readily reduced again to the metal by hydrogen and other reducing gases. Cuprous oxide is one of significance for welding, as it undergoes several changes and reactions which influence the weldability of the metal. Its melting point is 1234°C. Liquid copper dissolves cuprous oxide, but it is not soluble in the solid metal. It forms eutectic at a concentration of 3.6 per cent Cu_2O with a melting point of 1065°C.

Generally copper is deoxidised with phosphorous and silicon. Commercial type of copper normally supplied does not exhibit any strong tendency to crack when welded, but the presence of certain impurities combined with conditions of constraint may result in cracks in weld metal. Generally, copper is welded by gas and inert gas welding processes. Metal arc welding process is seldom used. Even in the welding of copper by these processes, considerable preheating is necessary because heat is rapidly dissipated from the weld region. Therefore interpass heating is also required and it should also be the same as that for preheating.

*Central Mechanical Engineering Research Institute, Durgapur 9.

Fusion of parent metal is impossible by normal manual arc welding process without preheating. It is also difficult to deposit fused metal in welding zone. Increase in current does not also help to fuse that parent metal, it may only increase the burning rate of electrode. In addition to this it is also difficult to restart welding with a new electrode in every case. Therefore, it was observed that instead of increasing the density of current, the arc voltage may be increased so that the total heat input in the welded area remains unchanged. But here the electrodes are double coated, one coating is metallurgical and the other is ionising in nature. In case of double coated electrode the arc voltage is increased and the heat input is more than the conventional electrode. Thus the detrimental effect of excessive pre- and interpass heating can also be avoided. By using double coated electrode, entire pre- and interpass heating arrangement may be eliminated.

Difficulties in manual metal arc welding

High thermal and electrical conductivity disturbs the arc stability. In near cathode and anode areas, as well as in the arc column, it is probable that the temperature is comparatively low so that the electron emission is made more difficult. This effect is particularly more effective with increase of plate thickness.

Feasibility of copper welding without preheating by manual arc welding process

Let us now examine the heat input necessary to burn the copper electrodes.

Heat input $Q = .24\ I.V.$

where, Q = heat input in calorie, I = current in amps, and V = voltage.

So, it appears that heat input is directly proportional to the product of current and voltage. Alternatively, either by increasing current or increasing the voltage, heat input may be increased.

From calculation it is observed that to melt 1 cm^3 of copper 880 cal of heat is necessary. Copper has very high thermal conductivity, about seven times higher than that of steel at room temperature. The thermal conductivity also increases with rise of temperature. Therefore, it is very difficult to change so much current necessary for welding copper without preheat.

Now, let us consider the increase of voltage. If the arc voltage is increased, ie, twice the conventional voltage, then heat input automatically becomes double without increasing the current. Alternatively, for same heat input the current could be nearly halved, and therefore, the electrode burn off rate would also be reduced. So, in case of copper welding by increasing the arc voltage, the electrode can be charged at a lower current.

Now every arc as in all normal conductors of electricity, offers an impedence to the flow of current dependent upon the discharge parameters accountable through the carrier density in the axial and radial directions. The welding arc is distinguished from other electrical discharges by the particle density of carriers of the flowing current as shown in Fig 1.

The arc consists of three connecting parts, the cathode region, the plasma column, and the anode region. The electrical power dissipated in each space or region is the product of the current flowing and potential across the region, ie,

$$E_{Total} = I.R = I(R_1 + R_2 + R_3)$$

The arc regions are optionally referred as the cathode fall space and anode fall space.

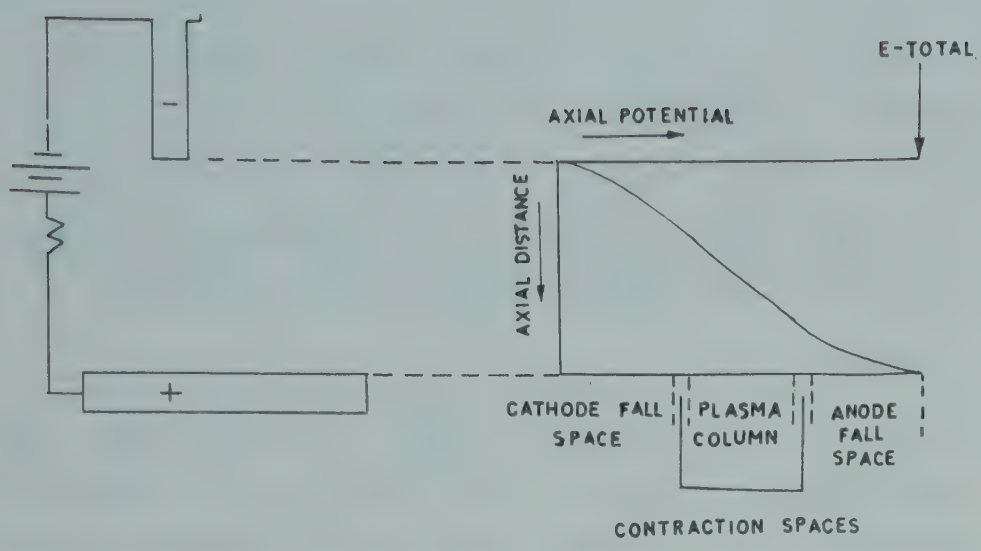


Fig 1
Distribution of arc potential

To maintain the arc discharge, emission of ions is necessary. When ions are emitted from the anode surface, the current flow as well as heat flow at anode are influenced. Current carried by plasma is composed of equal number of electrons and ions. The electrons which support most of current conduction flow out of negative terminal and move towards a positive terminal. The establishment of neutral plasma state by thermal means, ie, by collision process requires the attainment of equilibrium temperatures according to ionisation potential of the material from which the plasma is produced.

To ensure stable arc, additives in the form of coatings are provided in the case of consumable electrodes. Their presence in the form of oxide film or composite metal layers on the electrode provides high density electron emission.

For emission of ions from anode, a material must be present having greater ability to emit ions than the matrix material. Compounds and elements having high vapour pressure and low ionisation potential, present in the matrix of the material of lower vapour pressure and higher ionisation potential usually will emit ions from the anode. Positive ions formers are from alkali and alkaline earth elements.

Characteristics of the electrode

The type of electrode used for increasing the arc voltage has a double layer coating instead of single layer coating as in conventional type of electrode. The core wire is of deoxidised copper. First type of coating is metallurgical and gaseous type and the second one is ionising type. The first coating applied to the wire is a slag producing mixture which also produces gas to form a protective envelope around the weld as shown in the Fig 2. The first coating is extruded and it contains mainly slag and gas formers. The second coating is a mixture of high melting point materials forming a sheath. This sheath allows a long arc to be held giving a working voltage of 50-60 volts instead of 25-30 volts as in conventional welding.

Experimental procedure

Two sets of experimentations were conducted. In one set, welding was performed with conventional electrodes applying pre- heating and interpass heating. In another set, attempt was made to weld copper with the help of double coated electrode without pre- and interpass heating. Thickness of the plate in both cases was 10 mm. Investigation was restricted to plate of

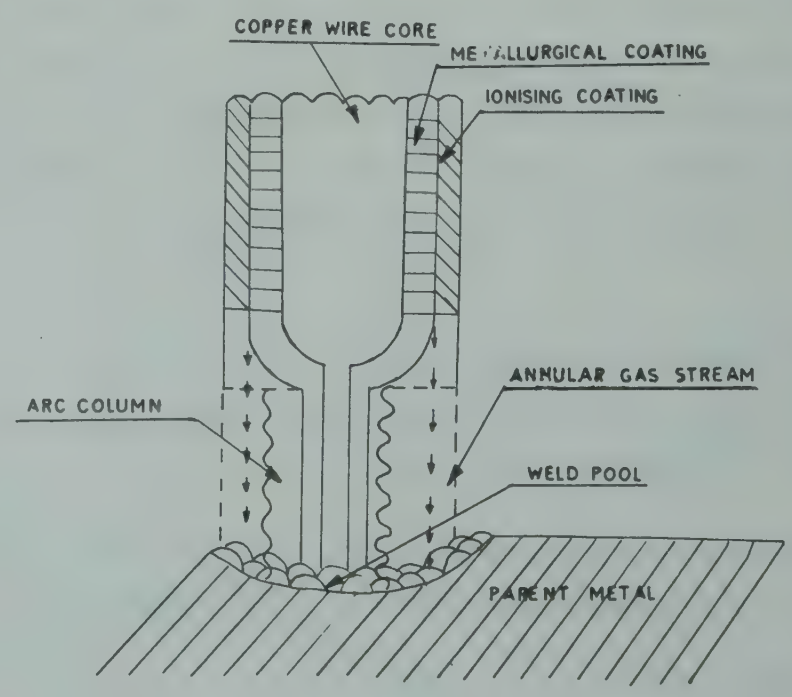


Fig 2
Coating of double coated electrode

thickness of 10 mm and plate with thickness of above 10 mm with larger heat sinks were not tried out. Direct current reverse polarity was also used in both cases. In all cases, the edges were cleaned mechanically and with 10 per cent sulphuric acid followed by washing and drying. Recommended joint design, groove angle and gaps were provided at the joint.

In case of the first set of specimens, preheating to about 600-650°C and interpass heating were provided. No pre- and interpass heating was given to a second set of the joint.

While welding the first set of specimens with conventional electrodes, after depositing each layer of bead, interpass heating was given so that temperature of the welded area reaches upto 600°C. Parent metal was covered with asbestos sheet to minimise the rapid cooling effect due to high thermal conductivity of the material.

While welding it was observed that slag removal is very difficult as the slag is sticky in nature. Pneumatic chiesel was used to remove the slag. Sometimes about half the thickness of bead had to be removed to get rid of the slag. The same procedure was followed in each case of burning electrode.

It is also important to adopt a well defined procedure when restarting a pass after changing the electrode owing to the high conductivity of the metal. The welding was resumed about ½" back from the weld pool so that when this point is reached the second time, the material will be sufficiently hot to allow full penetration to be obtained. Hot peening was performed after depositing each layer of metal.

In case of welding of copper by double coated electrode, recommended single V-joint design was provided. Electrodes were baked at 300 to 350°C for 2 hours. Electrodes were kept in the drying oven at about 300°C and taken out one by one fr the oven for direct use. The perfect dried electrodes melt at a uniform rate a provide high arc voltage thereby increasi the arc energy.

The electrode was moved along the joi in a straight line with slight weaving m tion keeping the electrode perpendicul to the surface of the plate as shown in t Fig 3. The arc was directed to parent ma terial to improve the melting of it. He no interpass heating and peening were pr vided. It was observed that slag remova was easier in comparison to the weldi done by conventional method.

Physical, metallurgical and mechanica tests were conducted to evaluate both type of joints.

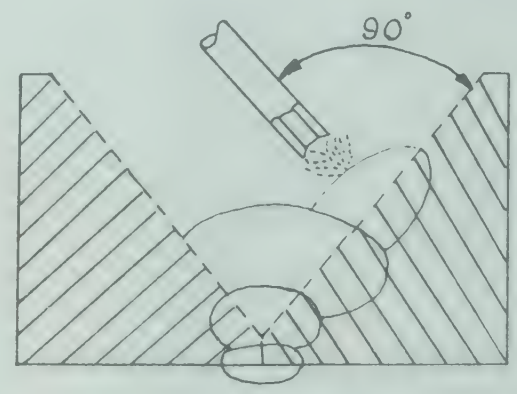


Fig 3
Movement of electrode on plate surface

Physical and mechanical tests

The joints were subjected to 180° ben tests. Fig 4 shows the results of ben test of conventional welding. It appears that the joint does not withstand 180° ben test. It may also be seen that proper fu sion from bead to bead does not take place Further, slag and other voids are presen at the joint (Fig 5). Fig 6 shows th radiograph of the sample welded by doubl coated electrode. It is evident that th joint is free from any porosities and othe voids and cracks. The joint was subjecte to bend tests. Although it does not with stand 180° bend test, it is clear tha

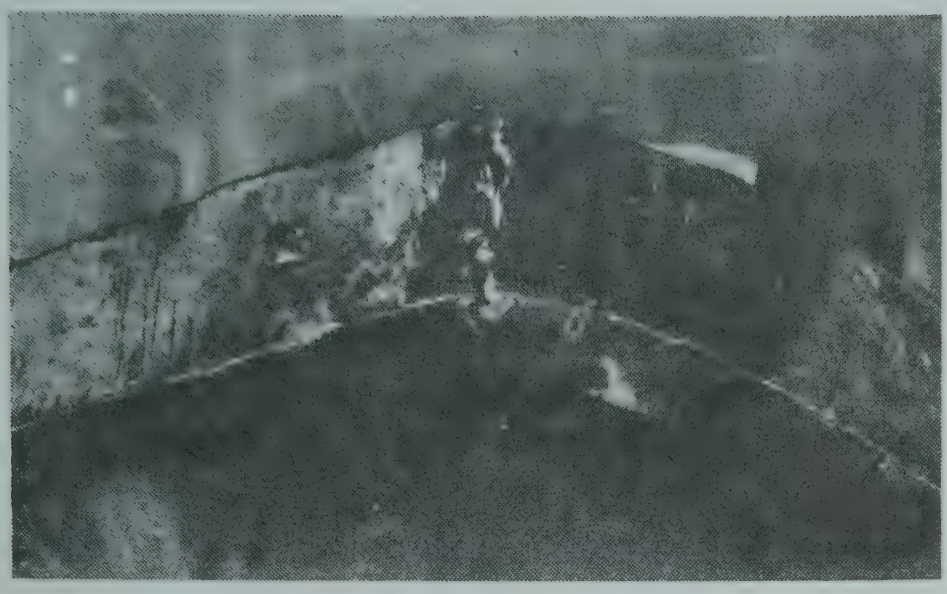


Fig 4
Specimen, welded with conventional electrode after bend test

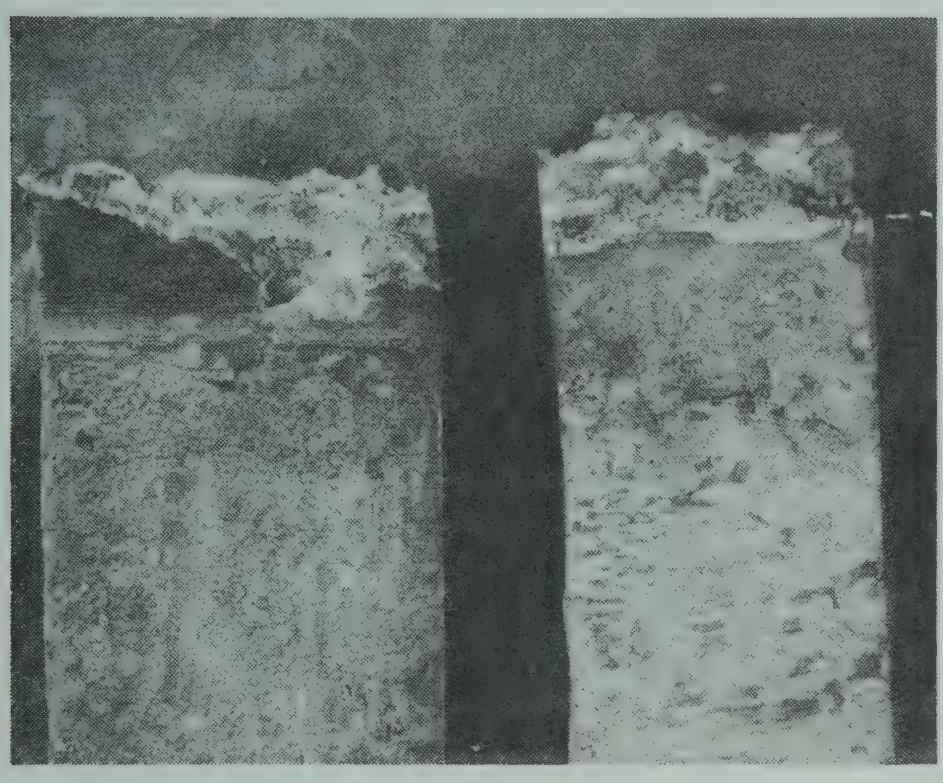


Fig 5
Specimen broken during bend test

proper fusion took place at the joint. Microhardness test was also conducted at the periphery. It appears from Fig 7 that the hardness of weld metal does not change appreciably.

Metallurgical investigation

Fig 8 shows the microstructure of the parent metal. From the microphotograph it appears that metal is free from oxide particles. Fig 9 is the microphotograph of the weld metal joined by conventional electrodes. It can be observed that porosities and inclusions are in the boundary line.

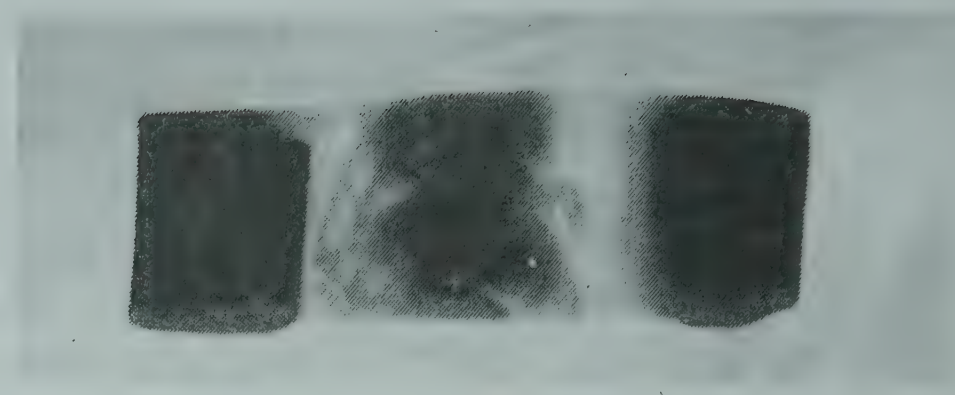


Fig 6
Radiograph of cross-sectional area of joint, welded with double coated electrode



Fig 7
Microphotograph of the micro-hardness survey area of the joint, welded with double coated electrode. It may be estimated from the indentation mark that there is no appreciable change in hardness of weld metal



Magnification 300 x Etchant $FeCl_3$

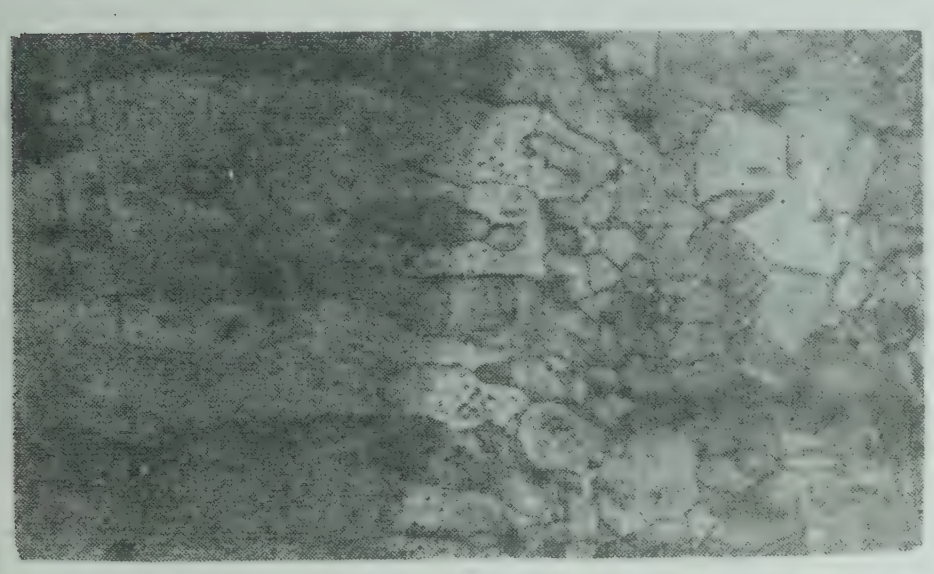
Fig 8
Microphotograph of the base material

This is probably due to oxygen absorption by weld metal during welding and due to non-removal of slag which is very sticky in nature. Fig 10 is the microphotograph



Magnification 120 x Etchant $FeCl_3$

Fig 9
Microphotograph of the joint, welded with conventional electrode



Magnification 120 x Etchant $FeCl_3$

Fig 10
Microphotograph of the joint area welded with double coated electrode without pre- and interpass heating

of the joint welded by double coated electrodes. It appears that the joint is free from voids and slag.

Discussion

From the experiments it appears that copper welding without preheating is possible by using the electrodes which can provide higher arc voltage. Adopting this process, formation of unfavourable Cu_2O - Cu eutectic precipitation at grain boundaries, hydrogen embrittlement and thermal distortion may be avoided.

It is also observed that slag removal is easier in case of double coated electrode welding than the conventional welding. Gas absorption such as diffusible hydrogen and oxygen are less in double coated electrode welding.

Conclusion

(i) Double coated electrode has more arc energy and deep penetration capacity.

(ii) By eliminating the preheating the unfavourable formation of Cu_2O-Cu eutectic at grain boundaries may be avoided.

(iii) This method can be applied to fabricate vessels and other structures of copper (thickness up to 10 mm) where preheating is not possible.

(iv) By adopting this method, use of argon may be eliminated in case of structural welding of copper.

Acknowledgement

The author likes to thank the Director, CMERI, Durgapur, for his kind permission to publish this paper.

General references

[1] E.G. West, **The welding of non-ferrous metals**, Chapman & Hall Ltd, London (1951) p 309.

[2] J. Wegrzyn, 'Welding of copper with deep penetration electrode', *British Welding Journal*, May 1967, p 283.

[3] **Welding Handbook**, American Welding Society, Vol 1, p 526

[4] Lessel, **The seathed electrode for welding of copper**, VDI, Berlin,

[5] 'Joining of copper', *AMAX Copper News*, Vol 1((1970) p 1.

EROSION, CORROSION AND FOULING OF TUBES IN FLUIDIZED BED BOILERS

PRABIR BASU AND M. DEBNATH

Abstract

Study of tube conditions in fluidized beds is important for the development of fluidized bed boilers. The authors review the earlier work on erosion, corrosion and fouling of tubes, and report their observations on tube erosion using Indian coal in a typical fluidized bed.

Introduction

In a fluidized bed boiler, the reheater and superheater tubes are located directly in the combustion zone. These remain in intimate contact with mobile ash particles to a much greater extent than in a PF boiler. Successful development of this type of boiler will largely depend on the capability of these immersed tubes to withstand the erosion, corrosion and fouling they are subject to. Much has been published on tube conditions in conventional boilers, but it is unlikely that these results can be directly applied to fluidized bed boilers, where combustion conditions are different from those in conventional boilers. Limited information is available on tube conditions in fluidized beds. The present communication attempts to review the existing results and present some data on erosion of tubes in fluidized bed of Indian coal-ash, which is much richer in the abrasive agent, silica (especially α-quartz) than the ash from UK or USA coal.

*Central Mechanical Engineering Research Institute, Durgapur 9.

Review of earlier work

Erosion, corrosion and fouling are three major causes of tube failure in boilers.

Erosion

Erosion is caused by direct impact of solids on the tube metals.

Lowy[1] presented a comprehensive review of erosion. He noted that the erosion is a function of the following:

(i) Size, shape, hardness and mass of impinging particles,

(ii) Incident angle and approaching speed of the particles,

(iii) Probability of inertial impaction, which brings in the additional factors such as velocity of the stream, particle terminal settling velocity, and geometry of the target surface.

All materials are not equally susceptible to erosion. Particles, striking perpendicularly on to a brittle surface, initiate and propagate cracks, and thereby allow relatively large fragments to disengage from the surface. In case of ductile materials, particles, glancing at low incident angles gouge out fragments much smaller than themselves.

Dependence of erosion rate on temperature may still be considered conflicting as both negative and positive temperature coefficients have been reported[2]. Although it is more reasonable to expect erosion

rate to be proportional to the second power of velocity, ie, the kinetic energy of incident particles, exponents of velocity above 2 have been reported by many workers. The opinions regarding the upper size of particles for tolerable erosion also vary, but in general it is believed to be in the region 5μ to 10μ. British Coal Utilisation Research Association[2] carried out experiments in a 0.6 m square bed of coal-ash. The bed particles were sized between 1.6 mm to 0.2 mm and it was fluidized with cold air at 0.9 m/s. The bed-ash contained about 12 per cent quartz by weight. The static bed depth was 450 mm - 550 mm. It expanded to 600 mm - 900 mm when fluidized. A bubble cap distributor with percentage opening 1.4 per cent was used.

Here, 48 specimen rings were clamped together on 3 rows of 25.4 mm OD tubes. The materials tested included mild steel and alloys like Bed Fox 36, Silver Fox 316 and Nimonic PE16.

The specimens were measured for weight and surface profile both before and after the experiment. After a total run of 100 hours, the specimens were examined under a microscope. It showed that much of the surface was 'peppered' with ash particles which adhered to the metal so strongly that even ultrasonic agitation in acetone could not remove them[2]. Profilometry measurements revealed increase in radial dimension between 0 to 1.9 micron. This increase was greater on the upper face but no sign of erosion was present. The weight gain of the specimen decreased from .0065 gm at the bottom to .0011 gm at the top of the tubes[2]. Although it was a carefully executed experiment, such increase in weight was not observed by any other subsequent worker.

Corrosion

Corrosion is largely attributed to the deposited alkali salts. Interaction of the deposite with the sulphur trioxide of the flue gas with the protective oxide of tubes forms a liquid phase containing pyrosulphates and/or complex sulphates. These accelerate the oxidation of superheater alloys[3]. Since the vapour pressure of alkali metal sulphates and chlorides are very low at 750-900°C, there will be less volatilisation of alkali salts and consequently less corrosion.

Early experiments on corrosion of tubes in fluidized beds were carried out at the Marchwood Engineering Laboratory of CEGB, UK. A 25.4 mm OD stainless steel corrosion probe was immersed into a 230 mm dia coal-fired fluidized bed. The bed was fired on Thoresby coal (0.85% Cl, 1.06% S) and Babington char (0.33% Cl, 0.6% S). The probe was examined after 72 hours run and no bonded deposit was found on any part of the probe surface when the bed temperature was upto 700°C. Further experiments were carried out with Ollerton coal (0.3% Cl, 1.33% S) and Pye Hill coal (0.42% Cl, 2.71% S). The observation for about 100 hours run can be summarised by stating that high chlorine coal is unlikely to cause serious corrosion provided the metal temperature is kept above the dew point of NaCl, ie, 575°C[1]. This dew point is to some extent dependent on the chlorine content of coal and bed temperature. Initial corrosion rate of type 316 stainless steel at temperature 550°C was 8.5×10^{-3} inch (216μ/1000 hrs) when fired by Thoresby coal at 700°C. This compares favourably with 7×10^{-3} inch (178μ/1000 hrs) corrosion rate under a comparable test condition in a PF rig. All evidences suggest that at metal temperature upto at least 600°C the tubes in a fluid bed boiler are not likely to suffer from surface carburization. With low chlorine coal, Ollerton, no serious corrosion was evident.

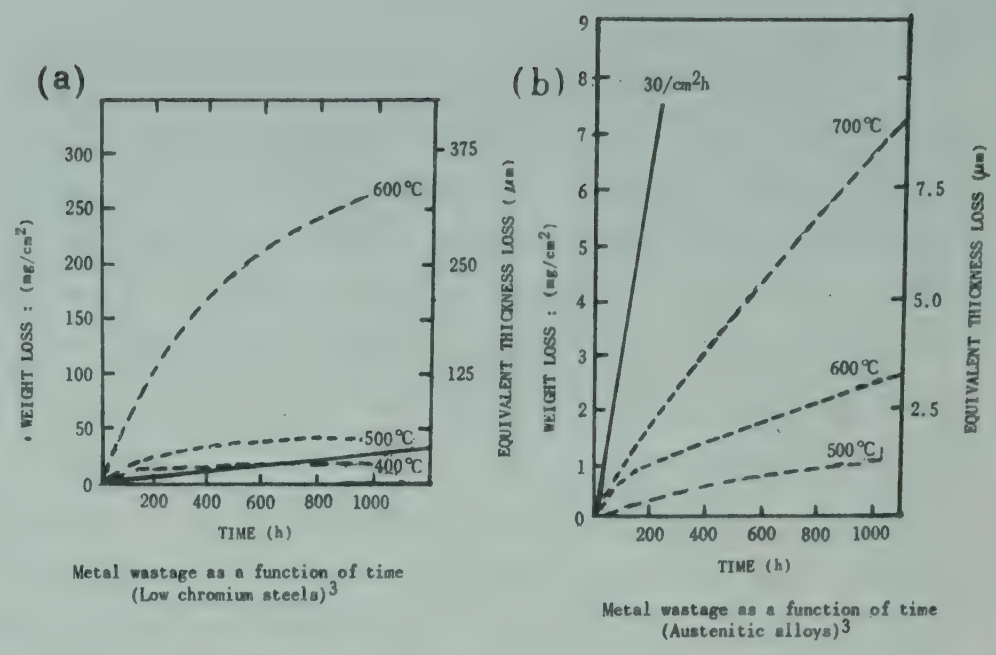
Cooke and Rogers[3] reported results of further long duration experiments. Their experiment covered these types of coal

ke Welbeck (1.3% S, 0.65% Cl), Newstead .7% S, 0.26% Cl) and Humphory No 7 (2.8% 0.1% Cl) which were burnt in three test gs. The fluidization velocity varied om 0.6 m/s to 2.4 m/s, while bed tempera- re was in the range of 800-850°C. The st specimens included the following loys:

(i) Medium carbon steel,
(ii) 1% Cr, 0.5% Mo steel,
(iii) 2.25% Cr, 1% Mo steel,
(iv) 12% Cr steel,
(v) Stainless steel type 316,
(vi) Stainless steel type 347,
(vii) Esshete 1250,
(viii) Nimonic PE16.

he tests were of 100 to 1000 hours dura- ion and metal temperature varied in the ange of 400-650°C.

The results suggest that satisfactory ube life can be obtained under normal bed perating conditions. Very little depo- ition was observed on tubes. Neither me- al loss nor intergrannular penetration as markedly affected by the nature of oal, pressure, fluidization velocity or ombustion condition. The observed higher orrosion rate with high chlorine coal ould have been aided by loss of fluidi- ation etc. Extensive sulphide penetra- ion was observed in presence of limestone nd dolomite in bed. Fig 1 illustrates etal wastage as a function of time. This hows that at low metal temperature, ini- ial corrosion rate is higher. Electric ower Research Institute, USA, sponsored a 000 hour corrosion test[4]. It was conduc- ed at CRE of National Coal Board, UK. his test revealed that stainless steels ype 304, 329, 347 are less prone to cor- osion attack in fluidized bed, but alloys uch as Inconel 671, 617, Incoloy 800, aynes 188 undergo sulphidation/oxidation, orrosion. Conditions which favour this orrosion are presence of calcium sulphate



Metal wastage as a function of time (Low chromium steels)[3]

Metal wastage as a function of time (Austenitic alloys)[3]

(a) Metal wastage as a function of time (low chromium steels)3, (b) Metal wastage as a function of time (Austenitic alloys)[3]

as deposit, low oxygen activity near metal surface, and metal temperature above 650°C[4].

Smirthwaits[5] carried out some tests with a number of stainless steel (18% Cr, 8% Ni) tubes. These tests were carried out in a coal fired (800°C) fluidized bed of sand. These air cooled tubes were examined under microscope after some hours of run, and was found that very little carbide has been formed. It was, however, concluded that the carbon inherent in the steel, and possibly a little from the atmosphere, precipitated as titanium or molybdenum carbide. Impact tests showed average increase in strength by 10-30%. Longer tests of 24 hours, however, showed less increase in strength probably because the peak of strength/precipitate size curve has been passed.

Fouling

Fouling is caused by the deposition of alkali salts which had been devolatilised during combustion. It is expected that the fouling in a fluidized bed boiler will be much less severe than that in a conventional boiler because (i) the maximum temperature of a fluidized bed boiler is 750° C - 900°C as against 1400° - 1700°C in a PF boiler and the vapour pressure of fouling agents, alkali, sulphates and chlorides

are very low at 750° - 900°C, and (ii) the vigorous motion of ash particles in fluidized beds helps in scrubbing off loose deposits from the tube surface.

Present investigation

Indian coal-ash by virtue of high ash fusion temperature[6] (Table I) makes an ideal material for fluidized beds; because the chance of bed agglomeration due to ash fusion is greatly reduced. But its richness in quartz increase the probability of tube erosion. So far, no data on erosion rate in fluidized bed fired on Indian coal is available. Furthermore, a need for checking the scanty data on British coal was also felt. Therefore, it was decided to measure the erosion and corrosion of tubes in a typical fluidized bed under hot and cold conditions.

Cold test

The experiments were performed in a fluidized bed combustor having a cross-section 450 mm x 450 mm. The distributor is straight hole orifice type. In the present experiment a bed of coal-ash is fluidized by cold air.

The test specimen was prepared from a 17.29 mm dia and 125 mm long carbon steel rod (composition C 0.63%, Si 0.24%, Mn 0.61%, S 0.025% and P 0.06%). It was ground to a fine surface finish. The sample was marked at one edge so as to designate the radial position of the surface profile. The specimen was placed under a Tallyrond machine and its profile was recorded on a profile recorder sheet. The specimen was then weighed in an accurate balance.

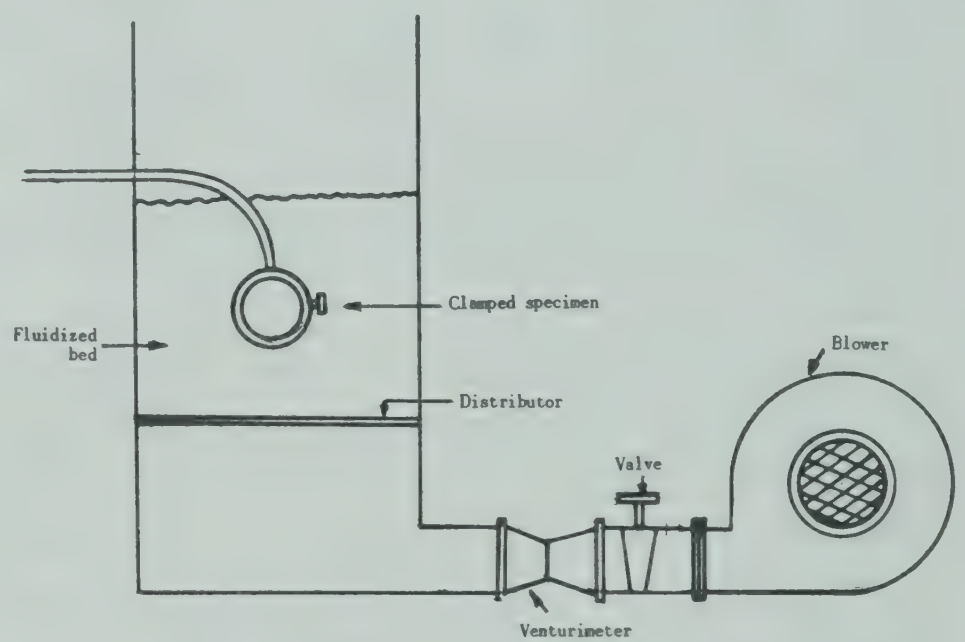


Fig 2
Schematic diagram of the test rig

It was clamped on two edges as shown in Fig 2. The assembly was immersed in the fluidized bed. The fluidizing velocity was kept constant at 50 cm/sec. The experiment was carried over a period of 16 days. During this period the bed was run for 110 hours in total. The specimen was not disturbed during this long run. After that the specimen was removed from the bed, cleaned and then examined under microscope for any change in surface structure. Surface of the specimen was again examined by the Tallyrond machine. It was then weighed in a precision balance.

Observation

Analyses of the bed material before and

TABLE I

Characteristic of ash from coal of different countries

Composition	India[6]	UK[7]	USA[8]	German[7]
	Percentage by weight			
SiO_2	62 - 68	25 - 50	20 - 60	25 - 46
Al_2O_3	18 - 27	20 - 40	10 - 35	15 - 21
Fe_2O_3	4.5- 12	0 - 30	5 - 35	0 - 45
CaO	0.3-2.5	1 - 10	1 - 20	2 - 4
MgO	0.1-1.5	0.5- 5	0.3- 4	0.5- 1
TiO_2	1.5-1.6	0 - 3	0.5-2.5	-
Na_2O & K_2O	0.1-1.1	1 - 6	1 - 4	-
SO_3	0.1-1.54	1 - 12	0.1-1.2	4 - 10
Ash fusion ID (°C)	1240°C--1480°C (melting)	1050°C--1350°C (melting)	1026°C--1537°C (melting)	

after 110 hours of cold run are given in Table II.

TABLE II

Size distribution of the bed material (coal ash) before and after the cold run

Size range (mm)	Per cent	
	Before	After 110 hours
2.8 - 2.0	0.66	0.3
2.0 - 1.4	3.1	1.33
1.4 - 1.0	25.0	10.0
1.0 - 0.6	11.7	19.0
0.6 - 0.3	46.8	42.0
0.3 - 0	12.6	27.3

Initial weight of the sample was 196.0249 gms and it reduced to 196.0227 gms after 110 hours of run. A total loss of 0.0022 gm has been detected due to erosion. It is equivalent to erosion rate of 0.294 $\mu g/cm^2/hr$. This result is in sharp contrast with that of BCURA[2] who observed a weight gain of 4 $\mu g/cm^2/hr$ (estimated). However, the present erosion rate is far below the maximum tolerable penetration rate on the fire side of tubes in conventional boiler, which is about 30 $\mu g/cm^2/hr$ [7].

The surface profile of the tube before and after run is reproduced in Fig 3. It indicates that erosion has made surface more smooth than before. Ovality of the specimen was 3μ at the middle before run. It has decreased to 1.5μ after 110 hours of run.

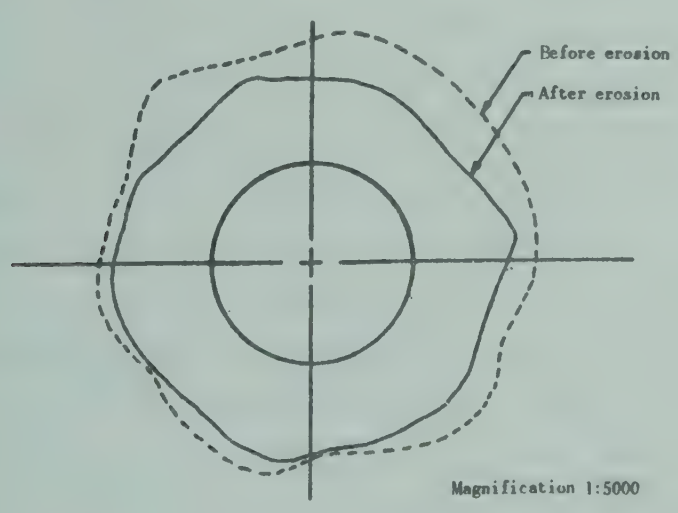


Fig 3
Surface profile of the tube before and after run

Metallurgical examination of the surface did not reveal any change, in the surface structure.

Hot test

In the hot test, a carbon steel tube of 19 mm OD was placed in a coal-fired fluidized bed. The bed, made of coal-ash of 1.3 mm mean size, was fluidized at 1 m/sec at 800°C. Water was passed through the tube. Outer surface temperature of the tube was around 125°C. The tube was removed from the bed after about 20 hours of run and examined carefully. The deposits formed on the tube (Fig 4) was found to vary circumferentially. It was thicker on the top than at the bottom, maximum thickness being 0.5 mm. Analysis of the deposit is given in Table III. No sign of erosion was apparent on the tube.

TABLE III

Analysis of deposit on boilder tube after hot run

Combustibles	43.2%
Ash	56.8%
Composition of the ash	
SiO_2	44.39%
Fe_2O_3	15.44%
Al_2O_3	38.65%
MgO	0.51%
Ni	Trace
Cu	Trace
Soluble Alkali	1:00%
Chloride	0.01%

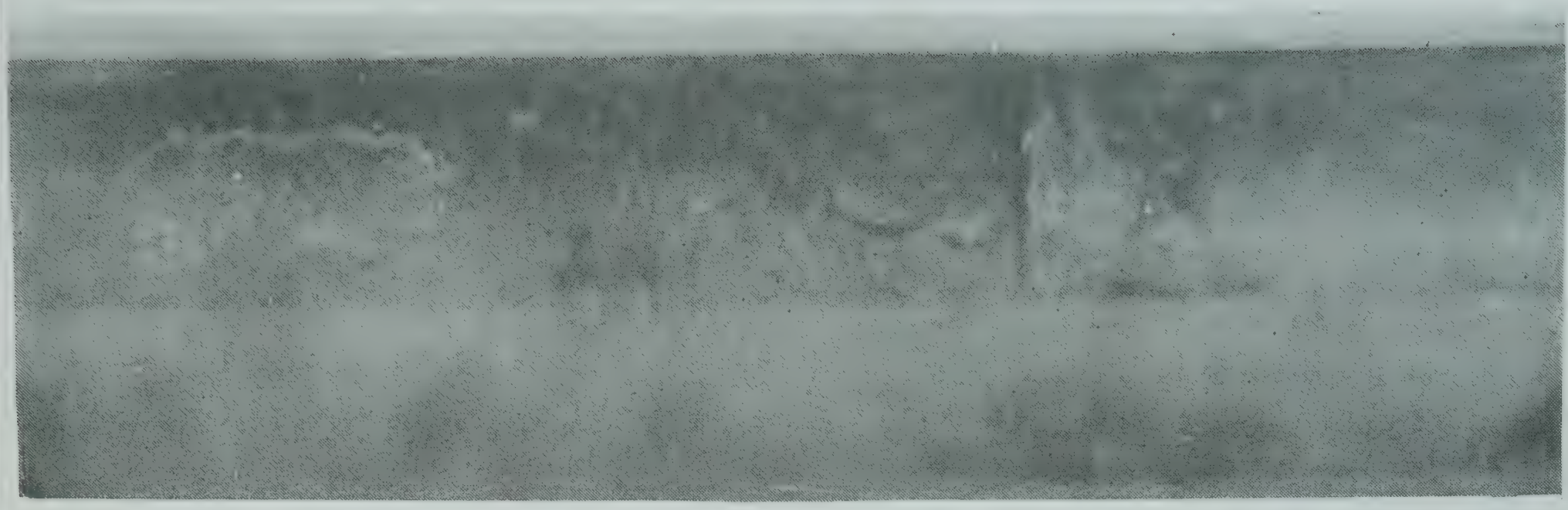


Fig 4
Photograph of tube after hot run in fluidized bed boiler

Conclusion

1. A literature survey indicated that the boiler tubes are less likely to be attacked by erosion and corrosion in fluidized bed boilers. Fire side corrosion will be less, especially in case of Indian coal which is poor in sulphur.

2. Erosion of tubes in fluidized bed is found to be 0.29 $\mu g/cm^2/hr$ in a cold fluidized bed made of ash from typical Indian coal and fluidized at 0.5 m/sec.

3. Some deposits were observed on a tube (metal temperature 150°C) which was located in a coal fired fluidized bed.

Acknowledgement

The authors thank Shri S.S. Nandi of CMERI for his valuable assistance in carrying out the experiments. Kind permission of the Director, CMERI, to publish this paper is also thankfully acknowledged.

References

[1] D. Lowy, Survey of the potential problems of erosion, deposition and corrosion in gas turbines driven by the exhaust from super charged fluidized bed boilers, BCURA Document No FCP 2 Pt 1 (April 1968).

[2] D. Lowy, E.S. Dingoor, Preliminary experiment on erosion of immersed boiler tubes in a fluidized bed, BCURA Document No FCP 3 (April 1969).

[3] M.J. Cooke and E.A. Rogers, 'Investigation of fireside corrosion in fluidized combustion systems', **Fluidized Combustion**, Institute of Fuel Symp, Ser 1 pp B-6 (1976).

[4] J. Stringer, R.D. La Nauze and E.A. Rogers, 'High temperature corrosion of metals and alloys in fluidized bed combustion systems', 5th International Fluidized Bed Combustion Conf, Washington (1977).

[5] Smirthwaits, 'Tube conditions in a coal fired fluidized bed', Undergraduate project report, Deptt of Metallurgy, University of Aston in Birmingham (1975).

[6] Y.P. Abbi et al, 'Development of fluidized combustion boilers for Indian coals', 69th Annual AICHE Meeting, Chicago (1976).

[7] R. Dolizal, **Large boiler furnaces**, Elsevere Publishing, p 80 (1967).

[8] R.H. Perry, **Chemical Engineering Handbook**, McGraw-Hill, 5th Edition, pp 9-15 (1973).

STATE LEVEL R&D COMMITTEE : INHERENT CONSTRAINTS DEFEAT BASIC OBJECTIVES*

After so many years of their functioning, there are certain ambiguities still in existence, in regard to some of the vital points which may be classed as inherent constraints, experienced or being experienced by many of the State Level R&D Committees all over the country. The main purpose of such Committees was to (i) develop an awareness in regard to R&D needs in a small industry; (ii) bring the problems, so encountered by small industries, to the attention of appropriate R&D institutions, national laboratories or research institutions; and (iii) to assist the industry concerned to come directly in contact with R&D institutions on mutually agreed terms - pertinent to the requisites of technology transfer.

Thus, the R&D Committee is just not an intermediary, as is the case with a Polytechnology Transfer Centre (PTC), but it has an important role in promotion of industrial growth as well as research and developmental activities. R&D being an expensive process, the industries normally shy away from such activity due to heavy financial burden. There are two distinct ways of looking at it.

1. Where the result of R&D is likely to be used by a single user industry and the cost is not prohibitive: In such case, industry - small or medium, does not lag behind in financing or sponsoring the project for its exclusive use.

2. Where the results (either in the form of new technology or improved technology) of such R&D exercises are likely to be used by industries in general and not necessarily a particular one: In such case, the small entrepreneurs would like the external funding without taxing their meagre financial resources.

Expertise and manpower for R&D are totally absent in such industry, R&D being a non-profitable and non-practicable proposition to it. Hence, National research agencies, academic and institutional organisations have to come forward to provide the technological base and cater to their R&D needs. But the difficulty of funding, particularly in regard to cases (2) above, has necessarily to be overcome. Though the national laboratories charge a fee with suitable concession for the R&D work of small scale industries, even then the share of cost of such developmental activities may fall beyond the means of the small and medium entrepreneurs.

Department of Science & Technology (DST) has a certain fund towards the provision in such cases. So has every State Government, in a limited scale. Problems referred by small industrial units are always scrutinised by experts listed in the panel prepared by SISI and the R&D Committee, before being forwarded to the DST or Small Industries Directorate of the State Government with a suitable recommendation for funding.

*Based on the key-note address delivered by Dr S.K. Basu, Director, CMERI, and Chairman, State Level R&D Committee for Small and Medium Industries, West Bengal, at the All India Get-together of Chairmen and Convenors of State Level R&D Committees held at the premises of Bengal National Chamber of Commerce and Industry, Calcutta on 7th February 1981.

But the experience of the State Level R&D Committee of West Bengal is very bitter and discouraging. In most of the cases, the Committee does not get a sympathetic consideration from either DST or State Government. Naturally, one feels inclined to question, under such situation, the very purpose and objective of R&D Committee. R&D Committee has no special fund at its disposal. DST sanctions rupees five thousand as the running expenses for holding meetings of the Committee, which itself is ridiculously low, compared with the number of Sub-Committees and their occasional meetings apart from normal meetings of the parent Committee. It has also to cater for dissemination of information, to communicate with industries and offer ad-hoc assistance of technical nature from time to time.

If R&D Committee is to function just as an intermediary unit or only as a referral one in character, then under the present circumstances, when PTCs are functioning in every State, its usefulness assumes an insignificant proportion. Should the Committee not wind it up, in such a case?

R&D Committee, even after so many years of functioning still remains an ad-hoc Committee without any secretariat facilities of its own.

Though in the State of West Bengal, R&D Committee, during the last 4-5 years, has helped some small scale industries successfully in developing new products and in solving technological problems, there are a large number of cases where problems could not be undertaken by R&D agencies due to paucity of adequate fund.

Recently, one of the constituent member organisations with the help of other experts, could compile a survey of the R&D needs of the small scale industries in Howrah region. But such surveys are needed for various disciplines wherein large number of small scale industries are facing a dire challenge in regard to their very survival. Who is to fund such a project? Is it not the need which could be identified as part and parcel to the specific needs of the State Government in their economic venture for national growth? But what happens, in such cases, is really disappointing and discouraging. It is the correct appreciation as well as sympathetic attitude that is needed to prevent the decelerating growth of small scale industries, noticed in some parts of the country, and encourage the budding entrepreneurs in their initial effort to establish industries.

The functions of the R&D Committees need to be communicated through various mass media. This is to encourage small industrialists to come forward with their challenging problems and to disseminate the knowledge and information available already. But who is to fund this activity? With State Government on one side and the Department of Science & Technology on the other, the R&D Committee really draws a blank and starve pitiably.

The experience of different State Committees may be different. But so far as West Bengal Committee is concerned, even the meetings are seldom attended by the representatives of the State Government, though the Committee deals with R&D problems (identification, referring to agencies for solution, and their follow-up) of the small scale industries of the State.

These are some of the findings of the State Committee and feelings of its Members. They should be looked into in a proper perspective, since the Committee's interest is to project its bright image and not a blurred and utterly confused picture, where it moves sluggish and in a directionless manner. Follow-up actions, realistic and application-oriented towards the country's vital needs, may be formulated and implemented on an urgent basis.

News and Views

Single spindle automatic turret lathe developed

The single spindle automatic turret lathe (42 mm capacity) developed by MERADO, Ludhiana, is the first indigenous design. Messers Accurate Engineering Works, Ludhiana have taken up its commercial manufacture and will soon be marketing this machine at half the cost of the currently available models based on the imported know-how. The firm has already received firm orders for supply of such machines from the user industry.

The MERADO designed machine has provision for six or eight station turret. It has five transverse slides including a compound slide at the rear and a separate swing type bar stop. The machine can be equipped with eleven different tools out of which six tools can operate simultaneously to perform any of the desired combination of operation, ie, turning, drilling, boring, reaming, tapping and threading, facing, parting and grooving. The provisions exist for adjusting angular position of the same in steps of 2°, and the 'camrise to tool traverse' ratio in a stepless manner which enable the machine to perform machining operation of a variety of turned parts with one set of cam. An auxiliary cam shaft has been provided with single revolution clutches which accelerates idle motion, viz, opening-closing, turret indexing, etc. This increases the overall production of the machine.

The designed machine provides 4 spindle speeds in one cycle with choice from 38 forward speeds and 190 reverse speeds and a wide range of feeds for various applications. The rationalised distribution of operations, and the convenience with which these can be selected, make the machine a versatile and efficient production tool.

CMERI observes Open Day

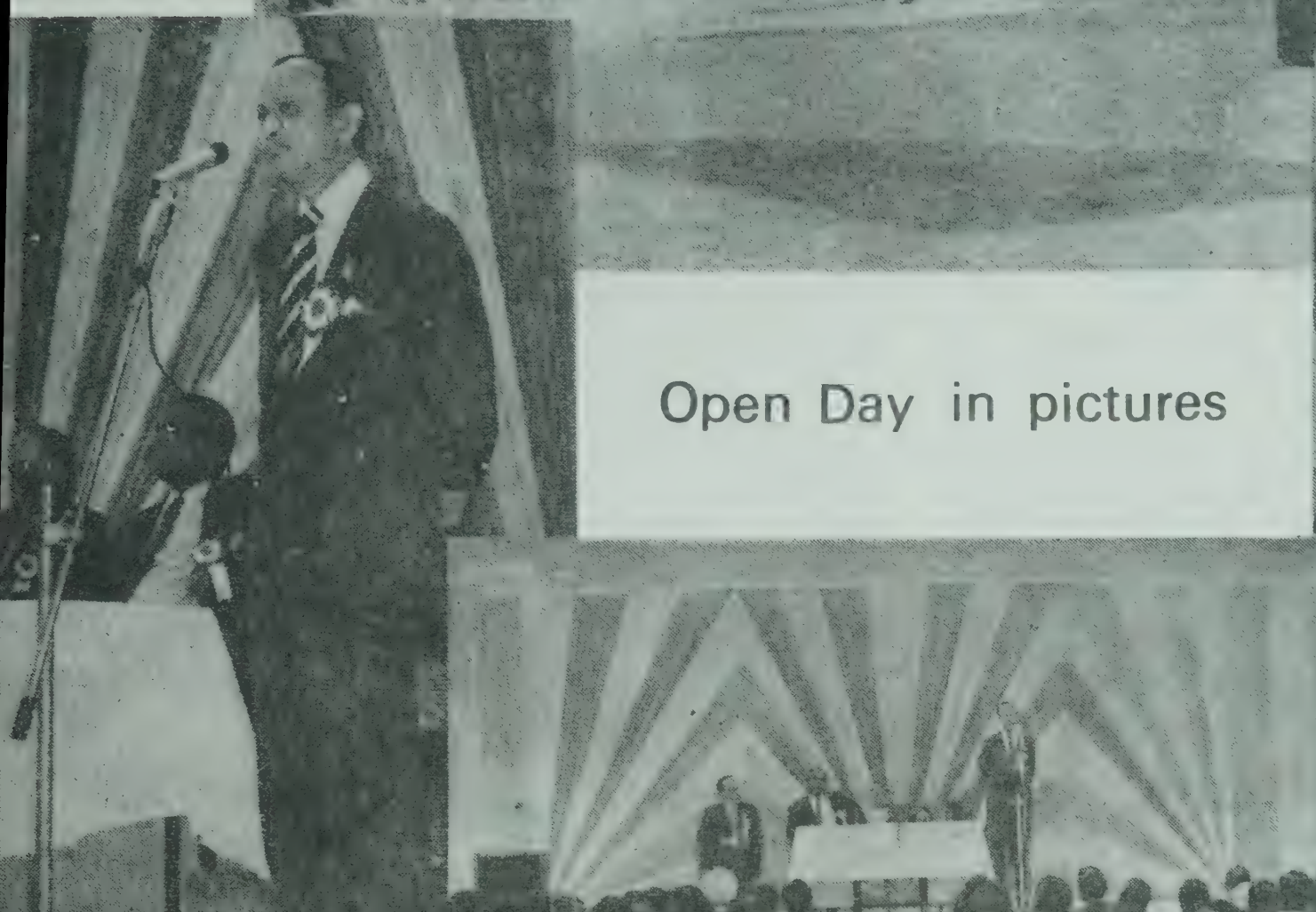
With a view to highlight the role of CMERI in promoting technology for rapid industrialisation of the country, and to provide a special opportunity to the industries to see and discuss the R&D facilities of the Institute, the Central Mechanical Engineering Research Institute, Durgapur, observed 16th February 1981 as an Open Day. It was also hoped that the Open Day would help the Institute in identifying certain areas of immediate interest to the regional and local industries.

The Open Day programme was inaugurated by Shri Kalyan Sen, President, Indian Chamber of Commerce, Calcutta. Dr S.K. Basu, Director of the Institute, welcomed the guests and the visitors, and Shri B.M. Sen, Deputy Director, moved the vote of thanks.

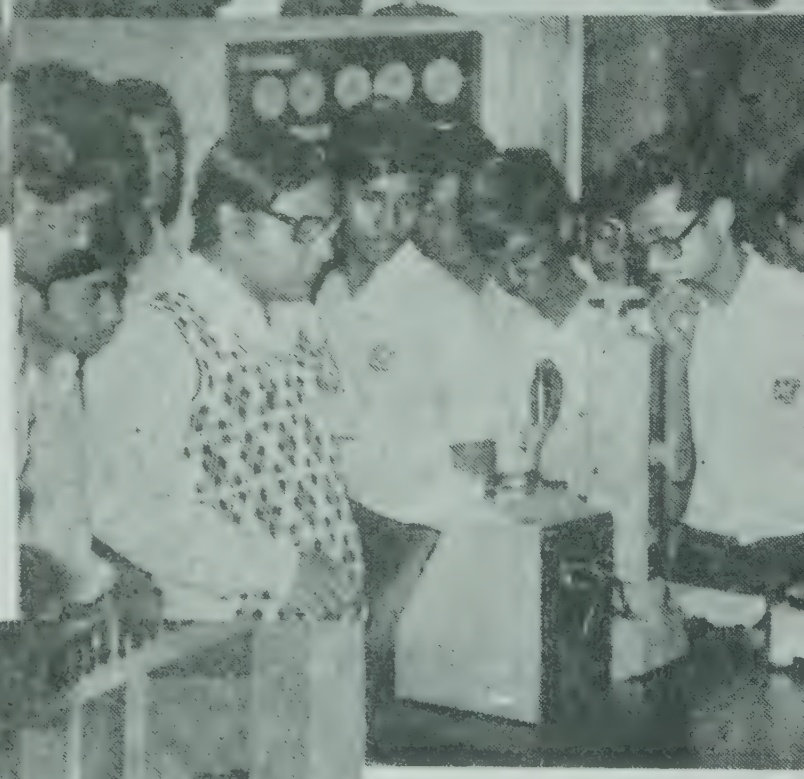
In his inaugural speech, Shri Sen referred to some of the pioneering work of CMERI and other national laboratories in the scientific and technological fronts. But, he said, these achievements do not get proper coverage in the newspapers, and



Open Day in pictures









so the industries and the public were grossly unaware of the excellent contributions made by these laboratories to national economy. Such Open Days were therefore the right opportunities for all concerned to know the work of our scientists.

Over 3500 people visited the laboratory on the occasion. Beside visits to the Institute's laboratories where live demonstration of prototypes and models were arranged, technical and business discussions were held with representatives of industries. The Institute's Display Room and technical film shows drew large crowds.

UNIDO to inaugurate ambitious project in India

Set in the lush hills of India's Andhra Pradesh State, the small farming community of Kothagudem will witness a turning point this November in the country's efforts to ensure self-sufficiency in iron and steel production. The occasion is the opening of a $24 million sponge-iron pilot plant intended to demonstrate how India's mini-steel plants can be fed a regular supply of ferrous material based on direct-reduction ironmaking.

Mini steel plants at present are largely dependent on the fluctuating scrap-iron market. Not only is India faced with a scarcity of ferrous scrap at reasonable prices, it also lacks a ready source of coking coal, another essential ingredient in steel production. In 1969, confronted by this dual problem, the Government of India turned to UNIDO for assistance.

The UNIDO answer was to construct a demonstration sponge-iron plant capable of producing daily up to 100 tons of 90 per cent metallic iron. UNIDO acted as an executing agency for the United Nations Development Programme which provided $5 million for the project, making it UNIDO's most ambitious undertaking to date. The balance came from the Government of India.

India has an abundance of non-coking coal, and by using it the plant is expected to show that sponge-iron can ensure dependable feedstock for the production of steel in the electric-arc furnace, while appreciably reducing capital costs. At the same time, UNIDO will provide training and research and development facilities in this important field.

Although the industrial technology is recent, sponge-iron production is the oldest method of obtaining iron. Archaeological evidence indicates the method was used in India as early as 800 BC. In modern times, however, most iron used for steelmaking has come from blast-furnaces. But the process is costly and suited mainly to large-capacity plants. It also requires good-quality coking coal which is not always readily available.

Recently, electric-arc furnace steel production has increased tremendously. The trend has been stimulated by proliferation, using this method, of smaller-capacity mini steel plants, especially in developing countries. Environmental considerations and the attractions of lower investment capital and operating costs have contributed to this popularity. While many varieties of steel are produced this way, the electric-arc method is dependent on the availability of scrap as the main raw material.

Since demand for scrap is expected to increase in the future, together with its cost, direct-reduction iron is a logical alternative to feed steelmaking furnaces. Direct reduction involves removing oxygen from iron-ore lumps or pellets without melting the iron. At a maximum temperature of 1100°C, the ore reacts chemically in a reducing atmosphere produced by burning coal or hydrocarbons such as natural gas or fuel oil.

The result is a highly metallic lump, honeycombed with holes and known as sponge-iron. It offers key advantages over scrap

in that it is uniform in composition, low in tramp or foreign elements and easy to handle.

Despite the lack of extensive natural gas resources, India has plentiful reserves on non-coking coal which are capable of sustaining a sponge-iron industry. This was a primary consideration when UNIDO agreed to assist in setting-up the Kothagudem iron plant. After evaluating various alternatives, the Government chose the so-called SL/RN process, which employs a rotary kiln and solid-fuel reducing agents such as non-coking coal.

Because sponge-iron production from this type of coal is sensitive to the characteristics of the raw materials, it was considered essential to build the Kothagudem plant as a demonstration unit. Various combinations of iron ores and coals could then be tested on a semi-commerical scale to provide data for future commercial sponge-iron plants. Plant construction began in June 1978. The Kothagudem plant will turn out not only some 30,000 tons of sponge-iron annually, it will also be the only operation of its kind in the world with the facilities to conduct studies on a laboratory, pilot plant and semi-commercial basis on varieties of iron ore and coal for sponge-iron. The demonstration plant should lead to commercial-size sponge iron installations in India designed to supply the additional 2 million to 3 million tons of iron per year now required by the mini steel plants.

The Kothagudem laboratories have been equipped to take into account the needs of other countries that are trying to cope with the global scarcity of coking coal. It exemplifies the UNIDO approach in encouraging third world countries to help each other in their industrialization process, using technology appropriate to natural resources and development priorities. The Organization is, therefore, considering development of the Kothagudem plant as a regional centre for direct-reduction studies.

Training will figure prominently at Kothagudem. Instruction is to be offered in operation, maintenance and process-control aspects of sponge-iron plants. Trainees are expected to attend from countries through the world as well as from all parts of India.

As underlined in 1979 by the UNIDO Second Consultations Meeting on the Iron and Steel Industry, at New Delhi, the consumption of steel by developing countries is in direct proportion to the pace of industrialization. In the face of rising costs for imported iron and steel, third world countries must took to their own natural resources and develop appropriate technologies for domestic conditions. With the opening of the sponge-iron plant in Kothagudem, UNIDO has forged new links in this direction, not only for India but also for the third world as a whole.

Modernisation plan for BSP

An ambitious rupees 400 crors modernisation plant, drawn up by Russian experts at the request of the Bhilai Steel Plant authorities, is awaiting approval of the Central Government. The Soviet report had been scrutinised by Indian specialists and MECON experts before it was sent to the Centre.

The programme basically aims at increasing the capacity of the existing units substantially, besides enabling the plant to perfect steel making and steel rolling technology to improve the quality of the products.

Steel producers raise prices

The ex-stockyard prices of the products of the main steel producers have been raised ranging from Rs 409 to Rs 1123 per tonne, depending on the variety, following the

hike of 20 per cent in steel prices from February 1981. The new prices have been given retrospective effect from February 9, 1981.

The highest increase is in respect of galvanised corrugated sheets. It amounts to Rs 1123. The latest ex-stockyard price was Rs 7385 a tonne in the tested variety of 0.80 mm sheets and Rs 7825 for 0.63 mm sheets. The lowest increase is in respect of angles (65 x 65 x 6/8/10 and 75 x 75 x 6/8/10 mm) which works out to Rs 409, the new stockyard price being Rs 3060.

GDR - India trade protocol

Trade between India and East Germany will increase further during 1981-85 according to a protocol signed in Berlin in late December 1980. Under the protocol, GDR will give India, among other things, machine tools, printing presses, diesel generating sets, agricultural machinery, electrical and electronic equipment and goods, chemicals and fertilisers. India will supply iron ore, textiles, tea, coffee and spices.

East Germany leads in explosive forming

The world's first mass-production, explosive forming process is saving its East German operators signigicant sums each year in the production of heavy duty axle cases.

Developed at VEB IFA-Automobilewerke in Ludwigsfelde by Dr Horst Steinicke, the new process employs a unique explosive-forming plant which completely cuts out high-cost presses and machine tools. Details are awaited.

Machining hard materials at reduced cost

Next to diamonds, cubic boron nitrade (CBN) is the hardest material known to man. A particular grade of CBN, known as CB50, is now being used as a new tool insert material and is said to be ideal for indexible tips for turning operations on very hard and difficult-to-machine materials by Sandvik, West Midlands, UK.

The Company claims that this can dramatically reduce the overall costs of machining components by eliminating grinding operations. Apart from hardness it has other advantages such as no chemical reaction with metals below 1000°C and practically no oxidation below the same temperature.

The new insert has a substrate of cemented carbide. A 0.9 mm layer of polycrystalline CBN is sintered on to the substrate at very high pressure and temperature.

Cobalt and nickel based super alloys can be machined with CB50. Upto now, most operations have included finish turning, but the normal metal removal rate is five times that of cemented carbide. The reason for this is that CB50 is stable upto 1000°C, and the workpiece material becomes soft instead and is substantially easier to machine.

Where the new material has particular relevance is in tackling flame treated bearing surfaces. Although intended to improve the bearing life, the process introduces production problem. Softer untreated sections can be turned, but the treated surface has to be ground.

This necessitates two machines, two set-ups, plus all the intermachine handling problems. In many cases, the components are large and the manufacturer does not have grinding machines with sufficient capacity which means the grinding operation has to be sub-contracted. The use of CB50 tools completes the work in one turning set-up and completely saves on grinding operations.

CRITICAL CONSIDERATION ON THE LIMITS OF OPERATION OF FLUID COUPLINGS

JHANKAR BASU, G.S. PATKI AND S. RAMACHANDRA*

Abstract

The steady state thermal considerations limit the maximum operating speed at different slips of a fluid coupling. Also depending upon the load characteristic, the start up heating decides the stability of a coupling. Other important considerations are on the basis of critical speed of the coupling shaft and centrifugal stress developed in the coupling material.

Introduction

The coupling geometry gives the power equation on the hydrodynamic theory. The power capacity of a coupling increases as the cube of the speed. But there is a definite limit for maximum operational speed of the coupling. Thermal consideration at the start up and during steady state operation decides the suitability of the coupling for a particular type of load and also limits its maximum speed. The critical speed of shaft is also an important consideration in design. Now, the increasing prime mover speeds with better balancing facilities necessitate the check on centrifugal stress. While starting the design of a fluid coupling it becomes essential to know the maximum speed at which the coupling can operate and also the type of load it can start easily. The design of transmission elements depends on these limiting considerations. During development of fluid coupling in CMERI it was found that these considerations are impo tant for a designer faced with the probl of designing a series of fluid couplin for wide range of industrial application

*Central Mechanical Engineering Research Institute, Durgapur 9.

Capacity equation

The torque transmission of a fluid coup ling can be expressed by the eqn[1]

$$T = \frac{Zb}{2\pi k_1} K_2 n_1^2 s \left[1 - \left(\frac{r}{R}\right)^2\right] \sqrt{1 + \frac{fL}{D}} \quad \ldots (1)$$

where,

T : torque input, kg-metre

Z : number of blades

b : blade depth, metre

n_1 : input speed (impeller), rpm

n_2 : output speed (turbine), rpm

r : inner radius of mean flow path, metr

R : outer radius of mean flow path, metr

L : length of mean flow path in the torus metre

D : Average hydraulic mean diameter o flow passage, metre

f : friction factor

K_1 : $\sqrt{R^2 - r^2}$

K_2 : $\dfrac{2\pi^3 \rho (R_1^4 - R_2^4) K_1}{\sqrt{1 + \frac{fL}{D}}}$

hike of 20 per cent in steel prices from February 1981. The new prices have been given retrospective effect from February 9, 1981.

The highest increase is in respect of galvanised corrugated sheets. It amounts to Rs 1123. The latest ex-stockyard price was Rs 7385 a tonne in the tested variety of 0.80 mm sheets and Rs 7825 for 0.63 mm sheets. The lowest increase is in respect of angles (65 x 65 x 6/8/10 and 75 x 75 x 6/8/10 mm) which works out to Rs 409, the new stockyard price being Rs 3060.

GDR - India trade protocol

Trade between India and East Germany will increase further during 1981-85 according to a protocol signed in Berlin in late December 1980. Under the protocol, GDR will give India, among other things, machine tools, printing presses, diesel generating sets, agricultural machinery, electrical and electronic equipment and goods, chemicals and fertilisers. India will supply iron ore, textiles, tea, coffee and spices.

East Germany leads in explosive forming

The world's first mass-production, explosive forming process is saving its East German operators signigicant sums each year in the production of heavy duty axle cases.

Developed at VEB IFA-Automobilewerke in Ludwigsfelde by Dr Horst Steinicke, the new process employs a unique explosive-forming plant which completely cuts out high-cost presses and machine tools. Details are awaited.

Machining hard materials at reduced cost

Next to diamonds, cubic boron nitrade (CBN) is the hardest material known to man. A particular grade of CBN, known as CB50, is now being used as a new tool insert material and is said to be ideal for indexible tips for turning operations on very hard and difficult-to-machine materials by Sandvik, West Midlands, UK.

The Company claims that this can dramatically reduce the overall costs of machining components by eliminating grinding operations. Apart from hardness it has other advantages such as no chemical reaction with metals below 1000°C and practically no oxidation below the same temperature.

The new insert has a substrate of cemented carbide. A 0.9 mm layer of polycrystalline CBN is sintered on to the substrate at very high pressure and temperature.

Cobalt and nickel based super alloys can be machined with CB50. Upto now, most operations have included finish turning, but the normal metal removal rate is five times that of cemented carbide. The reason for this is that CB50 is stable upto 1000°C, and the workpiece material becomes soft instead and is substantially easier to machine.

Where the new material has particular relevance is in tackling flame treated bearing surfaces. Although intended to improve the bearing life, the process introduces production problem. Softer untreated sections can be turned, but the treated surface has to be ground.

This necessitates two machines, two set-ups, plus all the intermachine handling problems. In many cases, the components are large and the manufacturer does not have grinding machines with sufficient capacity which means the grinding operation has to be sub-contracted. The use of CB50 tools completes the work in one turning set-up and completely saves on grinding operations.

CRITICAL CONSIDERATION ON THE LIMITS OF OPERATION OF FLUID COUPLINGS

JHANKAR BASU, G.S. PATKI AND S. RAMACHANDRA*

Abstract

The steady state thermal considerations limit the maximum operating speed at different slips of a fluid coupling. Also depending upon the load characteristic, the start up heating decides the stability of a coupling. Other important considerations are on the basis of critical speed of the coupling shaft and centrifugal stress developed in the coupling material.

Introduction

The coupling geometry gives the power equation on the hydrodynamic theory. The power capacity of a coupling increases as the cube of the speed. But there is a definite limit for maximum operational speed of the coupling. Thermal consideration at the start up and during steady state operation decides the suitability of the coupling for a particular type of load and also limits its maximum speed. The critical speed of shaft is also an important consideration in design. Now, the increasing prime mover speeds with better balancing facilities necessitate the check on centrifugal stress. While starting the design of a fluid coupling it becomes essential to know the maximum speed at which the coupling can operate and also the type of load it can start easily. The design of transmission elements depends on these limiting considerations. During development of fluid coupling in CMERI it was found that these considerations are important for a designer faced with the problem of designing a series of fluid couplings for wide range of industrial applications.

*Central Mechanical Engineering Research Institute, Durgapur 9.

Capacity equation

The torque transmission of a fluid coupling can be expressed by the eqn [1]

$$T = \frac{Zb}{2\pi k_1} K_2 n_1^2 s \left[1 - \left(\frac{r}{R}\right)^2\right] \sqrt{1 + \frac{fL}{D}} \quad \ldots (1)$$

where,

T : torque input, kg-metre

Z : number of blades

b : blade depth, metre

n_1 : input speed (impeller), rpm

n_2 : output speed (turbine), rpm

r : inner radius of mean flow path, metre

R : outer radius of mean flow path, metre

L : length of mean flow path in the torus, metre

D : Average hydraulic mean diameter of flow passage, metre

f : friction factor

K_1 : $\sqrt{R^2 - r^2}$

K_2 : $\dfrac{2\pi^3 \rho (R_1^4 - R_2^4) K_1}{\sqrt{1 + \dfrac{fL}{D}}}$

R_1 : outer radius of coupling, metre

R_2 : outer radius of coupling core, metre

S : $1 - n_2/n_1$ = slip.

The effect of blade thickness has been neglected and the slip is assumed to be low.

Taking $b = \frac{R_1 - r_2}{2}$, where, r_2 = inner radius of the coupling, the input horse power P can be derived from eqn (1) as

$$P = \frac{2\pi^3 \rho Z}{4500\ g}\ n_1{}^3 R_1{}^5 s G_F \qquad .. (2)$$

where,

G_F = geometric factor

$$= \tfrac{1}{2}\left[1 - \left(\frac{R_2}{R_1}\right)^4\right]\ (1 - \frac{r_2}{R_1})\left[1 - \left(\frac{r}{R}\right)^2\right]$$

For a particular series of coupling, the radii ratio, ie, R_1/r_2 = constant= $1/a$ (say) where $1 > a > 0$. So,

$$G_F = \left[1 - \left(\frac{1 + a^2}{2}\right)^2\right]\ (1 - a)\left(\frac{1 - a^2}{a^2 + 3}\right)$$

for coreless couplings, ie, outer core radius R_2 = inner core radius r_1.

Within the limit $0 < a < 0.6$, G_F can be expressed by the linear equation

$$G_F = 0.252\ (1 - 1.4a)$$

So, with ρ = 851 kg/m^3, the power equation becomes

$$P = 4700\ (1 - 1.4a)\ D^5\ (n_1/1000)^3$$

$$(Z/45)\ (s/0.04) \qquad .. (3)$$

The equation shows that with increase in diameter and speed of the coupling its power capacity increases. But the capacity is limited by other factors, viz, temperature rise of the coupling, critical speed of the shaft and centrifugal stress developed in the coupling wall.

Thermal considerations

A fluid coupling almost always operates under slip and thus generates heat, raising the temperature of the coupling and its contents. At the same time it dissipates heat to the surrounding through its wall. Considering the limiting thermal stress developed in the coupling material, the stability of the oil and the withstanding capacity of the seals, the temperature is not allowed to rise above a certain limit.

This heating phenomenon can be divided in three phases - start-up, transient, and steady state conditions.

The heat generation during start-up depends on the characteristic of prime mover and load inertia.

To accelerate the load from zero to normal running speed within a particular starting time, it is necessary for the coupling to transmit sufficient torque to overcome the resistance of the three forces friction, load inertia, and normal load.

Torque required for acceleration can be calculated assuming linear acceleration of the load.

$$T_{inertia} = J_L \times \omega / t$$

where, J_L = mass moment of inertia, ω = operating angular speed and t = time taken to reach ω from 0 speed.

Thus, starting torque = $T_S = T_{friction} + T_{normal\ load} + T_{inertia}$.

The first two terms depend on the type of load.

Time t is important where $T_{friction} + T_{normal}$ is very close to the starting torque of the prime mover, as then only a small amount of torque is left to accelerate the load. When the load is directly coupled, this condition causes slow starting of the electric motor which results in overloading and overheating and for the

nternal combustion engine, a complete in-
bility to start.

The starting time can be considerably educed if the coupling is fitted in the anner which allows the prime mover to tart unloaded and to accelerate to a point here maximum torque is available. In this ay more torque will be available to over-ome the inertia of the load.

The starting torque characteristics for ifferent types of loads are shown in Fig 1. n curve A, the load includes mostly cen-rifugal machines. In these cases, start-ng is easy. The curve B shows the loads ith large flywheels and high inertia com-onents, eg, presses, jaw, crushers, ham-er mills etc. In these cases, starting orque requirements exceed normal running orque but not to a great extent. In cur-e C, the load includes loaded conveyors, hoke-fed crushers, mixers, reciprocating umps etc. These machines require high reakaway torque to set them in motion and tarting torque is almost 2.4 times of the ormal running torque.

The heating characteristic of type C is onsidered. The conditions of other two ypes are simultaneously satisfied. During tarting, neglecting frictional torque

$$T_S = T_{inertia} + T_{normal\ load}$$

So, $T_{inertia} = 1.4\ T_{normal\ load}$

or, $J_L = \dfrac{1.4\ T_{n/l} \times l}{\omega}$

So, for a given starting time the allow-ble inertia of the load J_L can be calcu-ated.

Assuming constant power of the prime over, energy lost as heat during starting an be calculated as :

Energy lost in heat = Energy required or accelerating = $1.4\ T_{n/l} \times \omega/2 \times t$

Where $\omega/2$ is the average speed of the oad considering the constant acceleration f the load from 0 to ω

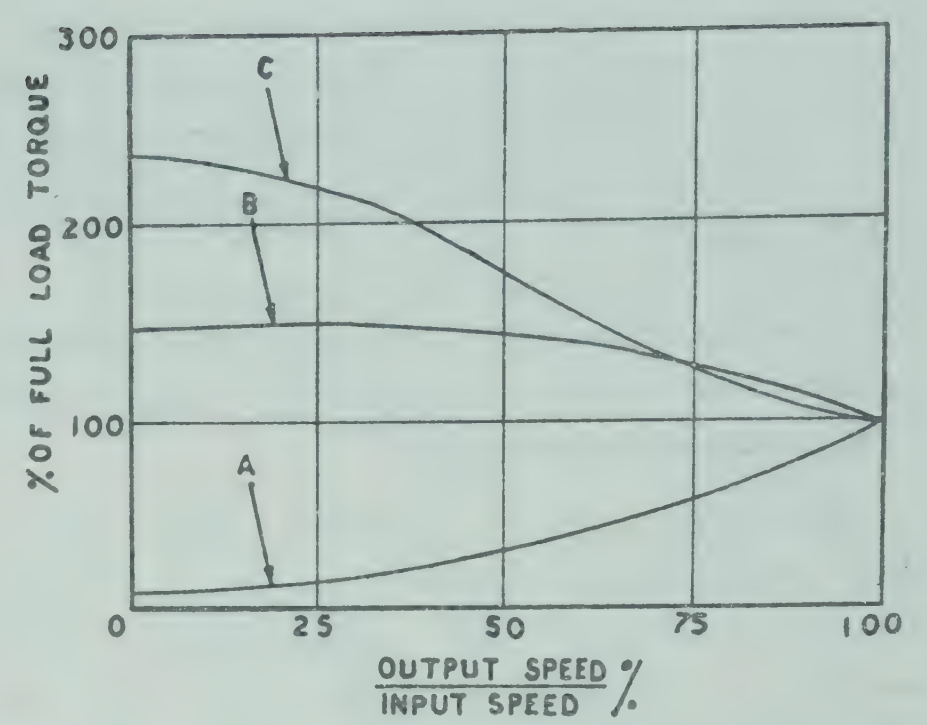


Fig 1
Torque demand characteristics of different types of machines

If $\Sigma(MS)_{oil} + \Sigma(MS)_{material}$ be the heat capacity of the coupling then for a particular starting time, temperature rise (ΔT) from initial value can be obtained. The heat dissipated during this short period is very much less than the heat generated and hence neglected.

$$[\Sigma(MS)_{oil} + \Sigma(MS)_{material}] \times \Delta T$$
$$= 1.4\ T_{n/l} \times \omega/2 \times t$$
$$= \tfrac{1}{2} J_L\ \omega^2$$
$$\text{So, } \Delta T = \frac{\tfrac{1}{2} J_L \omega^2}{\Sigma(MS)_{oil} + \Sigma(MS)_{material}}$$

The starting time depends on the starting torque. This time can be taken to be about 20 secs.

For practical calculations it can be assumed[2]

$\dfrac{\Sigma(MS)_{oil}}{\Sigma(MS)_{material}} = \dfrac{1}{1.3}$ for small couplings,

and = 1/3 for large ones.

The oils used in the coupling, are stable upto 80°C . But the oils can withstand much higher temperature for a short duration. However, for safety, fusible plugs are provided so that the temperature can

not rise more than this limit. A few of the low melting point alloys used for fusible plugs are BS 219-T (melting point 148 ℃), DIN 1707 (L-Sn63 PbAg) (melting point 178℃) etc.

Usually fusible plugs of 145℃ melting point are used. In special cases, this limit can go up to 180℃.

Once the load is started, the heating characteristics of the load passes through transient state. The temperature of the coupling changes according to the heat generation and heat dissipation. The heat generation will be dependent on the slip at which the coupling operates and can be calculated as -

Heat generation = Slip x power input.

Heat generation during this period, along with the heat generated during starting will be consumed by the coupling oil and material. A part of this heat will be dissipated to the atmosphere through the housing walls. The heat transfer to the atmosphere will be mainly by forced convection. Hence the heat transfer, ie, heat dissipation per unit time will depend on the heat transfer coefficient (h) and temperature difference (ΔT) between the wall and surrounding.

ΔT, for transient state is a function of time. Heat transfer coefficient between the wall and surrounding, as per Nusselt, for forced convection will depend on the area exposed and the speed of the coupling. Hence h can be expressed as -

$$h = \text{constant } (Q) \times D^m \times n^p$$

where m and p are constants.

The difference between the total heat generated and total heat dissipated will affect the temperature of oil at any instant.

(Total heat generated ~ total heat dissipated) = heat capacity of coupling x temperature rise or fall of the coupling and its content.

Since this temperature is time dependent it is difficult to calculate. However, from experiments it has been observed that this state is significant for a short duration and the temperature falls rapidly.

After sometime, the coupling reaches almost a steady state condition, ie, temperature of the oil and material does not vary with time. Hence, no heat is consumed by the coupling. So, for steady state condition the expression becomes.

Heat generated = Heat dissipated

ie, Slip x power input = Heat transfer coefficient x temperature difference between coupling and surrounding.

Or, $s \times HP = Ah \times \Delta T$

where A is the conversion factor from Kcal/sec to horse power.

Heat transfer coefficient h has been calculated from the performance curves of twin disc couplings[3], voith couplings etc and can be expressed as -

$$h = 0.00263\ n_1^{0.575}\ D^{2.5}$$

where D is in metres, n in rpm and h in Kcal per ℃ per sec.

Substituting HP from the general power equation

$$s \times 4700(1 - 1.4a)\ \left(\frac{s}{0.04}\right)\ \left(\frac{Z}{45}\right)\left(\frac{n_1}{1000}\right)^3 D^5$$

$$= 0.00263\ n_1^{0.575}\ D^{2.5}\ (\Delta T)$$

The permissible temperature for most of the oils is 80℃.

This expression for HC series of couplings developed in CMERI with $a = 0.3$ and $Z = 45$, has been taken as -

$$s^2\ n_1^{2.425}\ D^{2.5} = 9.7 \times 10^3$$

considering ambient temperature = 35℃,

By this expression permissible speeds of HC series couplings have been calculated for different slips.

In some couplings, hot oil from the coupling is drained out continuously. The oil is passed back in the coupling through coolers. This helps to run the coupling at higher slips.

Critical speed limit

The permissible speed of a coupling is also limited by the critical speed of the shaft.

The couplings are, usually, connected to the driving shaft through flexible discs to adjust minor misalignment of shafts. On the other end, rigid connection between the shafts and the coupling is provided. So cantilever bending of the shaft can be assumed. The critical speed, hence, may be calculated by the equation.

$$n_{cr} = \frac{30}{\pi}\sqrt{\frac{3EIg}{Wl^3}}$$

where

I = moment of inertia of the shaft

W = weight of the complete coupling and acting through CG

l = dis. ce of coupling CG from the supporting end.

For practical calculation for the couplings with the arrangements discussed earlier, the following proportionalities can be considered.

D = overall diameter of the coupling

d_{sh} = 0.16D to 0.2D = diameter of the shaft

l = 2 x flange width + 0.5 coupling width + clearance for end accessories = 3.0 d_{sh} + 0.2D + 0.1D

$l \approx 0.8D$

W = 0.574 x $10^2 D^3$ Kg where D is in metres.

Using these proportionalities, n_{cr} can be found out as -

n_{cr} x D = 2118 where n is in rpm and D is in metres.

The permissible value of the operating speed is maintained within 60 per cent of the critical speed.

So, n_{per} x D = 1270.

To maintain the permissible critical speeds the coupling parts and the assembly should be balanced properly.

Fig 2 shows the performance curve of a coupling designed in CMERI and its limits of operation.

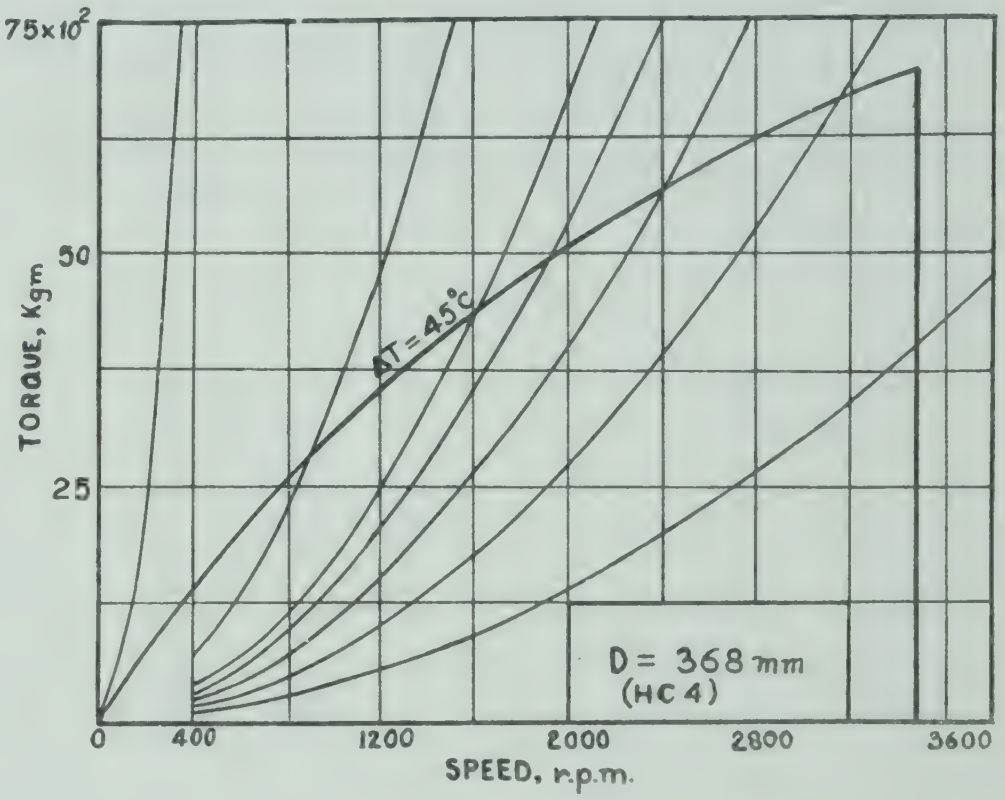


Fig 2

Performance characteristics and safe operating limits of HC 4 fluid coupling

Centrifugal stress

The limitation of the peripheral speed is connected with the strength of the coupling material. The peripheral speed is dependent on the diameter and rpm of the coupling.

By rough approximation, permissible peripheral speed can be taken as 120 m/sec for aluminium and 150 m/sec for steel coupling[4]. For aluminium coupling n_{per} can be calculated as

$n_{per} \times D = 2290$ where n is in rpm and D in metres.

This expression shows that n_{per} for a particular coupling is much more than that calculated on the basis of critical speed of the shaft or the temperature rise of the coupling.

However, if extra cooling arrangement and better balancing are done to increase the operating speed, the centrifugal stress developed should also be checked.

Conclusion

Maximum operating speed limit of a coupling is decided mainly on the basis of thermal consideration. Critical speed of the shaft is also checked. Centrifugal stress is found to be much within the permissible values for industrial couplings within their normal operating range. Starting torque requirement for which the transmission elements are designed, is calculated for high inertia load.

Acknowledgement

The authors thank the Director, CMERI, Durgapur, for his kind permission to publish the paper.

References

[1]G.S. Patki and B.S. Gill, 'The effect of blades on the performance of hydrodynamic couplings and dynamometers', *Mech Engg Bull*, 7(3) 80-88 (1976).

[2]R. Keller, 'The start-up of hydrodynamic couplings', VDI Report No 73 (1963) pp 41.

[3]E. Kickbush, 'Foettinger Kupplungen und Foettinger-Getriebe', Springerverlag, Barlin, pp 24-26 (1963).

[4]O.V. Yaremenko, T.I. Kononenko, 'Application of closed loop hydrodynamic clutches', *Russian Engg Jour*, L(11) 51-54 (1970).

OPEN SOLAR REGENERATION OF LITHIUM CHLORIDE BRINE

M. PRASAD AND P. KUMAR*

Abstract

It is attractive to have airconditioning in hot dry climate using open cycle solar absorption refrigeration where water works as refrigerant and lithium chloride brine as absorbent. The dilute brine can be regenerated in a solar collector-cum-desorber where free convection flow of ambient air removes water from it. The analysis of the regenerator is presented in mathematical terms. Its theoretical performance is found to be quite good for hot and dry climate conditions. The regenerator is well suited to be used with absorption refrigeration system for airconditioning applications.

Nomenclature

A	Regenerator surface area, m^2
C_p	Specific heat of brine, $WH(kg)^{-1}$ (deg K)$^{-1}$
C	Concentration of brine, Wt %
f	Function relating vapour pressure of brine with temperature and concentration
g	Acceleration due to gravity, $m(sec)^{-2}$
G_r	Grashof number
h_c	Convective heat transfer coefficient on brine surface, Wm^{-2} (deg K)$^{-1}$
h_{co}	Convective heat transfer coefficient on outer surface of the cover, Wm^{-2} ($^{\circ}K$)$^{-1}$
h_m	Mass transfer coefficient, $Kg\,m^{-2}(mmHg)^{-1}$
h_{fg}	Latent heat of vapourisation for water, $WH(kg)^{-1}$
I_t	Total solar intensity normal to regenerator surface, Wm^{-2}
K	Thermal conductivity, Wm^{-1} ($^{\circ}K$)$^{-1}$
l	Regenerator length, m
$\dot{m}$	Rate of mass transfer of water from brine to air, $Kg(hr)^{-1}$
$\dot{M}$	Flow rate of brine on regenerator surface, $Kg(hr)^{-1}$
P_{bo}	Vapour pressure of brine at regenerator outlet, mm Hg
p_w	Vapour pressure of solution, mm Hg
p_{wa}	Partial pressure of water vapour in ambient air, mm Hg
q_c, q_r	Convective and radiative heat transfer from brine surface respectively, Wm^{-2}
q_m, q_s	Energy used for mass transfer of water and sensible heating of brine respectively, Wm^{-2}
q_{cond}	Conductive heat loss from regenerator bottom, Wm^{-2}
q_a, q_{ca}	Solar energy absorbed at brine surface and cover surface respectively, Wm^{-2}
q_{ccda}	Heat transfer by conduction from inner surface of cover to air moving up due to buoyancy, Wm^{-2}
q_{cco} q_{cro}	Convective and radiative heat transfers from outer surface of cover respectively, Wm^{-2}
T	Temperature, $^{\circ}K$
V	Ambient air velocity, $m(sec)^{-1}$
x	Thickness, m
Ya, Yo	Humidity ratios of water vapour in ambient air and at brine surface respectively, Kg/Kg of dry air
α	Absorptance
η	Regenerator efficiency, $(q_m/I_t) \times 100$

*Central Mechanical Engineering Research Institute, Durgapur 9.

β	Coefficient of thermal expansion for ambient air, $(^{\circ}K)^{-1}$
θ	Regenerator tilt with horizontal, degree
τ	Transmittance
ρ	Reflectance
ϵ	Emittance
σ	Stefan Boltzman constant, $Wm^{-2}\ (^{\circ}K)^{-4}$
ν	Kinematic viscosity of ambient air, $Kg\ m^{-1}(Sec)^{-1}$

Subscripts

a	Ambient air
b	Brine
c	Cover
i	Insulation
bi	Brine at inlet
bo	Brine at outlet
ci	Inner surface of cover
co	Outer surface of cover.

Introduction

Solar airconditioning using absorption refrigeration is a well established phenomenon today[1,2]. The main charm of such a system lies in substantially reduced consumption of electricity for its operation. However, much effort is still needed to make it economically viable. The use of modified cycle and a better absorbent refrigerant combination are the two important steps in this direction.

A closed cycle absorption refrigeration system with water as refrigerant requires the complete system to remain under vacuum. Instead, if a regenerator open to ambient is used, not only that it remains at atmospheric pressure but the need of condenser is eliminated altogether. Moreover, when solar energy is used for absorbent regeneration, the solar collector itself works as regenerator for open cycle, whereas, a separate heat exchanger is required by closed cycle for this purpose. Thus open regeneration of absorbent makes the refrigeration system compact apart from reducing the leakage problem.

Open cycle solar absorption refrigeration systems, have been reported to perform well with LiCl-water and LiBr-water combinations in Turkmania (Russia)[3,4], first combination proving superior over the second. Large ambient wind velocity has been used for transferring water vapour from brine to air. However, contamination of brine is a problem with such regenerators. To reduce contamination, still type regenerator has been considered by Hollands[5] and Kakabayev and Golaev[6]. The disadvantage with such a regenerator is that efficiency drops down to a low value.

A simple open regenerator has been used by Mullick and Gupta[7] for the regeneration of calcium chloride brine where free convection of ambient air removes water vapour from hot brine surface. Such free convection regenerators are easy to fabricate and are less expensive. Nevertheless, the relative simplicity of a free convection solar regenerator belies the complexity of internal heat and mass transfer processes and a systematic and accurate method of analysis for such a regenerator has not been reported so far.

The objective of the present paper is to provide an up-to-date methodology for the analysis of open free convection solar regenerator and to predict its theoretical performance for the regeneration of lithium chloride brine in hot dry climates. Such a regenerator can be used in absorption refrigeration system for airconditioning.

Description

An inclined blackened corrugated metal sheet with a transparent cover at a distance of few centimetres is considered to make the regenerator in the present analysis (Fig 1). Dilute brine is evenly distributed at the upper end of the metal surface and flows down in a thin uniform film. Solar energy absorbed at collector surface raises the brine temperature which

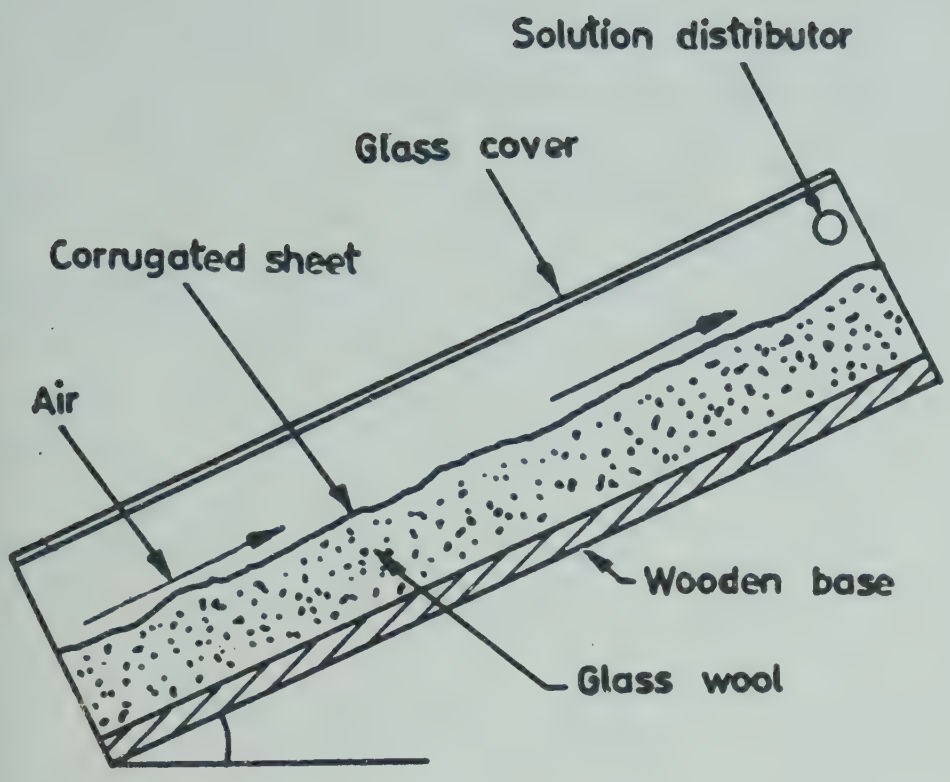


Fig 1
Open solar regenerator

gives rise to free convection flow of ambient air in the space between the metal sheet and the cover. Convective transfer of heat from brine to air is coupled with mass transfer of water vapour in the same direction and the brine coming out of regenerator is a concentrated one. It gets diluted by absorbing water vapour from evaporator, inside the absorber. Dilute brine is sufficiently preheated in a heat exchanger by extracting heat from the hot concentrated brine and is then sent back to the top of the regenerator.

Analysis

The steady state thermal analysis for the proposed free convection solar regenerator is presented in mathematical steps. It is assumed that the regenerator surface remains isothermal.

Energy absorbed by brine surface is

$$q = I_t \ \tau_c \ \alpha_b \qquad .. (1)$$

Energy balance at regenerator surface gives

$$q = q_c + q_m + q_r + q_s + q_{cond} \qquad .. (2)$$

Convective heat transfer from brine to air is

$$q_c = h_c \ (T_{bo} - T_a) \qquad .. (3)$$

where

$$h_c = (N_u K_b / l) \ [1 + \frac{p_{bo} - p_{wa}}{2020 - p_{bo}} \quad x$$

$$\frac{T_{bo}}{T_{bo} - T_a}]^{0.25} \qquad .. (4)$$

The factor under indices comes from enhanced buoyancy due to evaporation of water.

Average Nusselt Number is computed[8] as

$$N_u = 0.677 \left(\frac{P_r^{\,2}}{0.952 + P_r}\right)^{0.25} \quad G_r^{\,0.25} \qquad .. (5)$$

where,

$$g_r = \frac{g(\sin\theta) \ \beta \ (T_{bo} - T_a) \ l^3}{\nu^2} \qquad .. (6)$$

Dropkin's measurements[9] for air-water vapour system gives

$$h_c / h_m = 0.264 \qquad .. (7)$$

Thus, water vapour transfer from brine to ambient air is

$$\dot{m}/A = h_m \ (Y_b - Y_a) \qquad .. (8)$$

and heat energy utilised for this mass transfer is

$$q_m = (\dot{m}/A) \ h_{fg} \qquad .. (9)$$

Radiative transfer of heat from brine to the inside surface of the cover is

$$q_r = (T_{bo}^{\,4} - T_{ci}^{\,4}) / (\epsilon_b^{-1} + \epsilon_c^{-1} - 1) \qquad .. (10)$$

Sensible heating of the brine is given by

$$q_s = (\dot{M}/A) \ C_p \ (T_{bo} - T_{bi}) \qquad .. (11)$$

Conductive loss from the bottom of the regenerator surface is

$$q_{cond} = (K_i/x_i)(T_{bo} - T_a) \quad .. (12)$$

Heat transfer from inside surface to outside surface of cover, assuming a linear temperature profile through cover material, is given by

$$q_r + q_{ca} - q_{ccda} = (K_c/x_c)(T_{ci} - T_{co}) \quad .. (13)$$

where q_{ca} denotes radiant energy absorbed by cover and is expressed as

$$q_{ca} = I_t \alpha_c (1 + \tau_c \rho_b) \quad .. (14)$$

The first term on the right hand side gives the energy absorbed from incident radiation and the second term represents the energy absorbed from radiation reflected back from the brine surface.

Since free convection of air at brine surface which is inclined with horizontal is being considered, the air thickness between brine and cover may be treated as a conduction insulation to the inner surface of the cover for the case when T_{ci} is much closer to the T_a and buoyancy effects at cover surface are very small. Then, conductive heat transfer from inside surface of cover to the thin layer of air moving at brine surface is given by

$$q_{ccda} = (K_a/x_a)(T_{ci} - T_a) \quad .. (15)$$

The heat reaching the outer surface of the cover must be convected to the ambient air and radiated to the sky.

Thus,

$$\frac{K_c}{x_c}(T_{ci} - T_{co}) = q_{cco} + q_{cro} \quad .. (16)$$

where

$$q_{cco} = h_{co}(T_{co} - T_a) \quad .. (17)$$

and h_{co} is evaluated according to Whillier[10], from the relation

$$h_{co} = 5.7 + 3.8\ V \quad .. (18)$$

Radiative transfer of heat from outer surface of cover to the sky is

$$q_{cro} = \epsilon_c \sigma (T_{co}^4 - T_s^4) \quad .. (19)$$

Here sky temperature, T_s, is evaluated from Brunts' relation[11], expressed as

$$T_s = T_a \left[0.55 + 0.33\left(\frac{p_{wa}}{25.4}\right)^{0.5}\right]^{0.25} \quad .. (20)$$

Vapour pressure-temperature-concentration relationship for the solution under consideration is to be used from proper source and may be expressed in the form

$$p_w = f(T, C) \quad .. (21)$$

Finally, the percent regeneration efficiency is given by

$$\eta = \frac{q_m}{I_t} \times 100 \quad .. (22)$$

Discussion

The theoretical performance of the proposed open solar regenerator for the regeneration of LiCl brine is shown in Figs 2-6.

Evaporation rate of water per unit area from brine surface increases linearly with increase in insolation (Fig 2). Since average brine temperature also rises with insolation, thereby reducing h_{fg} marginally, the efficiency defined by equation (22) is characterised by a small curvature when plotted against insolation. Since regeneration efficiency drops down rapidly at lower insolations, it is advisable to use plain reflectors to enhance solar incidence on regenerator surface. It is for this reason that an insolation value of 1000 Wm^{-2} has been used for Figs 3-6.

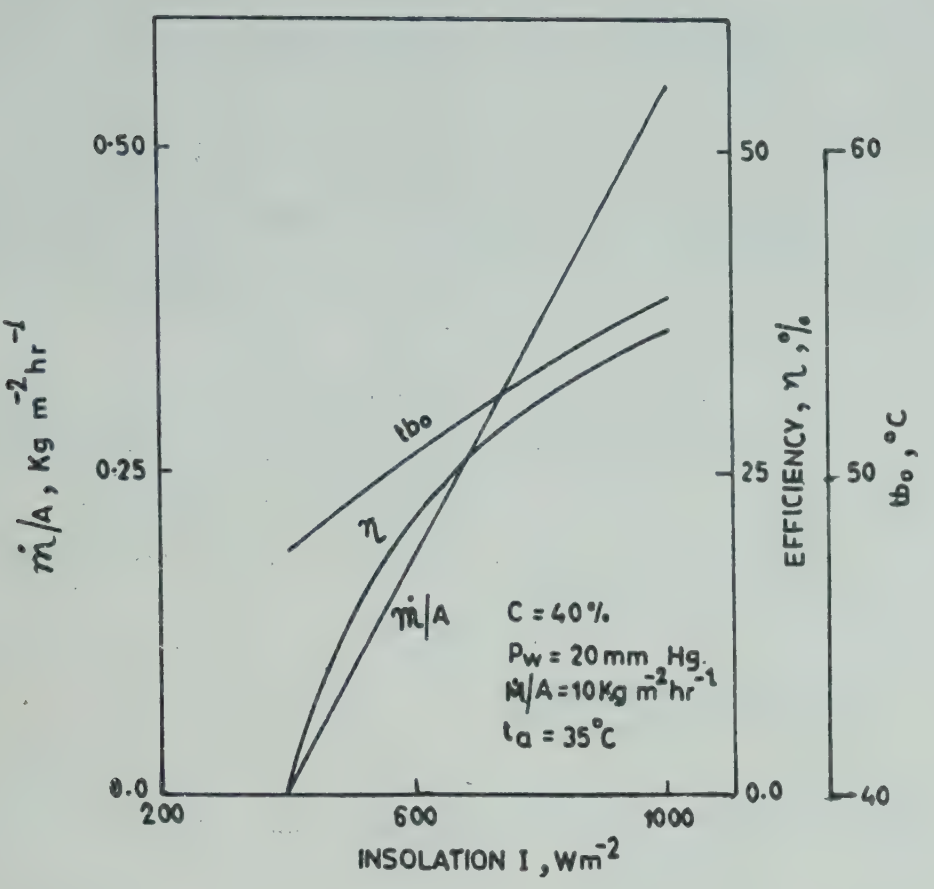


Fig 2
Regenerator performance with varying insolation

Fig 3 shows the effect of varying concentration on the regenerator performance. Water evaporation rate and regeneration efficiency drop down with increase in concentration due to associated decrease in vapour pressure of brine inspite of an increase in its temperature. Vapour pressure of water in ambient air has exactly similar influence on regenerator performance as that of brine concentration but at a smaller scale (Fig 4).

Flow rate of brine also affects the regeneration efficiency and the water evaporation rate adversely as expected (Fig 5). Nevertheless, the rates of decrease of both the quantities diminish with successive increase in brine flow rate. This characteristic makes it possible to have regeneration at a reasonably high efficiency even when brine flow rate is made comparatively large which may sometimes be required for satisfactory performance of absorption unit in refrigeration system.

It is interesting to note the effect of ambient air temperature on the regenerator performance as displayed in Fig 6. Not only the regeneration efficiency gets improved but also, the rate of increase of efficiency increases with rising temperature of ambient air. This characteristic of the regenerator makes it particularly suitable for airconditioning applications due to the fact that for a given flow rate of brine, it can be regenerated to higher concentrations for every increase in ambeint air temperature.

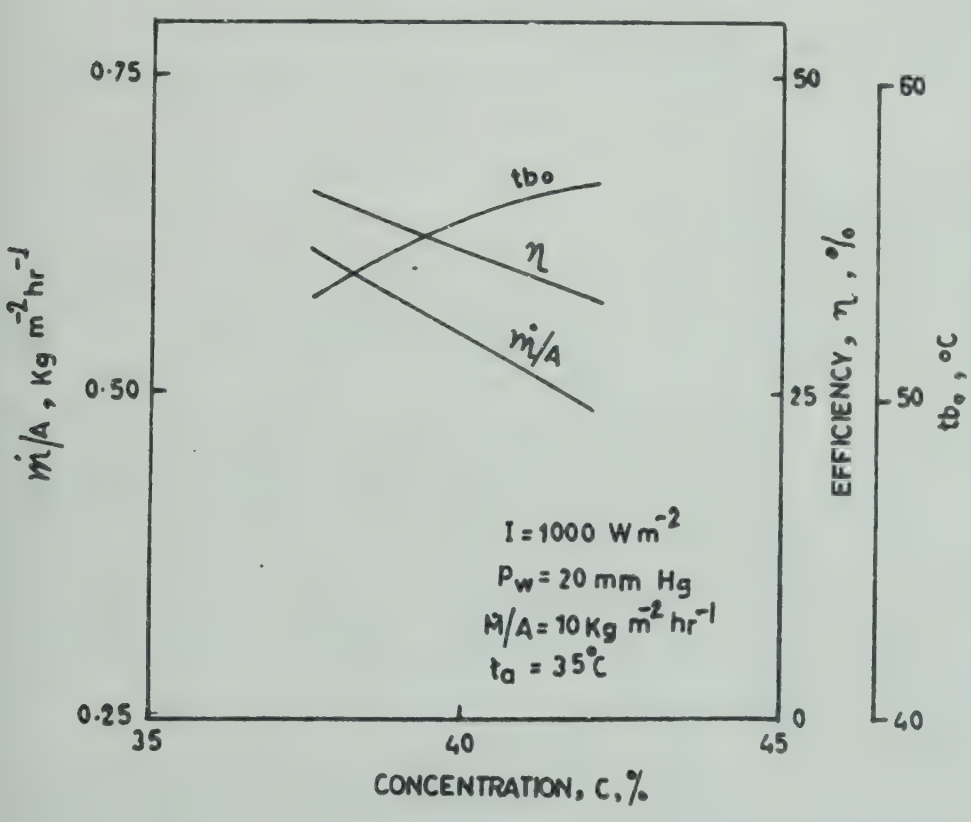


Fig 3
Regenerator performance with varying LiCl concentration

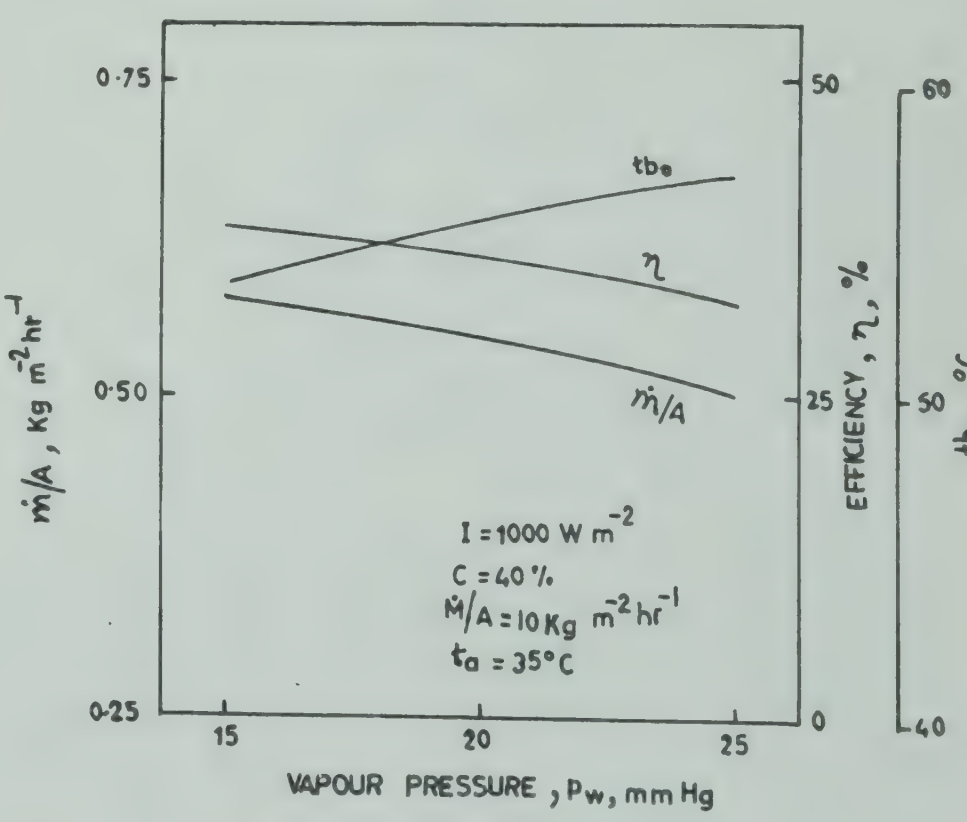


Fig 4
Regenerator performance with varying water vapour pressure in ambient air

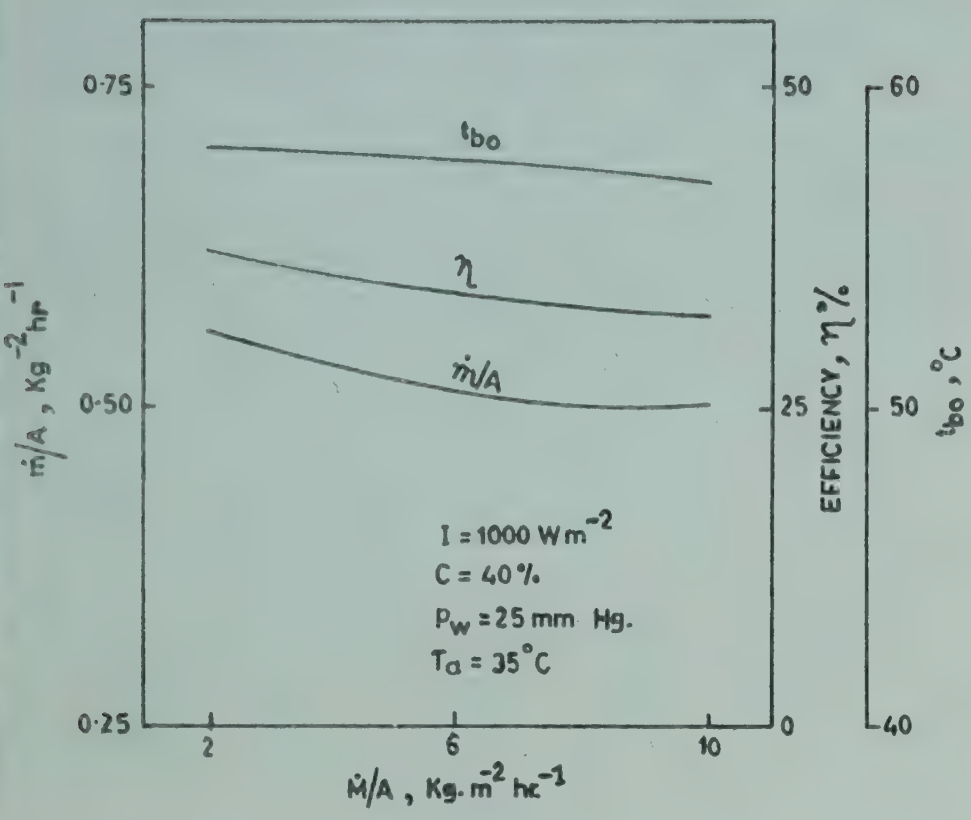


Fig 5
Regenerator performance with varying flow rate of LiCl brine

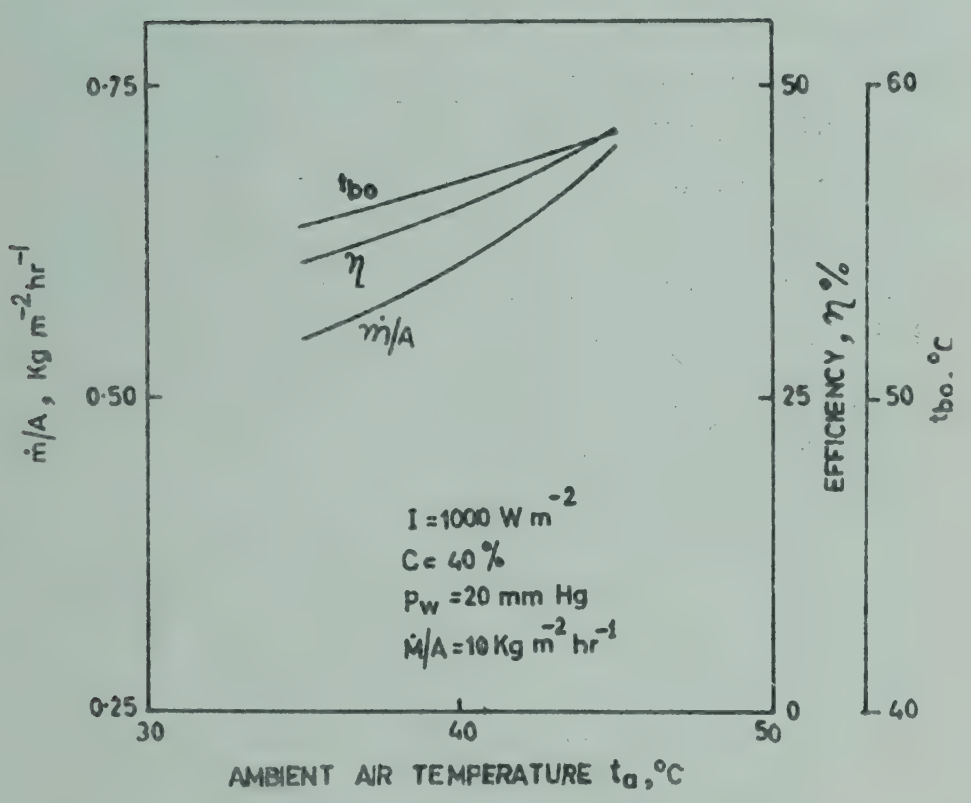


Fig 6
Regenerator performance with varying ambient air temperature

The thermophysical properties of the various substances and other important data used in present computation are given in Appendix.

Conclusions

1) It is possible to regenerate lithium chloride brine using an open solar regenerator at a reasonably high efficiency in hot dry climates.

2) The regenerator is well suited to be used with absorption refrigeration system for air conditioning and process cooling applications.

3) The resulting refrigeration system would be economical compared to closed cycle one having a solar energy operated regenerator and using same absorbent-refrigerant combination.

Acknowledgement

Thanks are due to the Director, CMERI, Durgapur, for his kind permission to publish the paper.

APPENDIX

The following data have been used for the solution of governing equations:

τ_c	= 0.82	α_c = 0.06	ϵ_c = 0.96
ρ_b	= 0.05	α_b = 0.95	ϵ_b = 0.95
V	= 1.39	K_c = 1.038	x_c = 0.003
T_{bo}-T_{bi}	= 10	K_i = 0.0465	x_i = 0.1
θ	= 23.75	K_a = 0.027	x_a = 0.05
l	= 1.17		

$f(T,C)$ for LiCl brine is taken from Threlkeld[12].

References

[1] J.A. Duffie et al, 'A study of a solar air conditioner', *Mechanical Engineering*, 85, p 31, August (1963).

[2] E.A. Farber et al, 'Operation and performance of the University of Florida solar airconditioning system', *Solar Energy*, 10(2) 91 (1966).

[3] A. Kakabayev and A. Khandurdyev, 'Absorption solar refrigeration unit with open regeneration of solution', *Applied Solar Energy*, 5(4) 69 (1969).

[4] V. Baum and A. Kakabayev, 'The use of solar radiation for creating comfortable temperature conditions in Turkmania SSR', *Proc ISEC*, New Delhi (India), p 1556 (Jan 1978).

(*Continued to page 59*)

FREE MASS IMPACT DAMPER HAVING LARGER CLEARANCES

S.Y. BHAVE* AND P.P. CHIKATE**

Abstract

An impact damper consists of a free mass that can have oscillating motion between two stops. If impacts are correctly arranged so as to be in phase opposition with the excitation, amplitude of vibration can be reduced effectively and considerably. However, the values of the optimum clearances predicted by the analysis are generally so small that such clearances are very difficult to obtain and maintain practically. Therefore this paper attempts to bring out the effect of clearances on the performance of the impact damper that are much larger than the theoretical optimum. It is shown that impact damper is very effective even for larger clearances. Effect of variation of clearance and free mass are given graphically.

Notation

d : clearance (total travel of free mass)
e : coefficient of restitution
f : excitation force (harmonic)
M : mass of the main system
m : mass of free-mass
p : natural frequency of the system
$q = \frac{F}{m}$: excitation per unit mass
r : frequency ratio
v : velocity of free mass between impact
x : displacement at time t
$x_{st} = \frac{F}{K}$: $\frac{\text{excitation force}}{\text{spring constant}}$
α : phase angle between excitation and impact
$\mu = \frac{m}{M}$: mass ratio
x_o : initial displacement of main mass M
$\dot{x}_o$: initial velocity of main mass M.

*Institute of Armament Technology, Pune 25.
**College of Engineering, Pune 5.

Introduction

An impact damper or impact vibration absorber is a device to reduce vibration amplitudes particularly at resonance condition. It consists of a free mass m (as shown in Fig 1) which is free to travel between two stops on the main system of mass M. As the main system vibrates because of excitation it creates impacts with the free mass.

The free mass impact damper acts in two ways. Firstly, it extracts some energy out of the system in the form of heat and noise. But this is a minor part of its function and some times this loss of energy should be avoided if the noise level is high and becomes irritating to the personnel. Secondly, the force of impact itself can be so phased that it is in opposition to the external force and thus acts as an absorber. To achieve this phase opposition proper choise of free mass m and clearances between two stops is necessary.

Right from the first paper[1] on the subject that appeared in 1945 many authors have studied the subject both from analysis and experimental points of view[2,3,4,5].

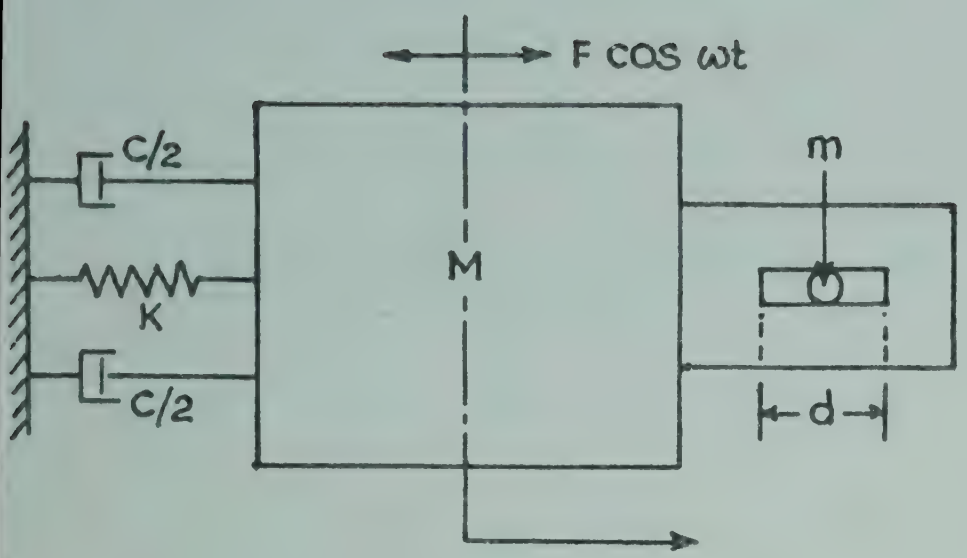


Fig 1
Theoretical model

Optimization of the system includes the proper choice of mass-ratio and clearance. However the optimum value of clearances is very small generally and no literature is available on the effect of larger clearance on the functioning of the impact damper. This paper brings out these effects from the experimental observations.

Theoretical analysis

The method of analysis used here follows closely that of Wartburton[4]. It is based on the assumption that two equispaced impacts occur in one cycle of the excitation force. Impact occurs instantaneously so that position of the system does not change during the impact but velocities of the masses change. The change is governed by the coefficient of restitution. Since the need of the damper is felt mostly in the region of resonance, analysis is presented for the undamped system at resonant frequency.

Fig 2 shows the position of the system after the first impact at the right hand stop and before and after the second impact at the left hand stop. For two equispaced impacts conditions at two impacts must be mirror images of each other.

Assuming that excitation leads the impact by phase angle and measuring time from the time of impact the equation of motion for the main system is

$$x = A\ Cos\ pt + B\ Sin\ pt + \frac{q\ Cos\ (\omega t+\alpha)}{(p^2 - \omega^2)} \quad .. \quad (1)$$

where A and B are constants which are to be determined from the initial conditions. Initial conditions are chosen as follows.

At $t = 0$, $x = x_o$ initial displacement,

$\dot{x} = -\dot{x}_o$ initial velocity.

Negative sign is chosen for the initial velocity as this will give better impact effect. With these initial conditions and allowing ω to reach $p(\omega = p - \epsilon)$ for resonant frequency, equation of motion becomes

$$x = x_o\ Cos\ pt - \frac{\dot{x}_o}{p}\ Sin\ pt + \frac{qt}{2p}\ Sin\ (pt + \alpha) - \frac{q\ Sin\ \alpha\ Sin\ pt}{2p^2} \quad .. \quad (2)$$

Now $x = -x_o$ at the second impact at $t = \pi/p$. This gives $Sin\ \alpha = 0$, ie, $\alpha = 0$ or $\alpha = \pi$ $\alpha = 0$ is not admissible for conservation of momentum equation and hence we choose $\alpha = \pi$. This shows that impact occurs at maximum force value.

Applying equation of conservation of momentum for the impact at $t = \pi/p$ gives

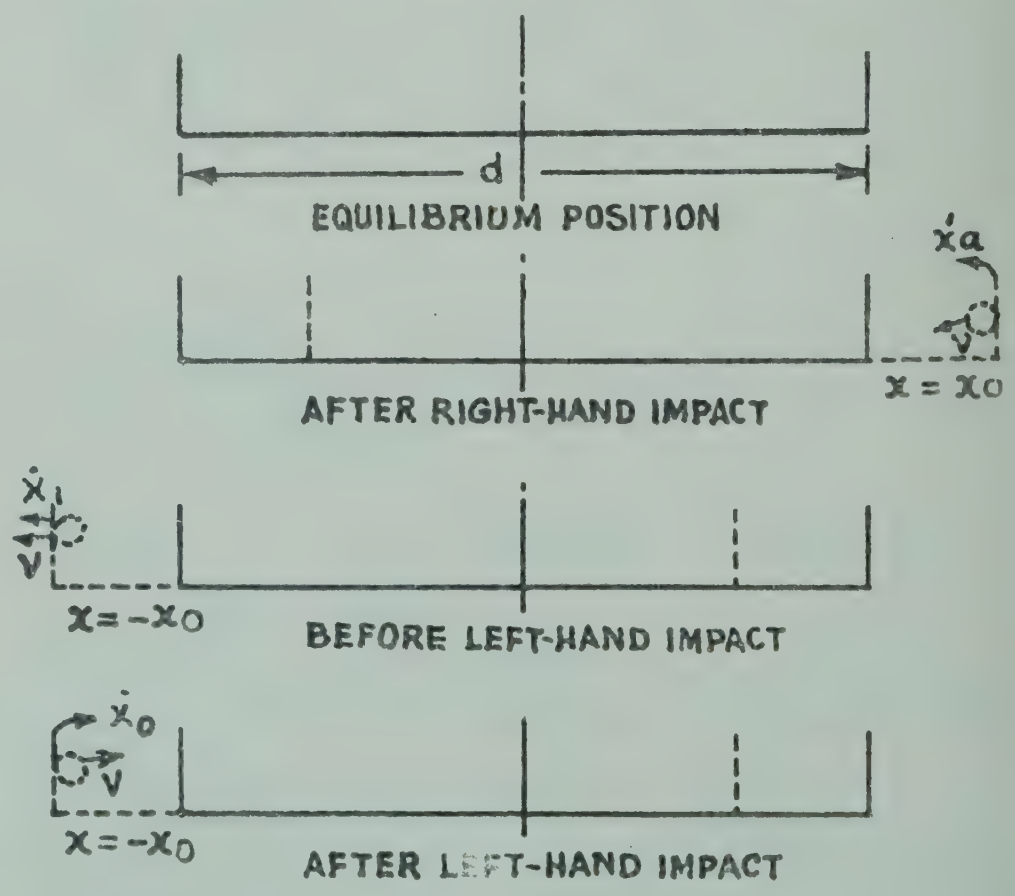


Fig 2
Positions of impacts

$$V = \frac{q\pi}{4p\mu} \qquad .. (3)$$

where $\mu = m/M$ mass ratio.

Since the free mass travels at uniform velocity between two impacts

$$d + 2x_o \cdot = \frac{\pi^2 x_{st}}{4\mu} . \qquad .. (4)$$

Using the notion of the coefficient of restitution for the velocities before and after the impact we get

$$\dot{x}_o = p(d + x_o)\ (1 - e - 2\mu e) \qquad .. (5)$$

Substitution from equations (4) and (5) makes the equation of motion

$$\frac{x}{x_o} = \left(\frac{\pi^2}{8} - \frac{d}{2x_{st}}\right) Cos\ pt - \left[\frac{\pi(1-e-2\mu e)}{4\mu\ (1+e)} + \frac{pt}{2}\right] Sin\ pt \qquad .. (6)$$

To find the time for $(x/x_{st})_{max}$ we differentiate and equate to zero.

$$\therefore \left(\frac{\pi^2}{8\mu} - \frac{d}{2x_{st}} + \frac{1}{2}\right) Sin\ pt + \left[\frac{pt}{2} + \frac{\pi\ (1-e-2\mu e)}{4\ \mu\ (1+e)}\right] Cost\ pt = 0 \qquad .. (7)$$

One of the possibilities is, if

$$\frac{d}{x_{st}} = 1 + \frac{\pi^2}{4\mu} \qquad .. (8)$$

We get $(x/x_{st})_{max}$ when $pt = \pi/2$.

And with this maximum amplitude becomes

$$x_{max} = \frac{\pi\ (1+\mu)\ (1-e)\ x_{st}}{4\ \mu\ (1+e)} \qquad .. (9)$$

It may be noted that this expression can be minimized by increasing μ and e. However e is limited by the expression

$$e < \frac{\pi + \mu\ (\pi - 2)}{\pi + \mu\ (\pi + 2)} \qquad .. (10)$$

With this value,

$$x_{max} = \tfrac{1}{2}\, x_{st} \qquad .. (11)$$

However it may be noted that eqn (8) is one particular solution of (7) and possibilities of other maxima can exist.

Another possible solution of (7) is for values of pt so small that $sin\ pt = pt$ and $Cos\ pt = 1$. For this condition also

$$x_{max} = \tfrac{1}{2}\, x_{st} \text{ exists} \qquad .. (12)$$

if eqn (8) is applied.

Results (11) and (12) indicate the possibility of a maximum at a time instant other than these two also.

Some authors[5] have put forward an analysis based on the assumption of two impacts per excitation cycle but time between two successive impacts is not equal. From their analysis it is observed that two equispaced impacts are not possible. However the experiments show that two equispaced impacts do occur giving the sinusoidal displacement function as shown in Fig 3. Their procedure was applied by the authors using microcomputers for the calculations involved. Since the procedure requires extrapolation of graphs to get certain values at resonant conditions it was found that discontinuities in the graph prohibit the extrapolation.

Eqn (8) gives the optimum value of clearance. This value of clearance as shown later is very very small to be obtained and maintained precisely. For example if $x_{st} = 0.01$ mm, $\mu = 0.1$ then $d = 0.25$ mm. To achieve and maintain this value for larger dampers will require a high precision in manufacture and assembly.

Hence this experimental work aims at studying the effect of larger clearances on the effectiveness of the damper.

Experimental set-up

The experimental set-up is fabricated to study the effect of impact damper on a system which is excited by rotary imbalance. Schematic arrangement of the set-up is shown in Fig 4. Photograph of the actual set-up is shown in Fig 5.

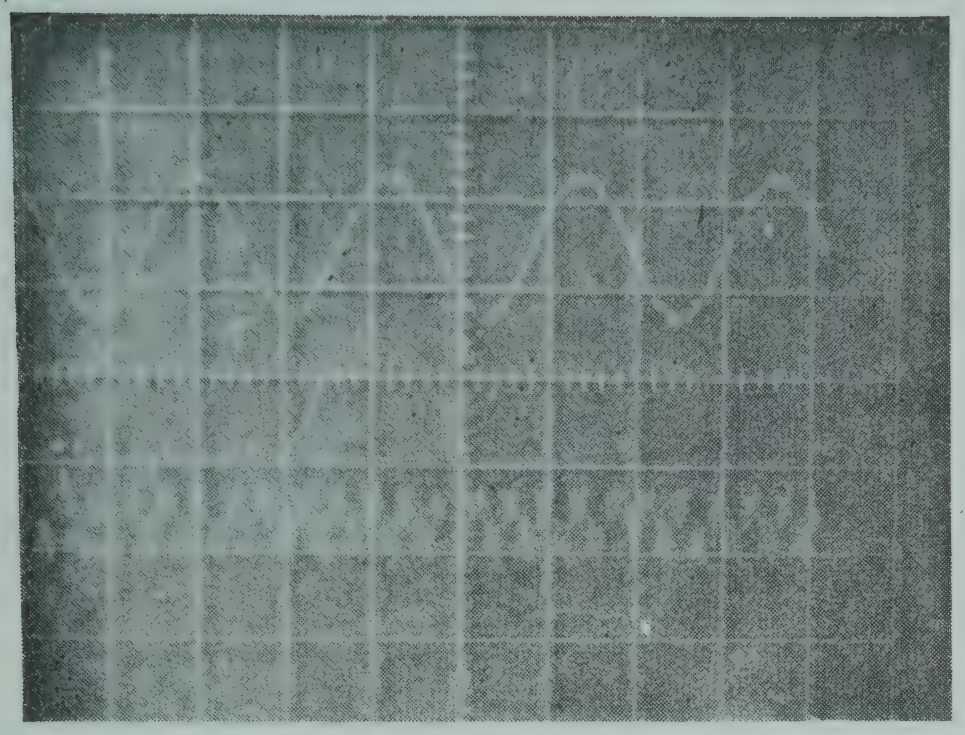


Fig 3
Sinusoidal displacement function of impacts

The apparatus consists of a base plate which is attached to a leaf spring. The spring is 70 times stiffer in vertical direction as compared to its stiffness in horizontal direction. Hence vibrations in horizontal direction can be studied in isolation. A motor is mounted on the base plate. A disc having imbalance about the axis of rotation is mounted on the motor and provides excitation to the system. A box is fabricated on the base plate and provides clearance for the round balls which act as free mass. Clearance is made adjustable by the movement of a screw. Balls are hung by a long thread to avoid any damping effect due to friction as well as any other effects due to gravity. Mass of the main system is kept constant during the experiment while free mass is changed. The experiment is carried out for four different balls masses which are given in Table I.

TABLE I

Free masses and mass ratio

(Mass of main system = 11.5 kg)		
Ball No.	Mass (kg)	Mass ratio
1	0.11818	0.01028
2	0.5	0.04348
3	0.9	0.06974
4	1.35	0.11740

Clearance for each ball is varied from 0.254 mm to 5.08 mm during the experimental programme. Speed of the motor is varied from very low values of speeds through resonance to higher values of speed up to 1400 rpm and above.

Natural frequency of the system is 10.2 Hz, damping factor is 0.001072. Excitation

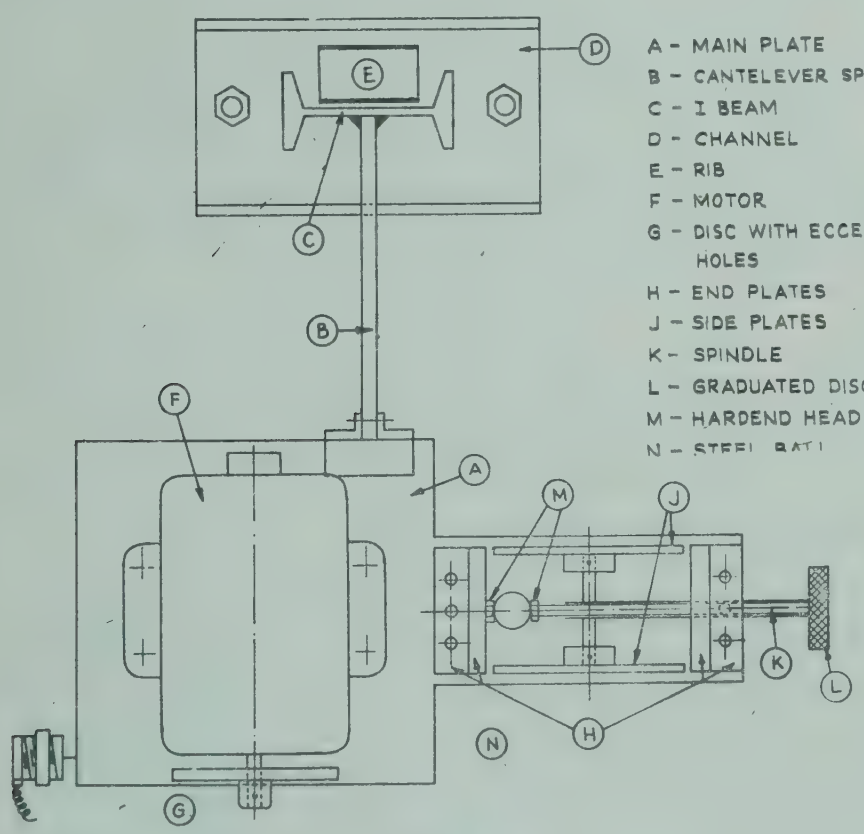


Fig 4
Line diagram for impact damper model

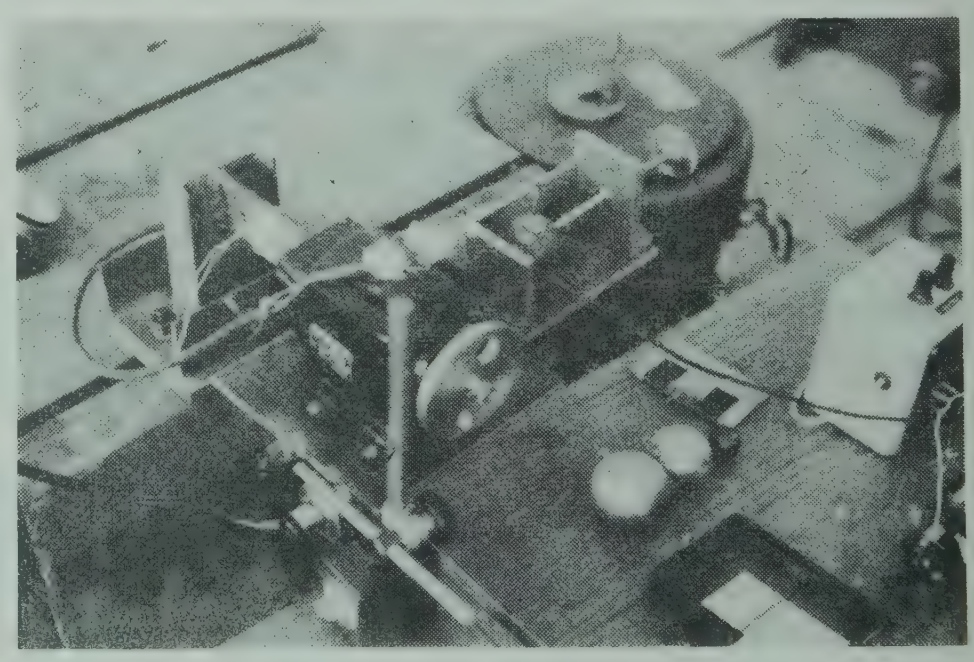


Fig 5
Experimental set-up

force at resonant frequency is 0.238 N and static deflection at resonant frequency is 0.047 mm.

In addition, arrangements were provided to record amplitudes of vibration, shape of the vibration and instant of impact.

Observations and discussion

Using formula (8) and (9) values for optimum clearances and maximum amplitude of vibrations for various mass ratios were obtained and these are given in Table II.

TABLE II

Theoretical values of optimum clearance and maximum amplitude of vibration

Mass ratio	Optimum clearance (d, mm)	Maximum amplitude at resonance (mm)
0.01028	1.219	0.0355
0.04348	0.577	0.0169
0.06974	0.178	0.0055
0.11740	0.106	0.0034

It may be noted that values of clearances are very small particularly for higher mass ratios while amplitude decreases with the increase in mass ratio. Calculations for coefficient e = 0.7 were carried out. Though optimum clearance value remains unchanged amplitude increases by a factor of 3.

Observations made during the experimentation are presented in the form of response curves in Figs 6, 7 and 8. Fig 6 shows the response of the main system without impact damper. Maximum peak to peak amplitude is 2.35 mm at 10.1 Hz. Fig 7 is response curve for the system when ball number 1 is used for various clearance values. Fig 8 is response curve for ball number 4.

Fig 9 shows the response of the system for the different masses but clearance is

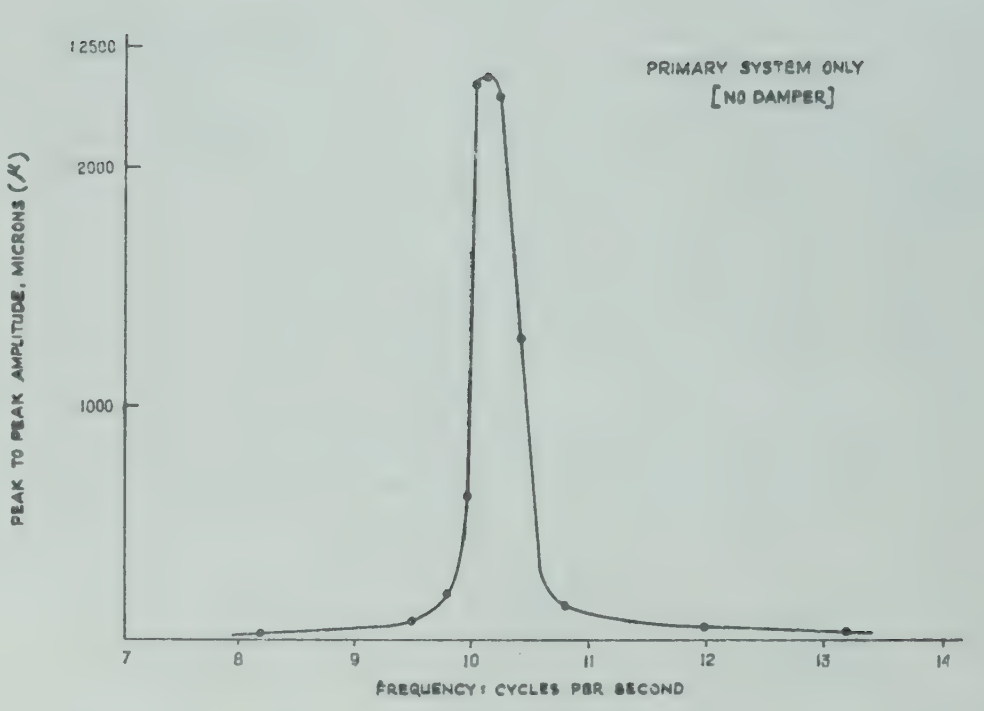


Fig 6
Response of the system without damping

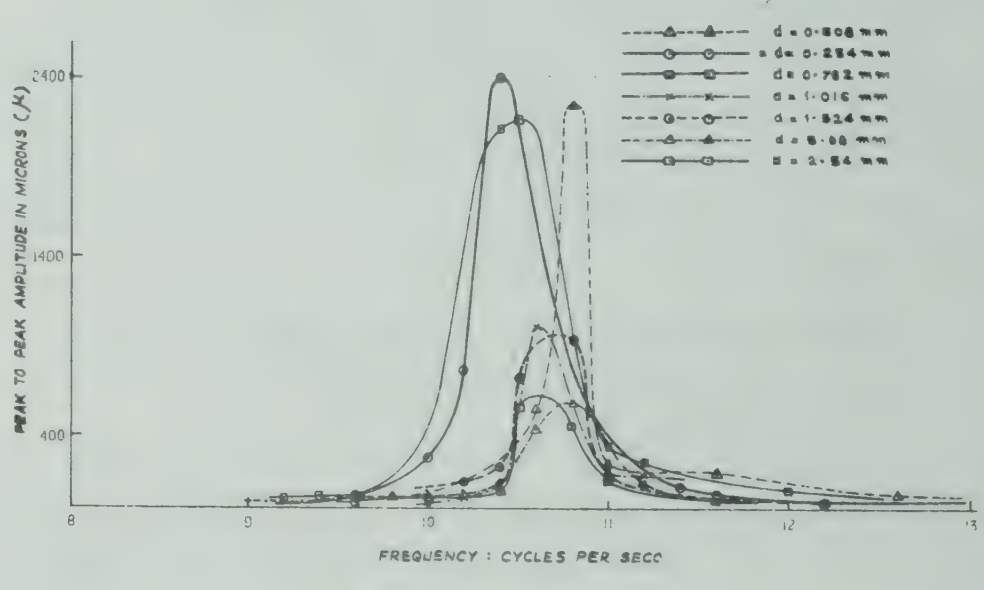


Fig 7
Response of the system for ball No 1

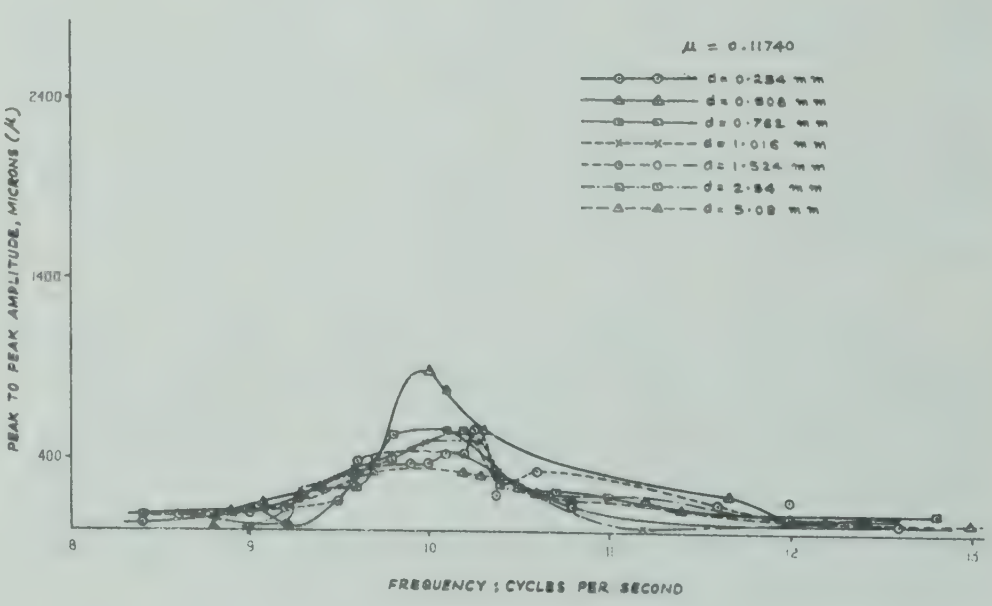


Fig 8
Response of the system for ball No 4

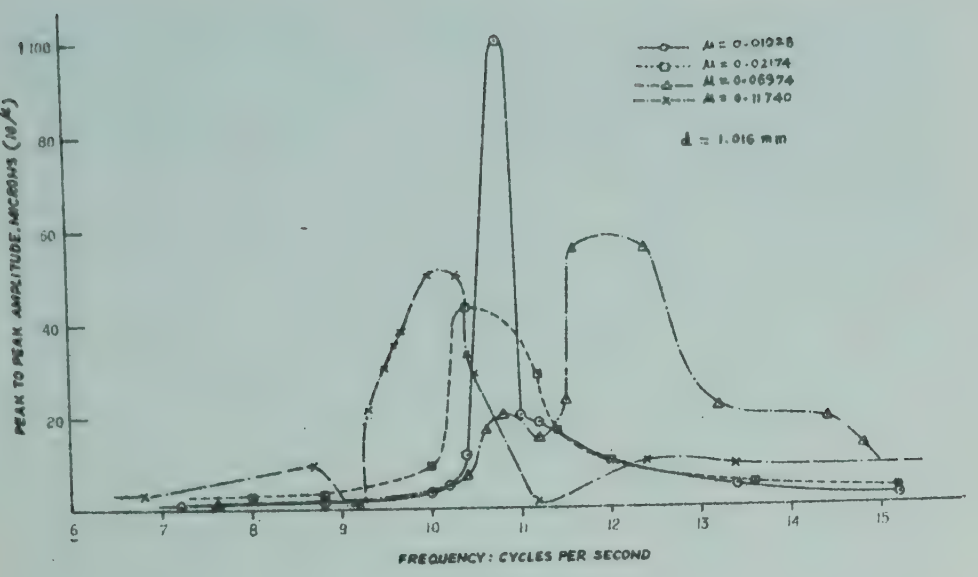


Fig 9
Response of the system for constant clearance

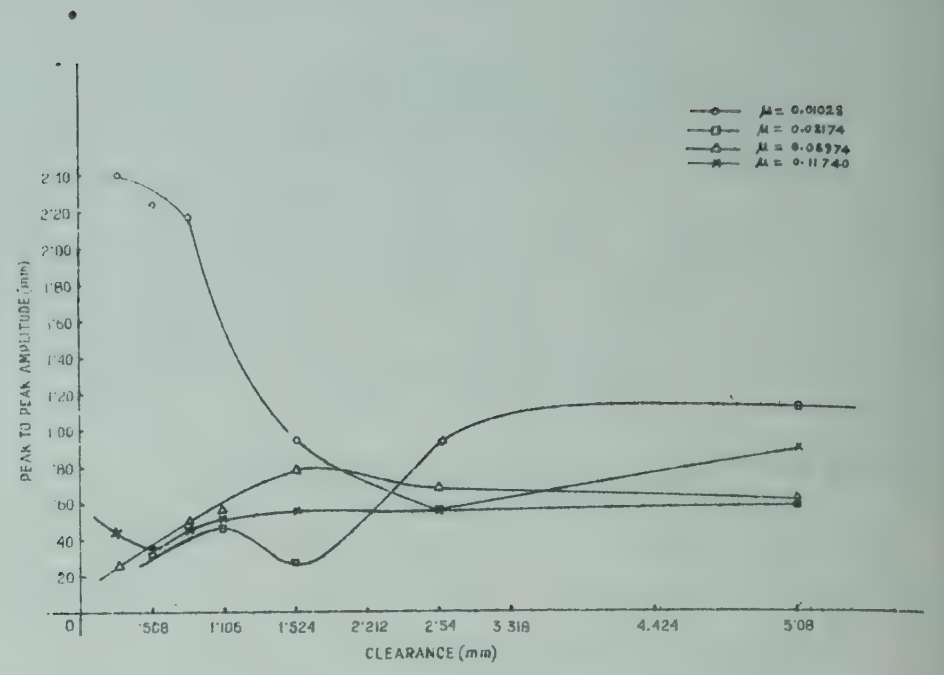


Fig 10
Variation of maximum amplitude with clearance

kept constant. Fig 10 is a graph of maximum amplitude at different clearance values for the four balls. Fig 11 gives variation in optimum clearance with mass.

A small damping present in the main system, and the impact duration are neglected in the theoretical analysis. This gives slight difference between theoretical and experimental values.

Other important observations made during the experimentation are as follows:

(1) For higher free mass values at higher speeds vibrations of the main system increased, they were irregular and damper was very noisy. At low speed values vibrations were again irregular but not noisy.

(2) At speeds on either sides of resonant speed particularly for bigger masses half-beats were observed. Amplitude of vibration at a particular speed increased slowly till maximum and then suddenly dropped down. Full beats were also observed in some cases.

(3) When bigger free mass with large clearance was used it was noticed that energy was not sufficient to push the mass from one side to the other side. This resulted in more than one successive impacts on the same side[6].

(4) Amplitude of vibrations with a damper never exceeds the value of amplitude

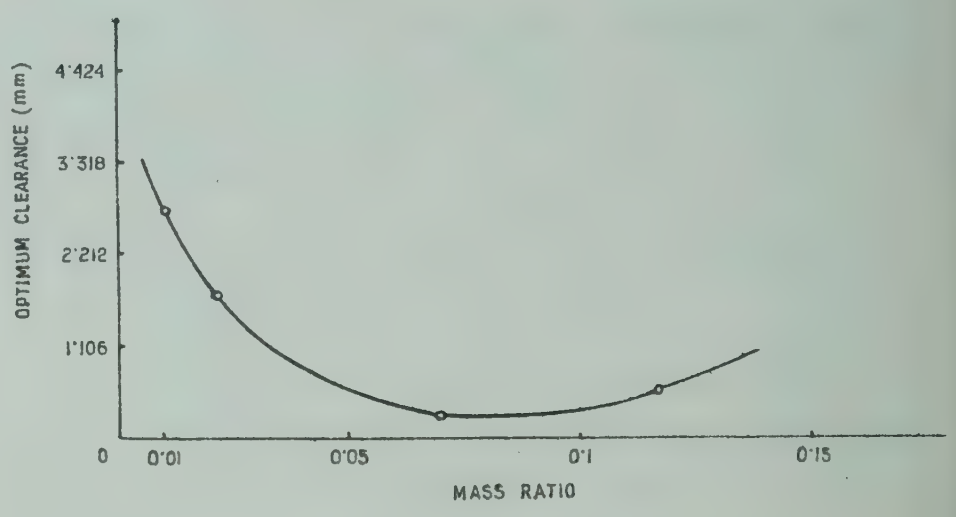


Fig 11
Variation of optimum clearance with mass ratio

of vibration of main system alone. Hence from this consideration impact damper is always desirable.

(5) Maximum reduction obtained in the resonant amplitude during this experimentation was of the order of 10.

Conclusion

(1) Impact damper is an effective device for reducing the amplitude of vibrations particularly in the resonance region.

(2) For each mass there is an optimum clearance that gives the maximum effectiveness.

(3) Optimum clearance is less for the heavier masses, and slight variation from optimum clearance does not affect the

ffectiveness of the damper to any great extent.

(4) As far as amplitude of vibration is considered, damper does not have any adverse effect near resonance region. But adverse effect is observed at higher speeds particularly for heavier free masses.

(5) Noise may be a source of irritation to the personnel.

Acknowledgement

Authors wish to express their thanks to Principal, College of Engineering, Pune; Head of Mechanical Engineering, College of Engineering, Pune; and Dean and Director, Institute of Armament Technology, Pune; for providing facilities to carry out this work.

References

[1] P. Lieber and D.P. Jensen, 'An acceleration damper - Development, design and some applications', *Trans ASME*, Vol 67, p 523 (1945).

[2] C.S. Duckwaid, 'Impact damping for turbine buckets', General Engg Laboratory, General Electric Report No R 55, GL, 108 (1955).

[3] C. Grubin, 'On the theory of the acceleration damper', *Trans ASME, Journal of Applied Mechanics*, Vol 23, No 3, p 373 (1956).

[4] G.B. Warburton, 'Discussion of C. Grubin'. *Trans ASME, Journal of Applied Mechanics*, Vol 24, No 2, p 322 (1957).

[5] M.M. Sadek, 'The behaviour of the impact damper', Proc IME, London, Vol 180, Pt 1, No 38, p 895 (1965).

[6] M.A. Velluswami and F.R.E. Crossiley, 'Multiple impacts of a ball between two plates', *Trans ASME, Journal of Engineering for Industry* Vol 97, Sr B, No 3, p 820, Aug (1975).

(*Continued from page 52*)

OPEN SOLAR REGENERATION OF LITHIUM CHLORIDE BRINE

[5] K.G.T. Hollands, 'The regeneration of lithium chloride brine in a solar still for use in solar air conditioning', *Solar Energy*, 7, p 39 (1963).

[6] A. Kakabayev and M. Golaev, 'Glazed flat surface as a solution regenerator for use in an absorption solar cooling system', *Applied Solar Energy*, 7(4) 80 (1971).

[7] S.C. Mullick and M.C. Gupta, 'Solar desorption of absorbent solutions', *Solar Energy*, 16, p 19 (1974).

[8] F. Kreith, Principles of Heat Transfer, International Textbook Company, Pennsylvania (1965), p 338.

[9] R.E. Treybal, Mass-transfer operations, McGraw-Hill, New York (1968), p 194.

[10] A. Whillier, 'Design factors influencing solar collector performance', Low Temperature Engineering Applications of Solar Energy, ASHRAE, New York (1967), p 27.

[11] G.V. Parmelee and W.W. Aubele, 'Radiant energy emission of atmosphere and ground', *Trans ASHVE*, 58, p 85 (1952).

[12] J.L. Threlkeld, Thermal Environmental Engineering, Prentice-Hall Inc, NJ, p 295 (1962).

DETERMINATION OF THE RELATIVE EFFECT OF THE PROCESS VARIABLES ON OVERCUT IN ECM

D. K. PRAMANIK*

Abstract

Values of overcut produced during electrochemical machining plays a great role in tool designing as because this is the only guiding factor for selecting the size of a tool for producing a particular size in the workpiece. But values of overcut is completely dependent on the values of the process variables. So it is very much beneficial to the production and design engineers to know the relative effect of the process variables on overcut. This paper deals with the determination of the relative effect of the process variables on overcut from the experimental data using a statistical technique.

Introduction

Although the electrochemical machining process has found a wide and, in many cases, competitive application in the aeronautics and space industry where exotic alloys and complicated shapes have to be machined, it must be noted that there are comparatively fewer applications of this process in other industries. The main reasons for this is the considerable cost on capital investment which demands an optimal method of operation for achieving the high machining accuracy and in finding out the optimal working conditions according to various machining tasks. It has been observed many times that the required results are achieved after extensive experiments are carried out on these expensive pieces. The difficulties arise mostly due to tne fact that the size and shape of the tool required to obtain a particular size and shape in the workpiece are not known.

Determination of the size of a tool for obtaining a particular size in the workpiece depends solely on the amount of overcut formed during machining. Now the overcut formed during machining is very much dependent on process variables like gap between electrodes (a), gap voltage (v), electrolyte concentration (c), electrolyte flow rate (f), and electrolyte temperature (t). Effect of these process variables on overcut has been found experimentally[1,2] and an equation has been formed relating overcut with the process variables.

This paper deals with the determination of the relative effect of the process variables on overcut employing statistical technique.

Experimental procedure and results

A series of experiments were conducted by using a square shaped tool having dimension 12 mm x 12 mm made of brass with a central hole of 6 ¢, in order to investigate the following -

(1) Effect of gap between the electrodes on the overcut produced while other parameters, eg, gap voltage, electrolyte concentration and electrolyte flow rate were

*Central Mechanical Engineering Research Institute, Durgapur 9.

kept constant.

(2) Effect of gap voltage on overcut when other parameters were kept constant.

(3) Effect of electrolyte concentration on overcut keeping other parameters constant.

(4) Effect of electrolyte flow rate on overcut keeping other parameters constant.

For each set of experiments, the area machined was accurately measured under a microscope. The overcut produced was calculated by subtracting the tool dimensions from the size of the cavity produced. Table I shows the values of overcut for different combinations of the process variables. For each combination four numbers of experiments were conducted. The values are tabulated below.

During experimentation special care was taken so that the difference of temperature of the electrolyte between the entry and exit of the machining path was kept at a minimum. In practice this value was kept within 0.2℃. As 0.2℃ variation on temperature does not appreciably change the electrolyte conductivity, ie, the amount of metal removal[3], effect of electrolyte temperature has not been considered in the analysis.

TABLE I

Values of overcut for different combinations of process variables

Electrolyte - Aqueous solution of sodium chloride

Electrode gap (mm)	Gap voltage (volts)	Electrolyte concentration (W/V)	Electrolyte flow rate (m/sec)	Overcut, mm Replica 1	Replica 2	Replica 3	Replica 4
0.4	5	8	14.6	1.31	1.25	1.32	1.35
0.5	5	8	14.6	1.62	1.58	1.64	1.6
0.4	6.5	8	14.6	1.56	1.49	1.57	1.66
0.5	6.5	8	14.6	1.66	1.66	1.64	1,80
0.4	5	10	14.6	1.56	1.37	1.40	1.19
0.5	5	10	14.6	1.66	1.66	1.68	1.69
0.4	6.5	10	14.6	1.376	1.52	1.23	1.31
0.5	6.5	10	14.6	1.74	1.69	1.64	1.81
0.4	5	8	20.7	0.475	0.52	0.535	0.46
0.5	5	8	20.7	0.895	0.893	0.93	0.91
0.4	6.5	8	20.7	0.82	1.125	0.76	0.52
0.5	6.5	8	20.7	1.307	1.31	1.24	1.38
0.4	5	10	20.7	0.636	0.75	0.42	0.575
0.5	5	10	20.7	1.21	1.52	1.36	1.17
0.4	6.5	10	20.7	1.62	1.41	1.33	1.6
0.5	6.5	10	20.7	1.68	1.67	1.65	1.39

Analysis of results

Relative effects of different factors which influence the final result of any experiment is quite essential to be found out for proper selection of process variables Yate gives an automatic method of computing all the factorial effect totals without writing down the algebraic expressions for the factorial effects[4]. Table II shows the values of overcut for different treatment combinations

TABLE II

Values of overcut for different treatment combinations

a = electrode gap, b = gap voltage, c = concentration and d = flow rate

	Replica 1	Replica 2	Replica 3	Replica 4	Total
(1)	1.31	1.25	1.32	1.35	5.2
a	1.62	1.58	1.64	1.6	6.44
b	1.56	1.49	1.57	1.66	6.28
ab	1.66	1.66	1.64	1.80	6.76
c	1.56	1.37	1.40	1.19	5.52
ac	1.66	1.61	1.68	1.69	6.64
bc	1.375	1.52	1.23	1.31	5.436
abc	1.74	1.69	1.64	1.81	6.88
d	0.475	0.52	0.525	0.46	1.98
ad	0.895	0.893	0.93	0.91	2.628
bd	0.82	1.125	0.76	0.52	3.22
abd	1.307	1.31	1.24	1.38	5.236
cd	0.635	0.75	0.42	0.575	2.38
acd	1.21	1.52	1.36	1.17	5.26
bcd	1.62	1.41	1.33	1.6	5.96
abcd	1.68	1.67	1.56	1.39	6.3

Applying the Yate's method of solution, results can be obtained as shown in Table III.

The first number in column 6 (effect total) is the grand total G. The succeeding factorial effects come out in the order in which the treatment combinations were written down With factors the process is continued until we reach column 6 (n). Factorial effect means have been obtained by dividing by $2^{n-1}r$, in this case 32. G is divided by $(2^n r)$ or 64 give the mean yield of the whole experiment.

An idea about these factors can be obtained from Table III. Ranking of the factors on the basis of effect means is as

TABLE III
Yate's method of analysis for finding effect total and mean effect

Treatment	Treatment total	(1)	(2)	(3)	Effect total		Effect mean
(1)	5.2	11.64	24.68	49.156	83.12	G	1.298
a	6.44	13.04	24.964	33.964	11.168	A	.348
b	6.28	12.16	14.064	4.284	9,024	B	.282
b	6.76	12.316	19.90	6.884	-2.608	AB	-.0815
c	5.52	5.608	1.72	1.556	5.632	C	.176
ac	6.64	8.456	2.564	7.468	0.4	AC	.012
bc	5.436	7.64	3.664	-0.436	.528	BC	.0165
abc	6.88	12.26	3.22	-2.172	-1.824	ABC	-.057
d	1.98	1.24	1.40	-0.204	-15.198	D	-0.475
ad	3.628	0.48	0.156	5.836	2.6	AD	.081
bd	3.22	1.12	2.848	0.844	5.912	BD	0.184
abd	5.236	1.444	4.62	-0.444	-1.736	ABD	-0.054
cd	2.38	1.648	-0.76	-1.244	6.040	CD	0.188
acd	5.260	2.016	0.324	1.772	-1.288	ACD	-0.04
bcd	5.96	2.880	0.368	1.084	3.016	BCD	0.094
abcd	6.30	0.34	-2.54	-2.908	-3.992	ABCD	-0.124

follows -

Rank 1 : electrode gap

Rank 2 : gap voltage, ie, current density

Rank 3 : electrolyte concentration

Rank 4 : electrolyte flow rate.

Conclusion

Ranking of the process variables as has been found out from the present experimental data may not be identical if any other electrolyte solution other than sodium chloride is used. Because, sodium chloride solution is characterized by its wild cutting properties which are more pronounced at higher current densities. But it is expected that the rankings obtained by using other common electrolytes except NaCl will be of same nature.

Acknowledgement

Author is thankful to the Director, CMERI, for his kind permission to publish this paper.

References

[1]D.K. Pramanik, S.B. Saha and A.K. De, 'Effect of process variables on shape reproduction in electrochemical machining', 6th AIMTDR Conf (1973).

[2]D.K. Pramanik, S.B. Saha and A.K. De, 'Mathematical formulation of overcut in electrochemical machining', Machine Building Industry (Oct 1974).

[3]D.K. Pramanik, T.K. Banerjee and A.M. Chatterjee, 'Electrolyte for ECM (II)', *Indian Machine Tools Journal*, XV(4) (Dec 75/Jan 76)

[4]W.G. Cochran and G.M. Cos, Experimental Designs. 2nd edn, Asia Publishing House (1959).

News and Views

PM addresses CSIR Directors' Conference

Smt Indira Gandhi, Prime Minister, and President of CSIR, inaugurated the 31st Conference of Directors of the National Laboratories of CSIR, held in New Delhi on 25-26 April 1981.

In her brief address Smt Gandhi urged the scientists to look beyond their work and help create an atmosphere which would take the country ahead. Though much had been said about the need for scientific temper in the country, 'we still remain very far from', she remarked.

Taking note of the difficult situation that India and in fact the whole world was passing through, the Prime Minister said, 'India has always geared itself to meet challenges, and it has on most occasions been able to come out stronger rather than weaker'. The present situation in the country demanded the mobilization of all resources, not only the financial ones but also the human as well as natural resources. She emphasized that the challenges were to be faced unitedly and in a constructive manner.

Agreeing that some useful suggestions which had been made could not be implemented for want of resources, the Prime Minister said, 'it was exasperating to see that though we had the capability but for lack of resources of adequate equipment we were not able to follow on all these things'. 'As far as we possibly can, we are trying to help our scientists', Smt Gandhi added.

Earlier, the CSIR's Vice-President Prof S. Nurul Hasan, in his welcome address mentioned the initiatives that had been taken up to further strengthen CSIR. He said that the four laboratories had come back to CSIR from the ministries to which they were transferred in April 1978. Also, the question of transferring back the three museums and ten industrial research associations was being reviewed. An autonomous Centre for Cellular and Molecular Biology had been set up at Hyderabad; a Regional Research Laboratory was being established at Bhopal; the Structural Engineering Research Centre had been bifurcated into two independent laboratories, one each at Roorkee and Madras, the Centre for the Study of Science, Technology and Development had been given the status of an independent centre; and there was a proposal to set up a CSIR Complex at Palampur, Himachal Pradesh. The CSIR Vice-President further said that the Council was building closer linkages with some of the economic ministries and major industries, especially in the public sector.

Referring to the report of the Working Group on Science and Technology, Prof Hasan said that CSIR had been given a major responsibility in many areas on national economic endeavour. In order that the CSIR laboratories make the desired contribution a review of all existing projects will have to be carried out. He hoped that with greater cooperation between CSIR, DGTD and

NRDC, the country's import bill on technology could be reduced. He also stressed the need for devoting greater attention to basic research, especially in frontier and interdisciplinary areas, and for this the CSIR's linkages with academic institutions were to be strengthened.

Prof Hasan assured the scientists that the Government was deeply conscious of the need to improve the working and living conditions as well as the career prospects of the scientists.

The Chairmen of the Coordination Councils of CSIR presented the major achievements in their respective groups.

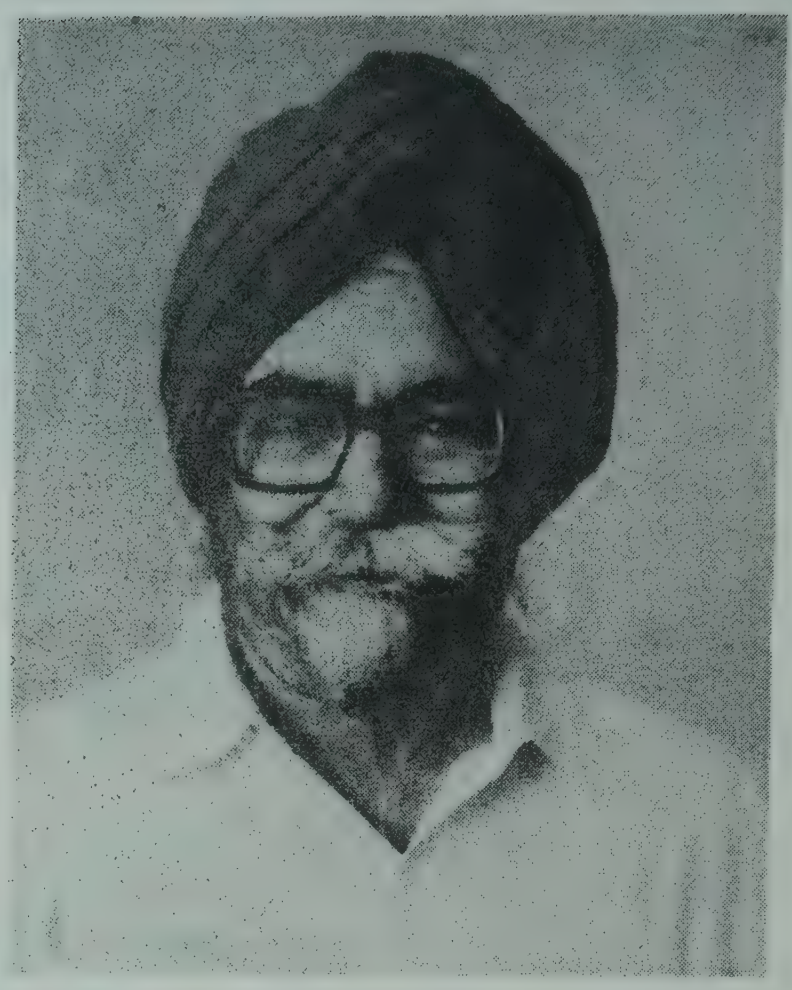
Among the items discussed at the two-day conference were : Functioning of Executive Committees, Research Advisory Councils, and Coordination Councils; Reviewing of performance of laboratories; Induction of new talent; Revision of procedures for creation of posts, and completion of probationary period; Simplification of recruitment procedures and merit promotion scheme; Distribution of royalty/premia; Housing and medical facilities; and Setting up of arbitration tribunals and joint consultative machinery.

Before inaugurating the conference Prime Minister declared open the CSIR Science Centre which in fact was the venue for the conference. She also released the first volume of a monograph 'Ores & Minerals of India-Benefication and Agglomeration Techniques for Industrial and Economic Exploitation' brought out by the National Metallurgical Laboratory (NML), Jamshedpur.

Dr G.S. Sidhu appointed DGSIR

Dr G.S. Sidhu has been appointed Director General, Scientific and Industrial Research. He is also Secretary (CSIR Affairs) to the Government of India in the Department of Science and Technology.

Dr Sidhu took over from Prof M.G.K. Menon on 5th May 1981.



Well known for his contributions in the field of industrial organic chemicals, drugs and pharmaceuticals, pesticides, and wood chemistry, Dr Sidhu was Director of the Regional Research Laboratory, Hyderabad, from where he retired on 31 January, 1981.

MERADO designs domestic gas stove

The Mechanical Engineering Research and Development Organisation (MERADO), Ludhiana, has developed an improved domestic gas stove. The tests conducted as per the Indian Standards test codes have given indications of marked improvement in thermal efficiency for Merado designed stove over that of the models currently available in the market.

The Merado designed gas stove gives a completely blue and stable flame. The gas consumption rates have been optimised keeping in view the functional requirements of the domestic stove.

The technical know-how has been transferred to Messrs Selection Appliances Private Limited, Ludhiana who have set a plant

for the production of 60,000 LPG domestic gas stove per year based on Merado design. Merado has also rendered its technical services to this firm for preparation of the detailed project report, machinery selection, plant layout, design of tooling, design of jigs and fixtures and two special purpose automatic machines required for the production of the gas stove.

New sponge iron production process

The Central Fuel Research Institute, Dhanbad, has developed a new process for the production of sponge iron. While known technologies involve reduction of iron ore by gases, generated by gasification of coal or char, in the new process no external reductant is necessary. The process consists of mixing iron ore fines of suitable quality with non coking coal usually 15 to 35 per cent of the iron ore. Water is then added to the mixture to make a paste, with addition of a small quantity of pasticiser, if required. The mix is then briquetted or extruded to desired shape. The mould shapes are then charged into suitable furnace in three different zones with temperatures ranging from 300° to 1100°C. The moulded shapes during passage through the furnace undergo a series of sequential reactions namely induration, reduction and incipient fusion. Sponge iron is then formed and is progressively cooled and discharged into a closed chamber with reducing atmosphere. The metalisation of the sponge iron produced varies from 70 to 92 per cent, the carbon content being only in the range of 0.22 to 1 per cent.

Beside reduction being intrinsic, the process is self supporting in so far its fuel requirement is concerned. The treatment of the performed shapes generates 12,000 to 15,000 cft of gas per tonne of sponge iron produced. The calorific value of the gas is 220 BTU per cft. The quantity of gas generated, is more than sufficient for sustaining the required temperature gradient in the furnace wherein direct production of sponge iron takes place, involving induration, reduction and incipient fusion - all in one step.

Engineering exports in 1980-81

Exports of engineering products from India were estimated at rupees 850 crores in 1980-81 against rupees 675 crores in the previous year, said Shri Manmohan Singh, President of the Association of Indian Engineering Industry, while talking to newsmen on 8th April 1981. Shri Singh also said that exports were getting more and more difficult. Industrial production was falling. The power situation was going from bad to worse and noncooperative attitude of the labour was also proving a great hinderence to production.

Export target raised

The Engineering Exports Promotion Council arranged a series of talks between the exporters representing various segments of engineering industry and the Commerce Ministry to consider India's engineering export target during 1981-82. Following these meetings the export target has been revised to rupees 1200 crores. At the beginning of the current financial year, the target was fixed at rupees 1150 crores.

SAIL's production goes up in 1980-81

The Steel Authority of India has closed 1980-81 with a happy note. The production of saleable steel was 4.746 million tonnes compared to 4.592 million tonnes achieved in 1979-80. The 1980-81 production was however about 10 per cent less than the target.

The total domestic supply of saleable steel during 1980-81 was around 8.54 million tonnes as against 8.28 million tonnes in 1979-80, an increase of three per cent. This increase was possible due to additional production at mini-steel plants and sales of imported steel.

Encouraged by the 1980-81 production, SAIL has fixed a target of 5.73 million tonnes of saleable steel for 1981-82.

Soviet help for building coal washery

The Soviet Union has agreed to take up construction of a large size coal washery plant in Jharia coal field by 1984-85. On completion, the plant will produce two to three million tonnes of washed coal per year for the steel plants. This agreement has been reached during the visit of the Union Minister for Energy, Shri A.B.A. Gani Khan Chowdhury, to the USSR in June 1981.

Robot usage

The British Robot Association, founded in 1977, held its first press conference in the second week of April 1981, with the object of revealing the details of a study it has concluded about robot usage and to announce an exhibition and conference in Brighton in mid May.

BRA defines an industrial robot as 'a reprogrammable device designed to manipulate and transport parts, tools or specialised manufacturing implements through variable programmed motions for the performance of specific manufacturing tasks'. Even at this relatively simple level of definition, the UK manufacturing industry still seems to be having difficulty in coming to terms with the concept.

UK has presently 371 installations, and is behind the USA, Sweden, Germany and Italy, and a long way behind Japan, where there are 16 times as many as British installation - although the definition of the robot may be different.

However, according to Tom Brock, the Executive Secretary of the BRA, the heartening aspect of the UK installations is that they are dotted in ones or twos over perhaps 180 users. In Italy the robots are all in operation in Fiat, Alfa Romeo and Olivetti. Britain thus has a potentially good base upon which to expand. Mr Brock believes robot usage will grow impressively in UK, perhaps 40 to 50 per cent per annum. Arc welding and assembly will be the key growth areas.

Mr Brock also said that Britain is now passing through a phase similar to that experienced in West Germany in 1973-74 when there was a great Government backed programme. Following that effort there are now 1133 installation. In UK, funding by the Department of Industrial Robotics is running at about £ 1.3 million a year, and may reach as much as £ 2.7 million a year. Among the bodies that DOI is presently supporting are the British Robot Association, Production Engineering Association, and the National Engineering Laboratory. Some joint research projects with industry are also financed.

SOME EFFECTS OF ELECTROLYTE FLOW MODE ON THE ANODE SHAPE IN ECM

V.K. JAIN* AND P.C. PANDEY**

Abstract

Finite element technique has been employed in this paper to analyse the effects of three different modes of electrolyte supply on the form, accuracy and nature of the surface produced in electrochemical hole sinking operation. The paper also presents computational aspects of the analysis.

Nomenclature

A_v : Applied voltage
a_o : Overcut in transition zone
C_e : Specific heat of electrolyte
E : Electrochemical equivalent
E_v : Effective voltage
F : Faraday's constant
F_F : Feed rate
I : Functional
J : Current density = E_vK/Y
K : Electrolyte conductivity
r : Radius
t : Machining time
T : Temperature
V : Electrolyte flow velocity
W : Width of anode
x : Distance in electrolyte flow direction
Y : Interelectrode gap
η : Machining efficiency
ρ : Density
α : Temperature coefficient of conductivity
α_v : Void fraction

Subscript

e : electrolyte or equilibrium
i,j : node numbers
m : work material
o : initial condition
t : condition at time 't'

* M.N.R. Engineering College, Allahabad
** University of Roorkee, Roorkee-72.

Introduction

Electrochemical machining (ECM) is defined as an accelerated and controlled anodic corrosion process[1] in which the anode is dissolved electrochemically to obtain the desired shape and size. For this purpose, a suitable electrolyte is pumped at high velocity through the inter-electrode gap (IEG) (Fig 1). The electrolyte removes reaction products, takes away the generated heat, does not permit deposition of metallic ions on the tool, etc. Low voltage and high direct current is passed through the IEG during cutting. This process has found wide application[2] in industries such as aerospace, nuclear, automobiles, missiles, turbines, rail-road, etc, because of its easy adaptability to different kinds of operations like turning, electrochemical grinding, boring (ECB), drilling (ECD) and wire cutting, etc. It offers advantages like, high metal removal rate (MRR) irrespective of strength and other mechanical properties of the work material, good surface finish, no residual

stresses in the machined component, etc. However, the authors feel that its applicability could further be enhanced if the basic process of electrochemical metal removal is studied in depth to include the effects of a number of interacting parameters and inherent inaccuracies associated with existing analytical models, used for tooling design in ECM.

Preliminary investigations by the authors have shown that the mode of electrolyte supply (ie, side flow, inward flow, outward flow, etc) has significant effect on the form accuracy and the surfaces produced. This paper makes use of the finite element technique (FET) to analyse the effects of the three different modes of electrolyte supply on the accuracy of holes produced in EC hole sinking operation. Temperature, current density and electrolyte flow velocity distribution within the IEG has also been computed and the detailed scheme of computation discussed.

Theory

Fig 1 shows the EC hole sinking operation for three different modes of electrolyte supply. From classical ECM theory equilibrium gap (Y_e) could be obtained as:

$$Y_e = E.E_v.K/F.\rho_m.F_F \qquad .. (1)$$

Eqn (1) gives inaccurate results because it is based on a number of simplified assumptions, viz, constant electrolyte conductivity, negligible effect of void fraction, etc. For accurate computation, the conductivity K should be calculated from eqn (2)

$$K = K_o(1 + \alpha \Delta T)\ (1 - \alpha_v)^{n'} \qquad .. (2)$$

where, $n' = 1.5$ when the voids are uniformly distributed. The temperature distribution within the IEG can be computed from the eqn

$$\frac{dT}{d} \quad \frac{J^2}{K.V.\rho_e\ C_e} = A_c.K \qquad .. (3)$$

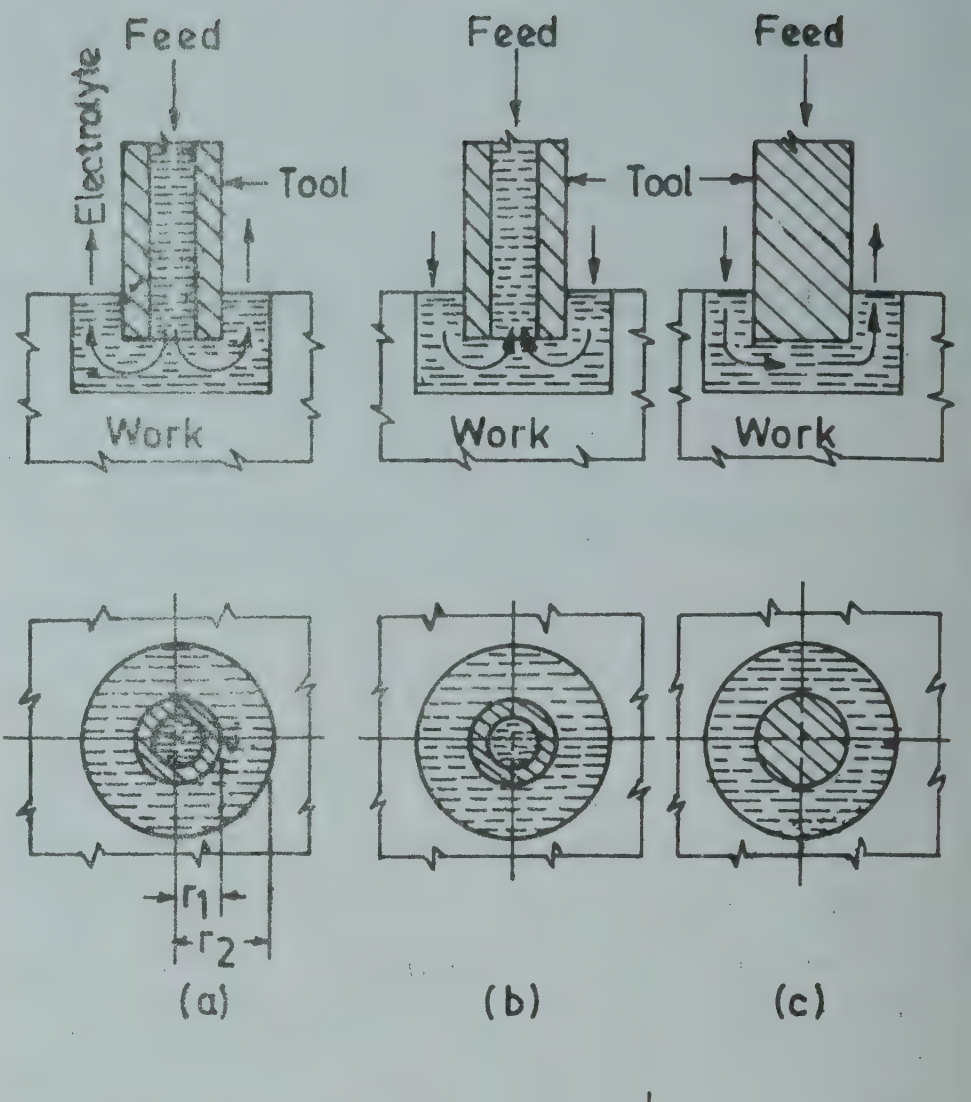


Fig 1
Schematic diagram showing electrochemical hole sinking operation: (a) outward flow (b) inward flow (c) side flow (d) unidimensional discretization of interelectrode gap

In order to evaluate the IEG at time t use of eqn (4) has been recommended by the authors[3].

$$Y_t = Y_o + (C' - F_F)\ \Delta t \qquad .. (4)$$

where, $C' = \eta JE/E\rho_m$. Eqn (4) would give correct values only if Δt is small and the feed rate has correctly been estimated.

For plane parallel IEG, the electrolyte flow velocity distribution is normally

estimated from the condition of volume constancy and neglecting the frictional effects. It is also assumed that the width W remains unchanged. Thus, we can write

$$V_i Y_i W = V_{(i+1)} Y_{(i+1)} W \quad .. (5)$$

However, in case of complex shaped IEG, eqn (5) would not give an accurate velocity distribution at any point in the gap. In such cases use of conformal mapping technique[4,5] could be useful.

Finite element analysis

The authors[6] have demonstrated the advantages of the application of FET to ECM tool design problems and have extended its use to the present case. The assumptions under which the present analysis applies are:

(i) Effects of anodic film, pH of electrolyte solution, intergrannular attack, microstructure, change in valency of work material during ECM, etc, are negligible.

(ii) Heat loss due to conduction and convection to the electrodes is negligible[7]. It is further assumed that reversible heat, heat due to chemical reaction, viscous heat and irreversible heat generated are small and hence negligible.

(iii) Metal removal is due to EC dissolution only.

(iv) Electric current lines flow perpendicular to the work and tool but for electric resistance computation the chordal distance between the two stations is considered.

$$\delta I = \int_{x_i}^{x_j} \frac{dT}{dx} \delta T - \int_{x_i}^{x_j} \frac{dT}{dx} \left(\delta \frac{dT}{dx}\right) dx = 0 \quad .. (6)$$

which on simplification reduces to

$$X = D.H. = K_m T^e \quad .. (7)$$

K_m is conductance matrix, T^e is element temperature and X is a column vector. For the case of ECD, it can be shown that

$$H = \frac{2 \pi K x_{ji} E_v^2}{ln (r_2/r_1)} \quad \text{and}$$

$$D = \frac{1}{(r_2^2 - r_1^2) V . \rho_e . C_e}$$

$$K_m = \int B^T B dx = \begin{bmatrix} 1 & -1 \\ -1 & 1 \end{bmatrix}$$

Substitution of the boundary conditions and assembly of the resulting equations[8] would yield a set of sparse, banded and symmetric matrix. The set of simultaneous equations could be solved by Gaussian elimination technique[9]. The computational procedure for model SGFET-11 used in this paper is given in Fig 2.

Experimental

ECD tests were performed on a set-up using cylindrical brass tools, mild steel workpieces and NaCl solution in water as electrolyte. During experimentation the input voltage across the electrodes was found to vary due to inherent characteristics of the process. Therefore, it was measured regularly at the intervals of about 300 seconds. The voltage which prevailed for about 66 per cent of the machining time during a cut was taken to be the true value of E_v. Machined anode shapes were measured using a tool maker's microscope having a measuring accuracy of 0.01 mm and using the replica technique. Tool-corner radii were measured using projection microscope.

Results and discussion

Fig 3 shows a comparison between the analytical and experimental temperature values[10] and a good correlation can be seen to exist between the two. Discrepancy in some of the cases is mainly due to the superfluous assumption of 100 per cent machining efficiency. In actual practice it is normally below 100 per cent.

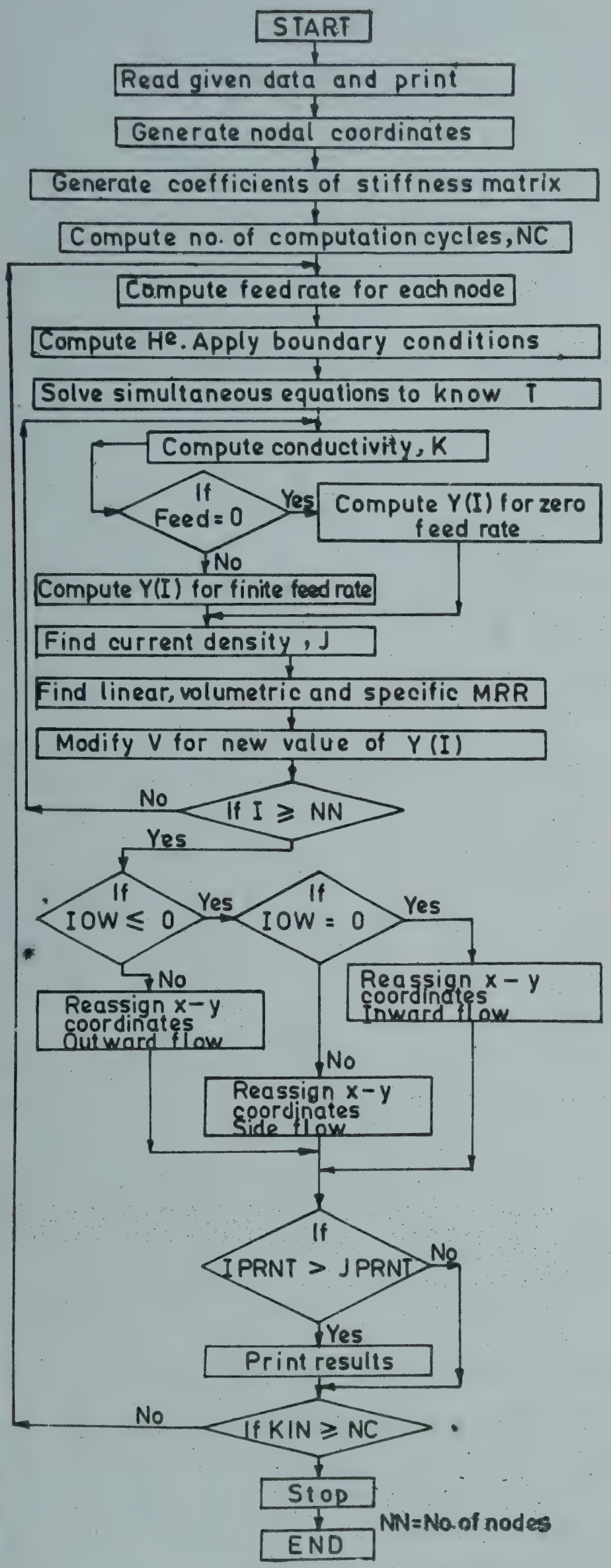


Fig 2
Computational scheme used in model SGFET-11

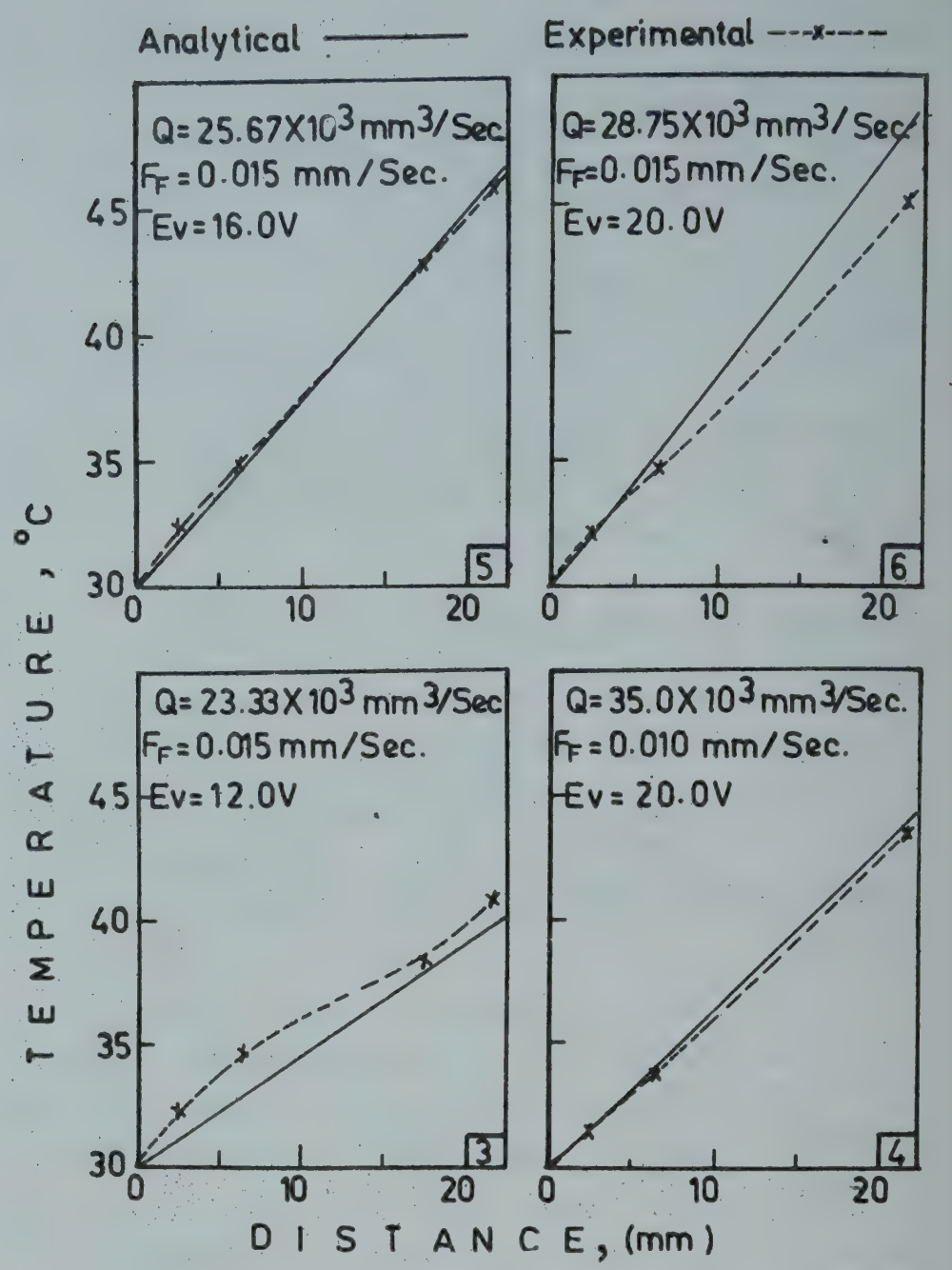


Fig 3
Comparison of analytical and experimental electrolyte temperature values

Fig 4 shows the anode profile obtained analytically and experimentally. The discrepancy between the two can be attributed to the assumed mean machining efficiency of 85 per cent, change in anodic dissolution valency with machining time[11] and lack of complete information about electrolyte flow specially near the corners. Also, the value of E_v varies in actual practice. However, the error due to these factors is not large and the validity of the FE analysis is thus established.

Fig 5 shows the surface generation during ECM for three different modes of electrolyte flow. It also gives variations in electrolyte temperature and current density. It is thus evident that the mode of electrolyte flow has a significant impact

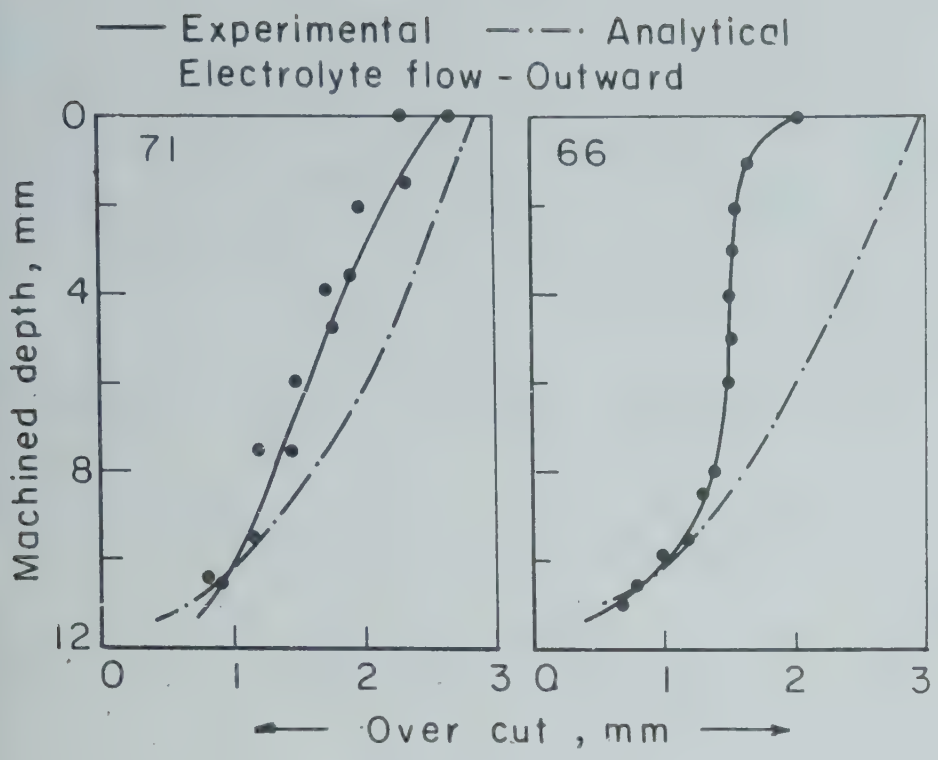


Fig 4
Comparison of analytical and experimental anode profile

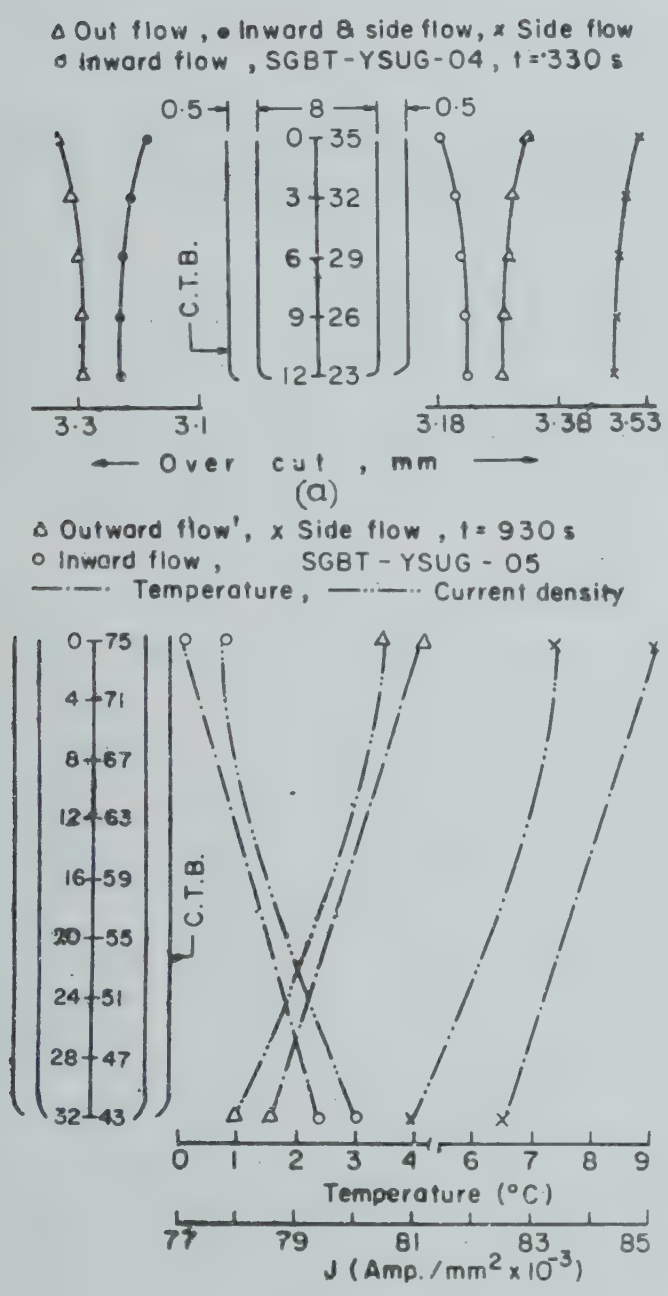


Fig 5
Effect of the mode of electrolyte flow on (a) anode shape, (b) temperature distribution and current density

upon the tolerances obtained during ECD. Further, it can be seen that inward mode of electrolyte flow yields minimum dimensional variations. The anode shape computation (Fig 4) in the present case is based on the assumption that the overcut in transition zone follows the regression equation (8) based on experimental data[12].

$$a_o = 0.10645\ Y_e + 0.04811 \qquad .. (8)$$

It has been observed during experimentation that in several cases of machining with radial outward flow the anode surface had striations present on it (Fig 6). This has been explained by Fluerenbrock[13] by sonic velocity. On the other hand, Cole[14] has attributed the formation of striations to a certain combination of electrolyte pressure and flow rate, not yet fully analysed. However, Opitz[15] has explained the presence of striations by the cavitation theory.

Thus, it is obvious that a knowledge of the electrolyte flow velocity distribution within the IEG is essential for accurate tooling design. Hence more work is in progress in this direction.

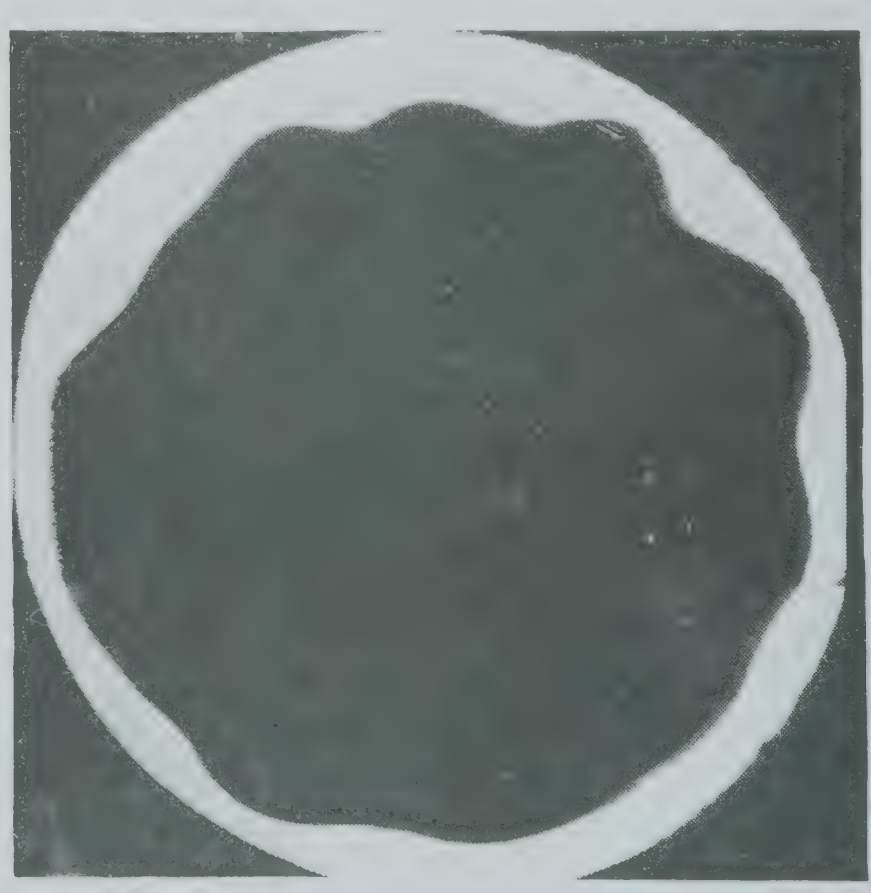


Fig 6
Magnified view of electrochemically drilled hole showing striations

Conclusion

From the above it is evident that for better dimensional precision, inward mode of electrolyte flow should be used. For anode shape prediction in ECM, model SGFET-11 based on finite element analysis gives accurate results. It is further concluded that the mode of electrolyte supply has considerable influence on the temperature distribution, current density, electrolyte flow rate and the rate of metal removal. A proper electrolyte flow rate, therefore, should be chosen to avoid the striations formation on the anodes.

References

[1]J.E. Bannard, 'Electrochemical machining', *Jour Appl Electrochem*, 7, pp 1-29 (1975).

[2]M.A. LaBoda, et al, 'Intricate pattern ECM on ferrous alloys,' *Jour Electrochem Soc*, 122, pp 1489-91 (1975).

[3]V.K. Jain and P.C. Pandey, 'An analysis electrochemical wire cutting process using finite element technique,' Proc 20th Int MTDR Conf, pp 631-36 (1979).

[4]K. Kawafune, 'Study on shapes processed by ECM', *Annals CIRP*, 17, pp 345-52 (1968).

[5]S.W. Yuan, **Fundamentals of fluid mechanics**, Prentice Hall of India (1976).

[6]V.K. Jain and P.C. Pandey, 'Design of ECM tooling using finite element technique,' Proc 8th AIMTDR Conf, pp 566-70 (1978).

[7]V.K. Jain and P.C. Pandey, 'On the heat transfer model for ECM using finite element technique,' Proc 5th Nat Heat & Mass Trans Conf, Hyderabad (1980).

[8]C.S. Desai et al, **Introduction to the finite element method**, East West Press, New Delhi (1977).

[9]L.L. Bhirud, **Matrix operations on the computers**, Oxford & IBH, New Delhi (1975).

[10]S.M. Bhatia, 'Effects of electrolyte conductivity on ECM process,' M Tech thesis, IIT Bombay (1971).

[11]P.J. Moir et al, 'Some effects of electrolyte flow rates on the electrochemical machining process,' Proc 16th Int MTDR Conf, pp 275-81 (1976).

[12]V.K. Jain, 'Analysis of ECM process for anode shape prediction,' Ph D thesis, University of Roorkee, Roorkee (1980).

[13]F. Fluerenbrock et al, 'Compressibility effects in electrochemical machining,' *Trans ASME*, Sr B, Vol 98, pp 423-30 (1976).

[14]R.R. Cole, 'Basic research in electrochemical machining - present status and future directions,' *Int Jour Prod Res*, 4, pp 75-85 (1965).

[15]H. Opitz, 'Electrochemical machining', Proc Int Prod Res Conf (ASME), pp 225-31 (1963).

ANGULAR DEFOCUSING OF PARABOLOIDAL REFLECTORS WITH OBTUSE RIM ANGLE AND TRUNCATED BOTTOM

M. PRASAD AND S.K. MAZUMDAR*

Abstract

Effect of angular defocusing on image contour and energy characteristic of paraboloidal reflectors having rim angle greater than 90° and with bottom truncated from above the focus is investigated theoretically applying ray analysis in accordance with the laws of geometrical optics. A distinct change is noticed in the image contour for a sagittal circumference in focal plane of the paraboloid under consideration, with angular defocusing, when compared to a paraboloid having rim angle less than 90°. The effect of angular defocusing on energy collection efficiency of the reflector-receiver system for the proposed paraboloid is not much severe and the system is suitable to concentrate solar energy for medium temperature power plant and process heating applications. Moreover, the receiver in the present case, being located at the bottom, can be easily aligned with its paraboloid without causing any shading of the reflector surface by the absorber or by its piping and supporting mechanism.

Nomenclature

C	:	a constant
f	:	focal length of the paraboloidal reflector, mm
N	:	number of sub-zones on reflector surface
Q_o	:	energy entering the receiver aperture in focal plane with perfect aiming ($\beta = 0$)
Q_β	:	energy entering the receiver aperture in focal plane with defocusing angle β
r	:	radius of receiver aperture in focal plane, mm
R	:	radius of reflector surface in an afocal plane, mm
R_a	:	reflector aperture radius, mm
l, m, n	:	direction cosines
$\vec{i}, \vec{j}, \vec{k}$	:	unit vectors along, X, Y and Z axes respectively
β	:	defocusing angle, deg
η_β	:	concentrator-receiver efficiency for defocusing angle β
θ	:	rim angle of the paraboloid, deg.

*Central Mechanical Engineering Research Institute, Durgapur 9.

Introduction

Paraboloidal reflectors are used to concentrate solar energy for high temperature applications such as in solar furnace and power plants[1-5]. The principle of design demands the incident rays to remain parallel to the paraxial axis which in turn requires precise tracking of the sun by the paraboloid. Nevertheless, this requirement is not fulfilled always due to practical limitations and the incident rays are often inclined to the paraxial axis. This phenomena is known as angular defocusing of the paraboloidal reflector.

The rim angle of a paraboloidal reflector is the angle made by a line joining the focus with any point on aperture circumference with paraxial axis (Fig 1). The rim angle may be acute, right angle or obtuse depending upon whether the aperture dia is less than, equal to or greater than four times the focal length, respectively.

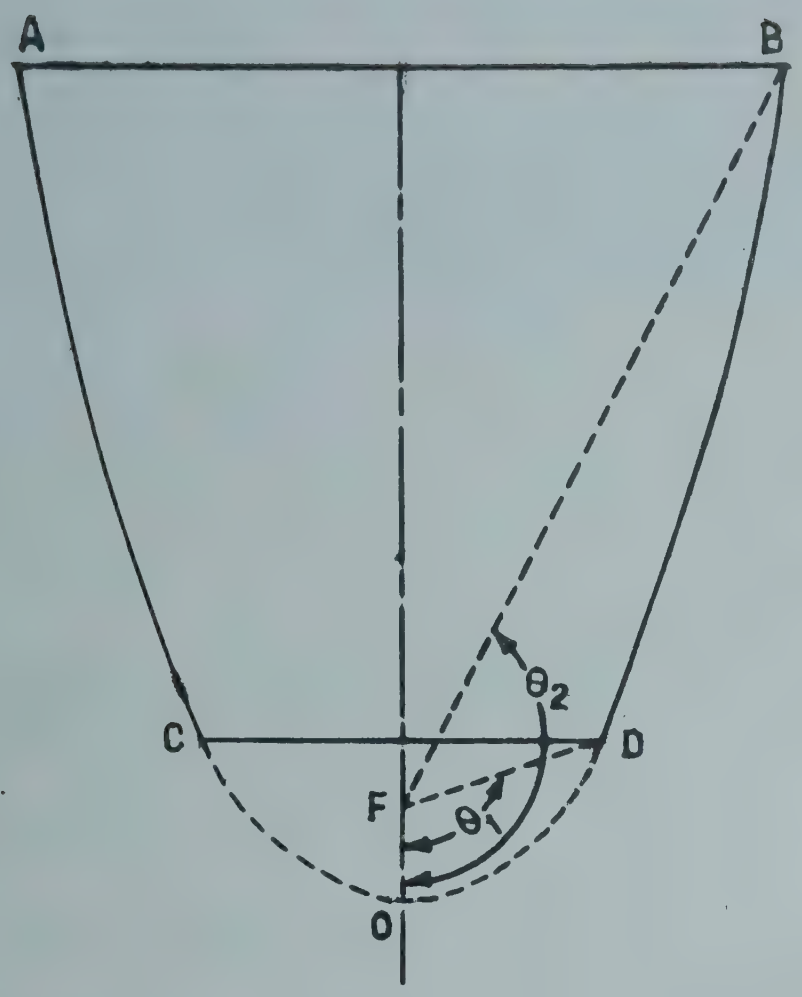


Fig 1
Paraboloidal reflector with obtuse rim angle and truncated bottom

Paraboloids with relatively higher focal lengths have been considered for solar furnaces[1-4] primarily due to the fact that they lead to high values of concentration ratio for a given rim angle. Also the solar concentration capability per unit area of the reflector surface added by increase in rim angle goes on diminishing for every increase in rim angle.

The above philosophy leads to the conclusion that it would be preferable to employ paraboloids with larger focal lengths and smaller (acute) rim angles for the concentration of solar energy for any high temperature application. Nevertheless, there are other important factors too, which must be given due consideration before deciding the specification of the paraboloid for applications other than solar furnaces, such as those for power plant and process heating. The power plant application of solar energy has become all the more important in view of acute energy crisis currently faced by human civilization.

The overall efficiency of a solar power plant is the product of the thermal efficiency of the heat engine and the collection efficiency of the solar collector; while the former will increase with increasing temperature of the working fluid, ie, with the increasing concentration ratio of the solar concentrator-receiver system, the latter will have a reverse trend. In general, the reduction in solar collection efficiency would be more pronounced than improvement in heat engine efficiency when working temperature is raised from moderate values. Therefore, solar concentrating arrangements when used for power plant applications are likely to have better cost effectiveness if working temperatures are kept relatively low, ie, moderate concentrations are used.

Apart from all that has been said above, acute rim angle of a paraboloidal reflector presents difficulties in making proper alignment between concentrator-receiver system and also leads to the shading of the reflector surface by the receiver, its piping and supporting mechanism. The problem of shading is particularly important with respect to power plant application in view of relatively large size of the receiver and its piping. However, these problems are completely solved if one uses paraboloidal reflector with obtuse rim angle and truncated bottom where the receiver is attached to the bottom of the reflector.

As mentioned earlier, angular defocusing of a paraboloidal reflector produces a highly adverse effect on energy concentration characteristics in the focal and afocal planes of the reflector. While there exists some literature on the effect of angular defocusing on image contour and energy distribution in the plane of interest for paraboloidal reflectors having acute rim angles[1-4], no such work has been reported, so far, for paraboloidal reflec-

ors with obtuse rim angle and truncated ottom.

The aim of the present paper is to ana-yse the effect of angular defocusing on mage contour and energy characteristic in he focal plane of a paraboloidal reflec-or having obtuse rim angle and with bottom runcated by an afocal plane above the ocus using ray analysis in accordance with he laws of geometrical optics.

nalysis

The paraboloidal reflector under con-ideration is shown in Fig 1. Following ssumptions are made :

(i) the paraboloid is geometrically per-fect

(ii) all the incident rays are parallel to each other,

(iii) the reflection takes place accor-ding to the laws of geometrical optics.

Following cartesian co-ordinate system s used for the analysis (Fig 2). Point 0 coincides with the apex of the paraboloid nd Z axis with its paraxial axis. Posi-tive Z is towards the apperture. X and Y xes are chosen such that angular deflec-tion β of the incident ray IP always lies towards positive X in the meridional plane XOZ.

Then, for any point P (x_o, y_o, z_o) on he reflector surface, we have

$$x_o^2 + y_o^2 = 4\,fz_o \qquad .. (1)$$

The unit vector along the incident ray IP, $\vec{n}_i$, is

$$\vec{n}_i = -\sin\beta\,\vec{i} - \cos\beta\,\vec{k} \qquad .. (2)$$

where $\vec{i}$, $\vec{j}$ and $\vec{k}$ represent unit vectors long X, Y and Z axes respectively.

Similarly, the unit vector along the eflected ray PR, $\vec{n}_r$, is

$$\vec{n}_r = l\vec{i} + m\vec{j} + n\vec{k} \qquad .. (3)$$

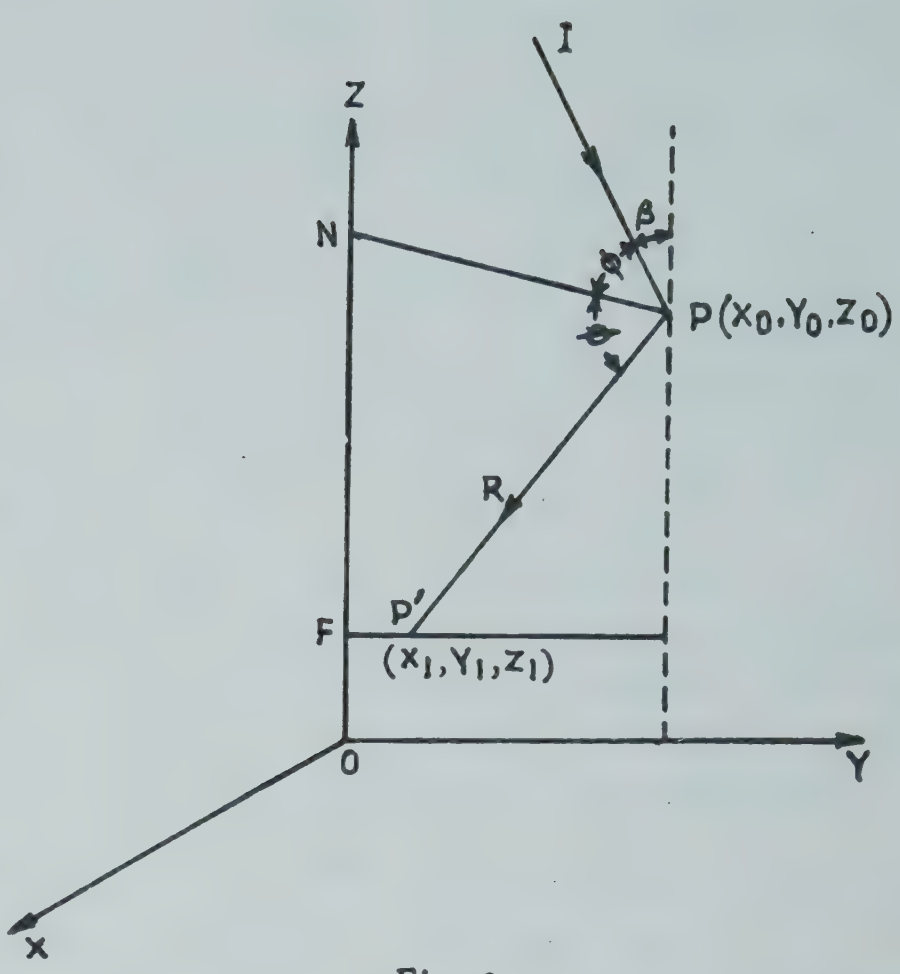


Fig 2

Coordinate system for geometrical ray optics analysis

where l, m and n are direction cosines of the reflected ray PR and are unknown. Let $\vec{n}_n$ be the unit vector along normal to the point P on the reflector surface. Then

$$\vec{n}_n = (-x_o/L)\,\vec{i} + (-y_o/L)\,\vec{j} + (2f/L)\,\vec{k} \qquad .. (4)$$

where,

$$L^2 = x_o^2 + y_o^2 + 4f^2 \qquad .. (5)$$

The unknowns l, m and n are determined from the laws of geometrical optics for the reflection of a ray, ie,

$$\vec{n}_i \cdot \vec{n}_n = -\vec{n}_r\,\vec{n}_n \qquad .. (6)$$

and $$\vec{n}_i \times \vec{n}_n = \vec{n}_r \times \vec{n}_n \qquad .. (7)$$

Solution of equations (2) - (7) results in the following three linearly independent algebraic equations in l, m and n.

$$x_o l + y_o m - 2fn = x_o \sin\beta - 2f\cos\beta \qquad .. (8)$$

$$2fl + x_o n = -2f\sin\beta - x_o\cos\beta \qquad .. (9)$$

$$y_o l - x_o m = -y_o \sin\beta \qquad .. (10)$$

From equations (8) - (10),

$$l = -[(4f^2 - x_o^2 + y_o^2)\sin\beta + 4f x_o \cos\beta]/L^2 \quad .. (11)$$

$$m = -[2y_o(-x_o \sin\beta + 2f\cos\beta)]/L^2 \quad .. (12)$$

$$n = [(4f^2 - x_o^2 - y_o^2)\cos\beta - 4fx_o \sin\beta]/L^2 \quad .. (13)$$

To investigate the image formation of reflector surface in any plane, the intersection of the reflected ray with that plane, should be determined.

The position vector of point P is

$$\vec{p} = x_o\vec{i} + y_o\vec{j} + z_o\vec{k} \quad .. (14)$$

Let P′ (x_1, y_1, z_1) be the point of intersection of the reflected ray PR with the plane of interest, then

$$\vec{p}' = \vec{p} + C\vec{n}_r \quad .. (15)$$

where $\vec{p}'$ is the position vector of P′ and C is a constant.

When the plane of interest is the focal plane, then

$$z_1 = f \quad .. (16)$$

and from equations (3), (14) and (15)

$$C = (f - z_o)/n \quad .. (17)$$

Finally equations (13), (15) and (17) give

$$x_1 = x_o - [\{(4f^2 - x_o^2 - y_o^2)\tan\beta + 4fz_o\}/(4f^2 - x_o^2 - y_o^2 - 4fx_o\tan\beta)](f - z_o) \quad .. (18)$$

$$y_1 = y_o - [2y_o(2f - x_o\tan\beta)/(4f^2 - x_o^2 - y_o^2 - 4fx_o\tan\beta)](f - z_o) \quad .. (19)$$

Equations (16), (18) and (19) establish the point P′. Similarly point of intersection of the reflected ray PR with any other plane can be found out. Considering several points on a sagittal circumference, obtained as intersection between an afocal plane and the reflector surface, the image of that circumference can be obtained on any plane. Repeating this procedure for different sagittal circumferences will give the image of the paraboloid as a whole.

For perfect tracking of the sun, ie, when $\beta = 0$, rays reflected from all points on the reflector surface pass through the geometric focus. But for $\beta \neq 0$, reflected rays get shifted from the focus.

The procedure used above to describe image formation of the paraboloid can also be employed to investigate the energy characteristic of the reflector-receiver system. The energy effect of angular defocusing manifests itself as a reduction in energy availability to the receiver, generally placed in the focal or a chosen afocal plane, due to degeneration of the focal spot. To account for this effect a concentrator-receiver efficiency with static angular defocusing by β, η_β, is defined as

$$\eta_\beta = Q_\beta/Q_o \quad .. (20)$$

where Q_β and Q_o are the energy entering the receiver aperture for a given defocusing angle (β) and for perfect aiming ($\beta = 0$) respectively.

To evaluate η_β through the principle of geometrical optics, the technique described in[1] is employed. The reflector surface is divided into a finite number of zones through concentric circles such that their projections on an afocal plane of the paraboloid are equal in area. Strictly speaking, the projections of angular zones on a plane perpendicular to the direction of the incident rays should be considered. However, for lower values of β the above mentioned system of division makes only a little difference. These zones are further divided into finite number of sub-zones having equal projected area on an afocal

lane. The reflected ray from the centre oint of each of the sub-zones on the re- lector surface is determined. Finally η_β s evaluated from

$$\eta_\beta = N_r/N_t \qquad .. (21)$$

here N_t is the total number of sub-zones n the reflector surface and N_r is the umber of those sub-zones, the rays reflec- ed from centres of which intersect the ocal plane in a circle of given radius ith centre at the focus. The concentrator- eceiver efficiency, η_β, evaluated for dif- erent values of β and aperture radius of he receiver in the focal plane (r) then ives the effect of angular defocusing on nergy characteristic of the paraboloidal eflector.

A computer program has been used to tudy the image contour and concentrator- eceiver efficiency of a paraboloid under ngular defocusing condition based on the nalysis presented above. The paraboloid onsidered has the same focal length (f = 39 mm) as that in reference[1].

Discussion

The image contour in the focal plane or two sagittal circumferences of the araboloidal reflector with obtuse rim an- le and truncated bottom (f = 639 mm, θ_1 = 00°, θ_2 = 150°) are shown in Fig 3 for wo values of the defocusing angle β (0.1° nd 10°). It is obvious that with angular efocusing, geometrical focus ceases to be he point at which all the reflected rays re collected. The point image degenerates nto a closed curve the complete loop of hich describes two turns in the focal lane corresponding to each sagittal cir- umference. For smaller defocusing angles tan $\beta \approx \beta$) this curve assumes the form of wo coinciding circles with centre shifted rom geometrical focus towards the direc- ion of angular defocusing as evident from ig 3a.

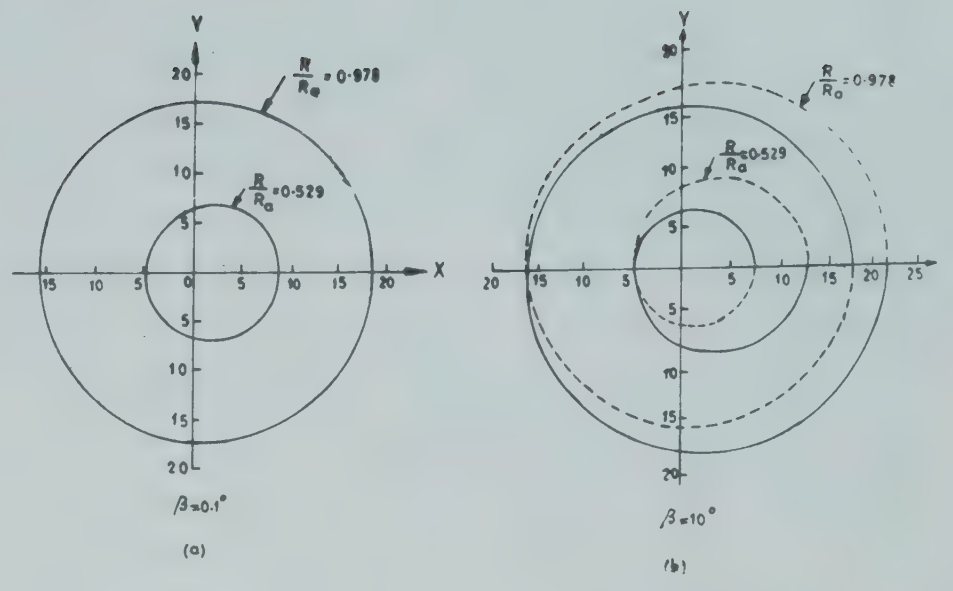


Fig 3
Image contour in the focal plane for obtuse rim angle of the paraboloid

Fig 4 shows the image contour in focal plane for the paraboloid having an acute rim angle of 60° and with same focal length as in Fig 3 (f = 639 mm). For smaller

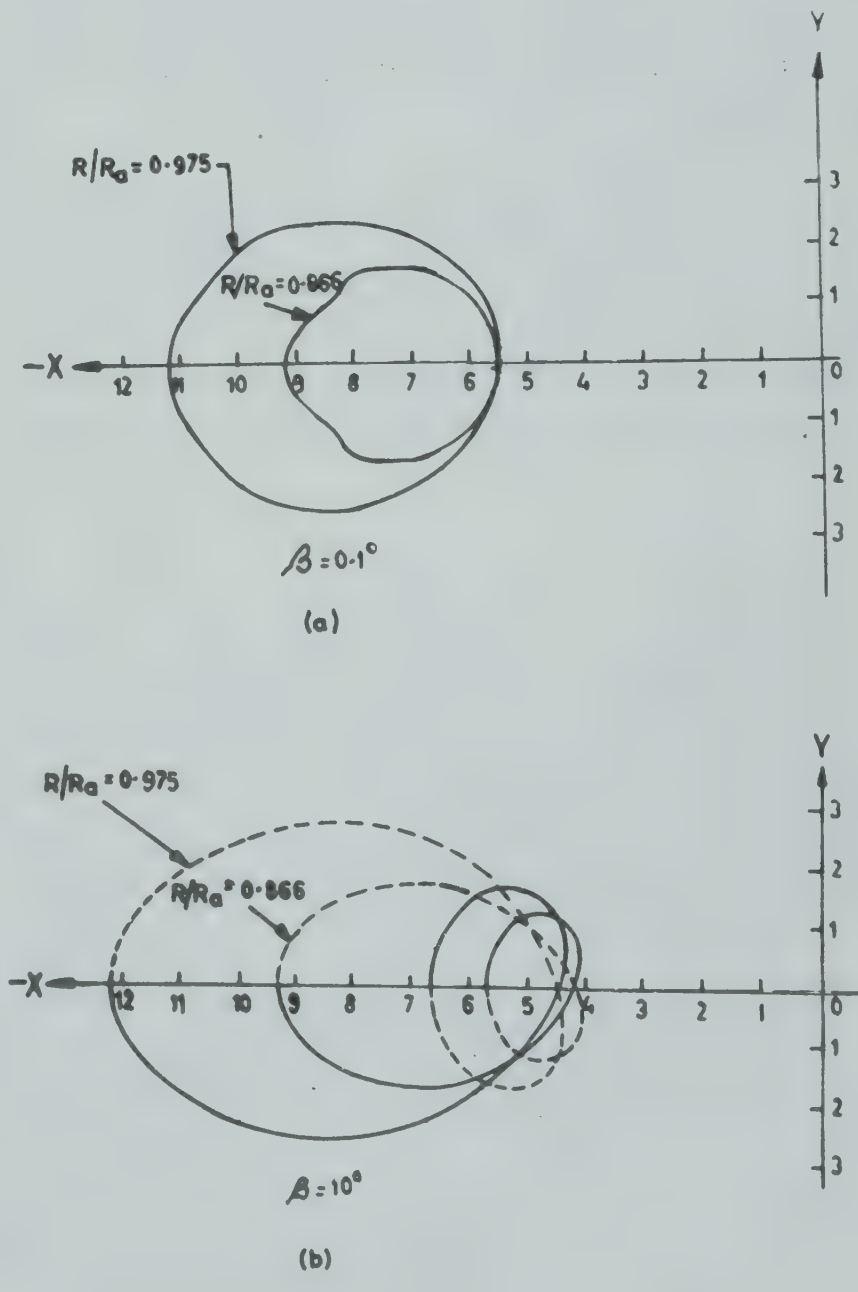


Fig 4
Image contour in the fo plane for
acute rim angle of raboloid

values of β ($\tan \beta \approx \beta$), the image contour (Fig 4a), again makes two coinciding complete turns for each sagittal circumference but the resulting configurations are not as close to a circle as in the case of a sagittal circumference above focus (Fig 3a). Moreover, while the image shift is towards the direction of angular defocusing in Fig 3a, it is reverse in Fig 4a. There exists a marked difference between the image contours of the two cases for higher values of β as displayed in Figs 3b and 4b, though the effective shift of image is similar as in Figs 3a and 3b respectively. In Fig 3b, the two complete turns of the image are almost circular but with different centres. On the other hand in Fig 4b, both the complete turns tend to be elliptical with the two major axes normal to each other.

Knowledge of the image contour makes tracking of sun by the receiver possible for comparatively small defocusing angles in case the tracking by paraboloid is inconvenient.

Plots for the variation of concentrator-receiver efficiency (η_β), with defocusing angle (β) are shown in Fig 5 for the paraboloid under consideration treating r/R_a as a parameter. As is to be expected,

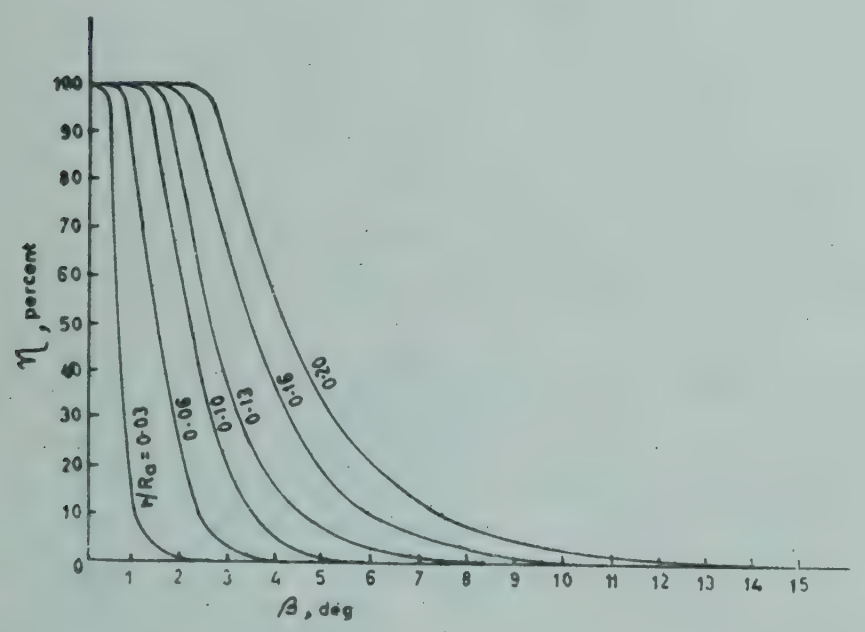


Fig 5

Variation of concentrator-receiver efficiency with β for the paraboloid with obtuse rim angle and truncated bottom

the efficiency increases with the increase in r/R_a and decreases with increase in β. However, the rate of decrease of η_β with increase in β drops rapidly as r/R_a is increased. For example, when r/R_a is 0.03, the efficiency falls to zero for a defocusing angle of 2.5°; whereas, for r/R_a equal to 0.2, the efficiency remains as high as 99.5 per cent at the above defocusing angle and falls to zero only at a value of β greater than 10°. Similarly, for a receiver radius equal to one tenth the aperture radius ($r/R_a' = 0.1$), an angular defocusing upto 1° does not have any diminishing effect on the availability of reflected energy to the receiver.

The above energy characteristics of a paraboloidal reflector with obtuse rim angle and truncated bottom under angular defocusing make it particularly suitable for medium temperature power plant and process heating applications due to rather large dimensions of the receiver involved.

Although it is difficult to achieve a geometrically and optically perfect paraboloidal reflector surface, the above analysis presents a sound qualitative picture of the image contour and energy characteristic for angular defocusing of the paraboloid under consideration. An elaborate quantitative treatment of the problem would require the consideration of random imperfections on the reflector surface, both at macro and micro levels.

Conclusion

1. Paraboloidal reflectors with obtuse rim angle and truncated bottom are well suited to concentrate solar energy as the receiver, located at the bottom, can be easily aligned with the paraboloid without causing any shading to the reflector surface.

2. The proposed system with moderate values of defocusing angle can be used for power plant and process heating applications.

3. For an angularly defocused paraboloid, the image contour in the focal plane corresponding to a sagittal circumference above the focus is much different compared to that for a sagittal circumference below the focus.

Acknowledgement

Thanks are due to the Director, Central Mechanical Engineering Research Institute, Durgapur, for his kind permission to publish the paper.

Reference

[1] R.A. Zakhidov and D.I. Teplyakov, 'Power characteristics of concentrator type solar devices under field tracking conditions,' *Applied Solar Energy*, 2(4) 31 (1966).

[2] R.A. Aparisi and Ya.G. Kolos, 'Concentration capacity of a paraboloidal mirror with angular defocusing,' *Applied Solar Energy*, 6(5) 9 (1970).

[3] I.M. Rubanovich, 'Theoretical investigation of the effect of the accuracy of the concentrator guidance system on the operation of solar energy devices,' *Applied Solar Energy*, 2(6) 13 (1966).

[4] I.M. Rubanovich, 'Effect of tracking accuracy on the efficiency of solar devices with paraboloidal concentrators,' *Applied Solar Energy*, 2(4) 39 (1966).

[5] J.P. Hartnett, Alternative energy sources, Academic Press, p 228 (1976).

FATIGUE IN ROLLING CONTACT - SOME SALIENT FEATURES

C.S. CHANDRASEKHARAMURTHY AND A. RAMAMOHANA RAO*

Abstract

Pitting due to surface fatigue is an important mode of failure in many machine elements experiencing rolling contact. This paper gives a critical discussion on the factors which influence the contact fatigue strength and some of the controvercial aspects of the present state of art of the subject.

Introduction

Gears, rolling contact bearings and cam and cam followers are examples of machine elements where contacts are usually described as 'line' or 'point'. Such concentrated contacts are governed by the elastic theory worked out by Hertz (for static loads) as early as 1881[1]. But in machine elements, the load is generally of cyclic nature due to the rolling of contacting bodies. Surface deterioration due to cyclical loads - called contact fatigue failure - has been the subject of investigation by many research workers for nearly half a century. The theory and practice of contact fatigue is of great technical importance and its understanding is essential for the rational design of gears and rolling contact bearings. Tribological, metallurgical and stress analysis aspects of non-conforming rolling contacts are exceedingly complex and not fully understood because of multifaceted interactions. The development of new materials, surface treatments and measurement and instrumentation techniques have opened up further possibilities of research in the field. Advances in technology have led to higher speeds and analysis has shown that high Hertz stresses at the outer race contacts caused by centrifugal force can seriously shorten the predicted bearing fatigue life of antifriction bearings[2].

The rolling contact problems can be classified into 'dry contact' and 'lubricated contact'. Dry contact problems like railway wheel on rail are usually treated as a separate topic and the following discussion essentially pertains to lubricated contacts. Table I gives a classification of concentrated contacts and their predominant mode of damage[3]. The modes of damage mentioned in the table are scuffing, pitting and abrasive wear. The form of surface failure frequently observed at the 'addendum' and 'dedendum' of spur gear flanks is known as scuffing or scoring. It occurs under high loads and high sliding speeds when the transient local temperature exceeds a critical value which is characteristic of the surface of materials and the lubricant applied. Abrasive wear is the surface deterioration due to the removal of layers of materials. In the absence of any lubricant, the wheel-rail interface will experience metallic contact and will be subjected to abrasive wear. Some examples of lubricated contacts are shown in

*Indian Institute Technology, Madras 36.

TABLE I

Classification of concentrated contacts

ypical pplication	Slip	Environmental conditions	Predominant mode of damage
all and Rol- er bearings	0	Lubricated	
ypoid gears	High	Chemically active lubricant	Scuffing
nvolute gears	Real but passes through zero at pitch line	Lubricated	Pitting
Wheel on rail	Zero in the absence of skidding	Atmospheric corrosion	Abrasive wear
Cam and cam follower	0	Lubricated	

the table, their essential mode of failure being pitting.

Factors affecting contact fatigue failures

Important factors influencing the failure of materials under rolling contact conditions are :

1. Contact stress
2. Hardness of surfaces
3. Materials and material pairing
4. Surface finish
5. Lubrication and
6. Slip.

The dominant parameter which determines the contact fatigue life is the contact stress. The general problem of the stresses produced by the local contact of elastic bodies has been treated by Hertz[1]. Hertz analysis is based on the assumptions of elastic and isotropic material behaviour, loading normal to the surface and a contact area whose dimensions are relatively small in comparison with the radii of curvature and with the dimensions of the bodies. Equations and charts for use in engineering design are available for stresses, deflections and contact dimensions for normally loaded unlubricated elastic contacts[4]. Equations should be used with care because studies have shown that small misalignments result in substantial changes in contact stress field and thus affect fatigue life[5]. When a lubricant is introduced into a rolling contact, the stress system is no longer strictly Hertzian[6].

Using disc machines, maximum contact stress versus pitting life curves have been plotted for different materials and operating conditions[7-11]. The pitting life is defined as the number of stress cycles that the material is subjected to before the formation of the first pit which is visible to the naked eye. Pitting life exhibits scatter and Log-normal and Weibull models have been used for fitting the data though no clear cut superiority of one model over the other has been shown[10]. The existence of a pitting limit and a well defined knee in the stress-life curves is controvercial.

In the case of cylindrical contacts, which represent the contact between spur gears, the contact stress is proportional to the square root of the applied load. Thus, if the allowable contact stress of a material can be raised two times, the load carrying capacity of the contact improves four times. This object is achieved by increasing the surface hardness. But, depending on the material and surface treatment, the hardness that can be obtained is limited. For the same surface hardness, the contact fatigue life can be different depending on the interaction of other factors. For example, pitting life increases as the depth of the hardened case increases[8,11]. But, the term case depth has no universally accepted definition. From a practical point of view, an effective case depth is defined as the depth at which 75-90% of the surface hardness prevails.

Some times the point at which hardness falls to R_c50 is taken as the case depth. When the case depth is small as in tufftriding and the original material has low strength and high ductility, plastic flow instead of pitting may become the mode of failure[12].

A large amount of work has been reported on material and surface treatment effects in rolling contact fatigue[13]. Case hardening, nitriding, tufftriding and ausforming have been shown to improve the contact fatigue resistance of materials[8,11,13-15]. Rolling contact fatigue behaviour of a large number of alloy steels and composites is not known. Light weight ceramic materials such as hot pressed silicon nitride have shown encouraging rolling element fatigue life results[16].

Unlike normal fatigue, mating of two elements is absolutely essential in contact fatigue. Not much work has been done on the effects of material pairing and hardness pairing. With respect to gears, the traditional practice is to mate a softer wheel with a harder pinion. During the running in period of such a pair, there will be plastic flow in the softer material allowing high points to be levelled down and shearing off of the asperities. This results in the reduction of the composite surface roughness of the pair and as a consequence in the improvement of the resistance to pitting. For optimum performance a tufftrided surface should be mated with another tufftrided surface[17].

It is generally considered that slag inclusion and other defects can act as starting points for contact fatigue cracks[18]. The steel making procedure can influence results and modifications and refinements within each process can improve contact fatigue life. Vacuum melting and degassing is beneficial, possibly because of smaller and better distribution of inclusions and less gas content[13].

Slip, also called as specific sliding and slide sweep ratio, is another factor which influences the contact fatigue life. Gear teeth and roller bearings subjected to high speeds and low loads experience slip. Some investigators have conducted roller tests both under pure rolling and rolling/sliding conditions. Contact fatigue life is reduced under rolling/sliding conditions compared to pure rolling. The effect of slip is to introduce a tangential force (frictional) in the contact area. Addition of tangential force to normal force alters the contact surface and subsurface stress distributions[19]. The maximum values of contact stresses become larger than those produced by normal force alone. The addition of frictional tangential forces results in the onset of tensile stresses in the region immediately behind the contact zone. Equations and charts which can be directly used in design are not available for stresses developed in lubricated rolling contacts subjected to combined normal and tractive loading. Another consequence of slip is the reduction in film thickness because of a rise in temperature due to the work done in sliding against frictional resistance. The combined effect of the reduction in film thickness and the tangential force is a reduction in contact fatigue life.

In the absence of lubrication, there will be no pitting and surface deterioration is due to removal of layers by wear. Lubricated surfaces generally exhibit pitting. A theory of the mechanism of formation of pits in the presence of a lubricant has been propounded by Way[20]. According to Way, a pitting crack first appears at the surface as a small 'v'. When this crack is suitably oriented, the lubricating oil pressure generated (in the crack) as a result of the normal load and rolling action helps in opening it and forming a pit. The contact fatigue life and the stress-

life relationship are affected by lubrication chemistry. The nature of the lubricant, any additives it may contain and the compatibility of the additives are factors which partially control the onset of failure[21]. It is generally felt that for a given material, finish and load, there is a critical oil viscosity such that oils of lower viscosity at the operating temperature promote pitting and oils of higher viscosity prohibit pitting . The possible reasons for this seem to be that the high viscosity oil cannot enter the crack and open it and the increase in oil film thickness and avoidance of metal to metal contact.

Speed has no direct effect on fatigue life, but has significant interaction effects with the nature of lubricant, slip and surface finish. The interaction effects have been studied by introducing a factor denoted by Δ which is defined as the ratio of minimum oil film thickness and composite surface roughness. The minimum oil film thickness is given by modified Dowson equation[23], and depends on the lubricant, speed, material and radii of curvature of the rolling contacts. If Δ is nearly equal to one, some amount of metallic rubbing may occur and continuous oil film ceases to exist. As a rough guide, $\Delta > 2$ usually suggests full elasto-hydrodynamic lubrication and $\Delta < 2$ boundary lubrication[24]. When a fully developed oil film eliminates metallic contact, there will be no wear or scuffing. But pitting will still occur because of cyclic stressing of the surfaces.

Conclusion

The above paper has attempted to give the reader an overview of the factors affecting contact fatigue strength. After starting from strength of materials aspects (contact stress and hardness) and going through material effects, it ends with tribological considerations. The interdisciplinary nature of the problem is brought out in the paper. Some of the gaps in the theory pertaining to pitting fatigue are indicated.

References

[1] H. Hertz, **Miscellaneous papers - On the contact of elastic solids**, translation by D.E. Jones, Macmillan & Co Ltd, London (1896).

[2] E.N. Bamberger and R.J. Parker, 'Effect of wall thickness and material on flexural fatigue of hollow rolling elements', *Jour Lubrication Tech*, Trans ASME, 100, pp 39-46 (1978).

[3] F.T. Barwell, 'Surface contact in theory and practice', Proc Instn Mech Engrs, 175(17), 853-76 (1961).

[4] Anon, **Contact phenomena**, Engineering Sciences Data Unit Ltd, London (1978).

[5] J.Y. Liu, 'The effect of misalignment on the life of high speed cylindrical roller bearings', *Jour Lubrication Tech*, Trans ASME, 93(1) 60-68 (1971).

[6] D. Dowson and G.R. Higginson, **Elasto-hydrodynamic lubrication**, Pergamon Press (1977).

[7] C.S. Nanjundaram and A. Ramamohana Rao, 'The effect of tufftriding on the rolling contact fatigue behaviour of 0.2 per cent plain carbon steel cylindrical specimens', *Materialprüfung*, 22(8) 332-35 (1980).

[8] K. Fujita and A. Yoshida, 'Surface durability of nitride-hardened aluminium - chromium - molybdenum steel rollers under pure rolling and sliding-rolling contacts', *Wear*, 53, pp 69-77 (1979).

[9] P.H. Dawson, 'Contact fatigue in hard steel specimens with point and line contacts', *Jour Mech Engg Sci*, 9(1) 67-71 (1967).

[10] S. Bhattacharyya et al, 'Chemical effects of lubrication in contact fatigue, Part II : The statistical analysis, summary and conclusion,' *Jour Lubrication Tech*, Trans ASME, pp 299-307 (April 1976).

[11] S. Ramanathan, 'Some investigations on surface failure in rolling contact fatigue', Doctoral thesis, Indian Institute of Technology, Madras (1977).

[12] A. Ramamohana Rao and G. Bechtloff, 'Preliminary investigations on the rolling contact fatigue behaviour of tufftrided St 37', to be published in *Materialprüfung*.

[13]D. Scott and J. Blackwell, 'NEL rolling contact tests - Accelerated service simulation tests for lubricants and materials for rolling elements', *Wear*, 17, pp 323-333 (1971).

[14]E.N. Bamterger, 'The effect of ausforming (hot and cold working) on the rolling contact fatigue life', *Jour Lubrication Tech*, Trans ASME, 89, pp 63-75 (1967).

[15]C.S. Nanjundaram, 'Some experimental investigations on the rolling contact fatigue behaviour of tufftrided surfaces', Doctoral thesis, Indian Institute of Technology, Madras (1980).

[16]R.J. Parker and E.V. Zaretsky, 'Fatigue life of high speed ball bearings with silicon nitride balls', *Jour Lubrication Tech*, Trans ASME, 97(3) 350-57 (1975).

[17]C.S. Nanjundaram and A. Ramamohana Rao, 'Optimum hardness pairing of tufftrided 0.2 per cent plain carbon steel surfaces in pure rolling contact', to be published in *Materialprüfung*.

[18]E.E. Shipley, Failure modes in gears, gear manufacture and performance, American Society for Metals, pp 107-136 (1974).

[19]J.O. Smith and C.K. Liu, 'Stress due to tangential and normal loads on an elastic solid with applicatron to some contact stress problems', *Jour Appl Mech*, Trans ASME, 20(2) 157-166 (1953).

[20]S. Way, 'Pitting due to rolling contact', *Trans ASME*, 57, pp 49-58 (1935).

[21]W.E. Littman et al, 'Chemical effects of lubrication in contact fatigue, Part III : Load-life exponent, life scatter and overall analysis', *Jour Lubrication Tech*, Trans ASME, pp 308-315 (April 1976).

[22]C. Lipson, Pitting and spalling, wear considerations in design, Prentice Hall, pp 63-73, (1967).

[23]D. Dowson, Elasto-hydrodynamic lubrication, Interdisciplinary approach to the lubrication of concentrated contacts, NASA SP-237 (1970).

[24]P.M. Ku, Tribology of gears, gear manufacture and performance, American Society for Metals, pp 73-106 (1974).

PEDAL PUMP FOR LIFT IRRIGATION

G.K. VERMA, R.K. VARMA AND K.N. RAO*

Abstract

The pedal pump developed at CMERI, is manually operated and suitable for rural application for lifting water from irrigation stream, ponds, open channels, shallow wells, etc. It is a medium head and high discharge pump. This paper discusses constructional details, principle of operation, efficiency, etc, of the pump.

Introduction

Seventyfive per cent of the people of our country live in rural areas and are mainly engaged in farming. The greater part of cultivated land is owned by the small and marginal farmers who are not capable to buy engine or electric power operated irrigation devices. The use of these devices are further limited due to non-availability of diesel or electric power everywhere.

The farmers are mainly using the manually or animal operated devices for irrigation purpose. The most widely used devices are : Swing basket, Paddle wheel, Counter poise lift, and Don.

These devices have varying performance characteristics satisfying various needs. For example, a swing basket delivers 3600-5000 l/h at a head of 1.2 metres and requires two operators. The paddle wheel may deliver as high as 18000 l/h but head is as low as 0.3 - 0.6 metre. A counter poise lift has low discharge of 2300 l/h at a head of 1.2 to 3 m. Don which is very popular in West Bengal, Bihar and Assam States, delivers 1200 l/h to 1500 l/h at a head of 1 metre.

In view of the requirement of the farmers for lift irrigation, manually operated pump of medium head and high discharge is in great demand. The Central Mechanical Engineering Research Institute, Durgapur, has developed such a pedal pump suitable for rural applications for lifting water from irrigation stream, ponds, open channels, shallow wells, etc. The average discharge of the pump is 6000 l/hr at a head of 2 metres. A farmer can irrigate about half acre of land if he works for 8 hours a day. The pump does not require any diesel or electric power.

Constructional details

General working arrangement and constructional details of the pedal pump are showing in Fig 1.

The pump consists of main body (1) having two chambers (2) and (3) fitted with unidirectional valves (4), (5), (6) and (7), suction and discharge chambers (8) and (9) fitted with inlet and outlet pipes (10) and (11) respectively, diaphragms (12) and (13) fitted on open ends of the chambers (2) and (3) connected to the pedal assembly (14) through links (15) and (16). The pedal assembly (14) having platforms (17)

*Central Mechanical Engineering Research Institute, Durgapur 9.

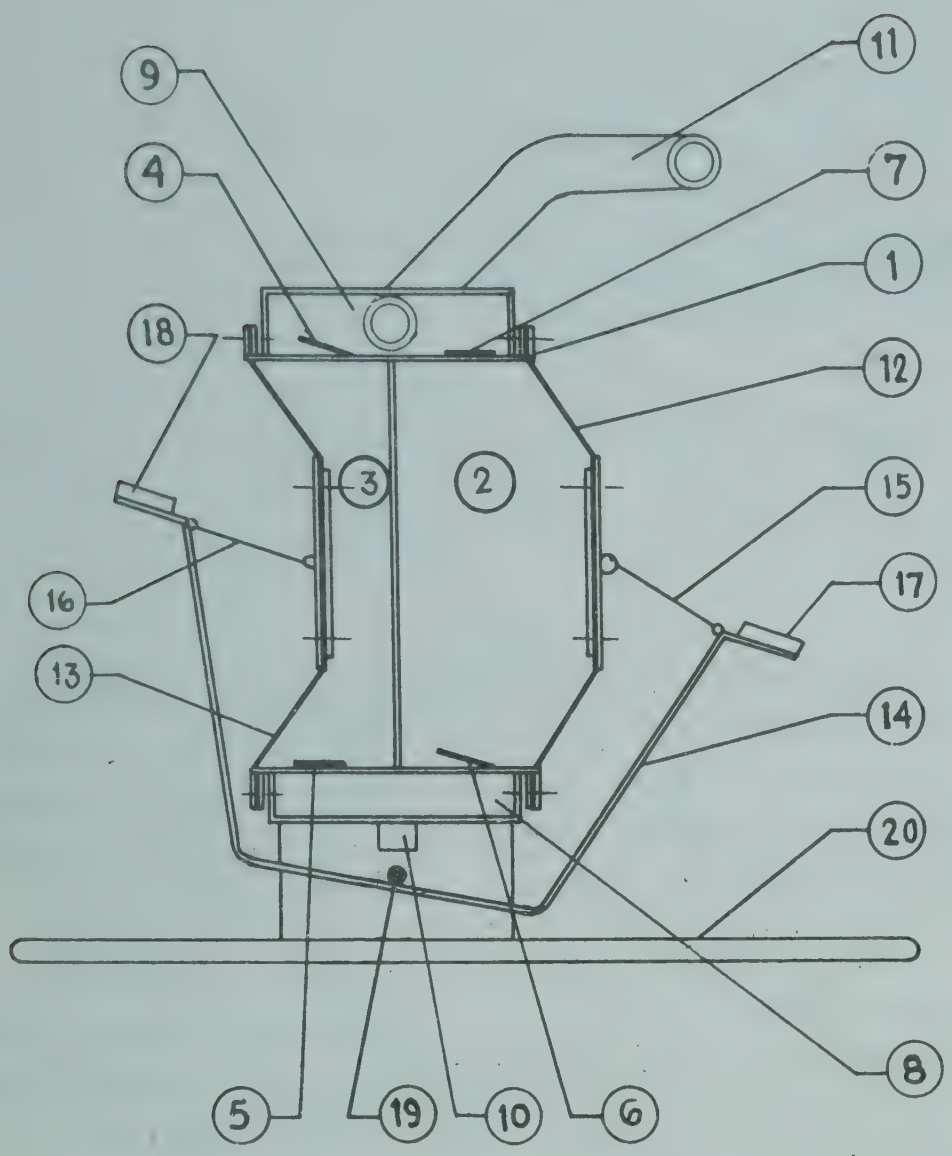


Fig 1
Constructional details (names of components described in the text)

and (18) are hinged on main body (1) with suitable bearing and pin assembly (19). The pump is mounted on a suitable base (20). A suitable tubular steel or bamboo support may be used for convenience of the operator.

The materials used for construction of the pump is described in Table I.

Principle of operation

The pump can be operated by a person standing on platforms (17) and (18) with the stand support. As the person standing on the platforms changes his body posture, his body weight is transferred to one of the platforms, say (17), causing movement of diaphragms (12) and (13) through links (15) and (16). As the pedal assembly is hinged to the main body (1), the platform (17) goes downwards and the other one (18)

TABLE I
Materials used

Part No	Name of parts	No of components	Materials used	Size/specification
1,2,3	Main body	1	MS sheet	SWG-11
4,5,6 & 7	Unidirectional valves	4	Rubber sheet	6 mm thick
8	Inlet chamber	1	MS	SWG-11
9	Outlet chamber	1	MS	SWG-11
10,11	Inlet and outlet pipes	1	MS tube	50 mm bore
12,13	Diaphragms	2	Truck tube	
14	Pedal assembly	1	MS tube	20 mm bore
15,16	Links	2	C-40	10 mm dia IS:1570
17,18	Platforms	2	MS angle and sheet	Angle 25x25x4 Sheet 5 mm thick
19	Bearing and pin assembly	2		
	Bush	2	Ph bronze	IS:28
	Pin	2	C-40	IS:1570
20	Base	1	MS angle iron	50x50x6x1 metre long

goes upwards. This in turn creates vacuum in the chamber (2) of the main body and the discharge valve (7) closes and suction valve (6) opens simultaneously causing lifting of water in chamber (2). At the same time the discharge of water takes place from chamber (3) due to closing of valve (7) and opening of valve (4) simultaneously. Similarly when the operator's weight is transferred to platform (18), the discharge takes place from the chamber (2) and suction occurs in chamber (3). Thus discharge and suction take place twice in each cycle causing continuous flow of water.

Performance of efficiency tests

Discharge of the pump is proportional to power if the head is kept constant. The power depends upon the physique of the operator. The power developed and the discharge obtained by different operators during the course of the testing, are shown in Table II.

The average weight of the operator being 60 kgs, he develops approximately 0.057 HP (45 watt).

Thus the average discharge

TABLE II

Results of performance tests

Sl No	Weight of operator (kg)	Power developed HP (approx)	Number of stroke/ minute	Discharge in litres/hour
1	45	.04	20	3950
2	50	.045	25	4950
3	60	.05	27	5400
4	61	.06	32	6400
5	62	.06	33	6600
6	63	.06	30	6000
7	65	.06	30	6000
8	73	.08	40	7950
Average	60	.0568	30	5906.25

$$Q = \frac{HP \times 75}{h}$$

where, Q = discharge in litres/sec

h = head in metres
= efficiency of pump operating

HP = power available for operating the pump.

Efficiency of pump

$$= \frac{\text{Actual discharge/stroke}}{\text{Design discharge/stroke}} \times 100$$

$$= \frac{3.328}{4.16} \times 100 = 80\%$$

Now h = 2 metres, HP = 0.057

$$\therefore Q = \frac{0.57 \times 75}{2} \times 0.8$$

= 1.71 lt/sec or 6156 lt/hr.

The discharge also depends upon the number of strokes that varies from man to man depending on individual physique and habit. Fig 2 shows the discharge-stroke relationship for different operators, and Fig 3 indicates the actual discharge at different heads. The difference between the theoretical discharge and actual discharge gives an indication about the leakage of the pump. This leakage is around 6 per cent at the head of 2 metres with normal working conditions.

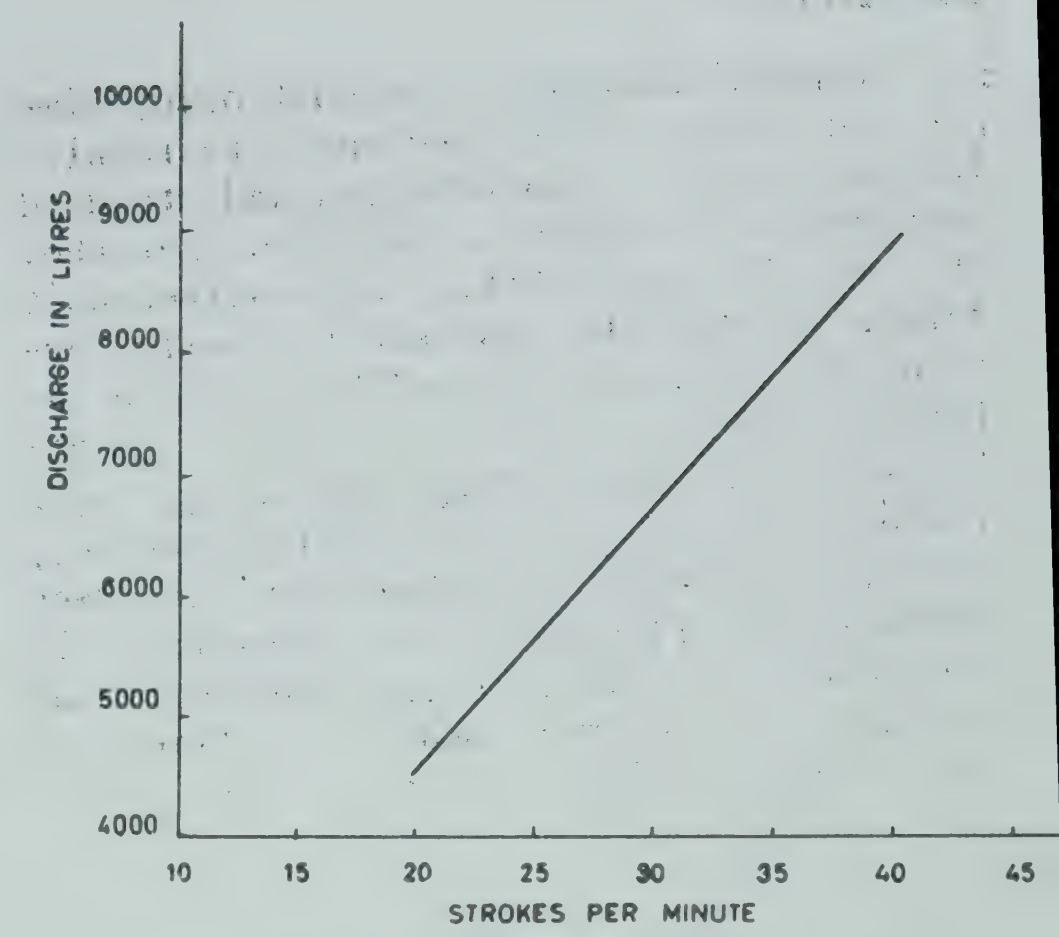


Fig 2
Strokes versus discharge characteristics

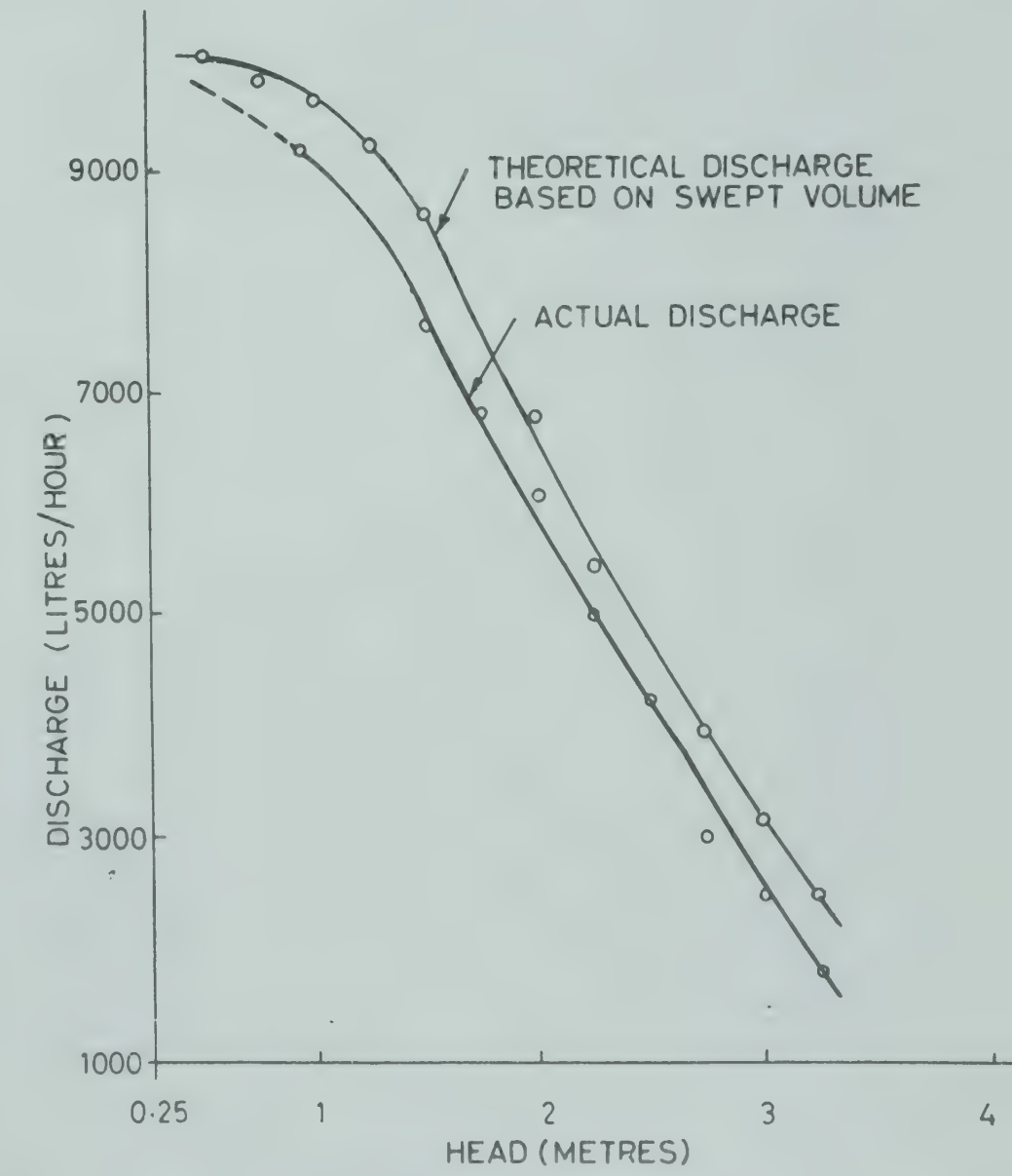


FIG 3 HEAD Vs DISCHARGE

Fig 3
Head versus discharge

Conclusion

The pedal pump is a low cost pump, simple in construction and easy to repair. The materials of construction and standard components have been so selected that they are easily available. The entire unit weighs about 35 kgs and can be easily carried by 2 persons or on bi-cycle to the field.

After successful field trials at different places in actual field conditions, technical know-how of the pump has been released to 14 small scale industries in West Bengal, Bihar, Uttar Pradesh, Maharashtra, Kerala and the Union Territory of Delhi. Many more industries are interested to take up this pump.

Acknowledgement

The authors thank Shri B.M. Sen, Deputy Director, CMERI, for his valuable suggestions and guidance in course of developing the pump. Thanks are also due to Shri S. Natarajan, Scientist, CMERI, for his valuable suggestions Thanks are also due to Prof S. K. Basu, Director, CMERI, for his kind permission to publish this paper.

News and Views

MERADO - Ludhiana releases know-how for turret lathe, reaming machine and gas stove

At a function held on 5 August 1981 at the Mechanical Engineering Research and Development Organisation (MERADO), Ludhiana, Prof S. Nurul Hasan, CSIR Vice-President, released the know-how of three MERADO developed products, viz, (i) single spindle automatic turret lathe, (ii) multispindle automatic reaming machine, and (iii) fuel-efficient LPG stove, to the industries which had sponsored developmental work on them. The opportunity was also availed of by this MERADO centre to demonstrate the working of the tractor-driven combine harvester, which it had developed under industry sponsorship and would be releasing after field trials.



Prof S. Nurul Hasan, CSIR Vice President, releasing technical know-how of multispindle reaming machine developed by MERADO, Ludhiana to Shri S.K. Malhotra of Friends Auto Industries, Phillaur. Dr G.S. Sidhu (sitting), Director General, Scientific & Industrial Research, presided. Also seen in the photograph are Shri Hardyal Singh (extreme left), Scientist-in-Charge of MERADO, Ludhiana and Dr S.K. Basu (extreme right), Director, CMERI, Durgapur

Driving home the point that India's development strategy was based on self-reliance, the chief guest Prof Nurul Hasan said in his address that in removing poverty and improving the living standard of the common man the creation of new trades, new industries, and new techniques was of paramount importance. We should produce goods not merely for our own use but for export to other countries, he added. In this context he made it clear that there was no conflict between big industry and small industry: without the help of small-scale ancillary industry large-scale industry cannot progress, and vice versa. The two are interdependent and both are relevant as far as development is concerned, the CSIR Vice President emphasized. Prof Nurul Hasan went on to say that to remove poverty it was necessary to create an environment in which more than half the population could depend on agriculture and the other half on industry. The chief guest underscored the role of science and technology in attaining such a goal.

In concluding his address, Prof Hasan complimented MERADO scientists and engineers on developing the machines which were being released to industry, and also the industrialists for sponsoring projects which had resulted in the development of the machinery.

Presiding over the function, Dr G.S. Sidhu, Director General, Scientific & Industrial Research, stated that the country had reached such a level of competence in research, design and engineering and also manufacturing capacity that it should look forward to exporting machinery and equipment in large numbers to a large number of countries. To be able to achieve this goal we should be competitive not only in price but in quality as well, said the Director General in a hortatory message to the engineering R&D organizations. He made special mention of the Central Mechanical Engineering Research Institute's Swaraj tractor, which licensed to industry by the National Research Development Corporation of India, had netted in royalties, at the rate of 2½% of sales, amounting to some Rs 30 million.

Referring to the phenomenal successes achieved by advanced countries like Germany and Japan in engineering industries, the Director General stated that for every shop floor engineer there were four R&D engineers behind the industrial scene in those countries. Exhorting enlightened industrialists to try this experiment, whose benefits are so obvious, Dr Sidhu said that if they could not set up their own R&D units, they could at least deploy, for every production engineer they employ in their establishment four R&D engineers in MERADO. Dr Sidhu, also mentioned many areas of successes achieved in R&D work in the country, which had not received publicity worthy of such achievements, as, for example, the Rs 130 million low-temperature carbonization plant set up in Andhra Pradesh entirely with indigenous know-how and equipment.

In his address, Dr S.K. Basu, CMERI's Director, said that MERADO's objective at the time of inception was to help industries maintain quality control, but over the years these organizations had developed sufficient expertise in design and development of a wide range and variety of machinery and equipment. Ludhiana's MERADO for instance, he said, had developed hosiery and knitting machines, agricultural implements, and even special-purpose machines, which are not tackled by institutes like the Central Machine Tools Institute. These centres also organized from time to time special courses for the benefit of engineering industry. Dr Basu also referred to the excellent rapport established between MERADO, Ludhiana and industry as a consequence of which industry had successfully absorbed the technologies for the production of a large number of machinery - the woollen knitting machine, to mention just one.

Shri Hardyal Singh, Scientist-in-charge of MERADO, Ludhiana, gave an account of his centre's work, ever since it came into being in 1965, towards modernization and growth of small-scale as well as medium-scale industries in the region.

MERADO develops combine harvester

This tractor-driven combine harvester, which MERADO, Ludhiana has designed and developed for a private industry (Jindal Combines Pvt Ltd, Sangrur), is more suitable to Indian conditions, especially because self-propelled combines are expensive and therefore beyond the reach of average farmers.

To be used with 35 hp tractors, the harvester can harvest crops like wheat, paddy, barley and soya bean. It is expected to have a field capacity of around 0.44 ha/hr (taking 2 kmph forward speed and 70% field efficiency).

Manual harvesting of headland is not required for the entry of this combine in the field as it has a cutter bar of 3.2 m which covers the pulling tractor.

The grain tank frame is hinged on to the chassis of the machine to enable easy assembly of the tractor. The machine has been provided with two steering wheels in the front and one wheel at the rear for even distribution of load, which does not affect the stability of the tractor by side pulls.

The harvester is driven by power take-off of tractor and is also steered by tractor steering. The header can be raised or lowered through a hydraulic cylinder the controls of which are within the reach of the operator sitting on tractor seat.

The know-how for the combine harvester will be released to industry following field trials.

Engineering units advised to concentrate on R&D

Inaugurating the fourth annual general meeting of the Federation of Engineering Industries in India, Mohd Fazl, Member of the Planning Commission urged the engineering industry to concentrate effectively on areas such as research and development, energy conservation, cost reduction and control over working capital.

Shri K.S. Rajan, Secretary (Technical Development) who also addressed the meeting felt in-house research and development units in industries had yet to make an impact in technological development. Technology being an essential industrial development, the Government had recognised the need for inducting advanced technology in certain areas where Indian skills and technologies were inadequate.

Md Fazal advocated that the industry should introduce morality so that marginal shortages in certain areas were not exploited to the detriment of the country.

Referring to the concept of cluster of industries, Md Fazl said, the state governments were engaged at present in devising suitable programmes for selected backward regions and when implemented the nucleus industrial complexes will provide new growth centres in backward regions.

The government hoped that through this scheme, it would be possible to concentrate on the limited resources in specific selected areas rather than spreading the resources thinly for providing infrastructure and other facilities. The ancillary and small units would also benefit by being close to a reasonably concentrated cluster of industries which would lead to a larger offtake possibility.

Engineering exports : EPI and BHEL lead

Engineering Projects India (EPI) and the Bharat Heavy Electrical Limited (BHEL)

have emerged as leading exporters for the period 1980-81. They are closely followed by Tata Exports, Tata Engineering and Locomotive Company (Telco) and the Projects and Equipment Corporation (PEC). All these companies have also improved upon their performances in the previous year.

This is revealed in a study of select engineering exporters conducted by the Association of Indian Engineering Industry (AEI).

The Engineering Projects India (EPI) led the race with export earnings of Rs 1216 million closely followed by BHEL which accounted for Rs 1100 million. Tata Exports, Telco and PEC followed with earnings valued at Rs 695 million, Rs 523 million and Rs 400 million respectively.

The association's study is based on response received from 207 member companies. Of these, only 197 have been included for purposes of analysis as these relate to physical exports of engineering goods. The share of these top five companies in 1979-80, was as follows: EPI (Rs 1005 million), BHEL (Rs 520 million), Tata Exports (Rs 546 million), Telco (Rs 450 million) and PEC (Rs 350 million).

The study reveals that the total exports of the 197 companies covered by AIEI increased from Rs 4678 million in 1979-80 to Rs 4830 million in 1980-81 thus registering an increase of 3.24 per cent.

The share of these 197 firms in the total exports of engineering goods was 72 per cent in 1979-80 which declined to 53 per cent in 1980-81.

The analysis further reveals that the western region, accounting for 49 per cent of the total engineering exports, has observed the highest growth rate at 12 per cent in 1980-81 over 1979-80. The northern region, on the other hand, has registered a decline in exports at 11.02 per cent for the same period.

Out of the 197 companies which were co
vered by AIEI, as many as 77 belonged t
the western region, 44 came from the north
33 from south and 43 from the east.

The 77 companies for the western regio
accounted for exports worth Rs 2380 millio
in 1980-81 constituting 49.28 per cent o
the total engineering exports of Rs 483
million by the 197 respondent companies
Similarly, the 44 firms in the northern
belt accounted for exports worth Rs 124
million in 1980-81 constituting 25.76 pe
cent of the total exports. Likewise, 3
firms in the southern region exported goods
worth Rs 629 million in 1980-81 constitu
ting 13 per cent of the total exports. The
43 companies from the eastern zone earned
Rs 576 million through exports.

Next energy meet

Scientists from all over the world
would meet at Mexico city in November this
year to review the recommendations of the
United Nations conference on new and re
newable sources of energy.

The official announcement came as the
two-week long deliberations on new and re
newable sources of energy held at Nairobi
came to an end on August 21.

The Mexico meeting will also plan prio
rities for their future work in the field
of energy problems.

About harnessing the solar energy, ex
perts have recommended to the international
community that national agencies should
prepare solar energy maps to make it pos
sible to improve solar radiation data.
They say the flow of energy from the sun
to the earth is virtually infinite, and
yet only one billion part of that energy
is intercepted by the earth.

The estimate that in 15 minutes the sun
radiates as much energy on earth as the
humanity consumes in every other form du
ring the whole year. The technological
problems of harnessing this enormous sour

ces of energy are formidable. The mastery of the appropriate technology requires the full cooperation of meterologists because of its fundamental characteristics, diurnal and seasonal cycles, the largely unpredictable vagaries of the weather, the low power density of the direct radiation and the largely unpredictable fact that it cannot be directly stored in its primary form.

The abundance of solar energy has attracted widespread interest for its utilisation. Flat collectors may be used economically in some areas for water and space heating, drying of crops and fishes and other agricultural purposes. However, despite its declining cost, the direct conversion of solar energy into electricity through pritovoltaic cells is still very expensive at more than $25,000 for per kilowatt capacity installed as compared to $1,000 for thermal and $2,750 for hydropower generation, transmission and distribution.

Research and development work are under way in many countries in this area as well as other applications of solar energy, including water pumping and cooking.

The technical panel on wind energy and ad-hoc groups of experts have suggested that a preliminary wind-resource inventory should be undertaken as soon as possible in all countries having some wind-powered electric generation systems. These are expected to be economically viable on a significant scale within the next five years.

The scope of the Nairobi conference was restricted by the United Nations General Assembly to 14 energy sources - solar, geothermal, wind power, tidal power, wave power and thermal gradient of the sea, fuelwood, charcoal, biomass conversion energy from draught animals, oil shale tar sands and hydropower. Eight technical panels were set up to study the various technical questions connected with each of these sources. The combined work of the various panels and groups appears in the form of 18 reports setting out their conclusions and recommendations.

The experts were in agreement that it seemed urgent to make a transition as quickly, equitably and smoothly as possible to an optimal energy distribution allowing the various sectors of the economy to diversity their energy supply arrangements.

Among the renewable sources, experts found the ocean resources as substantial. There are a few tidal sites in the world where the technology is probably economical compared to the cost of fossil fuels (oil and coal). While the tidal energy will make a useful contribution to world energy supplies over the next twenty years, it will not be large by global standards and will not make a major impact on the energy problems of the developing countries.

The technical panel on biomass energy has recommended that the United Nations should provide assistance to all those countries which have potentialities to exploit biomass energy.

Experts revealed that an immense unused hydropower potential is available with the developing countries. Only a small portion of the economic potential is utilised today. Of all renewable sources of energy, hydropower is expected to make a significant contribution in the energy field.

The conference recommended that collaboration of developing countries in the development of large-scale hydropower projects should be promoted.

Portable metal analyser

In conjunction with CEGB's Marchwood Engineering Laboratories, a small high technology company at Wheatley, Oxfordshire, has developed a fully portable metal analyser based on visible spectrum analysis and is to make the instrument under licence from the Board.

The unit is believed to be the first in which a complete analysis takes place with a digital read-out on the hand-held gun so that the operator does not, as with some existing instruments have to make a personal assessment of the visible spectrum.

Although there are cable connections to a box of electronics, the hand-held unit is completely portable and weighs only 3 kg.

Within the small space available the designers have included an electrode assembly to strike an arc at the metal surface, an optical system to capture the arc light, a prism to produce the spectrum and a rotary mirror system which turns the spectrum lines into a time domain to allow analysis.

The instrument was originally designed to overcome a persistent and potentially costly problem at generating stations where mild or low chrome steels find their way into boiler and heat exchanger components where higher-chrome steels had been called for in the specification.

The company, is thus offering an ini tial model that is able to differentiat between low chrome steels having up to 1 per cent chromium content, with a sensiti vity of 0.5 per cent.

Groundnut sheller

The Village Technology Unit, Easter Africa Regional Office, Kenya, has cons tructed a groundnut sheller formed like semi-cylindrical trough. The bottom of th trough is made of ½-in-square rigid wire mesh. It is equipped with a paddle whic can be rotated from the centre. The pad dle's blade can be adjusted so that it ma be either raised or lowered above the wire mesh.

Groundnuts are loaded into the troug and the paddle blade is set so that, whe moved backwards and forwards, it crushe the groundnut shell against the wire-mesh This falls into a box placed below. Th distance between the paddle blade and th wire-mesh is carefully set in order not t damage the groundnut kernels.

SOLAR STILL REGENERATOR FOR BRINE

M. PRASAD, P. KUMAR AND B.C. RAYCHAUDHURI*

Abstract

Brines are often required to be regenerated for their continuous use in a cyclic operation. Solar energy may be used to supply heat economically for such applications. A complete up-to-date design procedure for a solar still regenerator is presented and its performance is studied theoretically with lithium chloride brine.

Nomenclature

A	Regenerator surface area, m^2
C_c	Concentration of strong brine, wt % LiCl
C_d	Concentration of dilute brine, wt % LiCl
C_p	Specific heat of brine, $W(Kg)^{-1}(^{\circ}K)^{-1}$
f_w	Function relating vapour pressure of water with temperature
f_b	Function relating vapour pressure of brine with temperature and concentration
h_{co}	Convective heat transfer coefficient on outsideof the cover, $Wm^{-2}(^{\circ}K)^{-1}$
h_{fg}	Latent heat of vaporization for water, $WH(Kg)^{-1}$
I_t	Total solar intensity perpendicular to regenerator, Wm^{-2}
I_{ba}	Solar energy absorbed by brine, Wm^{-2}
I_{ca}	Solar energy absorbed by cover, Wm^{-2}
K_c, K_i	Thermal conductivities of cover and insulation respectively, $Wm^{-1}(^{\circ}K)^{-1}$
m	Evaporation rate of water, $Kg(hr)^{-1}$
M_d	Flow rate of dilute brine, $Kg(hr)^{-1}$
p_{bo}	Vapour pressure of brine at regenerator outlet, mm Hg
p_{ci}	Water vapour pressure at T_{ci}, mm Hg
$q_c, q_e,$ q_r	Convective, evaporative and radiative heat transfers respectively from brine surface, Wm^{-2}
q_{cond}	Conductive heat loss from bottom, Wm^{-2}
$q_{cco},$ q_{cro}	Convective and radiative heat transfer from outside surface of cover, respectively, Wm^{-2}
Q_s	Sensible heating of brine, W
T_a	Ambient air temperature, $^{\circ}K$
T_e	Effective sky temperature, $^{\circ}K$
$T_{ci},$ T_{co}	Cover temperature at inside and outside surfaces respectively, $^{\circ}K$
$T_{bi},$ T_{bo}	Brine temperature at inlet and outlet of regenerator respectively, $^{\circ}K$
V	Ambient air velocity, $Km(hr)^{-1}$
x_c, x_i	Thicknesses of cover and insulation respectively, m
α_b, α_c	Absorptivities of brine and cover respectively
η	$(q_e/I_t) \times 100$, % regeneration efficiency
β	$m/A(p_{bo} - p_{ci})$, mass transfer coefficient, $Kg\ m^{-2}\ (hr)^{-1}(mm\ Hg)^{-1}$
τ_c	Transmissivity of cover and condensed water film on cover
ρ_b	Reflectivity of brine
σ	Stefan-Boltzman constant, $Wm^{-2}\ (^{\circ}K)^{-4}$
ϵ_b, ϵ_c	Emissivities of brine and cover respectively.

Introduction

Solar energy can be efficiently used to supply heat for the regeneration of brines. For moderate temperature applications, flat

*Central Mechanical Engineering Research Institute, Durgapur 9.

plate collectors can effectively trap the solar energy and transfer it for regeneration.

The solar regenerator may be classified in three basic categories :

a) free convection regenerator,

b) forced convection regenerator, and

c) still regenerator.

Water gets transferred from dilute salt solution to ambient air, due to mass transfer taking place at the regenerator surface by free convection and forced convection of air for first and second types respectively[1]. The potential for this mass transfer depends upon water vapour pressure present in the ambient air and therefore requires a relatively dry climate. The solution, in these cases, will get easily contaminated as it comes in direct contact with the environment inside the regenerator and will thus need frequent purification.

Still regenerator is suggested to overcome the above shortcomings. Here, free convection of water vapour with fixed air mass takes place inside the regenerator which is closed from all the sides. Apart from the fact that the salt solution becomes free from environmental contamination threat, the humidity variation in the ambient air does not affect the performance of the regenerator and water evaporated from the regenerator is recovered. Thus still regenerator is most suitable for systems to be used in humid climate or where ambient air is not clean.

Solar still concept for the design of brine regenerator has been earlier mentioned by Hollands[2] and Kakabayev and Golaev[3]. Whereas Hollands deals with conventional still, of storage type, the design procedure suggested by Kakabayev and Golaev is an approximate one.

Thus, an accurate and general methodology has not been reported, till date, for the design of such regenerators. The ob jective of the present paper is to give systematic and up-to-date design procedur for the above still regenerator which ca be easily programmed.

Design considerations

The regenerator under consideration i an inclined solar still where dilute solution enters at the top and flows down in a thin film along the solar collector. A fraction of water evaporates from the brine surface, gets condensed on the regenerator cover and trickles down to its bottom in a separate channel from where it is removed away. Thus the outgoing solution from the regenerator gets concentrated in salt.

The design procedure for the proposed still regenerator in steady state is presented here in mathematical terms :

Energy absorbed by brine solution,

$$I_{ba} = I_t \, \tau_c \, \alpha_b \qquad .. (1$$

Energy balance at brine surface,

$$I_{ba} = q_c + q_e + q_r + Q_s/A + q_{cond} \cdot\cdot (2$$

Convection heat transfer from brine surface to inside of cover surface, q_c is given by[4]

$$q_c = 0.884 \, (T_{bo} - T_{ci}) + [(p_{bo} - p_{ci}) \, T_{bo}/(2020 - p_{bo})]^{1/3} \, (T_{bo} - T_{ci}) \qquad .. (3)$$

Water vapour pressure variation at brine surface is ignored and its value at regenerator outlet is used due to the fact that for inclined regenerators the motion of the vapour air mixture at the surface of the brine is directed upwards and thus the water vapour pressure for brine surface tends to approach the value p_{bo}. The simultaneous increases of temperature and concentration of brine further reduces the variation in water vapour pressure along regenerator length.

Inside cover temperature, T_{ci}, is assumed constant along the cover length as the circulation of water vapour air mixture will embrace the entire length for moderate values of regenerator inclination from horizontal and spacing between brine surface and the cover, thus making variation in T_{ci} very small.

Dunkle's analogy[4] is used to relate heat transfer to mass transfer, thus

$$q_e = 2.164\ (p_{bo} - p_{ci})\ q_c/(T_{bo} - T_{ci}) \quad .. (4)$$

Evaporation rate of water is determined by q_e

$$q_e = mh_{fg}/A \quad .. (5)$$

Radiative heat transfer from brine surface to inside surface of cover is

$$q_r = (T^4_{bo} - T^4_{ci})/(\epsilon_b^{-1} + \epsilon_c^{\ 1} - 1) \quad .. (6)$$

Sensible heating of dilute brine solution gives

$$Q_s = M_d C_p\ (T_{bo} - T_{bi}) \quad .. (7)$$

Conduction heat loss from the bottom of the regenerator is

$$q_{cond} = K_i\ (T_{bo} - T_a)/x_i \quad .. (8)$$

Heat transfer from inside surface to outside surface of cover gives

$$q_c + q_e + q_r + I_{ca} = K_c(T_{ci} - T_{co})/x_c \quad .. (9)$$

It is assumed that the temperature profile through the cover is linear.

Total heat absorbed by cover consists of two components, the one from direct insolation and the other from radiation reflected by brine surface.

Thus,

$$I_{ca} = I_t\ \alpha_c\ (1 + \tau_c\ \rho_b) \quad .. (10)$$

Energy balance at the outer surface of the cover is

$$q_c + q_e + q_r + I_{ca} = q_{cco} + q_{cro} \quad .. (11)$$

Convective heat transfer from the outer surface of the cover is

$$q_{cco} = h_c\ (T_{co} - T_a) \quad .. (12)$$

Where h_c according to Whillier[5] is

$$h_c = 5.7 + 1.095\ V \quad .. (13)$$

Radiative heat transfer from outside of the cover surface is

$$q_{cro} = \epsilon_c\ \sigma\ (T^4_{co} - T^4_e) \quad .. (14)$$

Where T_e is assumed to be 12 degree lower than T_a,

$$T_e = T_a - 12 \quad .. (15)$$

Also, $p_{ci} = f_w\ (T_{ci})$ .. (16)

$$p_{bo} = f_b\ (T_{bo},\ C_c) \quad .. (17)$$

Inlet and outlet concentrations of brine are related by

$$C_c = C_d\ M_d/(M_d - m) \quad .. (18)$$

Equations (1) to (18) determine the regenerator design.

Discussion

Various characteristics of the proposed regenerator are displayed in Figs 1-3 for $LiCl$-H_2O combination and the sample data are given in the Appendix.

The variation in the efficiency of regenerator with ambient air velocity is smaller compared to that with solar intensity as shown in Fig 1 and Fig 2 and confirms the possibility of using the system in localities receiving high values of solar insolation even if the ambient air velocities are small. Plain reflectors may also be used to obtain high values of solar insolation on regenerator surface.

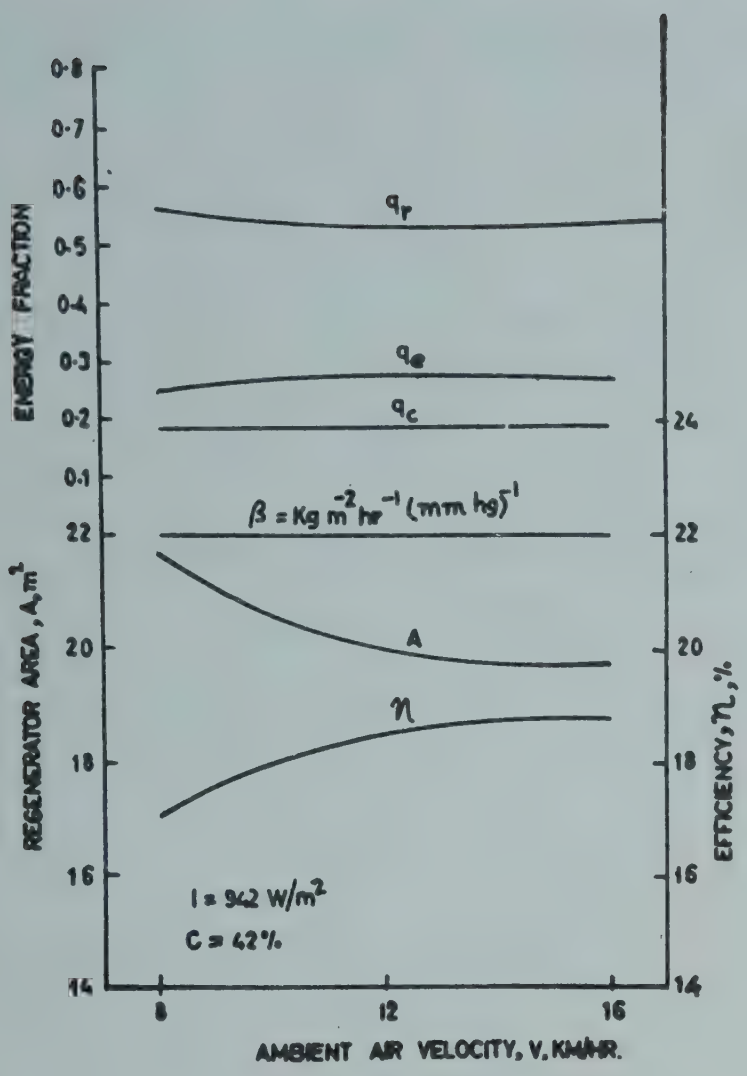


Fig 1

Regenerator performance with varying ambient air velocity

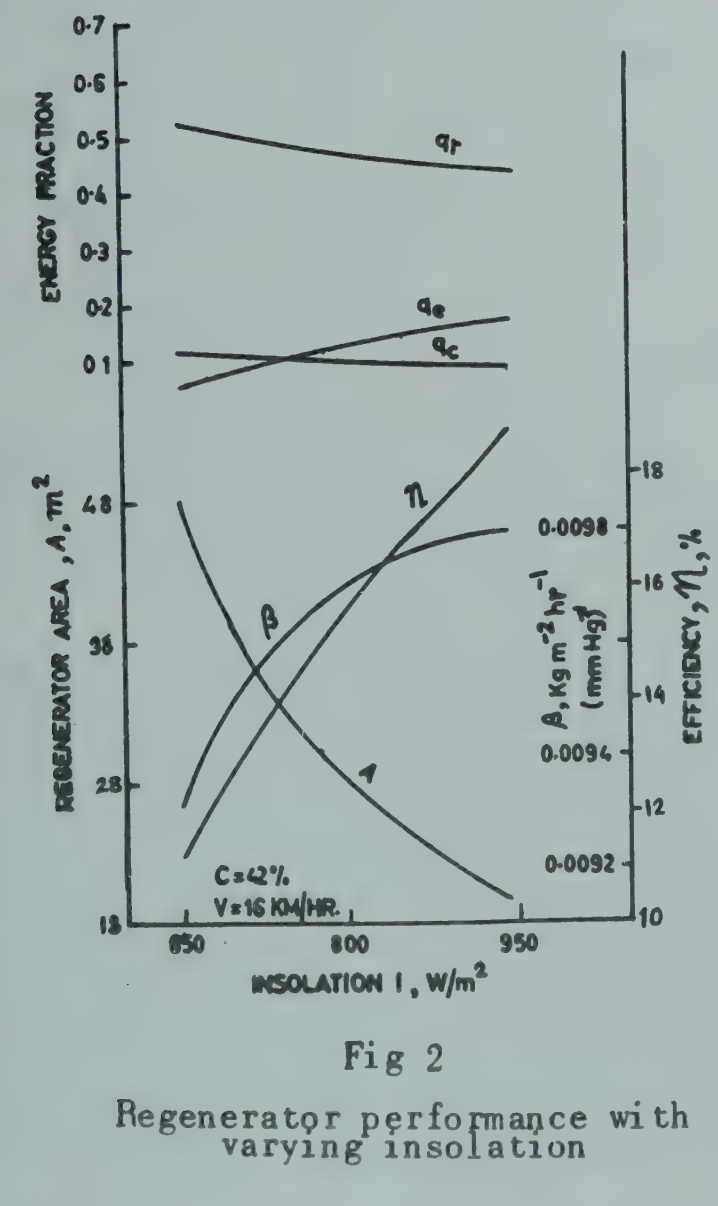


Fig 2

Regenerator performance with varying insolation

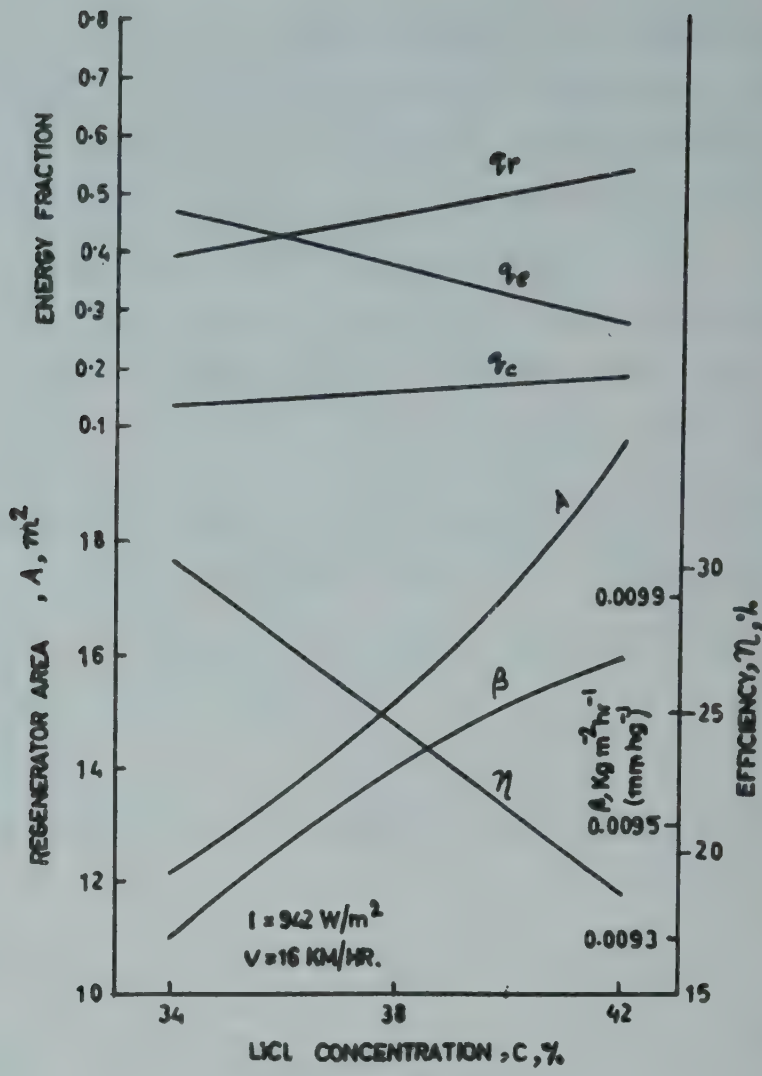


Fig 3

Regenerator performance with varying LiCl concentration

The η values reported by Hollands[2] are slightly higher than those computed in the present work. This is due to the fact that in Hollands' results, efficiency has been computed from the experimental data chosen for a time period when the effect of thermal inertia could be ignored. Similarly in his theoretical analysis, also, thermal inertia effect has been neglected. However, for a continuously flowing system discussed in the present work thermal inertia of brine will always be present and must be taken into consideration.

From Fig 3, β is found to increase slightly with increase in concentration of LiCl; however, regenerator surface area required for a given evaporation rate also increases, and that too, at a faster rate, because pressure potential for mass transfer drops down rapidly with increase in concentration.

The assumption made in equation (15) is reasonably good and gives the T_e values

very close to those obtained from Brunt's relation[7].

Conclusion

Solar still can be used satisfactorily for the regeneration of LiCl brine in a humid climate.

Acknowledgement

Thanks are due to the Director, Central Mechanical Engineering Research Institute, Durgapur for his permission to publish the paper.

Appendix

Sample regenerator design of LiCl-H_2O combination.

The following data are used -

$I_t = 942$	$\tau_c = 0.87$	α_c	$= 0.06$
$\epsilon_c = 0.96$	$\alpha_b = 0.9$	ρ_b	$= 0.1$
$\epsilon_b = 0.95$	$m = 5.1$	M_d	$= 143.0$
$V = 16$	$K_c = 1.038$	x_c	$= 0.003$
$K_i = 0.0465$	$x_i = 0.1$	$T_{bo}-T_{bi}$	$= 15$
$C_p = 0.745$	$T_a = 308$	C_d	$= 40.5$

$f_w(T_{ci})$ is taken from steam table and $f_b(T_{bo}, C_c)$ is used from Threlkeld[8].

The regenerator area comes out to be 19.8 m^2 with an efficiency of 18.72%.

A free convection regenerator[9] would require 14.4 m^2 of area for same solar insolation and for a water vapour pressure of 21 mm Hg in the ambient air.

References

[1] P. Gandhidasan, V. Sriramulu and M.C. Gupta, 'Performance characteristics of solar regenerators', Proceedings of the National Solar Energy Convention of Solar Energy Society of India, Dec 20-22 (1978) p 685.

[2] K.G.T. Hollands, 'The regeneration of lithium chloride brine in a solar still for use in solar air conditioning', *Solar Energy*, 7, 39-43 (1963).

[3] A. Kakabayev and M. Golaev, 'Glazed flat surface as a solution regenerator for use in an absorption solar cooling system', *Applied Solar Energy*, 7(4) 80-83 (1971).

[4] P.I. Cooper and W.R.W. Read, 'Design philosophy and operating experience for Australian Solar Stills', *Solar Energy*, 16, pp 1-8 (1974).

[5] A. Whillier, 'Design factors influencing solar collector performance', Low Temperature Engineering Applications of Solar Energy, ASHRAE, New York (1967) p 27.

[6] P.I. Cooper, 'The maximum efficiency of single-effect solar stills', *Solar Energy*, 15, p 105 (1973).

[7] G.V. Parmelee and W.W. Aubele, 'Radiant energy emission of atmosphere and ground', *Trans ASHVE*, 58, p 85 (1952).

[8] J.L. Threlkeld, Thermal environmental engineering, Prentice-Hall (1962) p 295.

[9] M. Prasad, P. Kumar and B.C. Raychaudhuri, 'Open cycle solar absorption refrigeration system for process cooling and air-conditioning applications', *CMERI Internal Report*, Dec (1978).

ENERGY LOSSES IN SMOOTH PIPE BENDS

USHA S. POWLE*

Abstract

The present paper deals with the graphical representation of energy losses in smooth pipe bends for turbulent and laminar flow. Nekrasov's empirical equations based on Abramovich's experimental results on bend losses and Blasius' and Nikuradse's well established results for straight pipe frictional loss are combined to develop equation for energy losses for turbulent flow. Equivalent friction factor f_b is presented as a function of Reynold's number for wide range of radius ratios and bend angles. Similar plot is obtained for laminar flow through 90° bends using experimental results by Kittredge and Rowley. The nomographs presented can be used for determining energy losses in curved elements involved in fluid machinery and fluid handling systems.

Introduction

Bends have considerable engineering importance in design and analysis of fluid handling systems and fluid machinery like turbines and pumping machines. A bend acts as an obstruction to flow causing additional loss of energy due to separation and turbulence in the case of both open and closed conduits. The study of energy losses due to bends will be useful for designing various systems involving curved elements.

The literature cited shows that extensive theoretical work[1,2] is carried out on turbulent and laminar flow in curved pipe or coil where flow is fully developed except initial entrance length. Comparatively very limited theoretical work[3] is done on energy losses in pipe bends. Upto 1950, experiments were carried out on bends with circular, square and rectangular cross-sections to study the flow phenomenon, energy losses and pressure and velocity distribution. Pigott[4,5] correlated the experimental work of previous investigators. Experimental results for bends of limited geometry were reported by Kittredge and Rowley[6] and Smith[7]. The most comprehensive work was presented by Ito[8] and Miller[9] where effect of Reynold's number, radius ratio, bend angle, length of upstream and downstream tangents on bend loss coefficient was investigated. Nekrasov[10] presented empirical equations for loss coefficients based on Abromovich's experimental results. Based on these results for bend losses and Blasius' and Nikuradse's results on straight pipe friction in smooth pipes, Powle and Kar[11] presented optimum radius ratios of pipe bends for turbulent flow regime.

*Indian Institute of Technology, Bombay 76.

Extensive experimental work is carried out by research workers in the field of energy losses in pipe bends, however the work is not systematically compiled for ready use as design charts. The present paper aims in giving graphical representation of energy losses in bends by using empirical equations and experimental results of previous investigators. The graphs presented can be used as nomographs by designers of fluid handling systems involving curved elements.

Analytical relations

Fig 1 illustrates the geometry of a pipe bend. For any bend with turbulent or laminar flow situation,

$$h_b = \frac{f_b L V^2}{2gd} = \frac{f_b R\theta V^2}{4gr} = K_c \frac{V^2}{2g} + \frac{f_s L V^2}{2gd}$$

$$= K_c \frac{V^2}{2g} + \frac{f_s R\theta V^2}{4gr} \quad .. (1)$$

This gives relation between f_b, k_c and f_s as

$$f_b = \frac{2K_c}{\theta R/r} + f_s \quad .. (2)$$

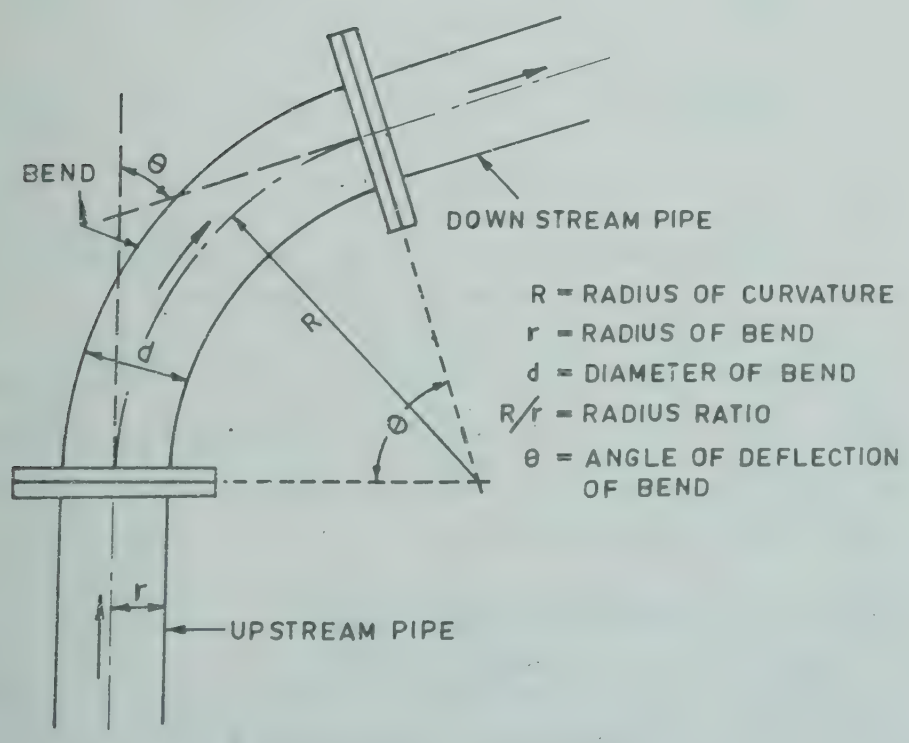


Fig 1
Geometrical parameters of bend

Equivalent friction factor for turbulent flow through smooth pipe bends

Nekrasov[10] proposed empirical expressions for K_c based on the experimental investigations of Abramovich for bend angle θ from 0° to 180° and radius ratio R/r from 1 to 25 as

$$K_c = A(\theta)\ [K_1 + K_2\ (r/R)] \quad .. (3)$$

where values of $A(\theta)$, K_1 and K_2 are given in Table I.

TABLE I

θ	A(θ)	K_1	K_2
90°	Sin θ	0.051	0.38
⩽ 70°	0.9 Sin θ	0.051	0.38
⩾ 100°	0.7 + 0.35 θ°/90°	0.051	0.38

The well established results of Blasius and Nikuradse[12] for turbulent flow in smooth straight pipes with circular cross-section are given as

$$f_s = f_1 + f_2/(N_R)^m \quad .. (4)$$

where values of f_1, f_2 and m are given in Table II.

Using empirical equations (3) and (4) in equation (2), equivalent friction factor for bend f_b can be determined for various values of bend angle θ, radius ratio R/r and Reynold's number N_R. Figs 2 to 7 show the variation of f_b with N_R for various values of θ and R/r.

Equivalent friction factor for laminar flow through 90° pipe bends

The work carried out on laminar flow

TABLE II

N_R	f_1	f_2	m
< 10^5	0	0.3164	0.25
> 10^5	0.0032	0.221	0.237

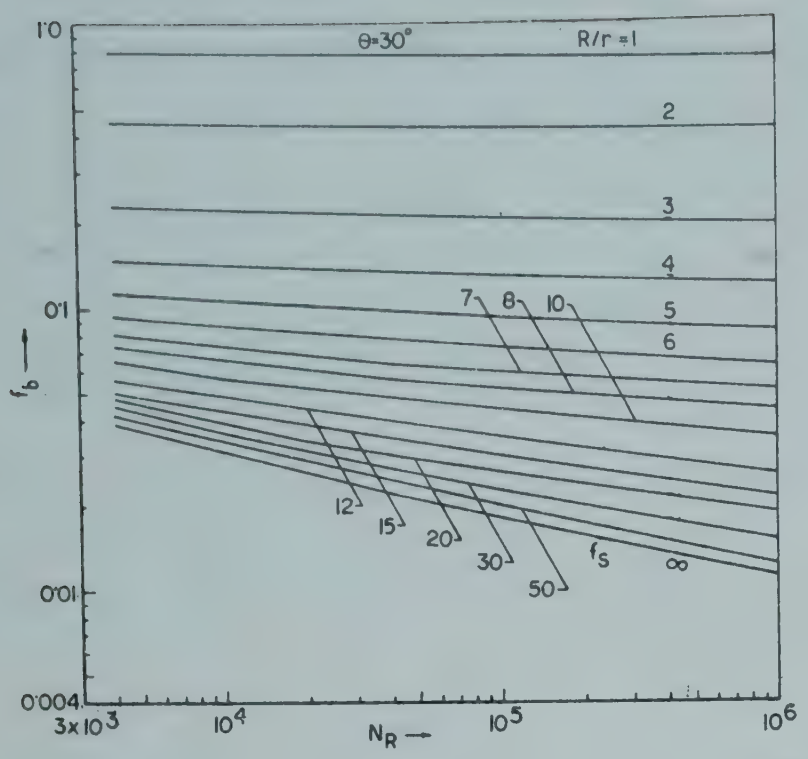


Fig 2

Variation of f_b with N_R for turbulent flow through 30° bends

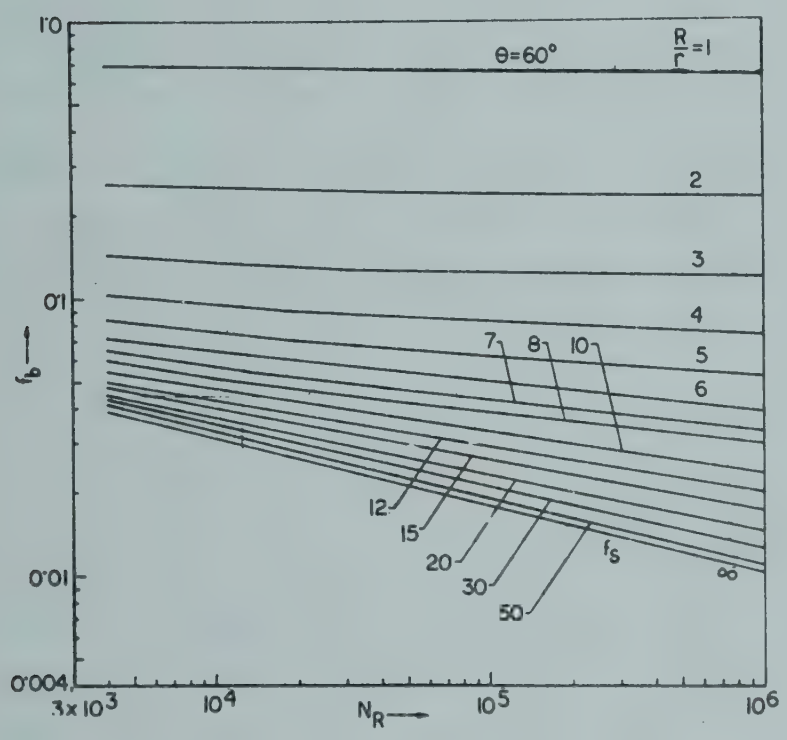


Fig 3

Variation of f_b with N_R for turbulent flow through 60° bends

through pipe bends is very limited. The only work reported so far is by Kittredge and Rowley[6] who presented experimental results for loss factor K_c as a function of Reynold's number for 90° bends with radius ratios of 4.52, 6.08, 13.06 and 23.42. Using these experimental results for K_c and taking $f_s = 64/N_R$ for laminar flow, values of f_b for these bends were determined by using equation (2). By interpolating these results, finally a plot presen-

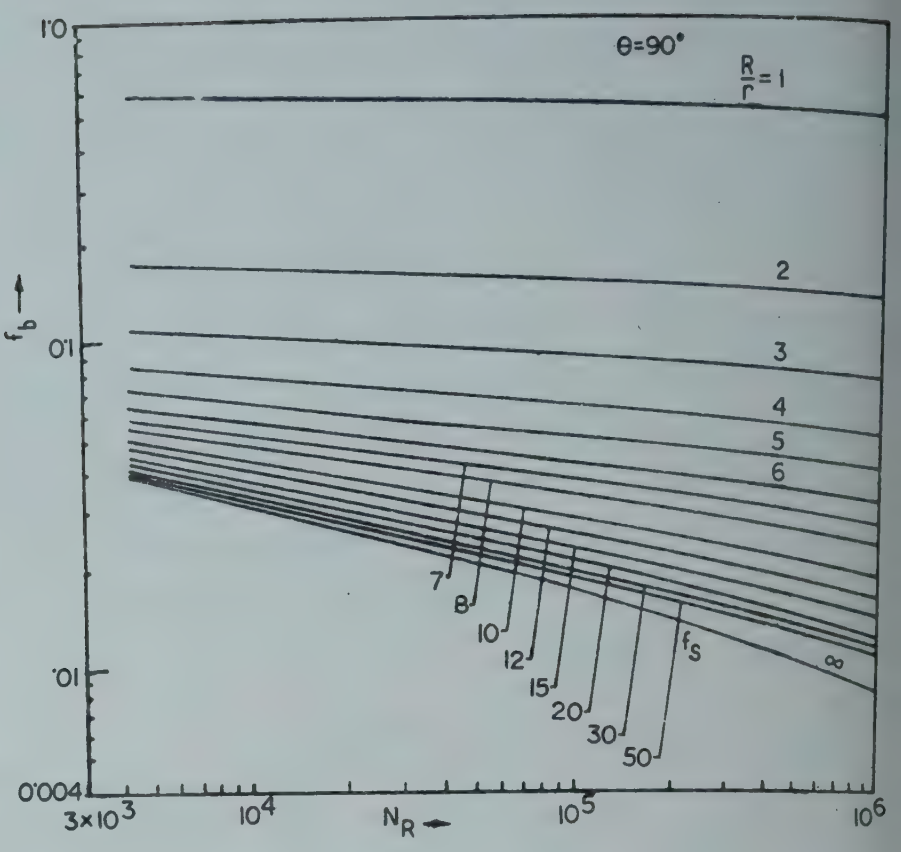


Fig 4

Variation of f_b with N_R for turbulent flow through 90° bends

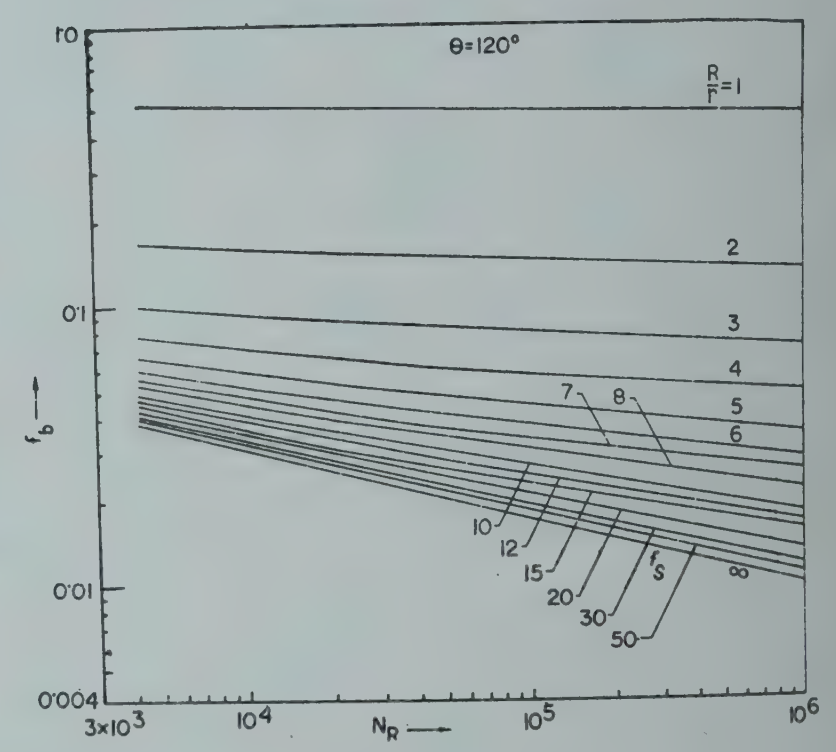


Fig 5

Variation of f_b with N_R for turbulent flow through 120° bends

ted in Fig 8 was obtained for f_b as function of Reynold's number for various values of radius ratios for 90° pipe bends with laminar flow situation.

Results and discussion

Results presented in Figs 2 to 7 show that the equivalent friction factor f_b for pipe bends with turbulent flow decreases with increase in Reynold's number N_R, in-

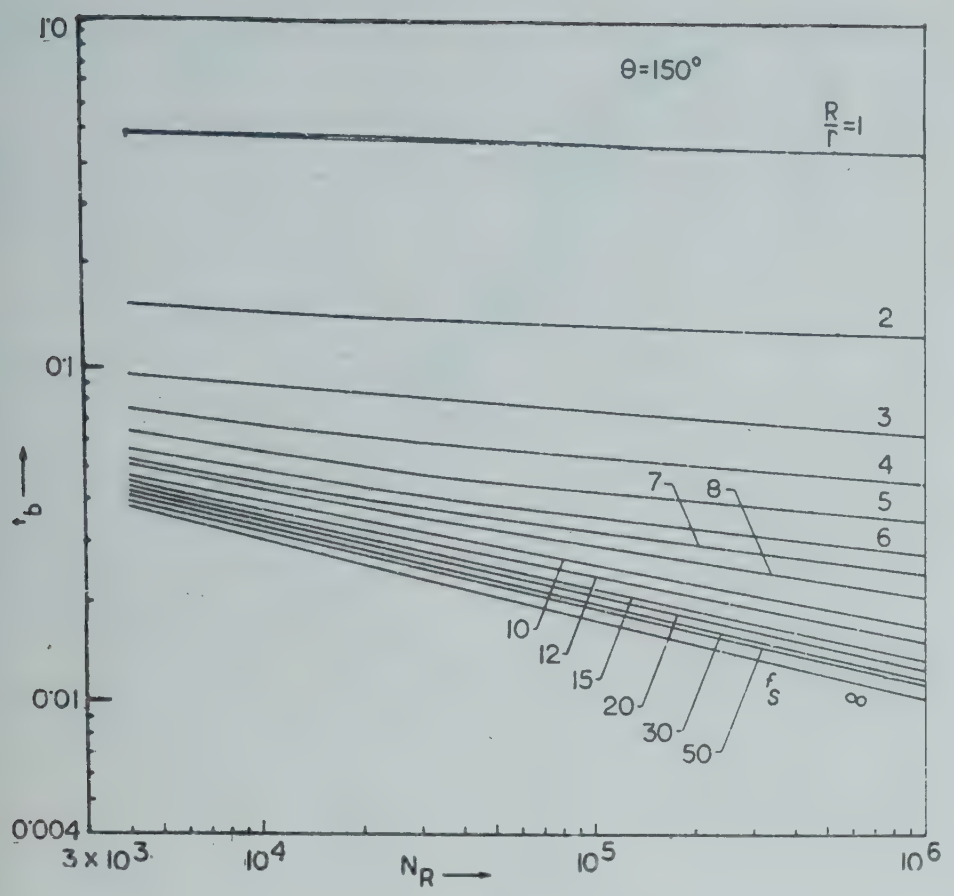


Fig 6

Variation of f_b with N_R for turbulent flow through 150° bends

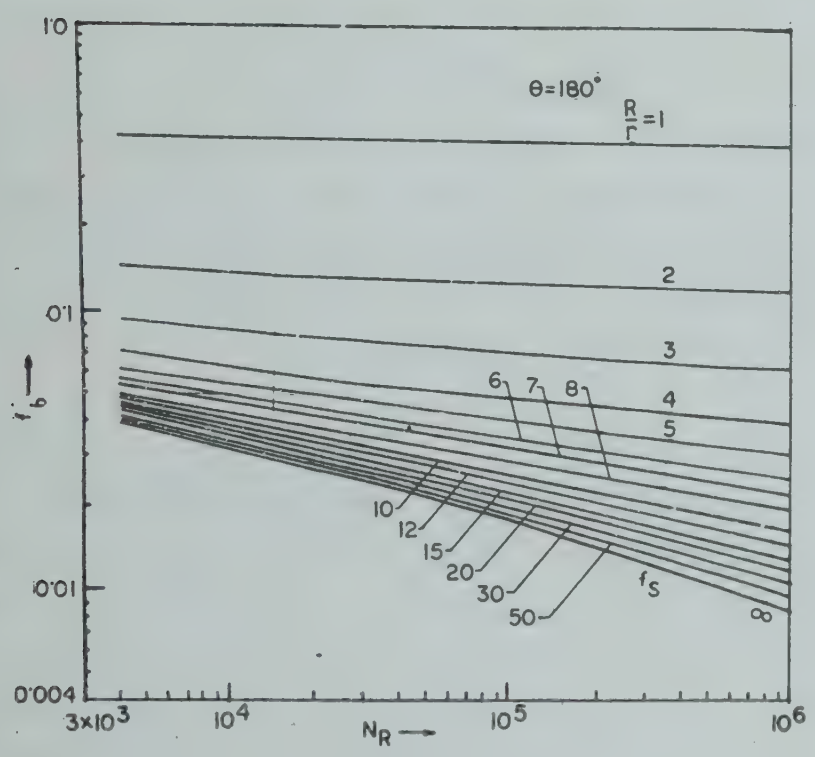


Fig 7

Variation of f_b with N_R for turbulent flow through 180° bends

crease in radius ratio R/r and increase in bend angle θ.

Figs 8,9 and 10 show the comparison of present relation with experimental results presented by Ito[8] It can be seen that the present relation for friction factor f_b compares very well with the experimental results by Ito and other investigators.

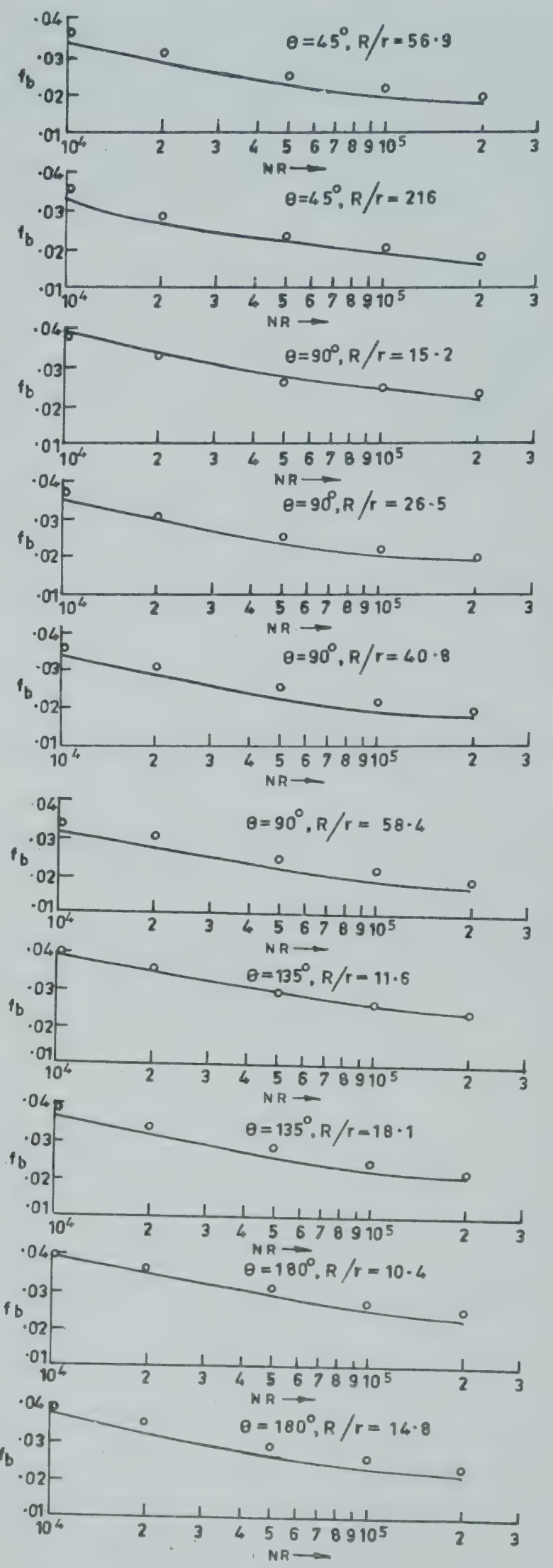


Fig 8

Comparison with results in Fig 6 by Ito[8]

The empirical equations proposed for loss factor K_c are based on the experimental results for ratio R/r from 1 to 25. How-

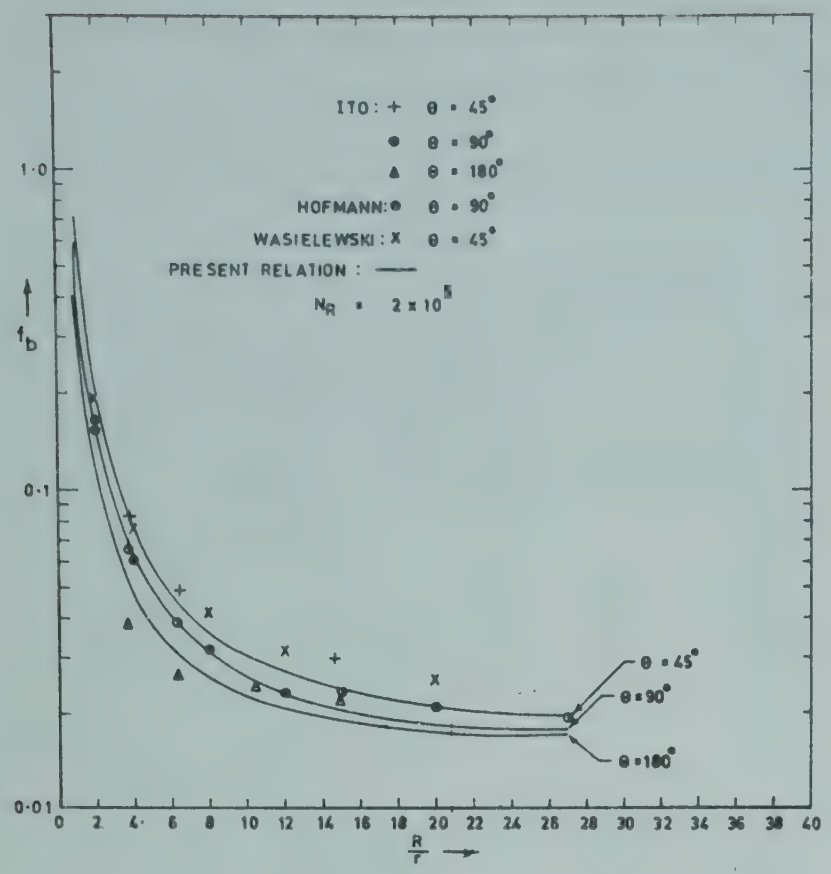


Fig 9

Comparison of present calculation with results of Ito[8]

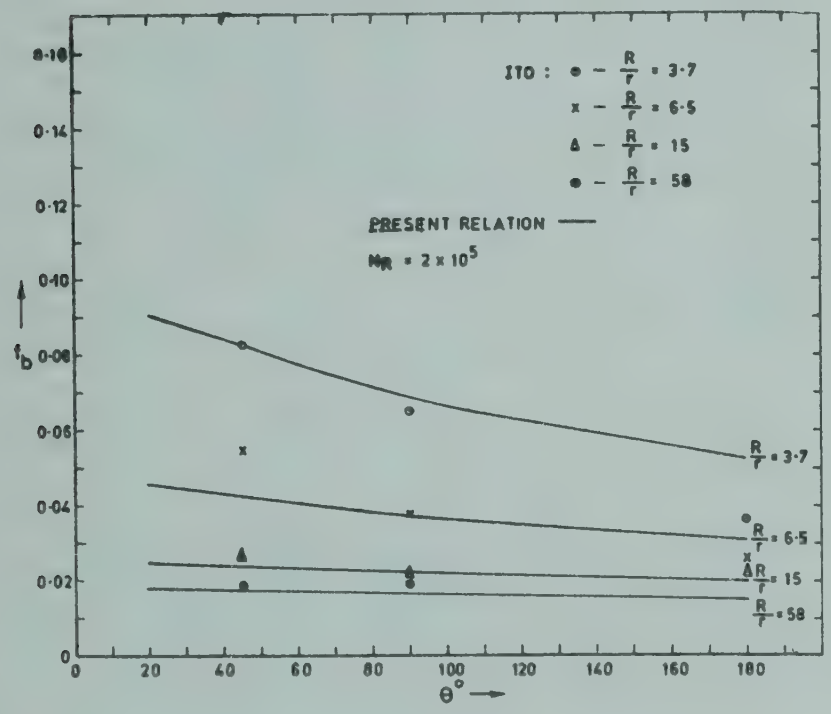


Fig 10

Comparison with results in Fig 8 by Ito[6]

ever the comparison shows that the experimental results for radius ratios greater than 25 also match very well with the present relation. The inclusion of radius ratios 30 and 50 in Figs 2 to 7 is thus justified.

Fig 11 presents the variation of equivalent friction factor f_b with Reynold's

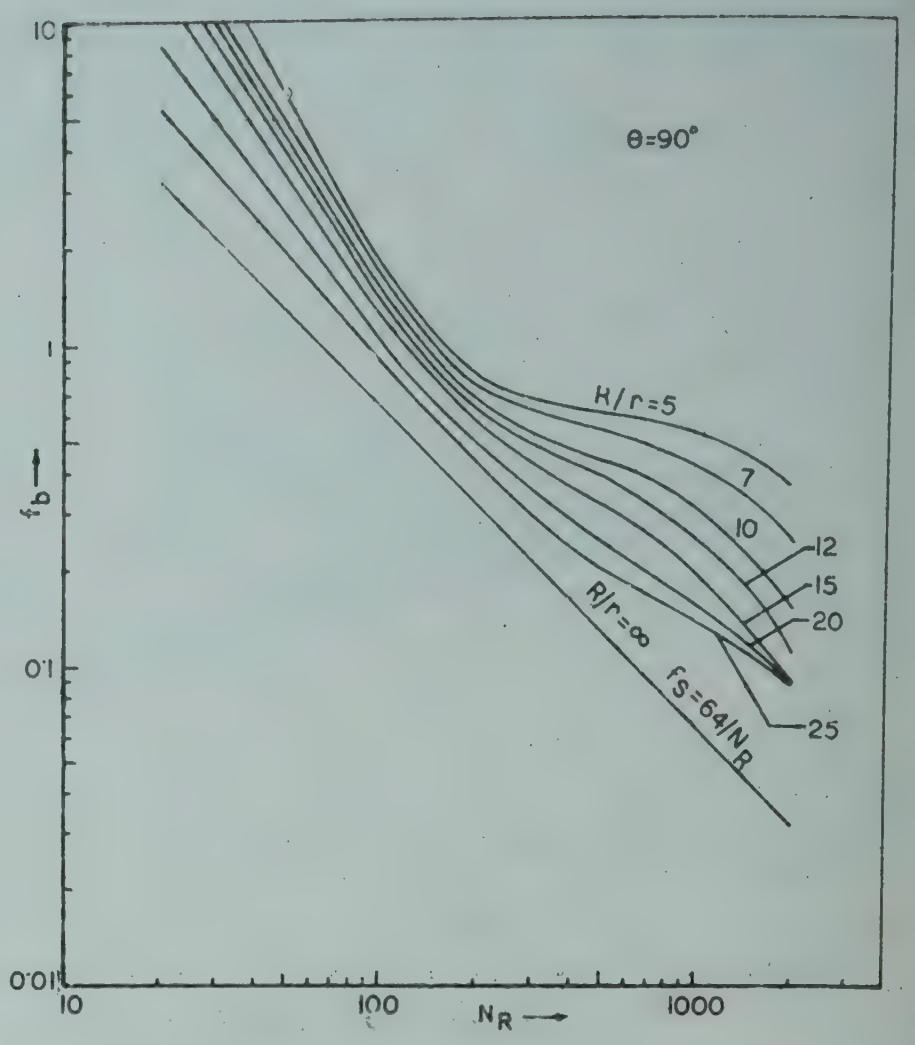


Fig 11

Variation of f_b with N_R for laminar flow through 90° bends

number for various radius ratios R/r for 90° pipe bends with laminar flow situation. Like turbulent flow, f_b for laminar flow is found to decrease with increase in Reynold's number and radius ratio.

The results in Figs 2 to 7 and Fig 11 can be readily used to determine the total energy losses due to bend h_b at given N_R by using relation $h_b = f_b\, R\theta V^2/4gr$. These graphs will be useful to estimate the losses in curved elements of specified geometry in fluid machines and fluid handling systems.

Conclusions

1. Equivalent friction factor of bend decreases with increase in Reynold's number and increase in radius ratio for both turbulent and laminar flow regimes.

2. Equivalent friction factor of bend decreases with increase in bend angle θ for turbulent flow regime.

Nomenclature

d	Diameter of the bend = $2r$
f_b	Equivalent friction factor of the bend
f_s	Friction factor for straight pipe
g	Acceleration due to gravity
h_b	Total energy loss in the bend
K_c	Curvature loss factor of the bend
L	Axial length of the bend = $R\theta$ where θ is in radians
N_R	Reynold's number = $\rho Vd/\mu$
r	Radius of the bend
R	Radius of curvature of the bend
R/r	Radius ratio
V	Average velocity of flow
ρ	Density of fluid
μ	Dynamic viscosity of fluid
θ	Angle of deflection of the bend.

References

[1]S.V. Patankar, V.S. Pratap and D.B. Spalding, 'Prediction of turbulent flow in curved pipes', *Jour Fluid Mech*, 67(3) 595 (1975).

[2]L.C. Truesdell (Jr) and R.J. Adler, 'Numerical treatment of fully developed laminar flow in helically coiled tubes', *AI Chem Engg Jour*, 16(6) 1010 (1970).

[3]Y.R. Reddy and S. Kar, 'Energy losses in smooth pipe bends', Proceedings of the International Symposium on High Velocity Flow, Indian Inst of Sci, Bangalore, No 133, p 19 (1967).

[4]R.J.S. Pigott, 'Pressure losses in tubing, pipes and fittings', *ASME Transactions*, 72, p 679 (1950).

[5]R.J.S. Pigott, 'Losses in pipes and fittings', *ASME Transactions*, 79(8) 1767 (1957).

[6]C.P. Kittredge and D.S. Rowley 'Resistance coefficients for laminar and turbulent flow through one and half inch valves and fittings', *ASME Transactions*, 70, p 1759 (1957).

[7]A.J.W. Smith, 'Flow and pressure losses in smooth pipe bends of constant cross-section', *Royal Aeron Soc Jour*, 67(631) 437 (1963).

[8]N. Ito, 'Pressure losses in smooth pipe bends', *ASME Transactions*, Series D, p 131 (1960).

[9]D. Miller, **Internal flow - A guide to losses in pipe and duct systems**, The BHRA Publications, England (1971).

[10]B. Nekrasov, 'Local features and minor losses', **Hydraulics**, Peace Publications, Moscow (1965).

[11]U.S. Powle and S. Kar, 'Optimum radius ratio for smooth pipe bends with turbulent flow', *Jour Inst Engrs (India)*, 56, Pt ME2, p 75 (1975).

[12]Blasius and Nikuradse, 'Experimental results of turbulent flow in smooth pipes', **Fluid Mechanics** by R.F.A. Pao, John Wiley & Sons Inc, p 243.

METALLURGICAL INVESTIGATION INTO TUBE FAILURES IN POWER PLANTS

A.B. MANDAL, B.K. GHOSH, A. BASU AND S. JANA*

Abstract

Failures in boiler tubes may occur due to various reasons. Central Mechanical Engineering Research Institute at Durgapur has often been involved in such failure analysis. In this paper some typical case studies of tube failures in various power plants mostly located in eastern India, have been documented.

Introduction

Although failures may occur in a relatively low percentage of the total boiler tubes used in a power plant, they may cause critical breakdowns leading to forced shutdowns of generation. Sometimes they may also lead to serious accidents causing wide attention and publicity. Failures are of extreme importance to plant operators, maintenance personnel, fabricators and suppliers. People, after all, learn from mistakes and hence, a correct diagonistic analysis of such failures help in their future prevention. The Central Mechanical Engineering Research Institute at Durgapur and its MERADO extension centres at Pune, Madras, Ludhiana and Cochin have often been involved in the investigation of such boiler tube failures. The present paper documents some of these investigations that the Institute and its extension centres had conducted in the past.

*Central Mechanical Engineering Research Institute, Durgapur 9.

Background information

The commonly observed tube failures may occur due to various reasons. Indeed, the conditions that may promote them are too numerous to list. However, in a broad generalization one may attribute the following factors to cause failures.

1. Deficiencies in design
2. Incorrect material selection
3. Poor material quality
4. Deficiencies in fabrication, lay-out and assembly
5. Deficiencies in operating conditions
6. Deficiencies in maintenance.

It is often found that no one reason but a combination of several of the above factors is responsible for the failure. A failure investigation and subsequent analysis should determine the primary cause of failure, and based on the conclusion, corrective actions should be initiated that will prevent similar failure.

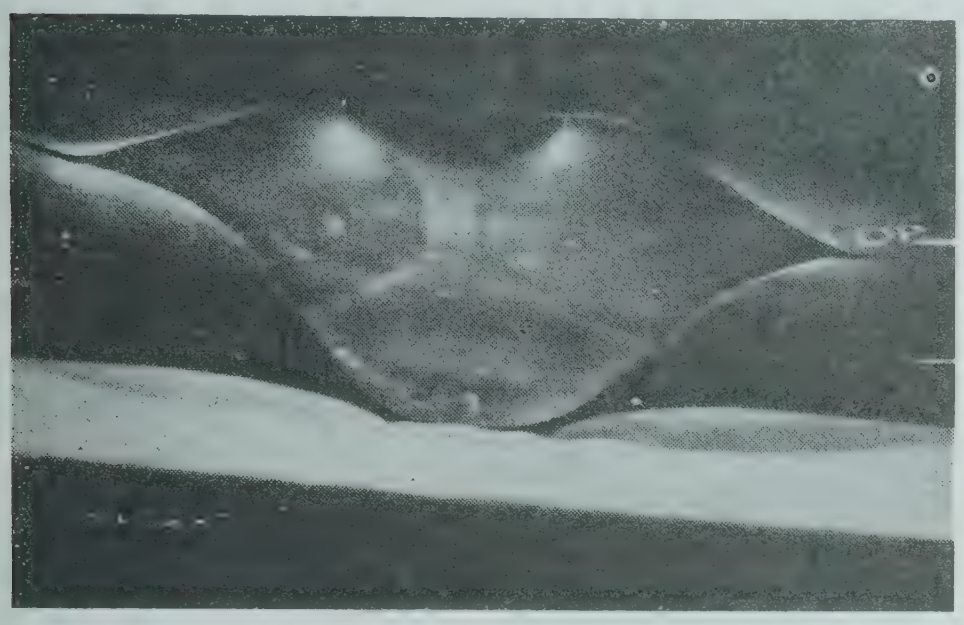
In the subsequent part of this paper cases of a few typical tube failures in power plants have been discussed to show how metallurgical investigations have helped establish the causes behind such failures.

Case studies

Case I

The power plant in this case reported

sudden failure of water wall tube in the front wall of the furnace. The location of the rupture was about 9 metres below the drum and about 30 metres above the lower header tube. The tube had opened up in a manner as shown in Fig 1. Considerable thinning of the ruptured edges was noticed.

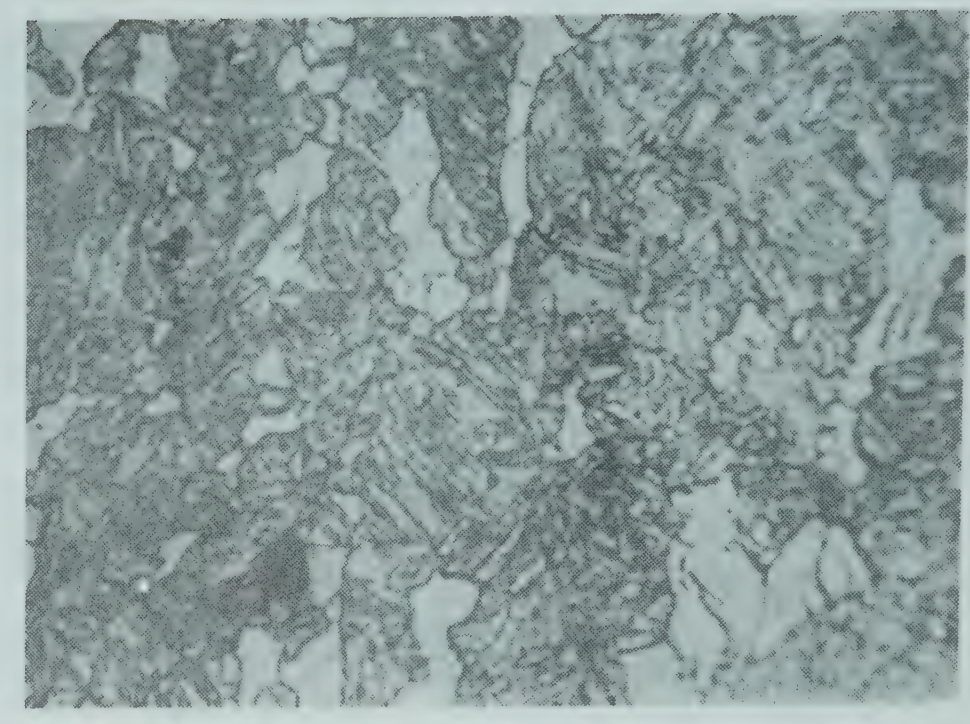


Mag 1/9 x

Fig 1
Thin-lip rupture of water wall tube

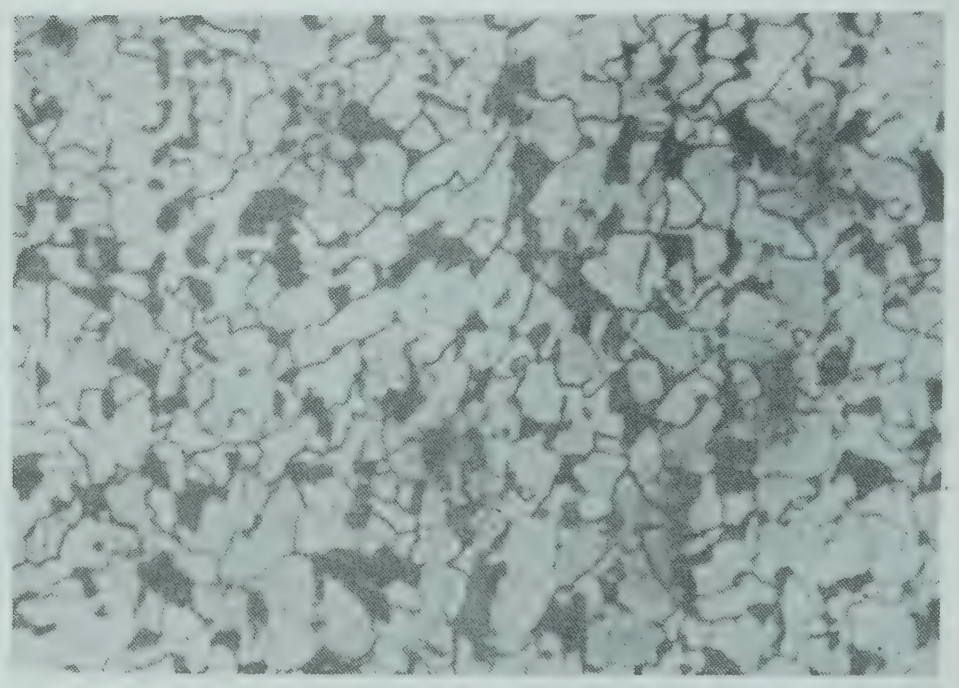
This is what is commonly known as 'thin-lip' rupture. There were no scales, corrosion products and pitting marks either on the inside or the outside surface of the subject tube. Investigations revealed that the tube underwent sudden overheating to a temperature in the range of 800° - 825°C. This weakened the tube which deformed plastically to a considerable extent before bursting occurred. This in turn released a flood of water and steam which quenched the overheated steel and thus produced a mixed martensitic-ferritic microstructure (Fig 2) in the area of rupture - which was in marked contrast to the normally observed pearlite-ferrite microstructure (Fig 3) of this class of steel.

It appeared that the subject tube failed due to sudden overheating over a very small and localized area. Water starvation in the tube due to obstruction to circulation appeared to be the likely reason behind this failure.



Mag 800 x

Fig 2
Microstructure of tube material in the area of rupture



Mag 150 x

Fig 3
Normal microstructure of the tube material away from the rupture

Case II

The power plant in this case reported rupture in one of its secondary superheater tubes. The tube opened out with a characteristic 'fish-mouth' appearance which was about 38 cmd long and 8 mm wide at its maximum (Fig 4). The rupture was accompanied by noticeable localised swelling. No scales were observed either on the inside or the outside of the tube.



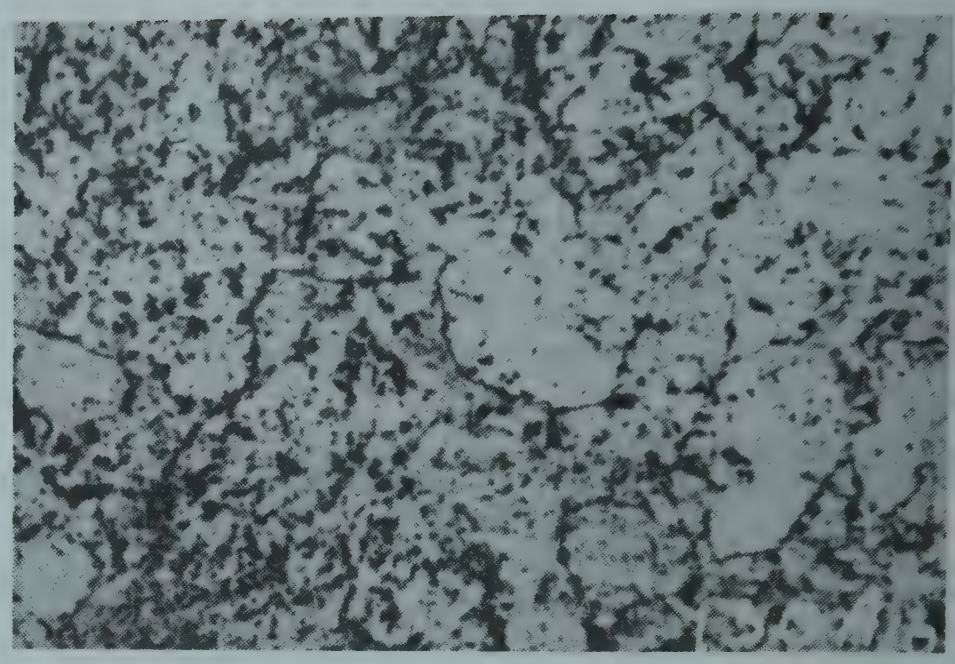
Mag 1/9 x

Fig 4
Fish-mouth rupture of secondary superheater tube

Microscopic examination of specimens taken from the vicinity of the rupture showed coalescence of fine alloy carbide particles in a matrix of ferrite (Fig 5) which was distinctly different from the normal microstructure (Fig 6) of this class of steel It thus appeared that the localised area of the tube was subjected to a temperature somewhat above the design temperature for a prolonged period. This alone could explain the spheroidization and coalescence of the carbides as seen in Fig 5. As a result of the prolonged overheating, slow and progressive plastic deformation took place in the affected area and finally rupture occured.

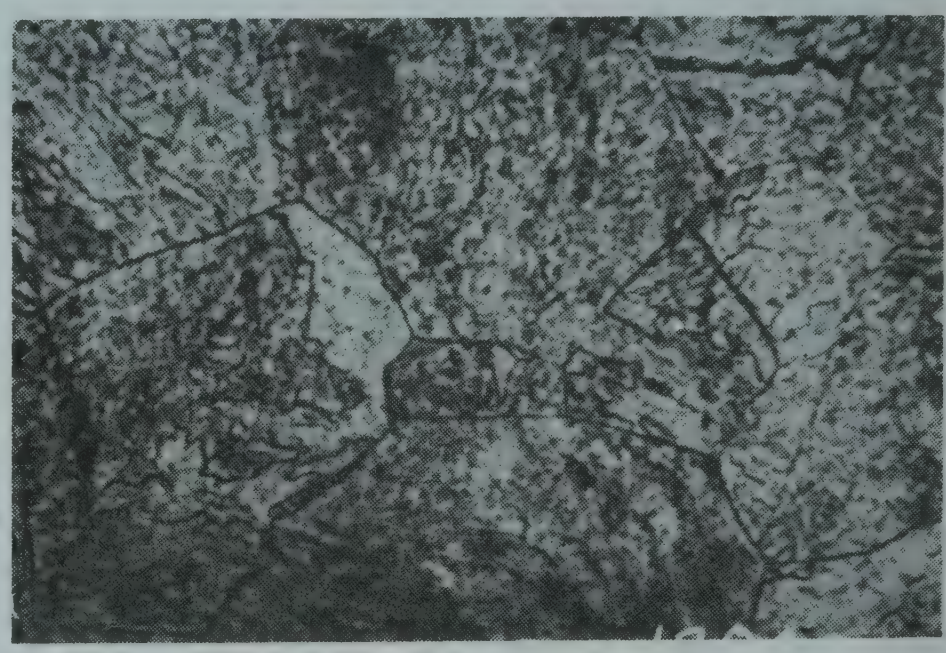
Case III

The economiser intermediate box drain tube in this power plant suffered a typical 'thick-lip' type rupture (Fig 7). There was evidence of a tightly adhering black scale on the outside surface of the subject tube. Investigations revealed that the tube was subjected to prolonged overheating. Intercrystalline penetration of oxide scales (the so-called oxide rootings) from the external surface of the tube (Fig 8), considerable decarburization and spherio-



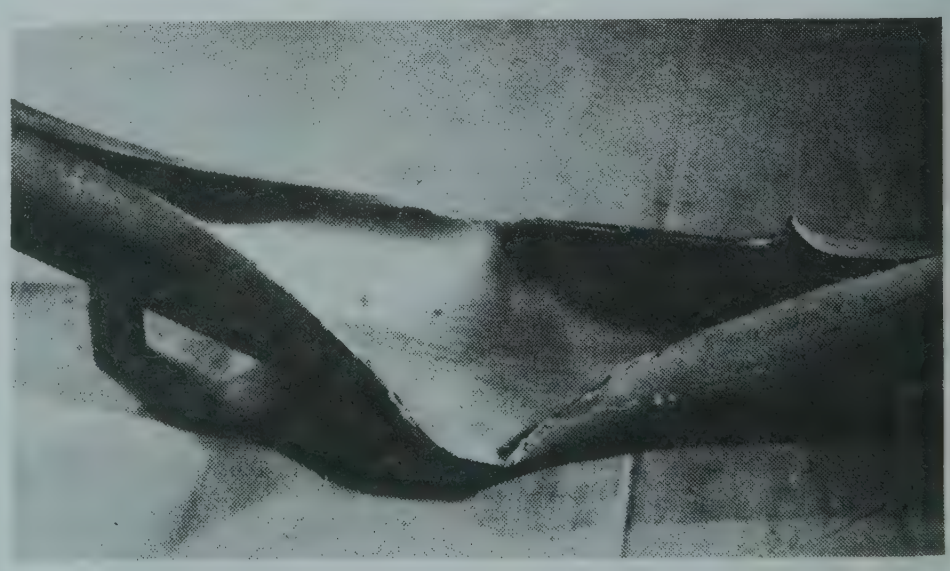
Mag 500 x

Fig 5
Microstructure of the tube in the vicinity of rupture showing coalescence of carbides



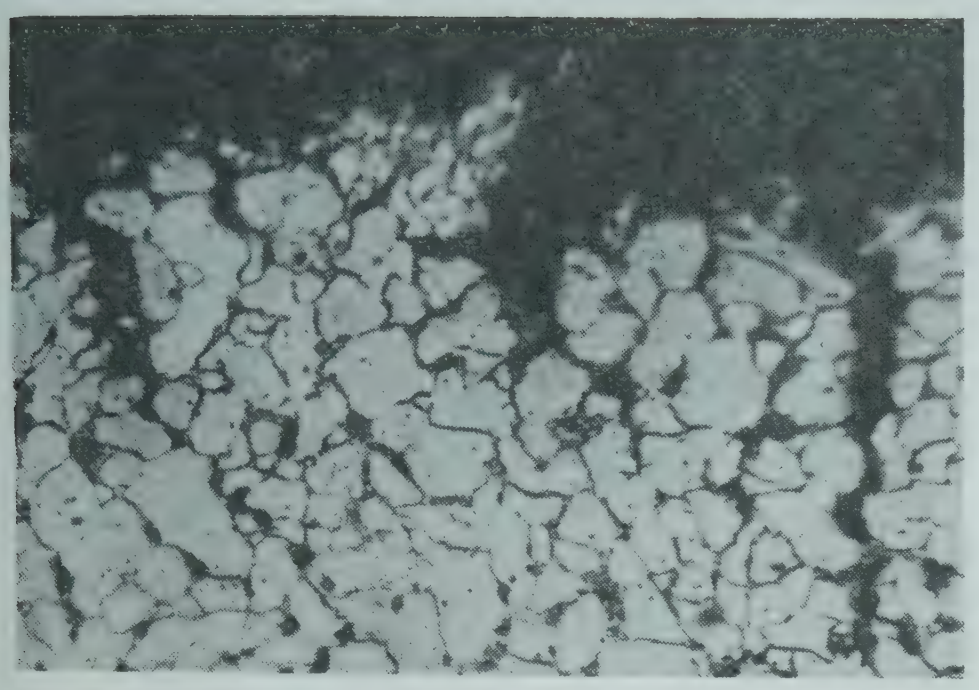
500 x

Fig 6
Normal microstructure of the tube material away from the rupture



Mag 1/9 x

Fig 7
Thick-lip rupture of economiser intermediate box drain pipe



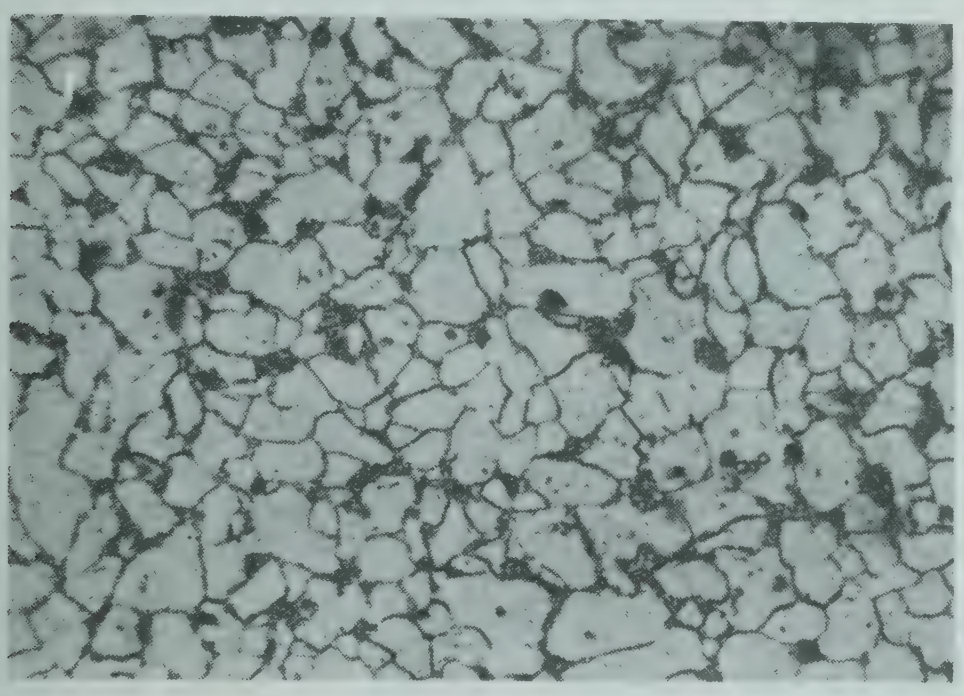
300 x

Fig 8

Oxide-rootings observed on the outside surface of the tube

dization of the matrix microstructure (Fig 9) spoke amply for slow and prolonged overheating.

The economizer tubes are located in the flue gas region of the furnace and thus overheating in this case appeared possibly due to formation of steam blanket inside the drain pipe. The power plant experienced similar failures in this drain pipe a few more times. Finally, they overcame the problem by replacing the pipe with a more expensive heat resistant alloy piping.



Mag 300 x

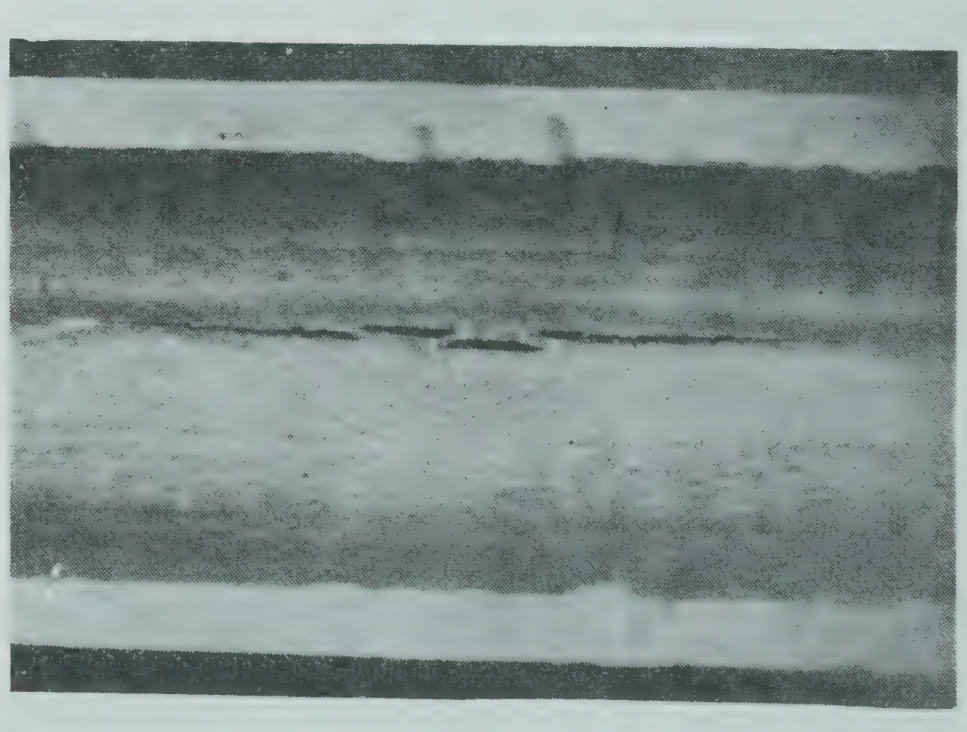
Fig 9

Matrix microstructure in the affected area showing extensive decarburization and spheroidization

Case IV

The secondary superheater tube in a power plant showed some longitudinal discontinuous cracks (Fig 10). The total length of the cracks was about 53 cms. The tube appeared to be quite clean with no internal or external scales. There was no evidence of any swelling, pitting or erosion marks. On dissection of the tube longitudinally, the bore surface was found to be uneven and noticeable ribs (alternate elevation and depression) were observed on the inside.

In this particular case, the failure appeared to be related to material defects in the tube. Formation of ribs on the bore surface during tube drawing seemed to have a major contributory effect towards this failure.



1 x

Fig 10

Propagation of the crack on the bore surface

Case V

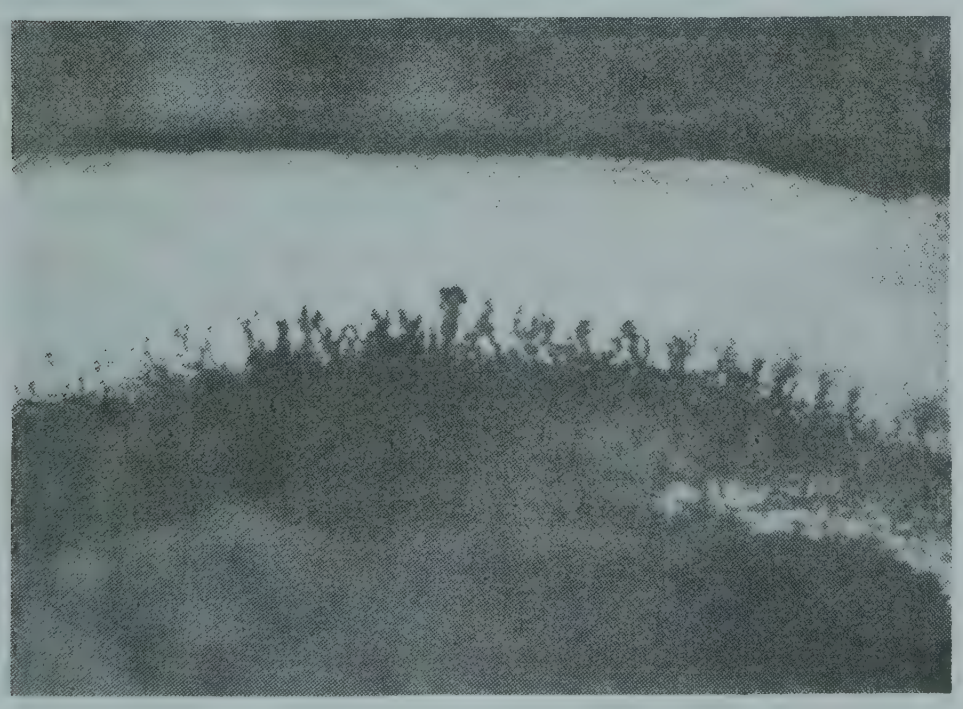
The power plant in this instance noticed leakage in one of the water wall tubes. The tube, however, ran for more than 60000 hours before the leakage started. On removing and sectioning the tube, the water side appeared to be extensively corroded (Fig 11). The tube wall had considerably thinned. Microscopic examination of the failed tube section in the vicinity of



1 x

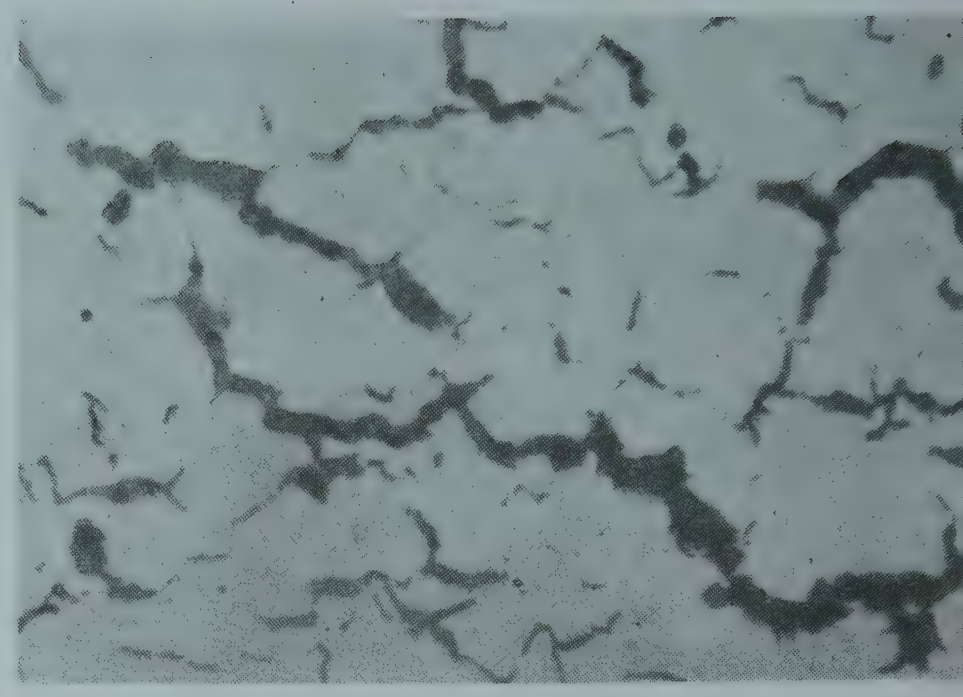
Fig 11
Corroded area on the water side surface

leakage disclosed a black porous zone on the inside surface of the tube (Fig 12). Microscopic examination revealed extensive discontinuous intergranular cracks and appreciable decarburization of the matrix in and around the affected area (Fig 13). The nature of failure appeared to be due to hydrogen damage in this particular instance.



Mag 5

Fig 12
Porous zone as observed on sectioning the tube

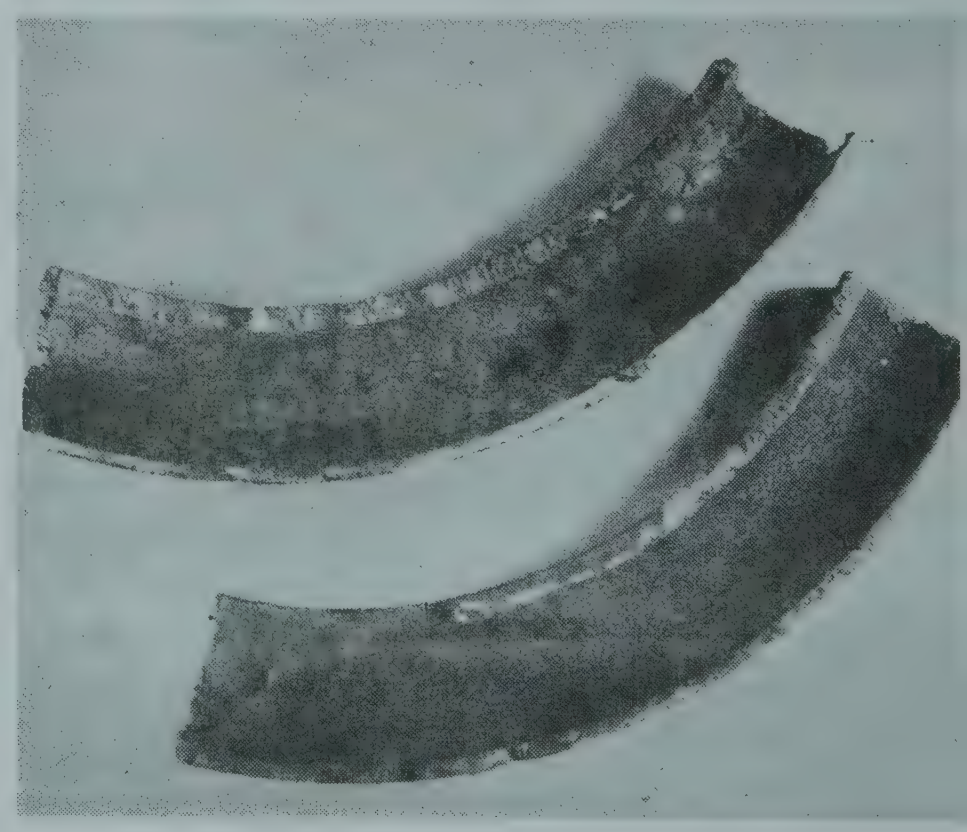


Mag 300 x

Fig 13
Discontinuous intergranular cracking due to hydrogen damage

Case VI

Boiler feed water line in a plant developed leaks along bends. There was very little external damage observed but on sectioning the tube, extensive internal damage in the form of cavities of geometrical shape were observed at the bends (Fig 14). On thorough investigation, it appeared that the cavities were essentially erosion



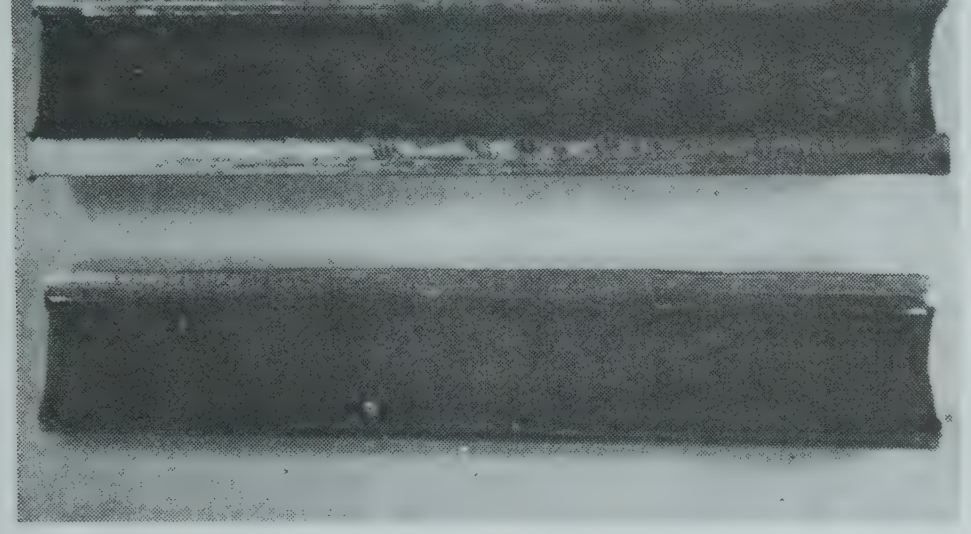
Mag 1/3 x

Fig 14
Cavities and internal damage at bend

pits caused as a result of repeated impingement of gas bubbles or solid particles on the bend surface. These types of pits are characterized by their sharp edged appearance and often their horse-shoe shape is due to turbulence produced by solid particles.

Case VII

After about 15 years of service, which was of course interrupted for periods of shutdown and repairs, the inlet header tubes of superheater in another power plant were found to be perforated. Several isolated and sharply defined pits were found on visual examination of the inside bore surface (Fig 15). There was a loosely adherent magnetic rust on the inside.



Mag 1/3 x

Fig 15
Isolated pits on the inside of the tube

Detailed micro- and chemical analyse of the tube and the deposits led to th conclusion that in this case the tube underwent internal corrosion under workin condition. This form of corrosion and pit ting usually occurs if boiler water is car ried into the tubes and is evaporated then thus leaving dry salts inside the tubes When the boiler is shut down, condensatio occurs in the tubes and this redissolve the salts to produce droplets of concen trated solution which initiate corrosion Once corrosion starts, it tends to continu whenever the boiler is shut down.

Conclusion

Failures of boiler tubes can occur du to a host of reasons. A correct diagnois tic analysis in the lines as shown in thi paper of such failures greatly helps powe plant engineers to identify their cause and remedy the drawbacks.

Acknowledgement

The authors gratefully acknowledge th valuable contributions made by various de partments and research workers at CMERI i conducting such investigations over th years, and the assistance of numerous powe plant authorities who have liberally spon sored and encouraged such investigations The authors thank the Director, Centra Mechanical Engineering Research Institute for his permission to publish this paper.

A REVIEW OF SURFACE ROUGHNESS MEASUREMENT TECHNIQUES

R.A. AGARWAL*, M.P. KUMARASWAMY AND S.K. BASU**

Abstract

This paper presents a review of surface roughness measurement technique. These techniques have been classified into two basic groups; the contacting type such as tactile and stylus method, and the non-contacting type based on optical and pneumatic principles. A brief description of techniques for measuring statistical parameters of roughness height has also been presented.

Introduction

A clear understanding of the functional characteristics of components needs quantitative assessment of surface roughness. Particular attention began to be paid to the problems of roughness measurement about the year 1930 and this attention has steadily increased till date when some knowledge of the subject is available in engineering plants practice.

Operational functions which are influenced by the surface condition of a component are dependent on two main characteristics of the surface : (1) the geometrical character, and (2) the metallurgical aspects. Greater effort has, however, been put to the assessment of the first characteristic, since it is closely and directly related to actual production techniques and, in general, requires a non-destructive type of test.

Instruments designed to assess the geometrical attributes of a surface are of two types, one having an output dependent on the three-dimensional character of the surface and the other limited to a two-dimensional analysis. To enable the many and varied parameters to be measured, instruments have been developed which incorporate different physical phenomena produced by surface conditions (eg, optical, electrical, hydraulic, pneumatic, mechanical etc).

No instrument has an infinite range of measurement. At one end the range is limited by the sensitivity and at the other end by its measuring capacity and the size of the specimen it can accommodate. The measuring ranges of some of the well known instruments are given in Table I.

Surface roughness measuring instruments can be broadly classified in two groups : (1) contacting type of instruments (tactile and stylus method), and (2) non-contacting type such as pneumatic and optical instruments. A brief description of important roughness measurement techniques is given below.

Taper sectioning method

In fact this is a destructive method of measuring surface roughness. In this method the specimen is sectioned at a very

*TELCO, Jamshedpur.

**Central Mechanical Engineering Research Institute, Durgapur 9.

TABLE I

Measuring ranges of instruments

	Technique	Surface	Comment	Height sensitivity
1)	Multiple beam Fizeau fringes	Silvered optical flat		$\lambda/100$
2)	Two-beam interference fringes	Uncoated optical flat or curved		$\lambda/50$
3)	Stylus instrument	Any optical surface	Surface profile shows both flatness and roughness	Variable ≈ 25 Å
4)	Holography	Any surface	Depth counter 0.75 - 2 x 10^5 can be obtained by immersing object in combination of liquids or gases	Variable $> 0.75\ \lambda$
5)	Multiple beam fringes of equal chromatic order (Feco)			~ 3 Å
6)	Light scattering			~ 10 Å
7)	Equidensity technique two-beam Fizeau fringes			$\lambda/50$ to $\lambda/2$
8)	While light speckle			0.6 to 6.4 μm

Note : 1 Å = 10^{-8} cm

shallow angle to the surface and the section is polished and examined microscopically. The magnification depends on the angle between the cutting plane and the plane of the surface (Fig 1).

$$\text{Magnification } M = L_1/H = \text{Cot } \alpha$$

However, this method can not be used for inspection because it destroys the surface examined.

Contacting type instruments

Tactile method

The simplest, cheapest and oldest way to measure surface roughness is the touch method (tactile method). Drawing an edge such as a finger nail or coin across the surface to be measured and comparing the feel or sound with that of a reference surface, consistent estimates with good accuracies can be obtained by skilled workers[2].

Rubert[3] has developed an instrument to perform tactile testing in which the coin or finger nail has been replaced by a thin

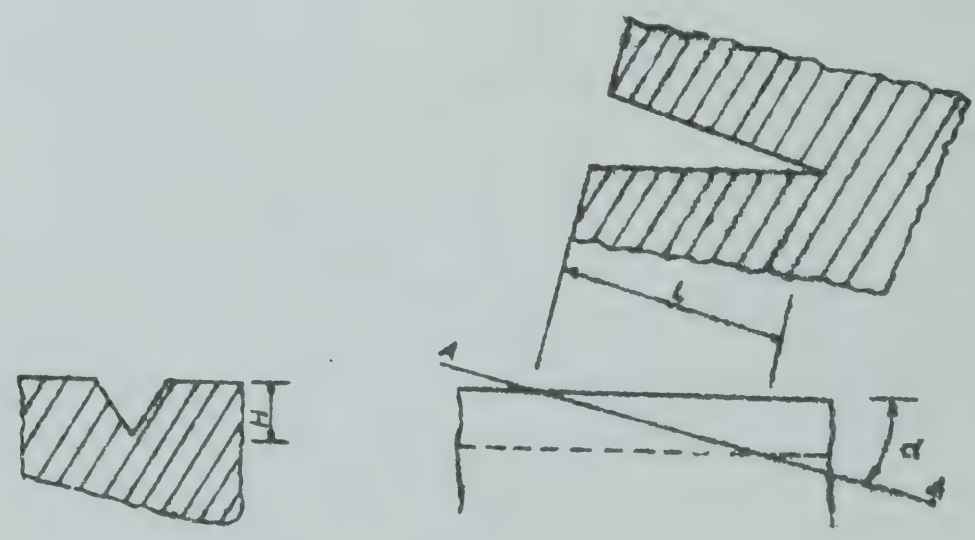


Fig 1
Taper section method

blade which buckles at an angle depending on the roughness (Fig 2). The judgement whether the surface is rough or smooth, must be done in comparison with standard specimens. Sets of machined specimens suitable for tactile comparison test are commercially available.

Stylus method

This is the most common method of measuring the surface roughness. The instrument consists of a sharply pointed stylus, which slides over the surface being tested. The vertical movement of the stylus is highly magnified and can be read off on a motor or recorded on a chart whose horizontal movement can also be magnified. Vertical magnifications are usually of the order of 10^3 to 10^5 times while the horizontal magnification of 20 and 100 is common. A recent development by Rank Taylor Hobson uses a vertical magnification of 10^5. Among the representative instruments are the Rank Taylor Hobson 'Talysurf', the perthometer. the Abbott profilograph and the Phillips roughness tester etc.

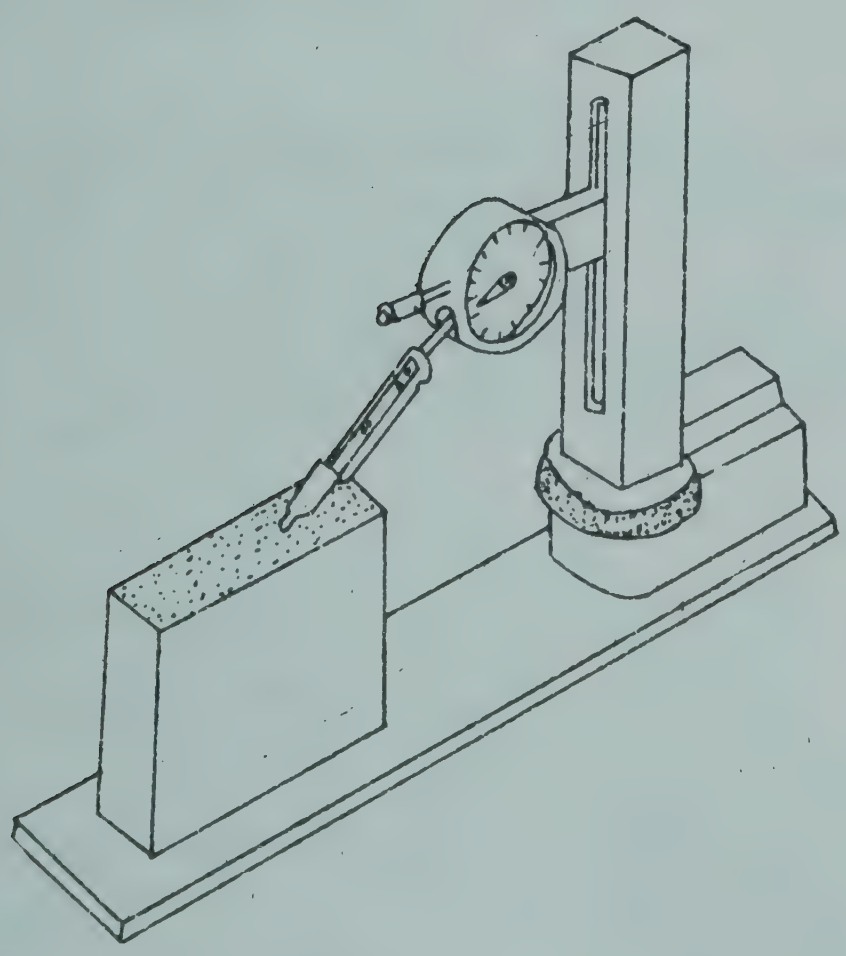


Fig 2
Tactile method

The fundamental requirements of an instrument are high magnification and very light operating force and the fitness of reproducing the result. The high magnification of the stylus movement can be achieved either by mechanical, optical, pneumatic or electrical means. Instruments based on these principles are available in the market. The Tomlison surface roughness tester is based on the principle of mechanical magnification. Forster and Kiesewetter surface roughness testers have optical magnification. Topograph instrument has pneumatic magnification. However, most of the popular instruments such as Rank Taylor Hobson 'Talysurf', perthometer etc have electrical magnification. One important advantage of the electrical magnification is the possibility of obtaining very high amplification in steps from 10^3 to 10^5 times. The transducers used for converting the mechanical displacement of the stylus into electrical signals are of mainly two types : (1) current or potential generating devices, and (2) carrier modulating devices (Fig 3)

The current generating method is one in which the stylus is connected to a small coil which moves with the stylus in the magnetic field of a permanent magnet. The current generated is proportional to the amplitude and the frequency of the stylus movement. Abbott profilograph is designed on this principle (Fig 3a)

In the piezo-electric method (potential generating instrument) a piezo-electric crystal is stressed in tension or compression as a result of the mechanical displacement of the stylus. Due to these stresses a voltage will be generated in the piezo-crystal which is proportional to the stylus movement. Phillips roughness tester is designed on this principle (Fig 3b).

The carrier modulating devices give an output signal which is dependent only on the position of the stylus. The signal remains constant while the stylus is in a given position. A high-frequency carrier signal is modulated by the variation in inductance of a differential coil arrangement in the pick-up. The coils constitute the arms of an AC bridge the output of which is amplified, demodulated and passed through a variable filter network to a roughness recording meter or directly to a trace recorder[4]. The Taylor Hobson 'Talysurf' and perthometer are designed on this principle.

The representation of the surface obtained by any stylus instrument is not a true reproduction of the actual surface. The distortions are due to different vertical and horizontal magnification[5] (Fig 4), finite size of the stylus point[6-10], dynamic response of the stylus[11,12] and its lateral deflection[13], and effect of surface datum, plastic deformation under stylus[14] etc.

Theoretically, to provide a true reproduction of the surface irregularities, the stylus tip radius should be zero and the cone angle of the stylus as small as possible. The usual cone angles of the stylii are 90° and 60° and the stylus shape may be conical, pyramidal or chiesel edged. In all cases the tip will have certain radius. Most of the commercially available instruments have tip radius varying from 0.5 μm to 15 μm[15]. The finite dimension of the stylus tips implies that the path it traces will not exactly follow the profile of the real surface. It may not enter deep and narrow valleys, and may record sharp peaks as cusps.

Nakamura[10] has analysed the distortion introduced by the stylus tip radius for surface waves of cosine and triangular waveforms. In case of cosine wave forms the error is not more than 10 per cent for the standard 2.5 μm stylus radius if the pitch of the irregularities is greater than 12 μm and total height less than 6 μm. The stylus can never bottom on a true triangular wave form.

V. Radhakrishnan[6] and D.E. Williamson[7] have analysed the influence of stylus tip

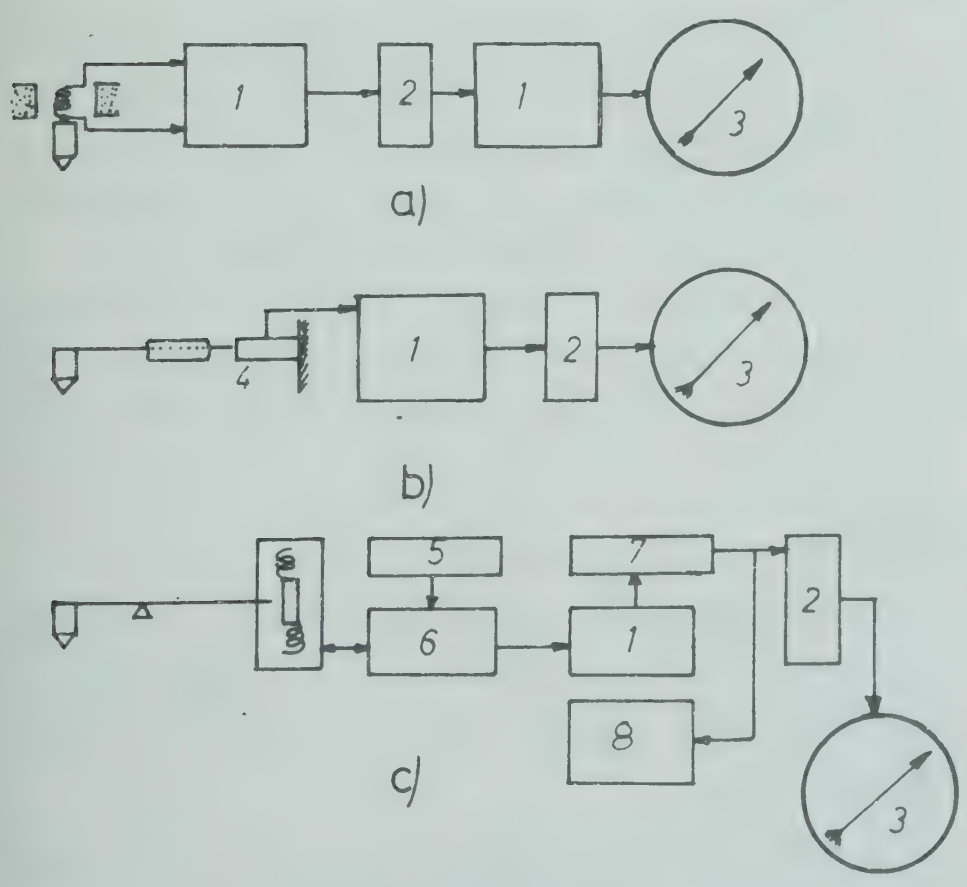


Fig 3
Schematic illustration of stylus instrument, (a) current generating, (b) potential generating, (c) carrier modulating. (1) Amplifier, (2) Filter, (3) Motor, (4) Piezo electric element, (5) Oscillator, (6) AC bridge circuit, (7) Demodulator, (8) Tracer recorder

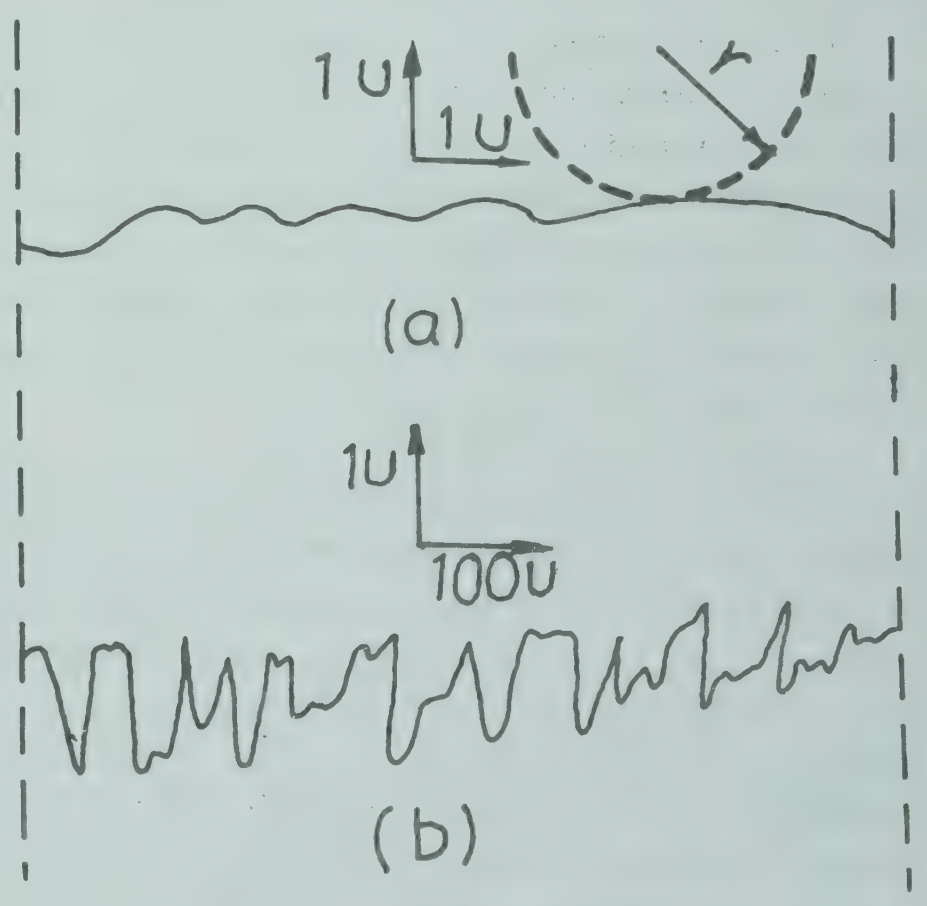


Fig 4
Distortion due to different vertical and horizontal magnification

radius on surface roughness value. Profiles having smaller wave-length get modified considerably even with small increase in the stylus radius. Thus ground, honed and electro-chemically machined surfaces show considerable variations in comparison to planned, spark eroded and turned profiles. The roughness values need not necessarily always decrease with increasing stylus radius. With certain profiles an increase *Ra* value was noticed with increasing stylus radius. This is possible due to thickening of the profile peaks and negligible change in the valley portion[6].

D.J. Whitehouse[8] has shown that for conventional finishing process such as grinding, diamond turning etc, the reduction in rms value is only 1 or 2 per cent. However, for the 10 μm stylus tip the loss of information may be 10 to 15 per cent.

Effect of dynamic response of the stylus[11,12] and its lateral deflection[13] have also been investigated by many researchers and shown to be negligibly small.

The movement of the stylus is generally measured relative to a selected datum. The datum is obtained by a skid which has relatively large radius of curvature (about 6 mm) compared to the stylus (about 10 μm). The use of any skid (or shoe) type pick-up automatically ensures a distorted trace of the surface since the output represents the relative movement between the skid and the stylus.

Some researchers[14] have observed surface damage due to the stylus movement specially on soft metal surfaces and have suggested that it can be a source of serious error. This has been refuted convincingly by Reason[16] and Williamson[17]. As Williamson comments, the analogy is with a bulldozer ploughing over a range of hills; the trail it left, though clearly visible, would follow the topography of the land sufficiently closely for most practical purposes.

The length of the surface sampled obviously influences the roughness values obtained. In 'M' system the effect of waviness is usually excluded by using standardised sample lengths. The instrument indicates the mean value of the measure taken from several such samples consecutively. It has been found that as the sample length increases, scatter of roughness values between samples decreases. Increase in sample length does not increase the RMS value but generally increases the numerical value of maximum peak to valley height. This is, because the longer the sample length the greater the probability of a high peak and a deep valley occurring in the sample[18].

Stylus method gives only a two-dimensional measure of surface finish at the position of measurement. However, a three-dimensional picture of surface finish can be achieved by tracing a number of parallel profiles on the surface[19].

Non-contacting type instruments

Surface roughness measuring instruments of non-contacting type are based on optical or hydraulic principles. Most of the optical instruments designed for roughness measurement are based on the principle of interferometry. The essential advantage of interferometric method is that it gives a picture of surface roughness over the area in the field of view.

Interferometric method

Surfaces which are sufficiently smooth and well finished to reflect light may be examined by making use of interference fringes.

Because of the wave nature and the rectilinear propogation of light, the generation of light interference is possible, as a rule, if two trains of light waves can be superimposed and shifted towards one another in their phase of vibration.

If the path difference is equal to half the wavelength of the light used ($\lambda/2$) or half of an odd multiple of it $\{(2p + 1)\lambda/2\}$, then two amplitudes which are a measure of the intensity cancel out and darkness arises. Thus the distance of two neighbouring interference fringes corresponds to a difference in height of $\lambda/2$.

The common type of interference microscopes can be classified according to the arrangement of beam splitting :

(1) The interference principle according to Linnik[20], with beam splitting between objective and eyepiece (Fig 5a),

(2) The interference principle according to Krug and Lau[21] with a beam splitting between objective and object (Fig 5b)

(3) The interference principle according to Ruhle, which was developed further by Tolansky[22], in which beam splitting occurs on the real wedge. These designs are described in great deal by Von Weingraber[23]. Of the above principles, the first and second cause two beam interference and the third causes multiple beam interference.

The mode of operation of the interference microscope by Linnik is shown in Fig 5a. The light emanating from a light source is split up into two partial bundles of rays on a cube beam splitter and the partial bundles phase through objectives 1 and 2. After reflection on the surface under examination (F1) and on the reference surface (F2) they are reunited on the cube beam splitter and are capable of interference. Surface F1 and F2 form a virtual wedge giving rise to interference of equal thickness. The spatial position and the angle of wedge can be altered by tilting F1 and F2, which makes it possible to alter the direction and the distance of the interference fringes appearing in the eyepiece.

In Krug and Lau's interference principle the beam splitting takes place between objective and object (Fig 5b), so that in

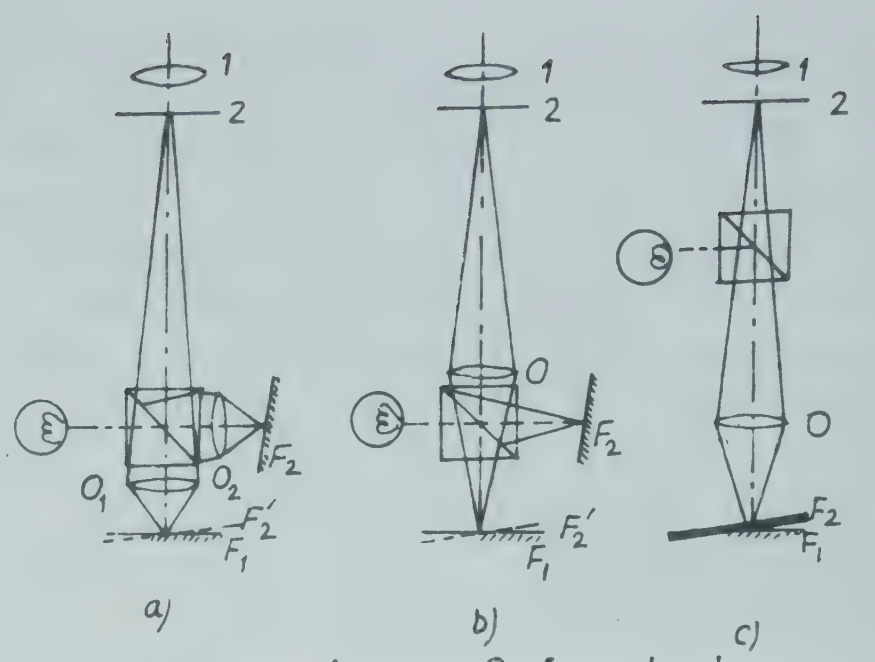


Fig 5

Interference arrangements, (a) Linnik's principle, (b) Krug and Lau's principle, (c) Ruhle's principle

contrast to Linnik's principle only one objective is required. The cube beam splitter with reference surface must be arranged between objective and object.

Ruhle's interference principle uses a beam splitting on the real wedge (Fig 5c). The wedge is formed by a thin glass plate (F2) and the surface under examination (F1). Part of the incident light is reflected on the lower glass plate and the remainder is reflected on the sample. If the distance between the sample surface and the glass plate is very small the partial bundles of rays thus generated are capable of interference after being reunited. The interferences are again studied microscopically in the conventional way. If the glass plate turned towards the sample is partially silvered, then the rays coming from the sample undergo repeated deflection and division which may cause multiple-beam interference. The multiple beam interference can only arise if the distance of the reflection surface to the sample is very small.

The Linnik principle makes it possible to realise highest apertures. This ensures full exploitation of the capability of

light microscope. The disadvantage is the intricacy of the apparatus required. The two objectives required must be highly identical optically; if not, the result will be diminution of contrast and a curvature of fringes. Interference with microscopes based on Krug and Lau principle is not influenced by the objective. However, the disadvantage of this is the limited aperture, since the cube beam splitter must be arranged between the objective and the sample.

The main advantages of multiple-beam interference over the two-beam interference are : better contrast of the narrow interference fringes and an improved possibility of evaluating fringe deflections. Further, such an arrangement can be easily designed individually by using incident light microscopes.

The disadvantage is that in commercial microscope the reference mirror is to be placed on the sample surface. Even if the mirror is made wear-resistant, it will be scratched after a short time, and cause the interference image to be disturbed. So the sample can be moved only when the mirror is raised, otherwise the mirror surface will be scratched. In contrast to the two-beam interference microscope that can operate without any handling, continuous viewing of the multiple-beam device during a shifting of the sample is impossible. Again due to participation in the interference by several partial beams coming from different spots of the surface, some kind of integration over a surface element is produced, and the total heights are falsified and described as too small under certain conditions. This applies primarily to curved surfaces which yield a permanently variable wedge angle.

Limits to interferometric measurement of roughness

The smallest measurable total height depends on the wavelength of the light used and on the character of the surface.

The total height of about 0.015 μm can be measured by two beam interference microscope. Whereas this lower limit for multiple beam microscopes is 0.005 μm, this lower limit can also be achieved by two-beam microscopes by producing 'equidensities'. Photographic equidensitometry technique was first described by Krug and Lau[24]. It is possible to get very sharp fringes of equal density. So called equidensities can be evaluated much more precisely than interferogram with hazy fringes. On account of the sharpness of the equidensities which can be regarded as contour lines like the interference fringes, the uncertainty of measurements can be reduced under favourable conditions to $\pm \lambda/200$ compared to $\lambda/20$ to $\lambda/60$ at best with interference fringes.

On rough surfaces (total height greater than 0.6 to 0.8 μm) the interference fringes are deflected to such a high degree that there course can not be followed. Total heights upto 30 μm can be measured interferometrically by means of Zehender method[25]. If the light of the partial bundle of rays falling on the sample is made to pass through a medium of the refractive index nj within the roughness, the wavelength of the light alters in terms of the equation

$$j = \lambda/nj$$

Thus we get a line standard of

$$L_M = \lambda 2.1/nj$$

If an oil immersion is used with $nj = 1.5$, then $L_M = 0.67\ (\lambda/2)$. For identical total height the deflections in the interference image will therefore be about 30 per cent greater than for observation in air (Fig 6a).

If, however, a transparent film replica (Refractive index nF) is made of the surface to be tested and put on the mirror

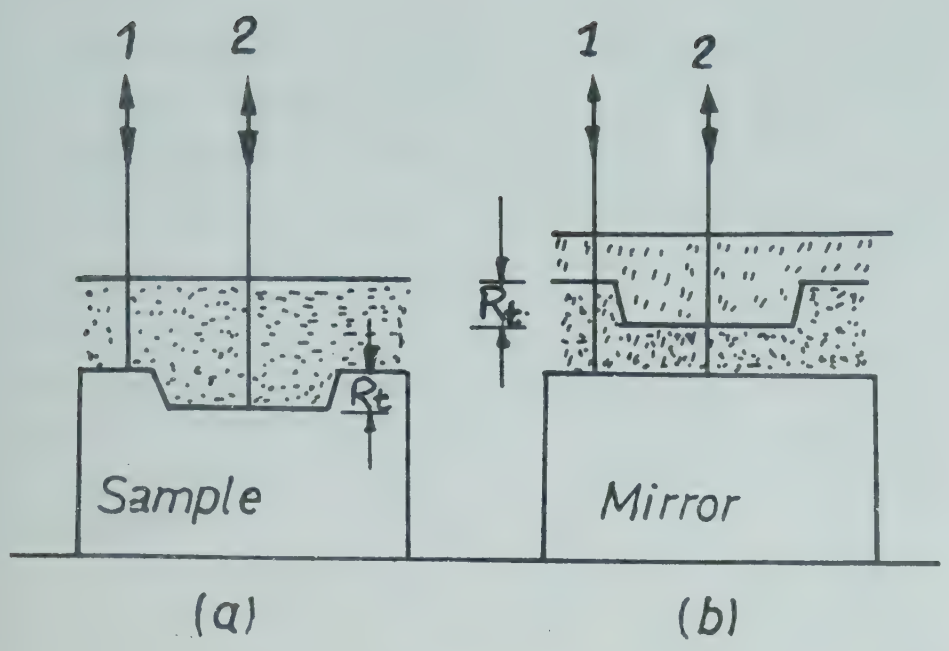


Fig 6

Interference method, (a) immersion method (b) Zehender method

surface on which there is an immersion agent, the partial bundle of rays passes through two media of different refractive indices within the range of roughness (Fig 6b). This yields a line standard of magnitude

$$L_M = \frac{\lambda}{2} \frac{1}{(n_F - n_j)}$$

Since the difference $(n_F - n_j)$ is always less than unity, the line standard becomes greater than for normal measurements. This procedure is referred to as the Zehender replica method[26].

Holographic interferometry

For an understanding of the application of holographic interferometry[27] to surface roughness measurement it is convenient to refer to Fig 7. In the configuration depicted in Fig 7, the object whose surface roughness is to be measured is photographed holographically. For this purpose the light from a laser is split into two beams. One beam denoted by U_o, illuminates the object and the other, denoted by U_r is the reference beam for holographically recording the light amplitude U_1 reflected from the object. In this figure the symbols have the following meaning : M_1, partially reflecting Mirror; M_2 and M_3 totally reflecting ultraflat mirrors; LP_1 and LP_2,

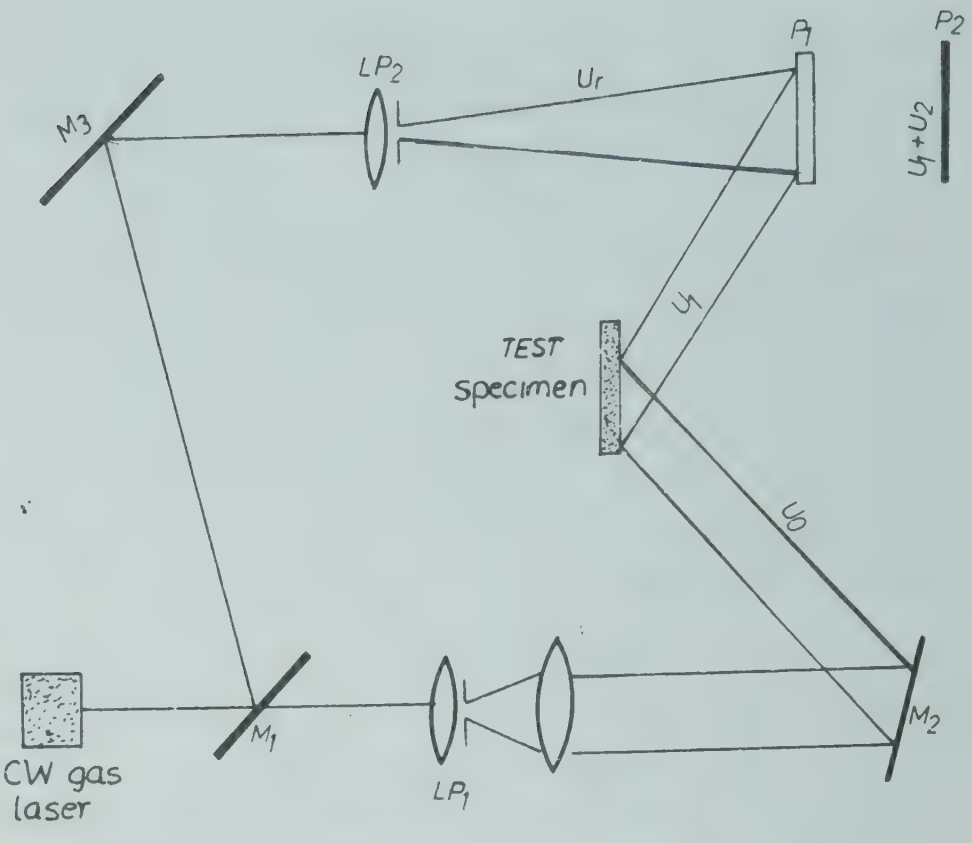


Fig 7

Principle of working of holographic interferometer

lens - pinhole spatial filters; and L_1, collimating lens.

The object beam is collimated in Fig 7 because all experimental test surfaces were planar, and a collimated object beam offers several advantages over an uncollimated beam. First, it has the advantage of good light efficiency because the reflected beam U_1 is principally specular reflection from the nominally flat test surface. In addition, it enables a simple mathematical formulation of the wavefronts U_1 and U_2 in the theoretical interpretation of the experimental data. In the experimental configuration of Fig 7, plane P_1 contains the hologram plate, and plane P_2 is the plane in which the interference pattern is observed. The object beam U_o sould be uncollimated if the average surface of the test object were nominally nonplanar.

A photographic plate is placed in plane P_1 and exposed to the superposition of U_1 and U_r. After developing, this plate is a hologram of the object. Whenever it is illuminated by U_2 at the proper angle a portion of U_r is diffracted, this being denoted by U_2. This complex light amplitude distribution is identical to the light

amplitude U_1 reflected from the object and carries enough information to form a virtual image of the object.

However, the most significant aspect of light amplitude distribution U_2 is its high correlation with U_1. An interference pattern is formed between U_1 and U_2 whenever the object is illuminated by U_o and the hologram plate by U_r. This interference pattern is a consequence of the imperfect registration of the hologram plate when it is returned to plane P_1 of Fig 7. The amount of misalignment is controlled by means of micropositioning differential screws which can rotate and translate the plate holder a small amount.

The contrast ratio of these fringes is determined by the ratio of the two light intensities and the mutual coherence or cross correlation between the light amplitude components U_1 and U_2. The latter is influenced by the spatial and temporal coherence of the incident light beam and by the roughness of the surface of the test specimen. If the light source (eg, spatially filtered laser beam) is sufficiently coherent, the cross correlation between U_1 and U_2 is determined primarily by the roughness of the test surface which is nominally flat (ie, of the order of the wavelength of the illuminating light source), the fringe contrast ratio is uniquely determined by the roughness of the test surface. The roughness of this surface is found by measuring the interference fringe contrast ratio in plane P_2, this being the theoretical basis of the present method of measuring surface roughness. It should be noted that mirrors M_1, M_2 and M_3 also limit the correlation between U_1 and U_2. However, in any practical instrumentation this influence is negligible compared to laser coherence.

The experimental procedure is to first make a hologram of the surface such that an interference pattern is obtained in plane P_2. The laser wavelength used here is 6328 Å. The optimum instrumentation for measuring the fringe intensity distribution is a scanning photocell. The aperture A of this photocell must be sufficiently large compared with the interference pattern in any fringe. However, it must be small compared with the fringe spacing to avoid errors introduced by variations in the average light amplitude over the aperture. Here aperture A has been circular having 1 mm diameter. The desired interference fringe contrast ratio was found by recording the output of the scanning photocell on a chart recorder. This output is proportional to the average fringe intensity over this aperture.

This method is sufficiently accurate for measuring surface roughness over the range from $0.05\ \mu < \sigma < 0.80\ \mu$ where σ is RMS value. Moreover, by using a laser whose wavelength is larger than λ = 6328Å, the validity of this method can be extended to larger surface roughness with greater confidence[28].

FECO scanning interferometer

Interferometry employing fringes of equal chromatic order (FECO) is used to determine the statistics of polished surfaces having roughness under 100 Å RMS. Height and slope distribution function, RMS roughness, RMS slope and modified autocovariance length distribution can be measured for optical surfaces. This method has been fully described by J.M. Benett[29]. By this method surface roughness as small as 8 Å RMS can be measured.

Description of FECO scanning interferometer

Multiple-beam fringes of equal chromatic order are formed when a collimated beam of white light undergoes multiple reflections between two partially silvered surfaces, one of which is the surface whose profile is being measured and the other is a super-

smooth reference surface. When the light is dispersed by a prism or grating, the FECO fringes occur as wiggly black lines in a bright continuum. The wiggles are contours in the wavelength regime of micro-irregularities on the pair of surface comprising the interferometer.

A schematic of the FECO scanning interferometer is shown in Fig 8. White light from a zenon arc A is collimated by lens L_1 and directed on to the interferometer I at normal incidence by means of beam splitter B. Lens L_2 focuses a magnified image m of I on the entrance slit S of a Bausch and Lomb constant deviation spectrograph, which contains collimating lens L_3, prism P, and focussing lens L_4. The resulting spectrum containing the interference fringes and mercury calibration lines (produced by a mercury lamp reflecting light into the system from the back of the beam splitter B) is formed at the focus of the lens L_4 and can be detected by the slow scan TV camera. Visual measurements of the RMS roughness can be made by using the direct reading scale on the spectrograph which is attached to a digital angular readout.

In this spectrum shown in Fig 8 on the right, the wiggly FECO fringe is the height profile of a rectangular area on the interferometer having a length of 1 mm and a width of about 2 μm. Thus the interference fringe contains information about surface detail with a height sensitivity of a few angstroms and a lateral resolution of about 2 μm, the resolution limit of the optical system.

To obtain surface statistics, a slow scan TV camera employing an image dissector tube scans the image, gathering data from one line at a time with the output going to a signal averager. A total of about 512 scan lines make up the TV frame, so each scan line contains information about the average height of an area 1 mm/512 = 1.95 μm by about 2 μm on the interferometer

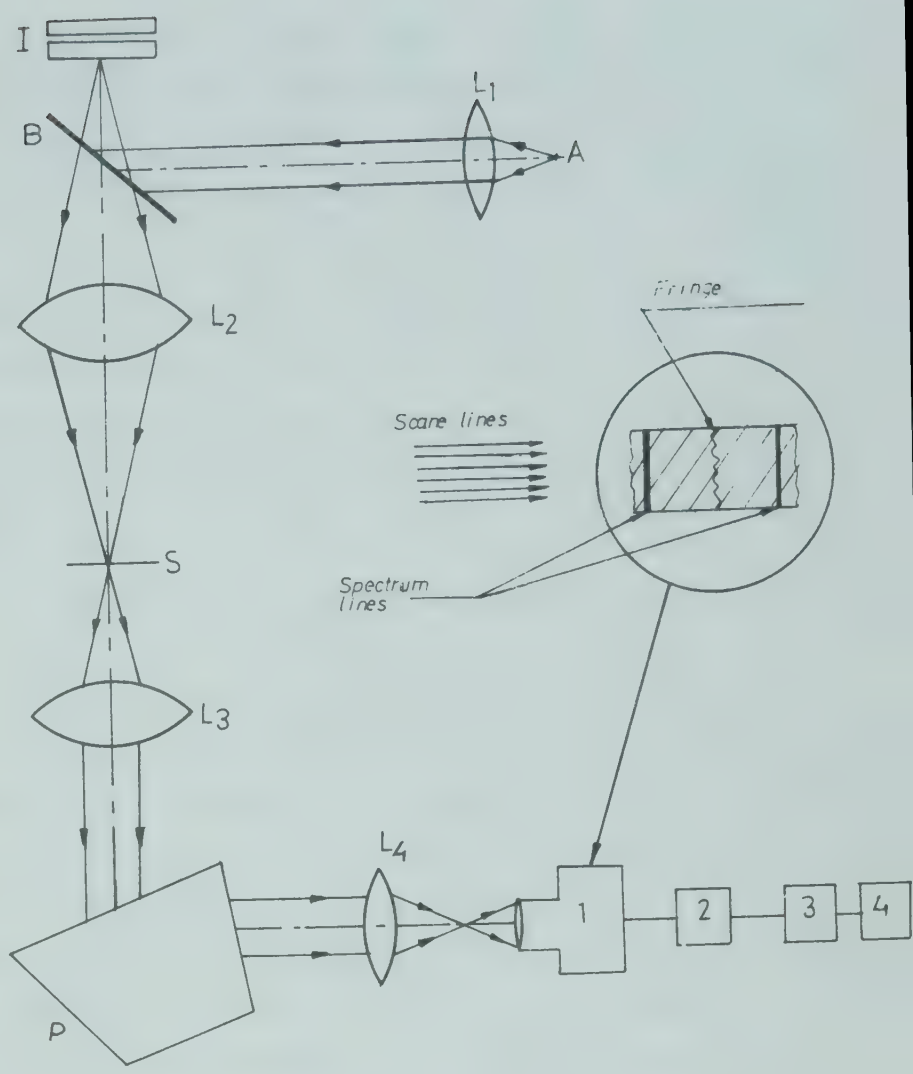


Fig 8
Principle of working of FECO scanning interferometer, (1) Slow scan TV, (2) Signal average, (3) Mini-computer, (4) Tale-type

surface. To obtain the statistical information, the digitized data from the signal averager are fed into a mini-computer (Hewlett-Packard model 2100 Å).

Fibre-optic transducer

A recent development in optical surface roughness measurement employs fibre optics. The instrument consists of a fibre optic probe and an associated metering unit. The probe is essentially a bundle of optical fibres terminating in a nylon shoe designed to accommodate flat, cylindrical, or spherical surfaces. Within the bundle, one group of fibres transmits light from a source in the metering unit to the surface under inspection, and another group receives the reflected light, which is electronically converted into a scaler value in the metering unit[30].

The probe is sensitive only to changes in the roughness or the colour of the sur-

face being inspected. In the event that the colour of a surface changes significantly enough to influence the surface finish, it is possible to use replica technique.

A distinct advantage of the fibre optics technique is that it can be used right at the machine tool, ie, in-process measurements can be made with the help of this instrument[31].

Light scattering by rough surfaces

Beckmann[37] has presented a theoretical development of the scattering of light by rough surfaces. For purposes of treatment, he has classified surfaces as periodic and random. A surface may be denoted by a function $\xi\ (x,y)$ where ξ is the deviation from a mean xy plane. The function can either be periodic or random. An electromagnetic wave with a propagation vector $\vec{k}$ and incident upon the surface at angle θ_1 with the Z-axis, is scattered in another direction making an angle θ_2 and θ_3 respectively with the Z and X axes. The problem then is to determine this field scattered in the arbitrary direction θ_2 and θ_3. Beckmann has obtained expressions for the scattering coefficient (defined as the ratio of the scattered field E_2 to the field E_{20} that would be reflected in the specular direction $\theta_2 = \theta_1$ and $\theta_3 = 0$ by a smooth, perfectly reflecting plane of the same dimensions and at the same angle of incidence at the same distance both for periodic and random rough surfaces respectively. Thus,

$$\rho_{mn} = \frac{F(\theta_1,\ \theta_{2mn},\ \theta_{3mn})}{\Lambda_x\ \Lambda_y}$$

$$\int_o^{\Lambda_x}\int_o^{\Lambda_y} exp\ (i.\vec{v}.\vec{r})\ dxdy \text{ and}$$

$$< \rho > = F/A\ \chi\ (V_Z)\ \rho_o$$

In the above equations Λ_x and Λ_y are periodicities of the surface in x and y directions, A the area subtending the surface S in the xy plane; F a function of the angles θ_1, θ_2 and θ_3; $\vec{V} = \vec{k}_1 - \vec{k}_2$ where $\vec{k}_1$ and $\vec{k}_2$ are propagation vectors of the incident and scattered electromagnetic radiations; $\vec{r}$ is the position vector describing the rough surface,

$$\chi\ (V_Z) = < exp\ (i\ V_Z.Z) > =$$

$$\int_{-\infty}^{\infty} p(Z)\ exp\ (i\ V_Z.Z)\ dZ$$

$p(Z)$ being the probability density of the random variable ξ assuming values Z and V_Z the Z component of V.

$$\rho_o = \frac{Sin\ (V_x.x)}{V_x.x} \cdot \frac{Sin\ (V_y.y)}{V_y.y}$$

is the scattering coefficient of a plane sheet of equal area $A = 4XY$. It will be seen in the two expressions for the scattering coefficient that the mean scattering coefficient is significantly different from zero only in the neighbourhood of the specular direction $\theta_2 = \theta_1$ and $\theta_3 = 0$.

Though it is theoretically possible to obtain the surface characteristics by the above treatment, there is as yet no experimental corroboration of this theory and the field is open for further work.

Specular reflection technique

The use of specular reflection measurements for the determination of surface roughness has been investigated by Benett and Forteus[33] and Devies[34] and experimentally verified by a number of authors whose results are summarized by Birkebak[35]. These results all show a significant correlation of specular reflection measurements with roughness as measured with a profilometer.

When a rough surface is illuminated with spatially coherent light and observed with a finite aperture optical system, speckle is seen (Fig 9). This speckle is produced because light is received at each point in

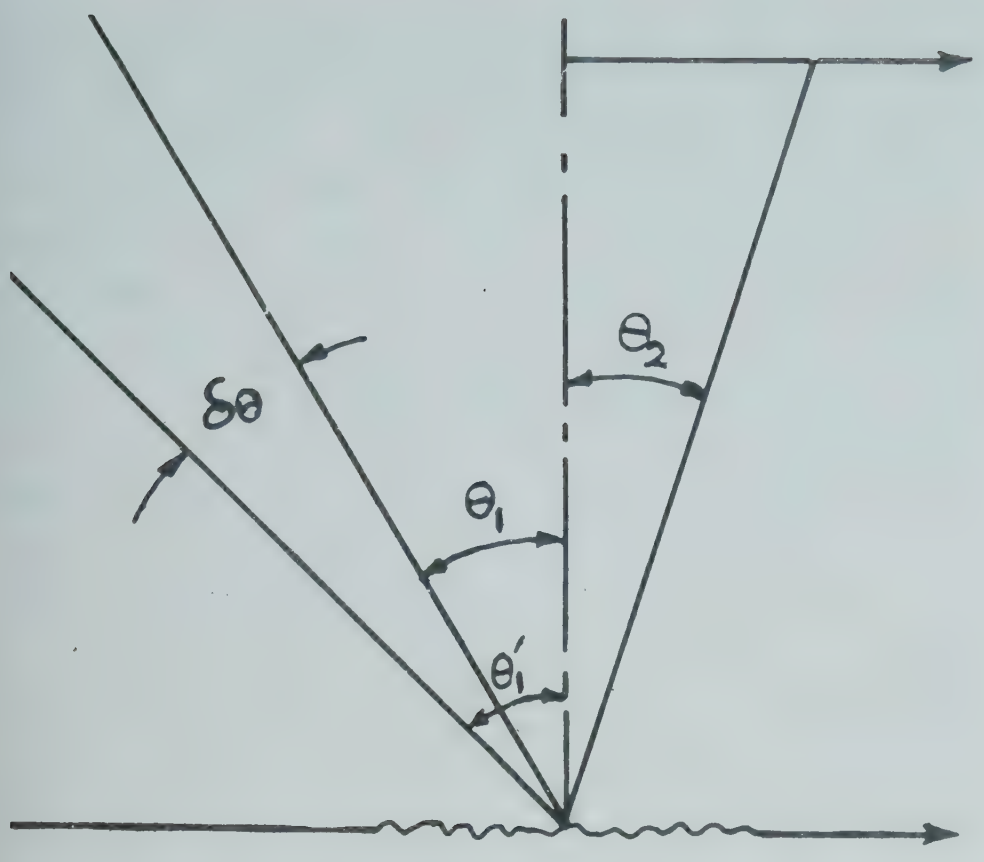


Fig 9
Specular reflection principle

the image from several different points on the object because of the resolution limitation of the system. The path-length of light from each point on the surface depends on the height of the surface contour at that point. If this height varies significantly across the width of the point spread function, interference effects will be seen that are known as speckle. The appearance of high contrast speckle depends on two conditions : (a) the interfering waves must have sufficient phase difference greater than half of wavelength to give complete destructive interference at some points in the speckle pattern, (b) the interfering waves must be temporarily coherent with respect to each other. The first of these two conditions causes the speckle contrast to be low for relatively smooth surfaces. Since an ideal mirror should not produce speckle, a curve of contrast vs roughness will drop to zero at the origin. The second of these conditions is easily satisfied with laser illumination for any surface roughness of interest. Thus the surface roughness can be determined by measuring the speckle contrast[36].

This technique gives useful results in the range of 0.2 μm to 3.2 μm.

This technique shows much promise for the development of an optical profilometer, because it separates out the average surface height deviation from other surface characteristics and is flexible enough to allow for some choice of roughness with cut-off.

The variation of the average contrast speckle intensity patterns against the receiving distance (distance between object surface and receiving plane) is characterized by the surface waviness of the objects[37]. If the object surface has a long wavelength profile, fully developed speckle patterns are observed even in the very near field of the surface. If, however, the object surface becomes almost flat only partially developed speckle patterns appear even at a receiving plane separated by a long distance from the object surface.

Optical profilometer

The optical profilometer (Fig 10) is useful for the examination of extremely fine micro-relief for which an error of less than 0.01 μm on the profile tracing is desirable[38]. It is also suitable for use on surfaces with roughness upto 60 μm. Its field of use is wider than that of mechanical profilometers, since its sensor is a diffraction spot with no material contact, and it can therefore be used without causing surface damage on fragile materials such as aluminium, films, varnish, plastics etc. Owing to the small diameter of the optical sensor, the profile-record it provides is definitely closer to the actual profile than that obtained with a profilometer with a diamond point. Spherical surfaces both concave or convex can also be examined with no special problems.

Glossmeter (reflectometer)

When light is reflected from a metallic surface, the reflection may be specular as in a plane mirror, or diffused due to light scatter. For a given material the specular

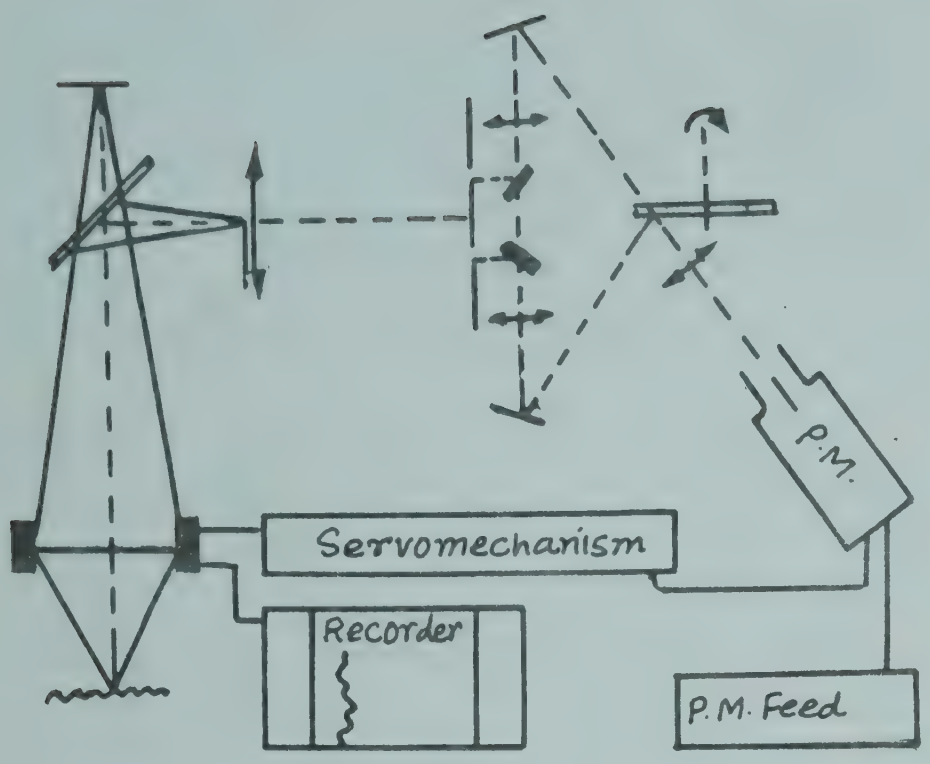


Fig 10
Working principle of optical profilometer

reflective properties depend on the geometric form of the surface texture, the physical state of the surface layer and the angle of incidence[28]. A good finish gives a sharp, well defined reflected image and hence an increased gloss value, whereas a poor finish scatters light and gives a fuzzy low resolution image thereby reducing the gloss value.

A glossmeter, in its normal design, consists of an illuminating collimator which sends out parallel light. The reflected light is assembled in a measuring collimator with a photocell as light registrator[39] (Fig 11).

When a light of intensity J falls on the surface under test such that the angle of incidence is α_o, the total reflected light with an intensity R can be divided into two parts, a direct reflected light with an intensity R_o and angle of reflection $\beta_o = -\alpha_o$, and a diffused reflected light scattered in different directions with an intensity R_d. Thus light R_s reflected from a reference standard also has two parts, the direct reflected light R_{os} and the diffused scattered light R_{ds}. It is shown[40] that the ratio R_o/R is dependent on the ratio of the magnitude of the RMS roughness to the RMS value of the slope of surface irregularities. The RMS value of the surface can be measured very accurately by using infrared light and measuring R_o/R on the test surface, and then on a surface with known RMS value and finally from the ratio of the reflectivities the RMS roughness can be determined. Motycka[41] showed that if the surface irregularities have a normal distribution curve, it can be related to the peak to valley height. Obradovich et al[42] have shown that assuming the distribution of the height of surface irregularities to be normal the relative reflection coefficient ρ can be used to determine roughness value. Since ρ is given by following formula

$$\rho = exp\ (-4\pi/\lambda . \sigma . cos\ \alpha_o)^2$$

where λ is the wavelength of light, σ the mean square deviation of the irregularity height and α_o is the angle of incidence. Since for normal distribution $\alpha = 1.25\ Ra$, this equation can be used to determine the roughness value Ra.

Pneumatic method

A three-dimensional assessment of surface roughness is possible by this method.

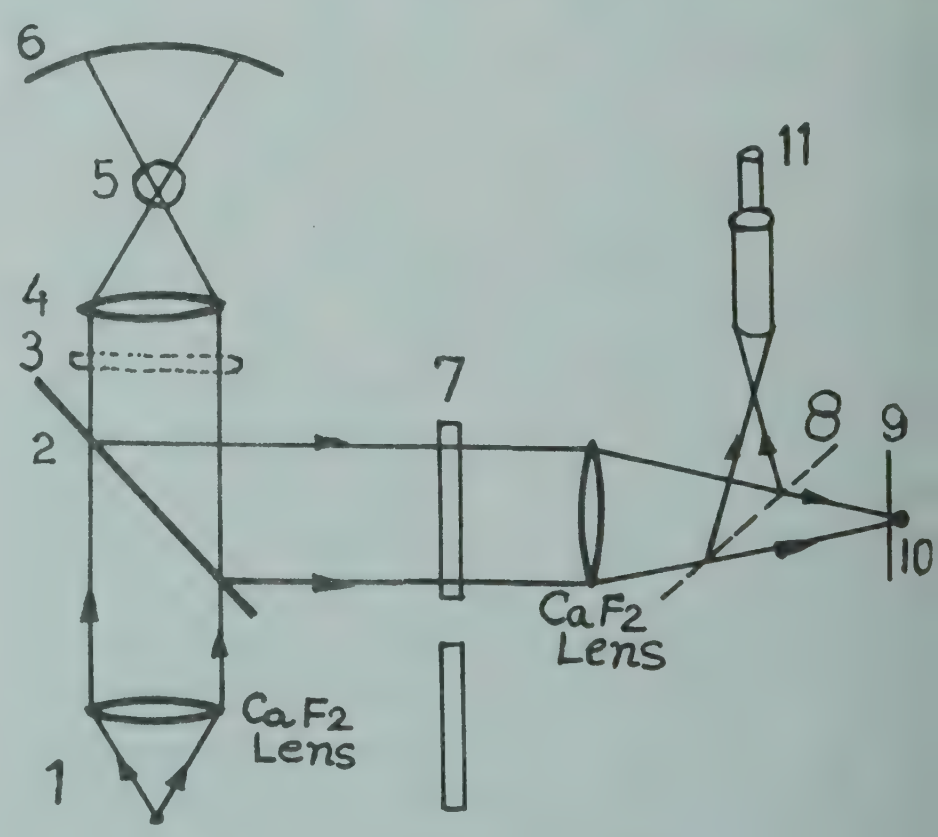


Fig 11
Working principle of glossmeter (after Bennet)

The working principle of this method depends on the fact that when a smooth surface rests over a rough surface, contact will be made only at a few points and the gap between the two is a function of the surface roughness. Pneumatic gauge can be used to measure this gap. The amount of the air discharge, measured by a special variable area air flowmeter or a rotameter determines the surface roughness. This gives and average roughness (CLA) over the area covered by the instrument.

This technique was initially used by Nicolau[43], who used a circular measuring head having a diameter of approximately 5 mm (Fig 12). If $Y = f(x)$ be the equation of the surface round the tip of the head, then the roughness G is given by

$$G = 1/\pi D \oint_o^{\pi D} y dx$$

M. Graneek et al[44] have used a slit type measuring head (Fig 12b) which can be used for both flat and cylindrical surfaces. V. Radhakrishnan et al[45] have used different shapes of measuring heads for roughness measurement. The roughness R_p can be calculated by dividing the air escapement area by the perimeter of the pick up.

Polyansky air flow meter based on pneumatic principle can be used for measuring roughness ranging from 0.32 μm to 10 μm. The disadvantages of this method are insensitiveness to smooth surfaces and lack of quantitative information.

Instrument for measuring statistical parameters

Now-a-days surface roughness is represented by statistical parameters such as number of peaks, bearing area, height distribution, autocorrelation analysis, spectral analysis etc.

Russell[46] has described a peak counter which can count the number and amplitude of peaks.

Bearing area curves are usually obtained

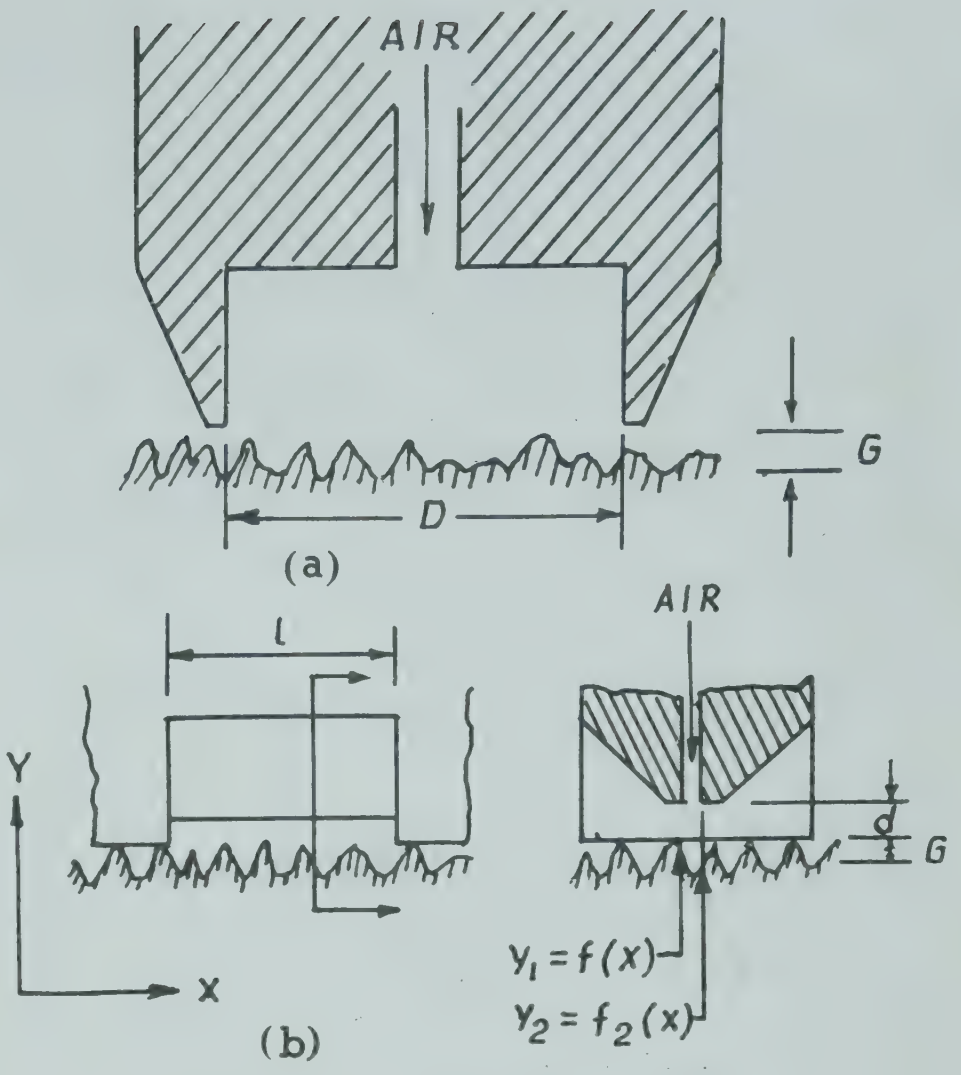


Fig 12

Pneumatic method, (a) circular head, (b) slit type head

manually from profilographs and is a hard work. A measuring instrument devised by Y. Oonishi[47] can be used for this purpose. The working principle of this instrument is fully described by Y. Oonishi in his work.

The instruments for the autocorrelation analysis, spectral analysis and for measuring slope and height distribution of surface irregularities have been fully described by Kubo[48]. Messers Hewlet Packard have devised a minicomputer which can directly be coupled with Taylor Hobson's Talysurf Model 4 for analysing surface roughness records for autocorrelation and spectral analysis. Fig 13 presents the working principle of an autocorrelator and frequency (spectrum) analyser. This consists of a roughness meter and an analogue autocorrelator. The signal proportional to the surface roughness waveform is transmitted from the roughness meter to the autocorrelator. The continuous signal of roughness wave is sampled at a distance of

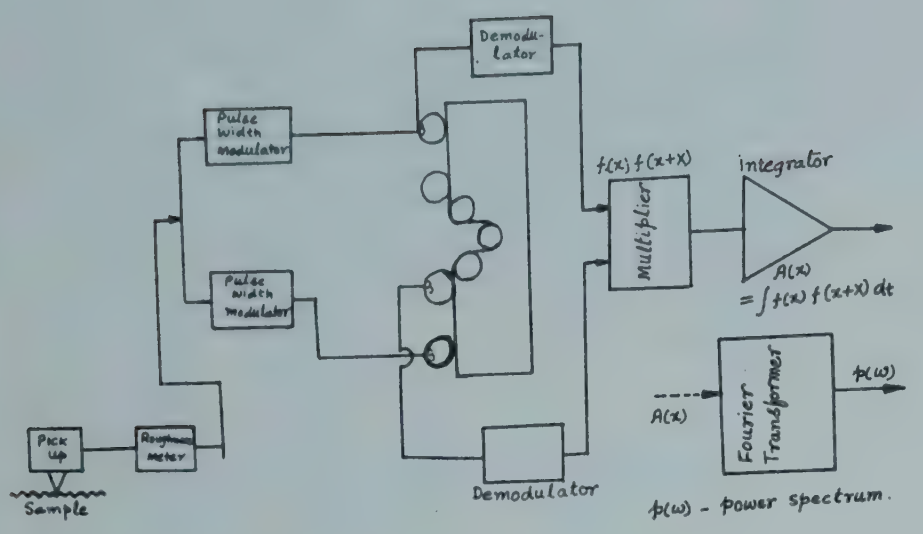


Fig 13

Principle of working of auto-correlator and frequency analyser

about 0.1 μm in the trace of stylus. The pulse width modulated signal is recorded on a double-track-magnetic tape by using two recording heads in parallel. The tape is used in the form of an endless loop. The tape speed is 95.2 mm/sec at recording and 381 mm/sec at playback. The signals from two playback heads are demodulated and multiplied by an electronic multiplier. The product signal is integrated on the operational amplifier. The displacement advances by one step automatically at the termination of a computation. Control signals are obtained at the switching electrodes, which are in contact with a couple of conductive film patches attached on the tape. The total number of steps of displacement is 162 in the device. One step corresponds to 0.25 μm for the first 20 steps to detect high frequency components. Then the steps are switched automatically to correspond to 2.5 μm in the residual 140 steps.

The roughness wave is sampled at 28,665 points in the time interval of 63 secs. The data greatly reduced to the autocorrelation function the value of which is given only at 162 points. These values are numerically read out from the recorded curve and Fourier transformed on a digital computer IPM 7090.

Thomas and King[49] have published a short review of the state-of-art of surface roughness measurements in engineering and have compiled extensive bibliographic notes on the subject. In this publication they have dealt with the methods of characterizing surface roughness, the methods of measurement, and applications. Their work covers the period from 1930 to 1975.

References

[1] H.R. Nelson, 'Taper sectioning as a means of describing the surface contour of metals', Proc Conf on Friction and Surface Finish, MIT (June 1940) p 217.

[2] M. Barash, 'Shop built instruments check surface finish', *Machinery*, 72, p 177 (1966).

[3] M.P. Rubert, 'Functional assessment of surface roughness', Proc Conf on Properties and Metrology of Surfaces, Inst Mech Engrs, 182, Pt 3K, p 350 (1967-68).

[4] E. Green, 'Review of surfaces texture measurement and its associated metrological problems', Proc Inst Mech Engrs, 182, Pt 3K, p 335 (1967-68).

[5] J. Halling, Principles of tribology, The McMillan Press Ltd, 1st Ed, p 21 (1975).

[6] V. Radhakrishnan, 'Does the stylus radius affect surface roughness measurements', *Tribology Ins*, p 101 (1977).

[7] D.E. Williamson, 'Tracer point sharpness as affecting roughness measurement', *Trans ASME*, 69, P 319 (1947).

[8] D.J. Whitehouse, 'Theoretical analysis of stylus integration', *Ann CIRP*, 23, p 81 (1974).

[9] T. Taukada, Y. Anne, 'An evaluation of machined surface topography (2nd report)', *Jap Soc Proc Engng*, 9, p 1 (1975).

[10] T. Nakamura, 'On deformation of surface roughness curves caused by finite radius of stylus tip and tilting of stylus holder arms', *Bull Jap Soc Proc Engng*, 1(4) (1966).

[11] S. Ajioka, 'Dynamic response of stylus', *Bull Jap Soc Proc Engng*, 1(4) 228 (1966).

[12] M.N.H. Damir, 'Error in measurement due to stylus kinematics', *Wear*, 26(2) 219 (1973).

[13] J.B. Agullo and J. Pagesfita, 'Performance analysis of the stylus techniques of surface roughness assessment a random field approach', Proc 15th IMTDR Conf, Birmingham, p 349 (1974).

[14] J.L. Guerrere and J.T. Black, 'Stylus tracer resolution and surface damage as determined by scanning electron microscopy', *Trans ASME*, Ser BJ Eng Ind, 94(4) 1087 (1972).

[15] J. Jungle and D.J. Whitehouse, 'An investigation of the shape and dimensions of some diamond stylus', *Jour Phys Eng Sci Instrum*, 3(6) 137-40 (1970).

[16] R.E. Reason, 'Surface finish and its measurement', *Jour Inst Prod Engrs*, 23, p 347 (1944).

[17] J.P.B. Williamson, 'Physical aspects of a surface', ASTME paper No. EM 68-513 (1968).

[18] H.B. Sharman, 'Influence of sample size and the relationship between the common surface texture parameters', *Proc Instn Mech Engrs*, 182, Pt 3K, p 416 (1967-68).

[19] R.S. Sayles and T.R. Thomas, 'Mapping a small area of a surface', *Jour Phys Eng Sci Instrum*, 9(10) 855-861 (1976).

[20] W. Linnik, 'An instrument for microscope interferometric study of reflecting objects (micro-interferometer)', *Compt Rend Acad Sci*, USSR, 21, (1933).

[21] W. Krug and E. Lau, 'Ein interferenzmikroskop fur Durch und Auflichtmikroskppie', *Ann Phys*, 329 (1951).

[22] S. Tolansky, Multiple beam interferometry of surfaces and films, Clarendon Press (1948).

[23] H. Von Weingraber, 'Optical methods for surface finish evaluation', Proc Int Prod Engng Conf, Pittsburg, p 659 (1963).

[24] W. Krug and E. Lau, 'Equidensitometry, a new measuring method for science and industry', *Feingeratetechn*, 1(9) 391-394 (1952).

[25] E. Zohender, 'An interference method for re-examining rough surfaces', *Z VDI*, 94(14-15) p 156 (1952).

[26] H. Trumpold, 'Limits of application of the interference methods for surface measurements', *Prod Inst Mech Engrs*, Pt 3K, p 241, (1967-68).

[27] W.B. Ribbons, 'Surface roughness measurement by holographic interferometry', *Applied Optics*, 11(4) 807-810 (1972).

[28] J. Halling, 'A reflectometer for the assessment of surface finish', *Jour Sci Instr*, 31, p 318 (1954).

[29] J.M. Bennett, 'Measurement of the rms roughness, autocovariance function and other statistical properties of optical surfaces using a FECO scanning interferometer', *Applied Optics*, 15(11) 2705 (1976).

[30] H. Adkins, 'A look at surface finish', *Amer Mech*, 113(18) 111 (1969).

[31] D. Spurgeon and R.A.C. Slater, 'In-process indication of surface roughness using a fibre-optics transducer', Proc 15th IMTDR Conf, Birmingham, p 339 (1974).

[32] P. Beckman, 'Scattering of light by rough surfaces', *Progress in Optics*, 6, p 55 (1967).

[33] H.E. Bennett and J.D. Porteus, 'Relation between surface roughness and specular reflection at normal incidence', *Jour Opt Soc Amer*, 51, pp 123-129 (1961).

[34] *Proc Inst Elec Engg*, 101, p 209 (1954).

[35] *Applied Optics*, 10, p 1070 (1971).

[36] R.A. Spragus, 'Surface roughness measurement using white light speckle', *Applied Optics*, 11(12) 2811-16 (1972).

[37] H. Fujii and T. Asakura, 'Development of speckle and its application to surface inspection', *Applied Optics*, 16(1) 180 (1977).

[38] Mille O. Dupuy, 'High precision optical profilometer for the study of micro geometrical surface defects', *Proc Instn Mech Engrs*, Pt 3K, p 255 (1967-68).

[39] J. Westwerg, 'Development of objective methods for judging the quality of round and polished surfaces in production', Proc Inst Mech Engrs, Pt 3K, p 260 (1967-68).

[40] H.E. Bennett, 'Measurement of smooth surface finishes', *Indust Qual Control*, pp 18-23, (1964).

[41] 10th Int Wiss Koll, TH Ilmenau (1965).

[42] K.A. Obradovich and F.M. Solodukho, 'Reflectometric methods of surface roughness measurement', *Measurement Technique*, 18(1) 59-62 (1975).

[43] M. Nicolau, 'Application du micrometre solex a la mesure de letat des surfaces', *Mechanique*, March-April (1937).

[44] M. Graneek, A.M. Lee and H.L. Wunsch, 'Application of pneumatic gauging to the measurement of surface finish', *Machinery*, 81, Sept (1952).

[45] V. Radhakrishnan and V. Sagar, 'Surface roughness assessment by means of pneumatic measurement', 4th AIMTDR Conf, Madras (1970).

[46] A. Russell, 'Peak counter for surface texture assessment', *Proc Inst Mech Engrs*, Pt 3K, p 327 (1966).

[47] Y. Oonishi, 'Measurement of bearing curves of surface profiles', *Bull Jap Soc Prod Engng*, 1(4) 249 (1966).

[48] M. Kubo, 'Instruments for statistical analysis of surface roughness', *Bull Jap Soc Proc Engng*, 1(4) p 255 (1966).

[49] T.R. Thomas and M. King, Surface topography in engineering - A state-of-the-art review and bibliography, BHRA Fluid Engineering Series, Vol 3 (1977).

News and Views

3 Crore worth export orders bagged

Indian companies have bagged export orders for machine tools worth about rupees 3 crores at the just-concluded fourth European machine tools exhibition at Hanover.

Mr S.D. Sulakhe, Secretary of the Indian Machine Tools Manufacturers' Association, which organised the country's participation, told that Indian companies also received export inquiries amounting to about rupees 3.5 crores. He hoped, a substantial number of these would result in actual export orders.

India mounted a big display of machine tools at the ten-day fair, rated the world's largest machine tools show.

Pig iron prices may come down

Increased production of pig iron in the public sector steel plants under the Steel Authority of India Limited (SAIL) coupled with the buffer import of pig iron will from now on improve its availability and its market price is likely to come down.

Aggregate production of pig iron during October was 141,800 tonnes as against 92,500 tonnes in September, registering an increase of 53.3 per cent. This, according to SAIL has also been the highest monthly production during the current financial year and has been exceeded only twice during the last 48 months.

This has been possible due to restarting of two blast furnaces at Bhilai and Bokaro which were down for capital repairs.

Meanwhile, the uptrend in steel production in the public sector steel plants, noticeable since October last year after a long period of low production, was maintained last month as well.

The plants at Bhilai, Bokaro, Burnpur, Durgapur and Rourkela aggregated saleable steel production of 472,500 tonnes in October. These plants have produced 66,600 tonnes saleable steel more than the 1980 October production, registering an increase of 16.4 per cent.

However, coal stocks at the plants continued to deplete, receipts being lower than consumption.

5 mini steel plants for N-E region

In a first major effort aimed at creating an adequate industrial infrastructure in the north-eastern region, the Union Government has decided to license five mini steel plants in this region.

This is expected to go a long way in meeting the regional requirements of steel which is said to be a major impediment in the rapid industrialisation of north eastern states comprising of Arunachal Pradesh, Assam, Manipur, Meghalaya, Mizoram, Nagaland, Tripura and Sikkim.

The Centre will help create an additional steel making capacity in this region to the extent of 98,000 tonnes per annum which include steel ingots and billets as also re-rolling facilities.

The decision to permit the setting up

f new mini steel plants in these states ollows Centre's eagerness also to ensure apid industrial growth in this hitherto ndustrially-backward area. The Deputy inister for Industry, Mr P.A. Sangma, has een charged with the responsibility of ndustrialisation of this region.

According to present reckoning, Centre as proposals to license a few textile ills, paper plants, chemical, vanaspati nd sugar mills as also steel units like tructurals, fabrication, tanks and ves-els and the like.

Besides, proposals to set up some units for manufacture of steel tubes, sacking and hessian, industrial packing, writing and printing paper are also proposed to be cleared in the current financial year.

In order to make sure that local entre-preneurial talents are encouraged, Mr Sangma s said to have inserted a new clause which ntails that majority equity participation will necessarily have to be that of locals n these states.

Sponge iron process

A seminar on SL/RN sponge iron process eld in New Delhi recently underlined the mportance of this technology and described t as the most appropriate one for a coun-ry like India which does not have high-uality coking coal for steel making.

Dr Janke, Executive Vice-President of urgi, a West German firm, pointed out that he significance of the SL/RN technology ay in the fact that it was more economical. mini-steel plant, based on sponge iron ould be set up at 60 per cent of the cost nd half the time involved in setting up a onventional steel plant he added.

He said, sponge iron can replace scrap n a large number of Indian arc furnaces nd as such, sponge iron units could be et up at several central locations of feed he arc furnaces of different regions.

The seminar was organised by Lurgi and Indian Institute of Metals, Delhi Chapter.

Automatic pultrusion machine for FRP structural sections

The Vikram Sarabhai Space Centre, Trivandrum, of the Indian Space Research Organisation has developed an automatic pultrusion machine for producing fibre reinforced plastic (FRP) structural sections of uniform cross-section in a continuous manner. FRP pultruded sections have the advantage of high strength to weight ratio, electrical and thermal insulation, corrosion resistance and energy storing capacity. Hence they will have a wide application in different sectors of the industry.

This machine has a puller unit consisting of two hydraulically operated puller heads which pull preset quantity of continuous fibre through a resin bath. Excess resin is removed by a squeezing arrangement. A preheater initiates gelling of the resin. The reinforced resin matrix then passes through a preformer and then through a heated die where the resin is cured and the section acquires its final shape. A start-up puller is also provided to start the operation until the continuous puller can take over the pulling. A diamond cut-off wheel with a preset counter cuts the continuous sections into required lengths.

The die is electrically heated in three independently controlled zones. Die temperatures are automatically controlled. A set of dies is provided with the machine. Other dies can be made for required shapes and sizes. Pulling speed is preset and is continuously variable.

This pultrusion machine can produce sections of a maximum cross-section of 60 mm x 60 mm. Maximum wall thickness is 8 mm.

At present this machine is designed to work on single line operation. However,

it can be modified to work on four lines of pultrusion on the same main frame and with the same hydraulic pack. This multiple line operation will be suitable for higher production rates of smaller sections.

The design of the machine has been optimised to work on polyester resin systems with glass fibre reinforcements. Use of other resin systems and other reinforcements is also possible but will require modifications of operating conditions and qualification trials.

Pressing parts together

Design for the high speed, low cost assembly of two components which can be pushed or pressed together is a new continuous assembly machine launched by Aylesbury Automation.

The entire unit is planned as a standard module with the availability of interchangeable tooling plates on the assembly head and, under normal operating conditions, assembly rates of up to 150 a minute can be reached.

Parts are fed into the company's vibrating parts feeders to a continuously rotating assembly head via gravity feed tracking. The two components are then pressed together by spring loaded plungers acting on a cam plate, the head being driven by a variable speed motor.

Although the new development should interest manufacturers wishing to increase productivity in the assembly of components, Aylesbury believes that its main success will lie in the area of plastics, packaging, cosmetics and electrical goods.

New process for zinc recovery

Australian scientists have developed a new residue treatment process which may increase the recovery of zinc worldwide by up to 5 per cent. The process has been developed at the works of the Electrolytic Zinc Company of Australasia Limited in Hobart, capital of Tasmania.

Scientists at the company, Australia's only zinc processing plant, have built a small experimental pilot plant, producing only half a tonne of zinc a day, to test the new process. Dr Rod Sinclair, manager of the research and development section at Electrolytic Zinc, said it was a new way of tackling an old problem - how best to remove unwanted iron from a solution containing zinc and other valuable metals. Most zinc plants throughout the world neutralise the solution and precipitate the iron as jarosite, a combined step which causes an unavoidable loss of zinc and other valuable metals in the jarosite residue.

The method being tested is a two-stage operation, separating the neutralisation and precipitation processes, Dr Sinclair said. It avoids the loss of valuable metals in the jarosite residue. Dr Sinclair said laboratory work had shown that zinc recovery at Electrolytic Zinc could be increased from 93 to 98 per cent. The recovery of lead and silver from zinc concentrates also could be increased by at least 20 per cent. The new process also produced an environmentally clean jarosite residue in the form of a pure iron compound.

Scientists at Electrolytic Zinc, which has secured provisional world patents for the process, first thought of the treatment in 1979. The company is spending more than 1.5 million Australian dollars to set up the small pilot plant to prove the process works as well under production conditions as it does in the laboratory. Processing exactly the same raw materials as the giant Electrolytic Zinc complex, the pilot plant, now operating on a limited scale, will be fully integrated by early 1983 and operational for two and half years at a total cost of 6 million Australian dollars. Every step will be self-contained, down to the final production of half a tonne of zinc

a day - a small fraction of the company's normal daily output of 600 tonnes. Dr Sinclair said that if the tests were sucessful, Electrolytic Zinc would spend 40-50 million Australian dollars modifying its equipment to incorporate the new process.

The Australian Industrial Research and development Incentives Board has provided a substantial grant for the experimental work. Established in 1916, Electrolytic Zinc is the second largest zinc processing plant in the world, with an annual production of 220,000 tonnes. Its output is exceeded only by the Cominco company in British Columbia. Electrolytic Zinc developed the original jarosite process during the 1960s. This raised the level of zinc extraction from the concentrate from 85 to 93 per cent, leading to a dramatic increase in world zinc production. Dr Sinclair said, by using the new process Electrolytic Zinc would increase its annual zinc production by more than 10,000 tonnes.

Fuel saving device

A device that cuts down fuel expenses by 25 to 40 per cent has been developed by Jose Concepcion of Makati, Metro Manila. This alco-diesel device, which is attached to the diesel engine, allows the use of 30 per cent hydrous alcohol and 70 per cent diesel oil.

In the Philippines, laboratory tests conducted by the National Science Development Board (NSDB) Centre for Non-conventional Energy Development and the Energy Research Development Centre showed that the device is efficient. Findings showed that with this device, a diesel engine attains 13.2 per cent more power and 10.7 to 22 per cent better mileage. The device can displace 15 to 39 per cent diesel fuel with low grade alcohol much cheaper than the former. It can also be used in any diesel engine for industrial purpose, like in farming and marine applications.

The device costs 3,000 to 10,000 pesos depending on the size and type of the engine. For an ordinary jeep or automobile, it costs 3,000 pesos.

BOOKS RECEIVED

(1) Managing Work-in-Process Inventory (Industrial Engineering Series, Volume 5). By Kenneth Kivenko, 1981, 240 pages, bound illustrated. $29.75 (price is 20% higher outside the US and Canada).

Managing Work-in-Process Inventory will be helpful to all manufacturing managers and planners, particularly those faced with intermittent production problems, to make informed policy decisions concerning the level of WIP inventory. This book integrates the accounting, engineering, and production aspects of WIP inventory and provides the necessary theories, models, mathematics, and practices for planning and controlling WIP inventory.

The text focuses on how work-in-process inventory affects each step of the manufacturing cycle, from the time work begins on materials and components to the delivery of the finished product, and how to plan and control each step of this cycle. The impacts of WIP inventory on job lead time, output mix control, machine utilization, and customer service are made clear, anddiscussions of operational auditing and performance measurement provide object measures for judging the effectiveness of inventory control policies.

Managing Work-in-Process Inventory is recommended to industrial engineers, financial executives, production planners, production and inventory control supervisors, management information systems, managers, purchasing personnel, and general management. This book will enable them to eliminate WIP inventory problems, improve production efficiency, decrease congestion and product damage, and enhance the on-

time delivery capability of the manufacturing firm.

(2) Improving productivity by classification coding and data base standardization : The key to maximizing CAD/CAM and group technology (Manufacturing Engineering and Materials Processing Series, Volume 5). By William F. Hyde, 1981, 352 pages, bound, illustrated. $35.00 (Price is 15% higher outside the US and Canada).

This book represents a comprehensive treatment of data classification, coding, and standardization available. Containing time-proven management tools for improving managerial and staff capabilities and the reduction of costs, this book also features instructions for their complete implementation.

All the terms have been defined, the basic theory has been provided, and practical examples readily applicable to the needs of the readers have been presented for the information data systems users, managers, and manufacturing, industrial and systems engineers. The emphasis is o improving productivity and staff by eli minating their redundant activities an improving their skills. Control and mana gement of data, representing the key ele ments of any business or institution yields a continuing and growing source o profits, maximizing the desired output fro a minimum input of essential resources.

Both the books are published by Marce Dekker Inc, 270 Madison Avenue, New York NY 10016, USA.

CSIR Vice President visits MERADO, Madras

Prof Nurul Hasan, Vice President, CSIR visited MERADO, Madras on 6th October, 1981. The Vice President was taken around the laboratories, where some important testing work were demonstrated to him. A brief review of some of the current projects was presented to the Vice President. He evinced great interest in them, particularly in the work undertaken for leather machinery manufacturers.



Prof Nurul Hasan during his visit to lab

mechanical engineering bulletin

Official organ of the Central Mechanical Engineering Research Institute—a laboratory under the Council of Scientific & Industrial Research, New Delhi

NUMBER 1 - 4, 1981

Publication, Editorial and Advertising Offices:
Central Mechanical Engineering Research Institute,
Mahatma Gandhi Avenue, Durgapur 9, India.

TABLE OF CONTENTS - PAPERS AND ARTICLES

NUMBERS 1-4, 1981

Number 1 (March), pp 3-33

1 Optimization of hand hoist by analytical structural modelling
by Jerry Kowalski and Waclaw Szyc .. 3

2. Calculation of the oil-flow rate for proper operation of a scoop type fluid coupling
by Jhankar Basu .. 17

3. Welding of copper without preheat - a study
by N.D. Das .. 20

4. Erosion, corrosion and fouling of tubes in fluidized bed boilers
by Prabir Basu and M. Debnath .. 26

5. State level R&D committee, inherent constraints defeat basic objectives .. 32

Number 2 (June), pp 41-62

1. Critical consideration on the limits of operation of fluid couplings
by Jhankar Basu, G.S. Patki and S. Ramachandra .. 41

2. Open solar regeneration of lithium chloride brine
by M. Prasad and P. Kumar .. 47

3. Free mass impact damper having large clearances
by S.V. Bhave and P.P. Chikate .. 53

4. Determination of the relative effect of the process variables on overcut in ECM
by D.K. Pramanik .. 60

Number 3 (September), pp 69-90

1. Some effects of electrolytic flow mode on the anode shape in ECM
by V.K. Jain and P.C. Pandey .. 69

2. Angular defocusing of paraboloidal reflectors with obtuse rim angle and truncated bottom
by M. Prasad and S.K. Majumdar .. 75

3. Fatigue in rolling contact - some salient features
by C.S. Chandrasekharamurthy and Ramamohana Rao .. 82

4. Pedal pump for lift irrigation
by G.K. Verma, R.K. Varma and K.N. Rao .. 87

Number 4 (December), pp 99-131

1. Solar still regenerator for brine
by M. Prasad, P. Kumar and B.C. Raychaudhuri .. 99

2. Energy losses in smooth pipe bends
by Usha S. Powle .. 104

3. Metallurgical investigation into tube failure in power plants
by A.B. Mondal, B.K. Ghosh and S. Jana .. 110

4. A review of surface roughness measurement techniques
by R.A. Agarwal, M.P. Kumaraswamy and S.K. Basu .. 116

AUTHOR AND SUBJECT INDEX

MECHANICAL ENGINEERING BULLETIN

NUMBERS 1-4, 1981

Agarwal, R.A., surface roughness measurement technique, (4) 116

Analyser, metal, portable, (3) 95

Analytical structural modelling, hand hoist, (1) 3

Angular defocusing, paraboloidal reflector, (3) 75

Anode shape, ECM, electrolyte flow, (3) 69

Automatic single spindle turret lathe, (1) 34

pultrusion machine, FRP structural section (4) 133

Basu, A., metallurgical investigation, tube failure, power plant, (4) 110

Basu, Jhankar, limits of operation, fluid coupling, (2) 41

Scoop type fluid coupling, (1) 17

Basu, P. corrosion. fluidised bed boiler tubes (1) 26

Basu, S.K., surface roughness measurement technique, (4) 116

Bends, pipe, energy losses, (4) 104

Bhave, S., free mass impact damper, (2) 53

BHEL, leads engineering exports, (3) 93

Boiler tubes, fluidised bed, corrosion, (1) 26

Books received, (4) 135

Brine, lithium chloride, solar regenerators, (2) 47

still regenerator, solar, (4) 99

BSP plan for modernisation, (1) 37

Calculation, oil flow rate, scoop type fluid coupling, (1) 17

Chandrasekharamurthy, C.S., fatigue in rolling contact, (3) 82

Chikate, P.P., free mass impact damper, (2) 53

Chloride lithium, brine, solar regenerator, (2) 47

CMERI open day, (1) 34

Coal washery, Soviet help, (2) 66

Combine harvester, MERADO develops, (3) 93

Committee, state level, R&D, inherent constraints, (1) 32

Conference, CSIR Directors, (2) 63

Constraints, inherent, state level, R&D Committee, (1) 32

Contact, rolling, fatigue, (3) 82

Copper, welding without preheat, (1) 20

Corrosion, fluidised bed boiler tubes, (1) 26

Cost reduced, hard material machining, (1) 38

Coupling, fluid, limits of operation, (2) 41

scoop type, oil flow rate, (1) 17

Critical consideration, fluid coupling, (2) 41

CSIR Directors conference, PM addresses, (2) 63

Damper, impact free mass, (2) 53

Das, N.D., welding of copper without preheat, (1) 20

Debnath, M., corrosion, fluidised bed boilers, (1) 26

Defocusing, angular, paraboloidal reflector, (3) 75

Determination, relative effect, ECM overcut, (2) 60

Developed combine harvester, (3) 93

domestic gas stove, (2) 64

single spindle automatic turret lathe, (1) 34

Device, fuel saving, (4) 135

DGSIR, Dr G.S. Sidhu, appointed, (2) 64

Domestic gas stove developed, (2) 64

East Germany leads explosive forming, (1) 38

ECM anode shape, electrolyte flow, (3) 69

overcut, relative effect of process variables, (2) 60

Effect, electrolyte flow, (3) 69

process variables, ECM overcut, (2) 60

Electrolyte flow, anode shape, (3) 69

Energy losses, smooth pipe bends, (4) 104

meet, (3) 94

Engineering export, (2) 65, (3) 93

units advised, R&D, (3) 93

EPI, leads engineering exports, (3) 93

Explosive forming, East Germany leads, (1) 38

Erosion, fluidised bed boiler tubes, (1) 26

Export, engineering, (2) 65, (3) 93

order, bagged, (4) 132

target, (2) 65

Failure, tube, power plant, metallurgical investigation, (4) 110
Fatigue, rolling contact, (3) 82
Features, rolling contact fatigue, (3) 82
Flow, electrolyte, anode shape ECM, (3) 69
rate, oil, scoop type fluid coupling, (1) 17
Fluid coupling, limits of operation, (2) 41
scoop type, oil flow rate, (1) 17
Fluidised bed boiler tube, erosion, corrosion, (1) 26
Fouling, fluidised bed boilers, (1) 26
Free mass impact damper, (2) 53
FRP structural section, pultrusion machine, automatic, (4) 133
Fuel saving device, (4) 135

Gas stove, domestic, MERADO develops, (2) 64
know-how released, (3) 91
GDR-India trade protocol, (1) 38
Germany, East, leads explosive forming, (1) 38
Ghosh, B.K., metallurgical investigation, tube failure, (4) 110
Groundnut sheller, (3) 96

Hand hoist, structural modelling, (1) 3
Hard material, machining, reduced cost, (1) 38
Harvester combine, MERADO develops, (3) 93
Hoist, hand, structural modelling, (1) 3

Impact damper, free mass, (2) 53
India-GDR, trade protocol, (1) 38
Inherent constraints, state level R&D committee, (1) 32
Investigation, metallurgical, tube failure, power plant, (4) 110
Iron, pig, price, (4) 132
sponge, production process, (2) 65, (4) 133
Irrigation, pedal pump, (3) 87

Jain, V.K., electrolyte flow mode, anode shape ECM, (3) 69
Jana, S., metallurgical investigation, tube failure, (4) 110

Know how, turret lathe, reaming machine, gas stove, (3) 91
Kowlaski, J., optimisation of hand hoist, structural modelling, (1) 3
Kumar, P., solar regenerator, (2) 47
solar still regenerator for brine, (4) 99
Kumaraswamy, M.P., surface roughness measurement, (4) 116

Lathe, turret, know-how released, (3) 91
single spindle, automatic, (1) 34
Lift irrigation, pedal pump, (3) 87
Lithium chloride brine, solar regenerator, (2) 47
Losses, energy, pipe bends, (4) 104

Machine, pultrusion, FRP structural section, automatic, (4) 133
reaming, know-how released, (3) 91
Machining hard materials, reduced cost, (1) 38
Mass, free, impact damper, (2) 53
Materials, hard, machining, (1) 38
Majumdar, S.K., defocusing, paraboloidal reflector, (3) 75
Measurement, surface roughness, (4) 116
MERADO designs gas stoves, (2) 64
develops combine harvester, (3) 93
releases know-how, (3) 91
Metal analyser, portable (3) 95
Metallurgical investigation, tube failure, (4) 110
Mini-steel plant, (4) 132
Modelling, structural, hand hoist, (1) 3
Modernisation plan, BSP, (1) 37
Mandal, A.B., metallurgical investivation, tube failure, (4) 110

NE region, mini-steel plants, (4) 132
New process, sponge iron production, (2) 65
zinc recovery, (4) 134

Oil flow rate, scoop type fluid coupling, (1) 17
Open-day, CMERI observes, (1) 34
Operation, limits of, fluid couplings, (2) 41
scoop type fluid coupling, (1) 17
Optimisation, hand hoist, modelling, (1) 3
Order, export, bagged, (4) 132
Over-cut in ECM, process variables, relative effect, (2) 60

Pandey, P.C., electrolyte flow model, anode shape, ECM, (3) 69
Paraboloidal reflector, angular defocusing, (3) 75
Parts, pressed together, (4) 134
Patki, G.S., limits of operation, fluid couplings, (2) 41
Pedal pump, (3) 87
Pig iron price, (4) 132
Pipe bends, energy losses, (4) 104
Plan, modernisation, BSP, (1) 37

Plant, power, tube failure, investigation, (4) 110
steel, mini, (4) 132
PM addresses Directors' conference, (2) 63
Portable metal analyser, (3) 95
Power plant, tube failure, (4) 110
Powle, Usha, S., energy losses, pipe bends, (4) 104
Pramanik, D.K., effect of process variables, over-cut in ECM, (2) 60
Prasad, M., defocusing, paraboloidal reflector, (3) 75
solar regenerator, lithium chloride brine, (2) 47
solar still regenerator for brine, (4) 99
Pressing parts together, (4) 134
Price, pig iron, (4) 132
steel, producers raise, (1) 37
Process, production, sponge iron, (2) 65
spong iron, (4) 133
variables, effect on over-cut, ECM, (2) 60
zinc recovery, (4) 134
Producers raise prices, steel, (1) 37
Production process, spong iron, (2) 65
SAIL's, goes up, (2) 65
Project, UNIDO, (1) 36
Pultrusion machine, automatic, FRP structural sections, (4) 133
Pump, pedal, (3) 87

Ramachandra, S., limits of operation, fluid couplings, (2) 41
R&D committee, state level, (1) 32
engineering units advised, (3) 93
Rao, A.R., fatigue in rolling contact, (3) 82
Rao, K.N., pedal pump, (3) 87
Rate, oil flow, scoop type fluid coupling. (1) 17
Raychaudhuri, B.C., solar still regenerator for brine, (4) 99
Reaming machine, know-how released, (3) 91
Recovery process, zinc, (4) 134
Reduced cost, machining hard material, (1) 38
Reflector, paraboloidal, obtuse rim angle, (3) 75
Regulator, still, solar, regenerator, brine, (4) 99
Regenerator, solar, lithium chloride brine, (2) 47
Review, surface roughness measurement, (4) 116
Rim angle, obtuse, paraboloidal reflector, (3) 75
Robot, usage, (2) 66
Rolling contact, fatigue, (3) 82
Roughness measurement, surface, (4) 116

SAIL's production goes up, (2) 65
Salient feature, rolling contact fatigue, (3) 82
Saving device, fuel, (4) 135
Scoop type fluid coupling, oil flow rate, (1) 17
Shape, anode in ECM, effect on electrolyte flow, (3) 69
Sheller, groundnut, (3) 96
Shidhu, Dr G.S., appointed DGSIR, (2) 64
Single spindle turret lathe, (1) 34
Smooth pipe bends, energy losses, (4) 104
Solar regeneration, lithium chloride brine, (2) 47
still regenerator for brine, (4) 99
Soviet help, coal washery, (2) 66
Spindle, single, turret lathe, (1) 34
Sponge iron process, (2) 65, (4) 133
State level R&D Committee, (1) 32
Steel plant, mini, NE region, (4) 132
producers raise price, (1) 37
Still regenerator, solar, (4) 99
Stove, gas, developed by MERADO, (2) 64
know-how released, (3) 91
Structural section, pultrusion machine, automatic, (4) 133
Study, welding of copper without preheat, (1) 20
Surface roughness measurement, review, (4) 116
Szyc, W., optimisation of hand hoist structural modelling, (1) 3

Technique, surface roughness measurement, (4) 116
Trade protocol, GDR-India, (1) 38
Tube failure, power plants, investigation, (4) 110
fluidised bed boiler, erosion, corrosion, (1) 26
Truncated bottom, paraboloidal reflector, (3) 75
Turret lathe, know-how released, (3) 91
single spindle, automatic, developed, (1) 34

UNIDO project in India, (1) 36
Units, engineering, advised, R&D, (3) 93
Usage, Robot, (2) 66

Variables, process, effect, ECM overcut, (2) 60
Varma, R.K., pedal pump, (3) 87
Verma, G.K., pedal pump, (3) 87
Washery, coal, Soviet help, (2) 66
Welding of copper without preheat, (1) 20
Zinc, recovery process, (4) 134